

UNIVERSITÉ DE STRASBOURG

ÉCOLE DOCTORALE Des Sciences Chimiques
Institut de Chimie - UMR 7177

THÈSE

présentée par :

Anaëlle Bolley

soutenue le : **04 septembre 2019**

pour obtenir le grade de :

Docteur de l'université de Strasbourg

Discipline/ Spécialité : CHIMIE

Catalyse de la polymérisation pour l'obtention de polyesters à caractères hydrophile biodégradable

THÈSE dirigée par :

M. Dagorne Samuel

Dr., Université de Strasbourg

RAPPORTEURS :

M. Rudolf Wehmschulte

Prof., Institut Technologique de Floride

M. Pierre Le Gendre

Prof., Université de Dijon

MEMBRES DU JURY :

M. Rudolf Wehmschulte

Prof., Institut Technologique de Floride

M. Pierre Le Gendre

Prof., Université de Bourgogne

M. Olivier Braun

Dr., SNF Andrézieux

M. Samuel Dagorne

Dr., Université de Strasbourg

PERSONNALITÉ INVITÉE

M. Cédric Favero

Directeur R&D-SNF, Andrézieux

UNIVERSITÉ DE STRASBOURG

ÉCOLE DOCTORALE Des Sciences Chimiques
Institut de Chimie - UMR 7177

THÈSE

présentée par :

Anaëlle Bolley

soutenue le : **04 septembre 2019**

pour obtenir le grade de :

Docteur de l'université de Strasbourg

Discipline/ Spécialité : CHIMIE

Catalyse de la polymérisation pour l'obtention de polyesters à caractères hydrophile biodégradable

THÈSE dirigée par :

M. Dagorne Samuel

Dr., Université de Strasbourg

RAPPORTEURS :

M. Rudolf Wehmschulte

Prof., Institut Technologique de Floride

M. Pierre Le Gendre

Prof., Université de Dijon

MEMBRES DU JURY :

M. Rudolf Wehmschulte

Prof., Institut Technologique de Floride

M. Pierre Le Gendre

Prof., Université de Bourgogne

M. Olivier Braun

Dr., SNF Andrézieux

M. Samuel Dagorne

Dr., Université de Strasbourg

PERSONNALITÉ INVITÉE

M. Cédric Favero

Directeur R&D-SNF, Andrézieux

REMERCIEMENTS

Un très grand merci à mon directeur de thèse, le Dr. Samuel Dagherne, pour m'avoir fait confiance tout au long du déroulement de ma thèse, pour l'opportunité qu'il m'a accordée de travailler au sein de son laboratoire sur mon sujet de thèse. Je le remercie également pour sa gentillesse, disponibilité et bien entendu pour les encouragements permanents qu'il m'a prodigués.

Je tiens bien évidemment à remercier la société SNF qui a financé et donc permis l'élaboration de ce doctorat.

Je tiens à remercier les membres du jury, le Professeur Rudolf Wehmschulte, le Professeur Pierre Le Gendre et le Docteur Olivier Braun pour avoir pris le temps et la peine de juger ce travail.

Je remercie bien évidemment toutes les personnes des services communs: Maurice, Bruno et Lionel du service RMN. Stéphanie du service de spectrométrie de masse, Lydia et Corinne de la «RX» ainsi que le personnel de l'analyse élémentaire.

Je remercie le Dr. Artem Osypenko, post-doctorant dans le laboratoire de Jean-Marie Lehn, qui a consacré du temps et m'a permis de réaliser mes purifications par chromatographie.

J'aimerais remercier également l'informaticien de la fac de chimie, Mr. Jean-Christian Pont pour sa réactivité exceptionnelle face à mes demandes spécifiques ainsi que le Dr. Aurélie Guidez qui m'a apporté son aide afin de mettre en page ce travail.

Un grand merci aux membres du service commun d'analyses et caractérisations des polymères à l'Institut Charles Sadron, ainsi qu'à l'équipe de la plateforme Chemlab de l'ECPM, qui m'ont permis la détermination de nombreux résultats physico-chimiques.

Je finirai par remercier mes parents pour leur soutien inconditionnel au cours de ces années.

ABBREVIATIONS AND REPRESENTATIONS

AcC: Acetyl cellulose

$\alpha\epsilon\text{CL} = \text{Cl-CL}$: α -chloro- ϵ -caprolactone

Anh: Anhydrous

a. u.: Atomic units

Bn: Benzyl

Conv.: Conversion

Corr: Correction

Cy: Cyclohexyl

DCM: Dichloromethane

DSC: Differential Scanning Calorimetry

ΔH : Enthalpy variation

Equiv.: Equivalent

FDA: The Food and Drug Administration

FLPs: Frustrated Lewis Pairs

GPC= SEC: Gel Permeation Chromatography= Steric Exclusion Chromatography

k_{app} : Apparent rate constant

$\epsilon\text{-CL}$: ϵ -Caprolactone

ROP: Ring Opening Polymerization

h: Hours

IFT: Interfacial Tension

IPr* = 1,3-bis{2,6-bis(diphenylmethyl)-4-methylphenyl}-1,3-dihydro-imidazol-2-ylidene

ⁱPr: *Iso*-propyl

^tBu: *Tert*-butyl

k: Kinetic rate

L-lactide: (*S,S*)-lactide= (3*S*)-cis-3,6-dimethyl-1,4-dioxane-2,5-dione

m-PEG-OH: monomethyl methoxy-capped polyethylene glycol

M: Molecular concentration at a given time

M_0 : Molecular concentration at $t = 0$

*m*CPBA: *meta*-Chloroperoxybenzoic Acid

Meso: (*R,S*)-lactide

Me: Methyl
M_n: Molecular mass
Min.: Minutes
M_w: Molecular weight
NHC: *N*-Heterocyclic Carbene
NMR: Nuclear Magnetic Resonance
NY11: Nylon 11
PBS: Poly(butylene succinate)
PCL: Polycaprolactone
PDI: Polydispersity index
PES: Polyethersulfone
PE: Polyethylene
PEG: Poly(ethylene glycol)
PHB: Poly-β-hydroxybutyrate
PHBV: Poly(hydroxybutyrate-3-hydroxyvalerate)
PLA: Polylactide
PLLA: Poly(*L*-lactic acid)
PS: Polystyrene
PTMC: Poly(trimethylene carbonate)
Rac: Racemic
RT: Room Temperature
Salen: *N,N'*-bis(salicylaldehyde)ethylenediamine
Sec = s: Second
T: Temperature
T_c: Crystallization temperature
T_g: Glass transition temperature
T_m: Melting temperature
TGA: Thermal Gravimetric Analysis
Theo: Theoretical value
THF: Tetrahydrofuran
Tol•: Toluene
Vs.: Versus

“Je suis reconnaissant envers tous ceux qui m’ont dit NON car, grâce à eux, je l’ai fait MOI-MEME”

Albert Einstein

Table of contents

GENERAL INTRODUCTION	1
I. Biodegradable materials	2
I. 1. Background and significant categories of biodegradable materials	2
I. 2. Factors affecting the biodegradability of polymers	5
I. 3. Cyclic polyesters/polycarbonates via Ring Opening Polymerization	6
II. Polylactic acid	7
II. 1. Different ROP mechanisms of lactide	8
II. 2. PLA stereochemical considerations and physical properties	11
II. 2. 1. Stereochemical considerations	11
II. 2. 2. Physical properties	12
III. Water-soluble polymers	13
IV. Presentation of Ph.D. works	13
CHAPTER I	18
CONTROLLED PRODUCTION OF POLYLACTIDE BIOMATERIALS UNDER MILD CONDITIONS USING N-HETEROCYCLIC CARBENE GROUP 13 COMPLEXES	18
I. Introduction	19
II. General characteristics of NHCs	19
II. 1. Electronic properties	20
II. 2. Steric properties	21
III. Metallic adduct synthesis supported by NHCs ligands	21
IV. Properties and applications of group 13 metals	22
V. Results on the synthesis of new adducts	24
V. 1. Sterically bulky NHC group 13 adducts	24
VI. Synthesis of NHC-supported group 13 metal alkyl cations	28
VII. ROP of <i>rac</i>-lactide with the IMesMMe₃ complexes.	30
VII. 1. ROP of lactide with IMesGaMe ₃ (<i>catalyst 4</i>)	32
VII. 2. ROP of <i>rac</i> -lactide with IMesInMe ₃ (<i>catalyst 5</i>)	36
VIII. [IMesAlMe₂(OEt₂)]⁺ <i>catalyst 6</i> for the ROP of <i>rac</i>-lactide	39
IX. Conclusion	44
CHAPTER II	50
SYNTHESIS OF PEG-CO-PLLA AMPHIPHILIC COPOLYMERS USING DIFFERENT CATALYSTS UNDER MILD CONDITIONS	50

I. Introduction	51
II. <i>N,O,N</i>-supported Al(III) and Ga(III) amido chelates 2 and 3: synthesis and structure	54
II. 1. Synthesis of <i>N,O,N</i> ligand 1	54
III. Synthesis and structural characterization of <i>N,O,N</i> group 13 complexes	54
III. 1. Synthesis of complexes	54
III. 2. ROP of PEG- <i>co</i> -PLLA with <i>catalyst 2</i>	57
III. 3. ROP of PEG- <i>co</i> -PLLA with <i>catalyst 3</i>	60
III. 4. Comparison of the activity of the metal center between the two κ^3 - <i>N,O,N</i> catalysts	62
IV. Use of a biocompatible zinc catalyst for PEG-<i>co</i>-PLLA copolymerization	66
IV. 1. Zinc properties	66
IV. 2. Synthesis of $\text{tol}\cdot\text{Zn}(\text{C}_6\text{F}_5)_2$ catalyst	66
IV. 3. ROP of <i>L</i> -lactide in presence of PEG with $\text{tol}\cdot\text{Zn}(\text{C}_6\text{F}_5)_2$ <i>catalyst 4</i>	67
V. Use of a magnesium catalyst for ROP of <i>L</i>-lactide in presence of PEG	70
V. 1. Magnesium properties	70
V. 2. Synthesis of $\text{Mg}(\text{THF})_2(\text{C}_6\text{F}_5)_2$ <i>catalyst 5</i>	70
V. 3. ROP of PEG- <i>co</i> -PLLA with $\text{Mg}(\text{THF})_2(\text{C}_6\text{F}_5)_2$ <i>catalyst 5</i>	71
VI. Bulk conditions	74
VII. Conclusion	75
CHAPTER III	81
SYNTHESIS OF POLY(ALPHA-CHLORO-EPSILON-CAPROLACTONE)	81
I. Introduction	82
II. Synthesis of α-chloro-ϵ-caprolactone (Cl-CL)	82
III. ROP of chloro-caprolactone using a magnesium catalyst	85
III. 1. Polymerization of Cl-CL using $\text{Mg}(\text{THF})_2(\text{C}_6\text{F}_5)_2$ <i>catalyst 1</i> /BnOH system	85
IV. $\text{tol}\cdot\text{Zn}(\text{C}_6\text{F}_5)_2$ as catalyst for the ROP of chloro-caprolactone (Cl-CL)	97
V. Use of Salen catalysts for the ROP of alpha-chloro-epsilon-caprolactone	100
V. 1. Synthesis of two different salen-based catalysts	100
V. 2. Kinetic comparison of <i>catalyst 3</i> vs. <i>catalyst 4</i>	102
V. 3. Stability of Cl-CL' ROP above RT	105
V. 4. Use of salen aluminium alkoxide 4 as ROP initiator of Cl-CL at RT	108
VI. Extension of the P(Cl-CL) chain length	113
VI. 1. 250 equivalents of P(Cl-CL)	113
VI. 2. 500 equivalents of P(Cl-CL)	118
VII. Coordination-insertion mechanism	120
VIII. Calibration curve obtained by ^1H NMR and by GPC as a function of different Cl-CL equivalents.	122
VIII. 1. 75 equivalents of Cl-CL	123
VIII. 2. 100 equivalents of Cl-CL	124
VIII. 3. 150 equivalents of Cl-CL	125
VIII. 4. 170 equivalents of Cl-CL	127
VIII. 5. Calibration curve plot	128

IX. Immortal ROP	129
X. Functionalization of the poly(α-chloro-ϵ-caprolactone)	132
X. 1. Substitution of the chlorine pendant group according to Williamson reaction	133
X. 2. Hydrogenation of the polymer mixture obtained after the Williamson reaction	134
XI. Conclusion	135
CHAPTER IV	138
COPOLYMERS, DIBLOCKS AND STEREOCOMPLEX FORMATION AND THEIR PHYSICOCHEMICAL PROPERTIES	138
I. Introduction	139
II. Synthesis of PEG-co-P(Cl-CL)	139
II. 2. IFT measurements.	144
II. 2. a. IFT explanation and measurements principle	144
II. 2. b. IFT Results on the different copolymers	145
III. Synthesis of P(L/D)LA-<i>b</i>-P(Cl-CL) diblocks and stereocomplex	146
III. 1. Diblocks synthesis	146
III. 2. Stereocomplex formation	154
IV. Thermal gravimetric analysis TGA	157
IV. 1. Theory about TGA	157
IV. 2. P(Cl-CL) homopolymer TGA analysis	158
IV. 3. Diblocks and stereocomplex TGA studies	159
V. DSC studies	161
V. 1. Theory about DSC	161
V. 2. Homopolymers, diblocks and stereocomplex DSC studies	161
VI. Conclusion	163
CONCLUSION AND PERSPECTIVES	166
EXPERIMENTAL SECTION	170
GENERAL PROCEDURE	171
Materials	171
Nuclear Magnetic Resonance	171
Size-exclusion chromatography (SEC) analysis	171
MALDI-TOF analysis	172
Elemental analysis	172
X-ray crystallography	172
CHAPTER I	173

Syntheses	173
Crystal data	179
Polymer Synthesis	180
Polymer characterization	180
NMR spectroscopy	180
Size-exclusion chromatography (SEC) analysis	181
Supporting data	181
CHAPTER II	182
Syntheses	182
Crystal data	187
Polymer synthesis	188
Polymer characterization	188
NMR spectroscopy	188
Size-exclusion chromatography (SEC)	188
Supporting data	189
CHAPTER III	190
Typical procedure for Cl-Cl polymerization	190
Typical procedure for immortal Cl-Cl polymerization	190
Syntheses	190
Crystal data	195
P(Cl-Cl) characterization	196
NMR spectroscopy	196
Size-exclusion chromatography (SEC) analysis	196
General procedure for Williamson reaction	196
Supporting data	197
CHAPTER IV	209
Polymer characterization	209
IFT measurements	209
Thermogravimetric Analysis (TGA)	209
Differential Scanning Calorimetry (DSC)	209
General procedure for diblock's formation	210

Stereocomplex formation	210
Supporting data	211
RESUME DES RESULTATS IMPORTANTS	222

General introduction

I. Biodegradable materials

I. 1. Background and significant categories of biodegradable materials

Since 1940, mass production of polyolefin plastics has increased rapidly.¹ The most common plastics, which account for approximately 80% of the European plastic demand, are polyethylene (PE), polypropylene (PP), poly(vinyl chloride) (PVC) and polystyrene (PS) (Figure 1).²

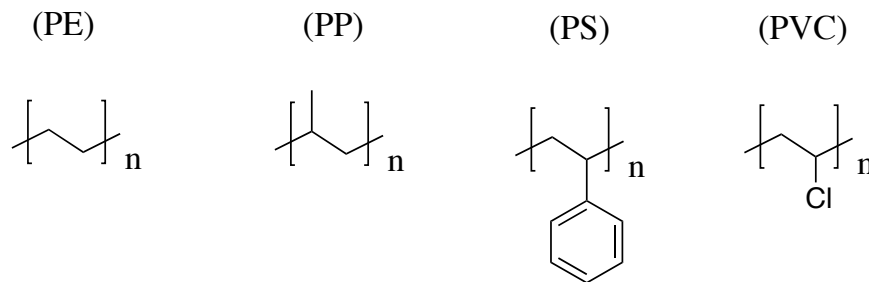


Figure 1: The most widely used polyolefins

The consumption of plastic materials has experienced a substantial expansion, and they are now the most widely used materials. These materials have a wide range of applications from packaging to electronic fields.³

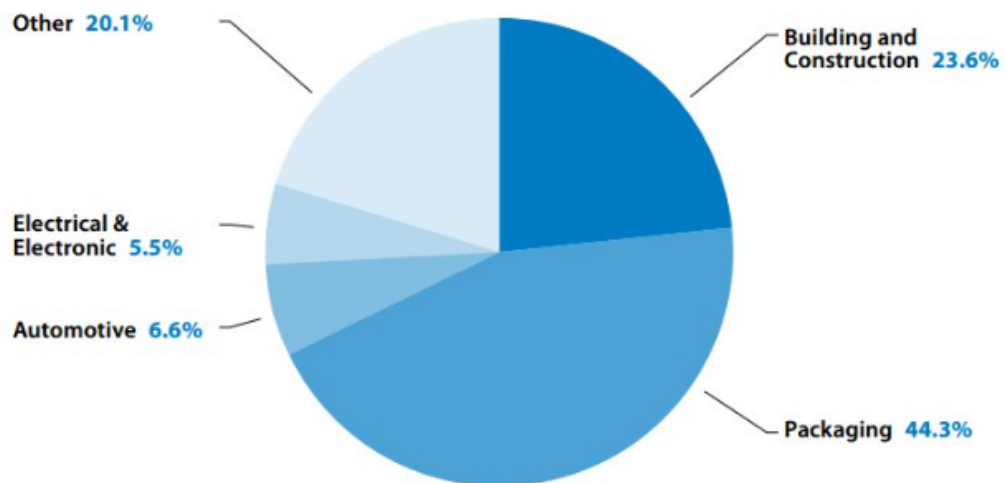


Figure 2: European plastics demand by segment

(Source: PlasticsEurope Market Research Group (PEMRG) 2015)

Polyolefins, however, are derived from fossil resources and more than 90% of these plastics are not renewable and, for the most part, are not recyclable, more scarce and expensive.⁴ These materials represent an environmental problem, mainly with regard to disposal after use.⁵ For this reason, they present a «non-zero carbon footprint».⁶

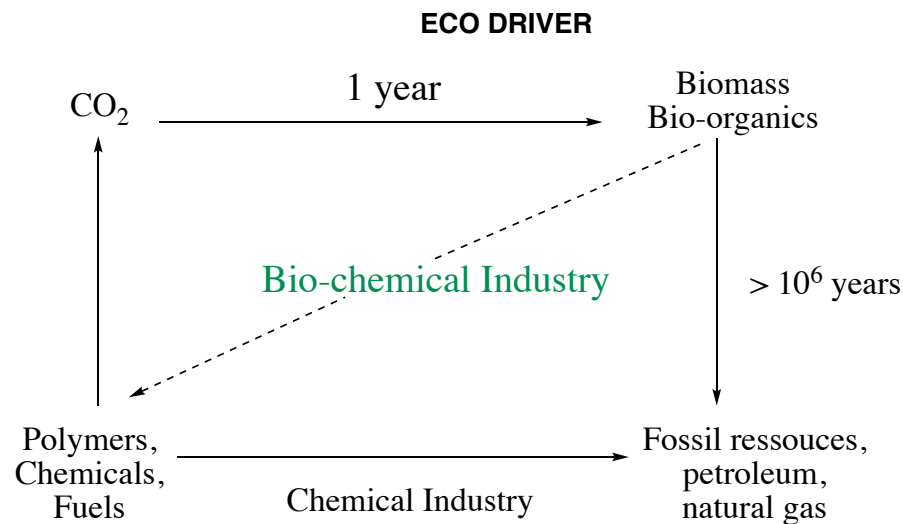


Figure 3: Carbon life cycle

Bio-sourced⁷ and biodegradable⁸ polymers may then be a viable alternative to plastics of petrochemical origin.⁹

To overcome the problems mentioned above, some strategies involving the production of a high degree of degradability (more than 60% of conversion after 28 days)¹⁰ have been undertaken. Biodegradable¹¹ and bio-sourced polymers (*e.g.*, plastics synthesized from biomass or renewable resources)¹² can constitute a viable alternative to plastics from a petrochemical origin and are already used in many fields, for example as packaging, biomedical devices and nanotechnology. These materials can be categorized as follows:

- Polymers from agro-resources (biomass products)¹³: cellulose, chitin, and starch
- Polymers from microorganisms¹⁴ : Poly(hydroxybutyrate) (PHB), Poly(hydroxybutyrate) (PHBV)

- Biotechnology polymers (synthesis from bio-sourced monomers)¹⁵: Polylactide (PLA)
- Polymers from synthesis¹⁶: Polycaprolactone (PCL), Poly(trimethylene carbonate) (PTMC)

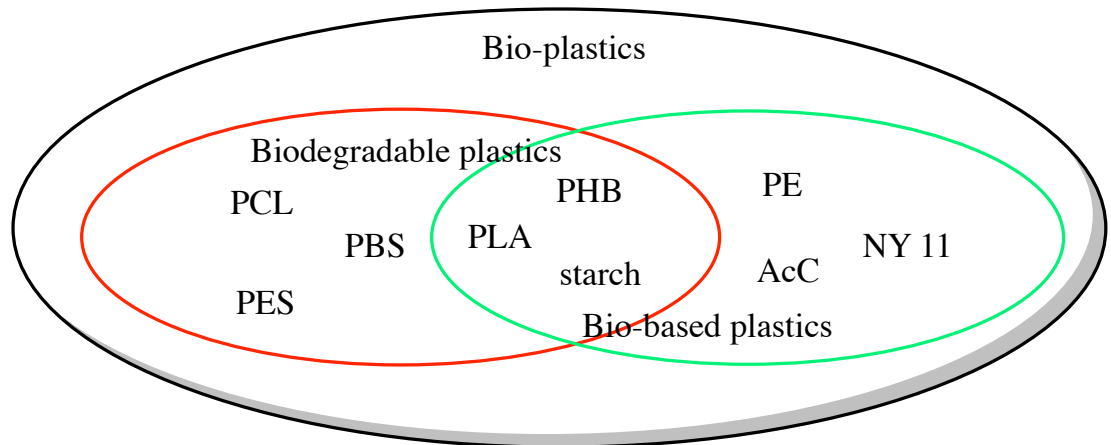


Figure 4: Bio-plastics comprised of biodegradable plastics and bio-based plastics

Figure 4 shows the inter-relationship between biodegradable and bio-sourced plastics. On the one hand, PCL and PBS are petroleum based, but they can be degraded by microorganisms. On the other hand, PHB, PLA and starch are produced from biomass or renewable resources and are biodegradable. Whilst PE and NY 11 can be produced from biomass or renewable resources, they are not biodegradable. Another point we can see with AcC is the biodegradation depending on the degree of acetylation; with a low acetylation, it can be degraded whilst with high substitution ratio it is non-biodegradable. Biodegradable polymers are a promising solution in order to limit the use of fossil feedstocks because they are environmental-friendly and can be produced from renewable feedstocks (wheat, corn). Also, the analyses of the life cycles of these materials tend to show a lower impact on different environmental factors (warming, soils nitrification, ozone emission, etc) and can offer significant advantages such as increased soil fertility, low accumulation of bulky plastic materials in the environment and reduction in the cost of waste management. Biodegradability is a natural process in which organic materials are decomposed (**Figure 5**). In many cases, the adherence of microorganisms on the surface of plastics is followed by the colonization of the exposed surface, which is the major mechanism, the degradation of plastics by hydrolysis in two-steps by enzymatic process¹⁷: the enzyme binds to the polymer

substrate then catalyses a hydrolytic cleavage then polymers are degraded into low molecular weight oligomers, dimers or monomers and finally mineralized to water, carbon dioxide, methane (in the case of anaerobic degradation), etc. and new biomass is produced.¹⁸

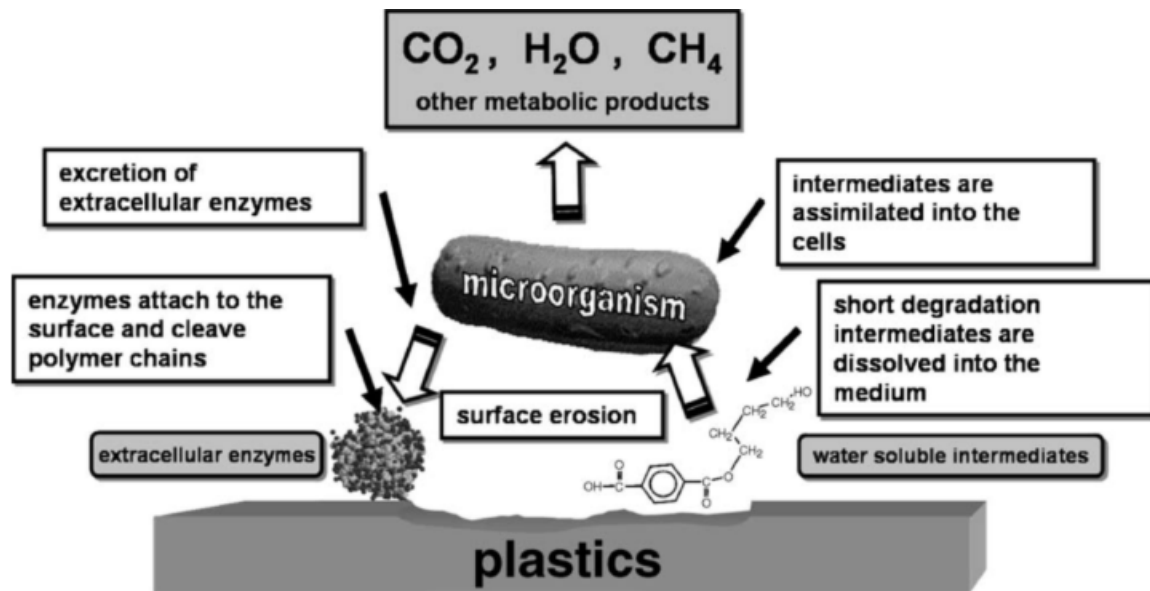


Figure 5: General mechanism of enzymatic catalyzed hydrolytic polymer degradation¹⁹

I. 2. Factors affecting the biodegradability of polymers

The chemical and physical properties of plastics influence the mechanism of biodegradation:

- The surface conditions, surface area, hydrophilic/hydrophobic properties
- The first order structures: chemical structure, molecular weight, and molecular distribution
- The high order structure: glass transition temperature, melting point, and modulus of elasticity, crystalline structure

Increasing the molecular weight of the polymer decreases its degradability, the crystalline part of the polymer is more resistant than the amorphous region and for example, the rate of degradation of PLA decreases with an increase in crystallinity of the polymer.^{20,21} The melting point of polyesters (**Table 1**) has an important effect on the enzymatic degradation of the polymers. The higher it is, the less biodegradable the polymer is.²²

Name	Chemical structure	T _m (°C)
Polyester	-O-(CH ₂) ₆ -O-CO-(CH ₂) ₄ -CO-	60
Polycarbonate	-O-(CH ₂) ₄ -O-CO-O-(CH ₂) ₄ -O-CO-	65
Polyurethane	-NH-(CH ₂) ₆ -NH-CO-O-(CH ₂) ₄ -O-CO-	180
Polyamide	-NH-(CH ₂) ₆ -NH-CO-(CH ₂) ₆ -CO-	240
Polyamide	-NH-(CH ₂) ₆ -NH-CO-(CH ₂) ₄ -CO-	265

Table 1: Chemical structures of aliphatic polyester, polycarbonate, polyurethanes, and polyamides with their melting temperature (T_m)s

In that regard, we can easily see that aliphatic polyesters and polycarbonates show high potential for use as biodegradable plastics.

I. 3. Cyclic polyesters/polycarbonates via Ring Opening Polymerization

Biodegradable polyesters/polycarbonates previously mentioned can be obtained via different routes: polycondensation,²³ enzymatic process²⁴ or by Ring Opening Polymerization (ROP) of cyclic esters/carbonates monomers²⁵ as ϵ -caprolactone (ϵ -CL), lactide (LA) or trimethylene carbonate (TMC).

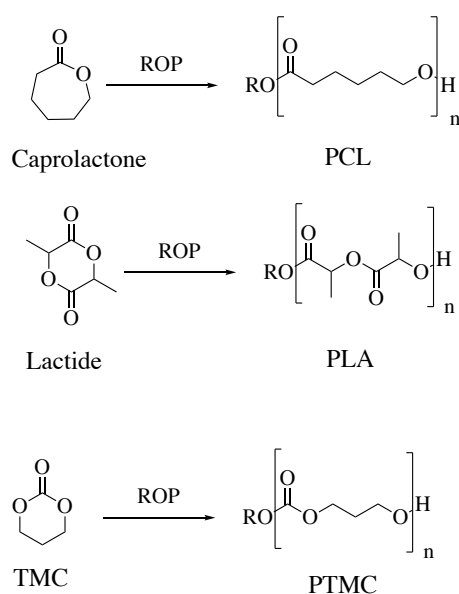


Figure 6: Cyclic polyesters/polycarbonates obtained by ROP of cyclic monomers

II. Polylactic acid

PLA was the first bio-sourced polymer to be commercialized²⁶ and is still the most used biopolymer: the aliphatic polyester backbone is intrinsically sensitive to water and heat but bioassimilable too since the hydrolysis in physiological environment gives lactic acid, a non toxic component that is then eliminated via the Krebs cycle as water and carbon dioxide. It is a compostable polymer too. In the presence of microorganisms, in conditions of humidity and proper temperatures, the polymer is partially degraded (more than 60% in less than six months).²⁷ Nowadays, two industrial processes permit the PLA synthesis. The first developed by Cargill (Nature work) is initiated by tin (II) octanoate ($\text{Sn}(\text{Oct})_2$) but the possible toxicity of tin along with current limitations of the produced PLA (limited thermal and mechanical properties) would require the development of biocompatible metal-based ROP catalysts. A second industrial process permits to immediately polymerize lactic acid through polycondensation but requires diphenyl ether, a toxic solvent.

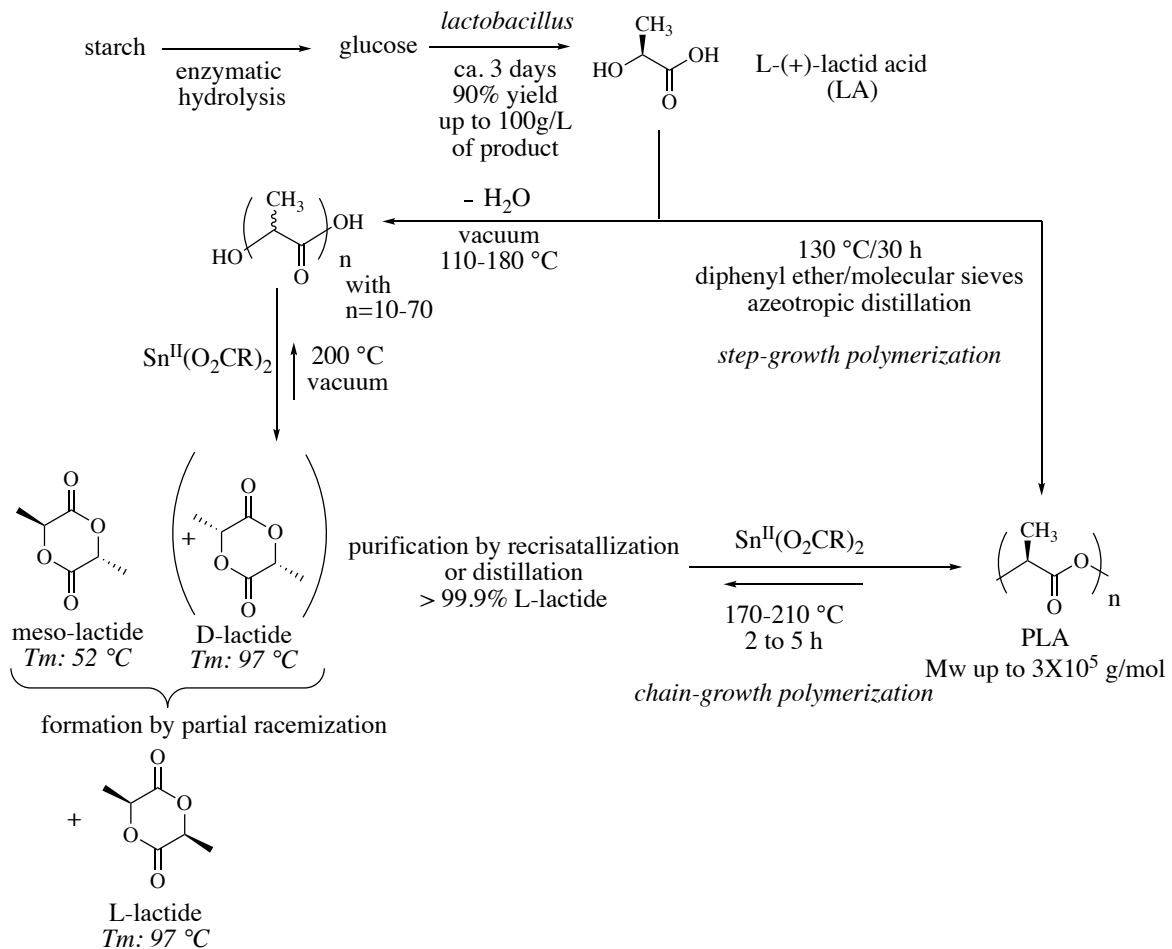
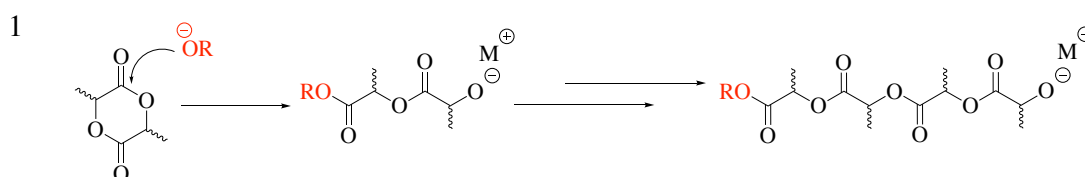


Figure 7: Industrial processes of PLA synthesis

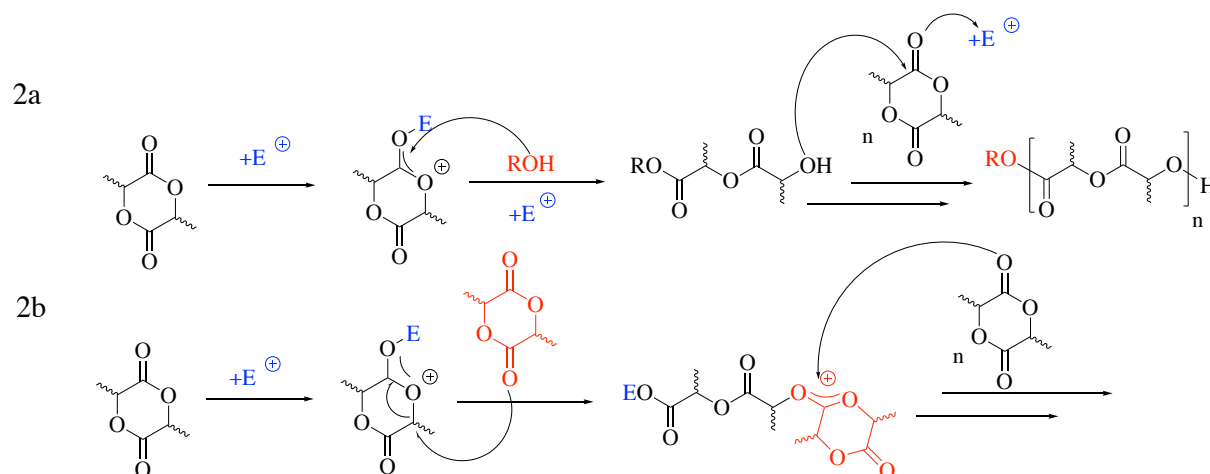
II. 1. Different ROP mechanisms of lactide

The generally accepted mechanism for ring opening polymerization involves initiation by either an anionic, cationic, activated monomer mechanism or a coordination–insertion. Because of the highly reactive anionic reactants that hinder the growth of chain, the anionic polymerization becomes a cause of undesirable reactions (racemization, decomposition reaction and other side reactions). Cationic polymerization can cause racemization too because of the nucleophile reaction on the active center.²⁸

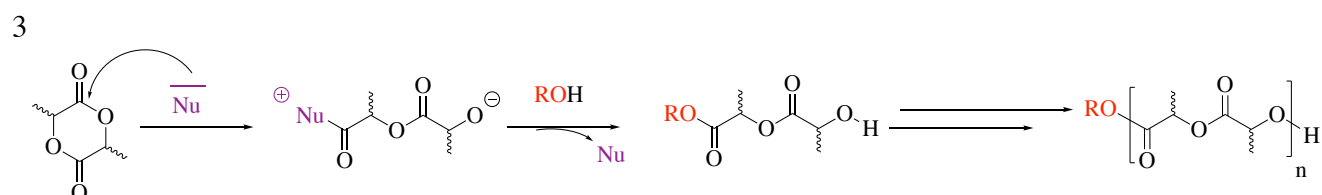
1: Anionic polymerization.²⁹



2a: Cationic polymerization, electrophilic monomer's activation, 2b: Cationic polymerization: activated end chain mechanism.³⁰



3: Nucleophilic ROP.³¹



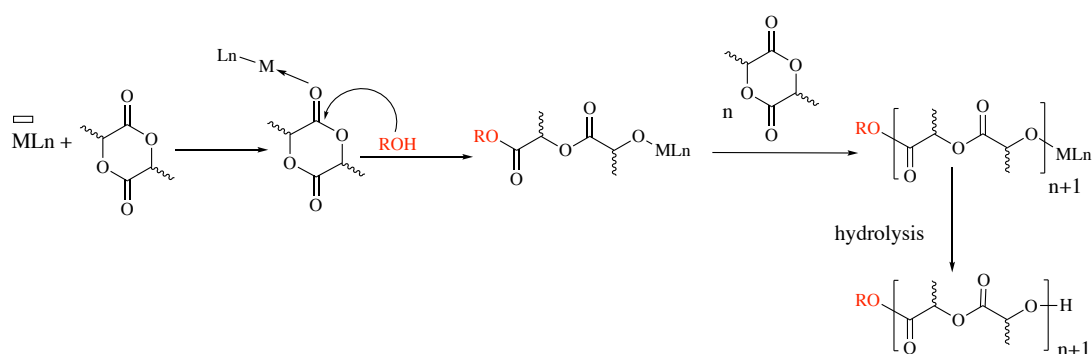
4: Activated monomer mechanism.³²

Figure 8: Different ROP mechanisms

The most classical mechanism is the general coordination-insertion ROP:³³

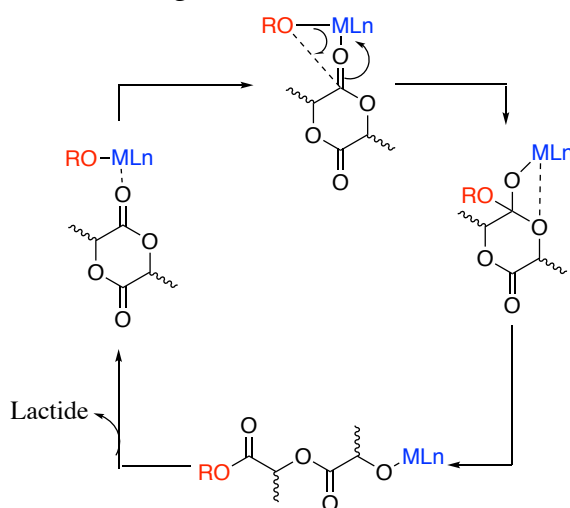


Figure 9: General coordination-insertion mechanism for *rac*-lactide ROP by an OBn-MLn complex

The mechanism operates via coordination of the lactone to a Lewis acidic metal alkoxide complex (RO-MLn), which activates the carbonyl function. Then, the monomer inserts into the metal-alkoxide bond via a nucleophilic attack on the carbonyl carbon. Acyl bond cleavage results in the ring opening then chain propagation by incorporation of the following monomers. The hydrolysis of the active metal-alkoxide bond leads to the formation of a hydroxyl function on one chain end while the other end is bonded by the alcoholate.

Dittrich and Schulz firstly formulated this three-step coordination-insertion mechanism for the ROP of cyclic esters/carbonates in 1971.³⁴ Then, Kricheldorf³⁵ and Teyssié³⁶ reported the first experimental proof for this mechanism in the late 1980s. This kind

of polymerization is called «living polymerization» and allows a control of PLA chain length formed by the initial stoichiometry in the monomer. There is an important interest in metal-based initiators (*e.g.*, alkoxide metal) bonded to a ligand that would display higher catalytic activity and lead to polymers with controlled chain length.³⁷ Without undesirable reactions, for this controlled polymerization, there is a linear correlation between the polymer molecular weight as the ROP proceeds and monomer conversion; however, in such coordination-insertion polymerization, the molecular weight control depends on the $k(\text{propagation})/k(\text{initiation})$ ratio. Inter-/intra-molecular chain transfers between macromolecules with chain scission is the most often observed “side” reaction in the polymerization of heterocyclic compounds. The extent of transesterification is strongly dependent on reaction conditions, tending to be more prolific when reaction times are long and with higher temperatures, but has also been found to be dependent on the nature of the metal initiator. These transesterifications side reactions can occur both intramolecularly leading to macrocyclic structures and shorter chain, and intermolecularly to give a chain redistribution.³⁸ These side reactions result in broader molecular-weight redistribution and deterioration of physical properties of the polymer.

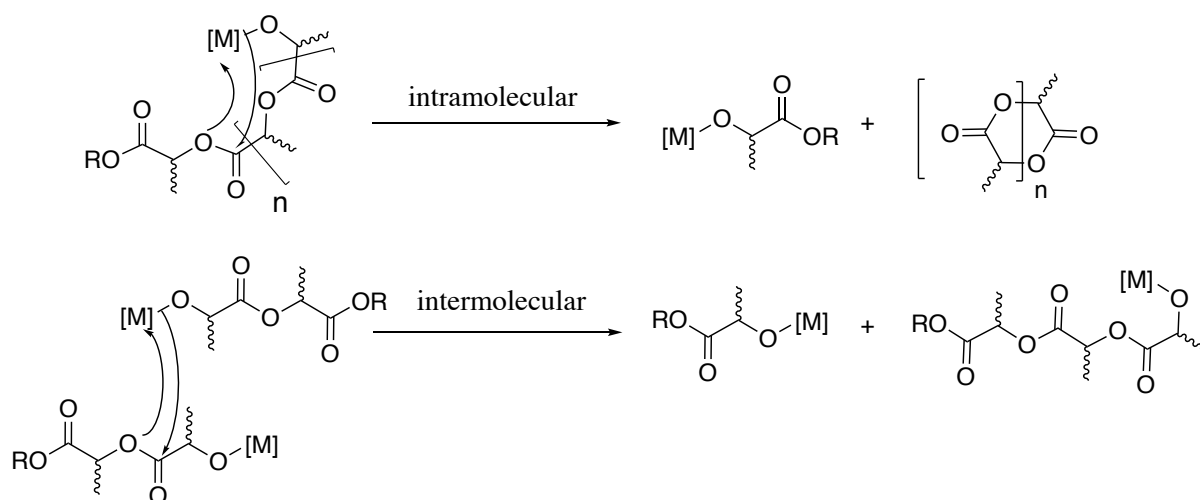


Figure 10: PLA intramolecular and intermolecular transesterification side reactions

For a successful polymerization control, an initiator must have a very good activity, an initial ring-opening rate faster than the propagation step, and restricts the side transesterification reactions during the polymerization.

Generally, alkoxide and amido complexes of oxophilic and Lewis acidic metals are excellent to initiate the ROP of cyclic esters ROP like lactide by the typically

coordination-insertion mechanism. The effect of initiating group was investigated by Chisholm and co-workers within the series of compounds, and the rate of lactide ring-opening was reported to follow the order $X = \text{NMe}_2 > \text{OMe} > \text{O}^i\text{Pr} > \text{O}^i\text{Bu} > \text{OPh}$. The electronic and steric properties of the initiating group influence the ROP and the stability of the ring-opened product.³⁹ Another advantage of such ligand-supported metal initiators is the possibility of stereoselectively polymerization of *rac*- and *meso*-lactide into stereoregular PLA through appropriate ligand design.

II. 2. PLA stereochemical considerations and physical properties

II. 2. 1. Stereochemical considerations

Due to the presence of two stereocenters per monomer unit (**Figure 11**), lactide has two diastereomeric forms leading to a variety of possible polymer microstructures for PLA, which have an effect on the mechanical properties of the polymer.⁴⁰

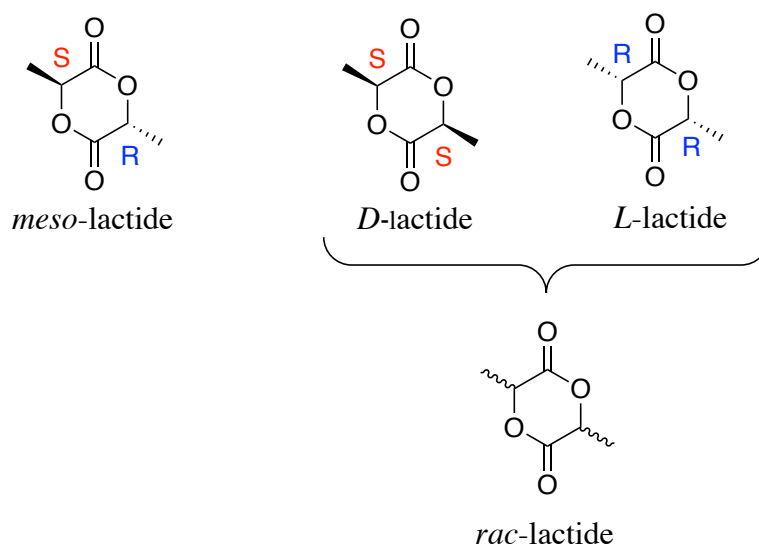


Figure 11: Lactide's diastereoisomers

ROP of *rac*- or *meso*-lactide with stereoselective catalysts able to promote the addition of monomers based on their stereochemistry has allowed the synthesis of stereoblock, heterotactic⁴¹ and syndiotactic⁴² PLAs. Atactic and heterotactic PLA are amorphous materials while isotactic PLA (PLLA, commercialized form of lactide, and PDLA) is a semi-crystalline thermoplastic. The obtention of isotactic PLA arises from either the polymerization of *L*-

lactide (or *D*-lactide) or by a stereoselective (*iso*-selective) polymerization with a *rac*-lactide catalyst.⁴³

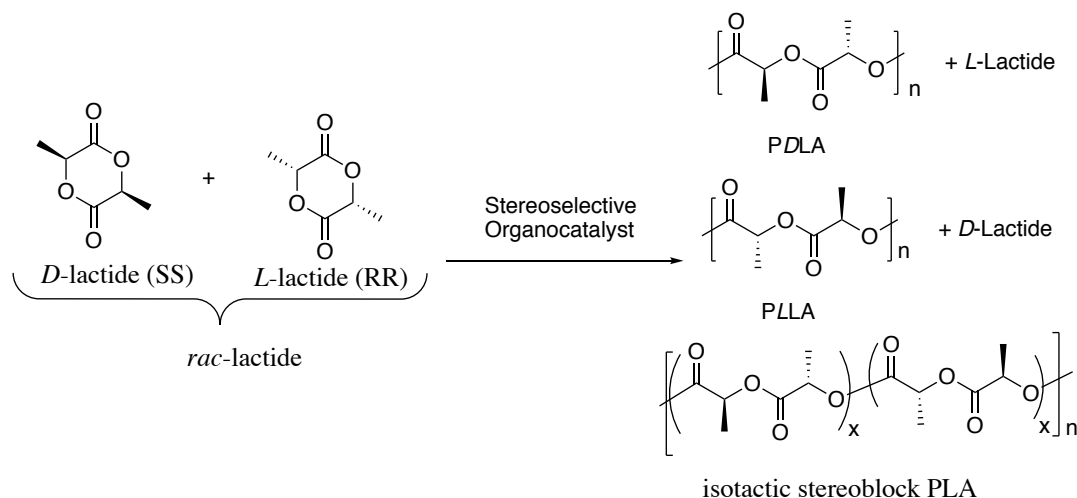


Figure 12: Stereoselective ROP of *rac*-lactide

II. 2. 2. Physical properties

The tacticity of resultant PLAs greatly affects their physical properties. Pure isotactic poly(*L*- or *D*-lactide) is a semi-crystalline material with a melting point of about 170 °C. The stereochemistry of the polymer has only little effect on glass transition temperature T_g , which is typically between 55 and 60 °C. However, atactic, as well as heterotactic PLA, which are amorphous, have a lower T_g because the more amorphous the polymer is, the lower the T_g is (**Table 2**). As for the syndiotactic PLA, it is a semi-crystalline polymer having a T_g of 34 °C and a melting temperature reported respectively by Coates (152 °C) and Okuda (119 °C).⁴⁴ In addition, the polyester having the highest melting point is the poly(lactic) acid stereocomplex (a racemic mixture of PLLA and PDLA).^{45,46,47}

Polymer	Tacticity	$T_g/^\circ\text{C}^{\text{a}}$	$T_m/^\circ\text{C}^{\text{b}}$
Poly(lactic acid) ^c	Atactic	45-55	---
Poly(lactic acid) ^c	Isotactic	55-60	170
Poly(lactic acid) ^d	Syndiotactic	34	151
Poly(lactic acid) ^d	Heterotactic	<45	---
Poly(lactic acid) ^d	Stereocomplex	65-72	220-230

^a Glass transition temperature. ^b Melting temperature. ^c Figures quoted from Jérôme et al.⁴⁸ ^d

Figures quoted from Tsuji.⁴⁹ ^e Figures quoted from Nozaki et al.⁵⁰

Table 2: Thermal properties of PLA

III. Water-soluble polymers

Amphiphilic polymers consist of hydrophobic and hydrophilic components. This kind of polymers is widely used in smart materials⁵¹ research according to their own structure design. They show high performance in various applications, for example, in advance delivery carriers, tissue engineering, surface modification, flocculant and many other applications throughout industry.

Water-soluble, hydrophilic polymers are very limited. The most common materials are: polyethylene glycol (PEG),⁵² polyacrylamide (PAM),⁵³ poly(vinyl alcohol) (PVA),⁵⁴ poly(vinyl pyrrolidone) (PVP),⁵⁵ and sodium polyacrylate (SP) (**Figure 13**).⁵⁶ Many of them are widely used as water-treatment agents or food additives and appear to be expelled in large volume into river water like wastewater.⁵⁷ Moreover, the biodegradation rate of these polymers in the natural environment isn't sufficiently fast and they are not bio-sourced polymers.

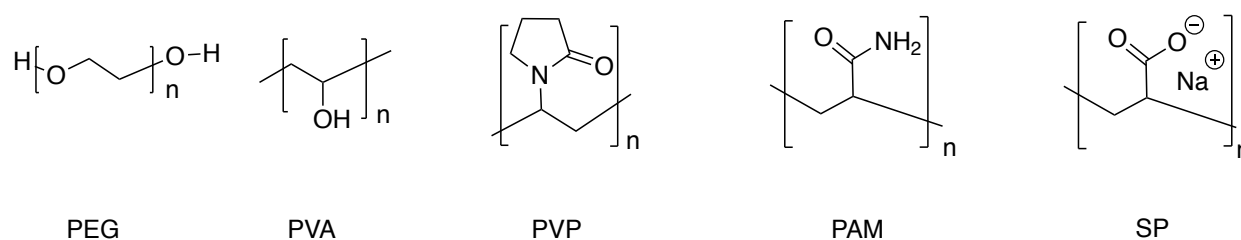


Figure 13: Structure of five principal water-soluble polymers

IV. Presentation of Ph.D. works

The present Ph.D. studies aims at the controlled production of biodegradable polyesters, including novel hydrophilic and amphiphilic materials based on biodegradable polyester backbones, using well-defined organometallic initiators (with, for the most part, earth-abundant and non-toxic metal sources) that operate under mild conditions. The results are divided into four different chapters described below:

- Chapter I: Controlled production of polylactide biomaterials under mild conditions using *N*-Heterocyclic carbene group 13 complexes

This chapter focuses on the synthesis of several *N*-heterocyclic carbene group XIII metal adducts and cationic species. These prepared compounds act as efficient ROP initiators of *rac*-lactide, allowing access to linear PLA under mild conditions.

- Chapter II: Synthesis of PEG-*co*-PLLA amphiphilic copolymers using different catalysts under mild conditions

In this chapter, the copolymerization of PEG polymer with *L*-lactide using different catalysts allows access to PEG-*co*-PLLA copolymers with controlled chain length. These copolymers exhibit an amphiphilic character due to the hydrophilic properties of the PEG segment.

- Chapter III: Synthesis of Poly(α -chloro- ϵ -caprolactone)

This chapter deals with ROP studies of a little explored monomer, α -chloro- ϵ -caprolactone, for the controlled production of poly(α -chloro- ϵ -caprolactone) whose functionalization may open the way to a wide range of amphiphilic polyesters.

- Chapter IV: Copolymers, diblocks and stereocomplex formation and their physicochemical properties

New copolymers, diblocks and stereocomplex were synthesized with PEG and PLA copolymeric segments in order to modify the properties of P(α -chloro- ϵ -caprolactone) homopolymer. The physicochemical properties of the resulting materials were studied by different methods: IFT, TGA and DSC.

IV. References

- [1]. W. D. Sauter, M. Taoufik, C. Boisson, *Polymers* **2017**, *9*, 1-13.
- [2]. A. L. Andrady, M. A. Neal, *Phil. Trans. R. Soc. B* **2009**, *364*, 1977-1984.
- [3]. S. Slomkowski, S. Penczek, A. Duda, *Polym. Adv. Technol.* **2014**, *25*, 436-447.
- [4]. (a) S. Mecking, *Angew. Chem. Int. Ed.* **2004**, *43*, 1078-1085. (b) A. Andrady, *Polym. Rev.* **1994**, *34*, 25-76.
- [5]. (a) D. K. A. Barnes, F. Galgani, R. C. Thompson, M. Barlaz, *Phil. Trans. R. Soc. B* **2009**, *364*, 1985-1998. (b) Y. Mato, T. Isobe, H. Takada, H. Kanchiro, C. Ohtake, T. Kaminuma, *Environ. Sci. Technol.* **2001**, *35*, 318-324. (c) J. G. B. Derraik, *Mar. Pollut. Bull.* **2002**, *44*, 842-852.
- [6]. A. Dormer, D. P. Finn, P. Ward, J. Cullen, *J. Clean. Prod.* **2013**, *51*, 133-141.
- [7]. S. Rebouillat, F. Pla, *J. Biomater. Nanobiotechnol* **2016**, *7*, 167-213.
- [8]. R. A. Gross, B. Kalra, *SCIENCE* **2002**, *297*, 803-807.
- [9]. A. Steinbüchel, *Curr Opin Biotechnol.* **2005**, *16*, 607-613.
- [10]. <http://www.oecd.ilibrary.org/environment/oecd-guidelines-for-the-testing-of-chemicals-section-3-degradation-and-accumulation-2074577x> (as on 22 decembre 2014).
- [11]. D. D. Katti, S. Lakshmi, R. Langer, C. T. Laurencin. *Adv Drug Deliv Rev* **2002**, *54*, 933-961.
- [12]. V. V. Myasoedova, *Russ. J. Gen. Chem.* **2017**, *87*, 1357-1363.
- [13]. L. Avérous, P. J. Halley, *Biofuel Bioprod Biorefin* **2009**, *3*, 329-343.
- [14]. D. Byrom, *Trends Biotechnol* **1987**, *5*, 246-250.
- [15]. K. Sudesh, T. Iwata, *CLEAN – Soil, Air, Water* **2008**, *36*, 433-442.
- [16]. M. A. Woodruff, D. W. Hutmacher, *Prog. Polym. Sci.* **2010**, *35*, 1217-1256.
- [17]. Y. Tokiwa, B. P. Calabia, C. U. Ugwu, S. Aiba, *Int. J. Mol. Sci.* **2009**, *10*, 3722-3742.
- [18]. R. -J. Mueller, *Process. Biochem* **2006**, *41*, 2124-2128.
- [19]. J. Rydz, W. Sikorska, M. Kyulavska, D. Christova, *Int. J. Mol. Sci.* **2015**, *16*, 564-596.
- [20]. T. Iwata, Y. Doi, *Macromolecules* **1998**, *31*, 2461-2467.
- [21]. H. Tsuji, S. Miyauchi, *Polym. Degrad. Stab.* **2001**, *71*, 415-424.
- [22]. Y. Tokiwa, T. Suzuki, *J. Appl. Polym. Sci.* **1981**, *26*, 441-448.
- [23]. W. H. Carothers, *Chem. Rev* **1931**, *8*, 353-426.
- [24]. A. Kumar, B. Kalra, R. A. Gross, *Chem. Rev.* **2001**, *101*, 2097-2124.

-
- [25]. *Handbook of Ring Opening Polymerization*, ED. P. Dubois, O. Coulembier, J. -M. Raquez, Wiley-VCH, Weinheim, **2009**.
- [26]. J. Lunt, *J. Polym. Degrad. Stab* **1998**, *59*, 145-152.
- [27]. NatureWorks, www.natureworksllc.com
- [28]. C. Lee, S. Hong, *Mod. Chem. appl.* **2014**, *2*, 1-5.
- [29]. O. Dechy-Cabaret, B. Martin-Vaca, D. Bourissou, *Chem. Rev* **2004**, *104*, 6147-6176.
- [30]. Y. Sarazin, M. Schormann, M. Bochmann, *Organometallics* **2004**, *23*, 3296-3302.
- [31]. N. E. Kamber, W. Jeong, R. M. Waymouth, R. C. Pratt, B. G. G. Lohmeijer, J. L. Hedrick, *Chem. Rev* **2007**, *107*, 5813-5840.
- [32]. F. Hild, L. Brelot, S. Dagorne, *Organometallics* **2011**, *30*, 5457-5462.
- [33]. K. Nakano, N. Kosaka, T. Hiyama, K. Nozaki, *Dalton Trans.* **2003**, 4039-4050.
- [34]. W. Dittrich, R. C. Schulz, *Angew. Makromol. Chem.* **1971**, *15*, 109-126.
- [35]. H. R. Kricheldorf, M. Berl, M. Scharnagl, *Macromolecules*, **1991**, *21*, 286-293.
- [36]. P. Dubois, C. Jacobs, R. Jérôme, P. teyssié. *Macromolecules*, **1991**, *24*, 2266-2270.
- [37]. J. Kleine, H. -H Kleine, *Makromol. Chem.* **1959**, *30*, 23-38.
- [38]. S. Penczek, A. Duda, R. Szymanski, *Macromol. Symp.* **1998**, *132*, 441-449.
- [39]. M. H. Chisholm, E. E. Delbridge, *New J. Chem.* **2003**, *27*, 8, 1167-1176.
- [40]. A. P. Dove, *Chem. Commun.* **2008**, *48*, 6446-6470.
- [41]. M. Cheng, A. B. Attygalle, E. B. Lobkovsky, G. W. Coates, *J. Am. Chem. Soc.* **1999**, *121*, 11583-11584.
- [42]. T. M. Ovitt, G. W. Coates, *J. Am. Chem. Soc.* **1999**, *121*, 4072-4073.
- [43]. G. W. C. T. M. Ovitt, *J. Am. Chem. Soc.* **2002**, *124*, 1316-1326.
- [44]. J. -C. Buffet, A. Kapelski, J. Okuda, *Macromolecules* **2010**, *43*, 10201-10203.
- [45]. J. Shao, J. Sun, X. Bian, Y. Cui, Y. Zhou, G. Li, X. Chen, *Macromolecules* **2013**, *46*, 6963-6971.
- [46]. J. Zhang, H. Sato, H. Tsuji, I. Noda, Y. Ozaki, *Macromolecules* **2005**, *38*, 1822-1828.
- [47]. A. C. Silvino, P. S. Corrêa, M. L. Dias, *J. Appl. Polym. Sci.* **2014**, *131*, 40771/1-40771/2.
- [48]. X. D. Lou, C. Detrembleur, R. Jérôme, *Macromol. Rapid Commun.* **2003**, *24*, 161-172.
- [49]. H. Tsuji, *Macromol. Biosci.* **2005**, *5*, 569-596.
- [50]. K. Nakano, N. Kosaka, T. Hiyama, K. Nozaki, *Dalton Trans.* **2003**, 4039-4050.
- [51]. H. N. Gray, D. E. Bergbreiter, *Environ Health Perspect.* **1997**, *105 Suppl 1*, 55-63.
- [52]. J. Israelachvili, *Proc Nati Acad Sci USA* **1997**, *94*, 8378-8379.

-
- [53]. B. Xiong, R. D. Loss, D. Shields, T. Pawlik, R. Hochreiter, A. L. Zydney, M. Kumar, *npj Clean Water* **2018**, *1*, 17, 1-9.
- [54]. A. Aina, A. Morris, M. Gupta, N. Billa, N. Madhavani, R. Sharma, S. Doughty, V. Shah, Y. Boukari, *JPB*, **2014**, *2*, 1-6.
- [55]. F. Haaf, A. Sanner, F. Straub, *Polymer Journal* **1985**, *17*, 143-152.
- [56]. A. Pradesch, *IJSRST*, **2017**, *3*, 568-576.
- [57]. S. Naidoo, A. O. Olaniran, *Int. J. Environ. Res. Public Health* **2013**, *11*, 249-270.

Chapter I

Controlled production of polylactide biomaterials under mild conditions using *N*-Heterocyclic carbene group 13 complexes

I. Introduction

In the early 1960's, Wanzlick^{1,2} and Öfele³ first investigated the reactivity and stability of *N*-heterocyclic carbenes (NHCs), and then shortly after reported their application as ligands for metal complexes. However, it was only after the isolation by Arduengo *et al.*^{4,5} of the first free NHC in 1991 that the study of this new class of ligands took off. This is explained by the ability of these ligands to form strong bonds with many transition and main group metal centers in low oxidation states as well as high oxidation states,⁶ leading to metal-carbene complexes with a remarkable stability.⁷ These ligands have found multiple applications in some of the most common catalytic transformations due to the stability of NHC-supported metal catalysts.^{8,9} Also, when M is an electropositive and high oxidation state metal center, the polar character of the NHC–M bond may also be a source of reactivity for the activation of polar substrates. In this area, we became interested in the coordination chemistry and associated reactivity of group 13 metal NHC–MMe₃ [M = Al(III), Ga(III), In(III)] adducts for the catalytic ROP of *rac*-lactide.

II. General characteristics of NHCs

NHCs are defined as neutral heterocyclic compounds containing a divalent carbon atom¹⁰ with at least one nitrogen atom in the ring structure.¹¹ Within these criteria fall several classes of carbene compounds with various substitution patterns, featuring ring saturation¹², differing ring sizes^{13,14} and degrees of heteroatom stabilization¹⁵ (**Figure 1**).

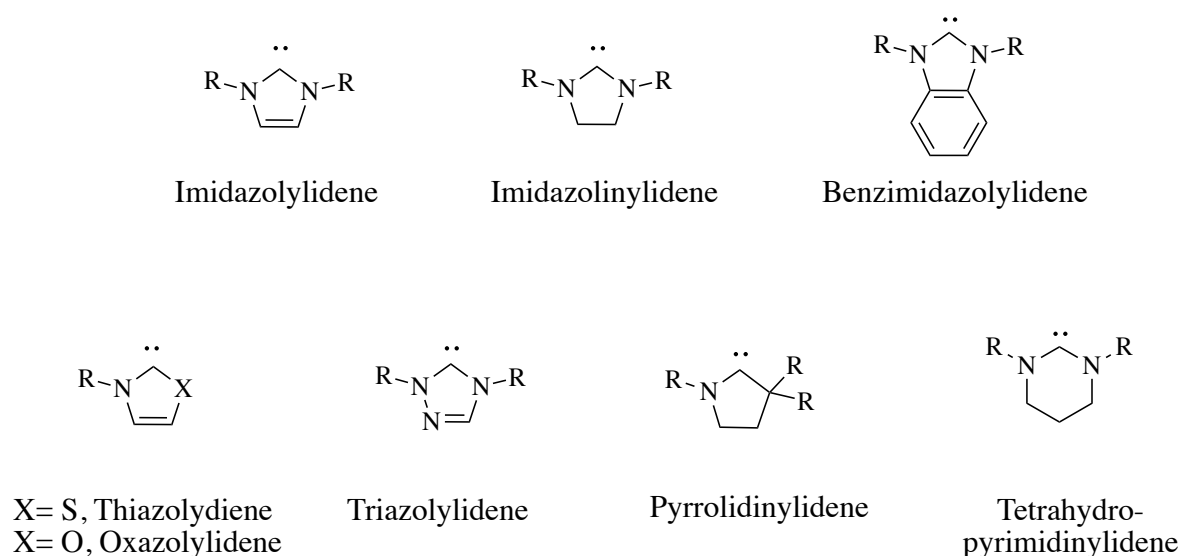


Figure 1: Families of NHCs

Electronic and steric properties of these ligands can easily be modified.¹⁶ Variations are possible on R substituents bonded to nitrogen atoms. A sulfur¹⁷ or oxygen atom¹⁸ can also replace one nitrogen atom in the heterocycle, allowing modification of the electronic properties of NHCs. Finally, heterocyclic carbenes with four,^{19,20} five,²¹ six,²² or seven²³ membered-rings, as well as acyclic diaminocarbenes, have been described.^{24,25,26}

II. 1. Electronic properties

NHCs are electron-rich and strong neutral σ -donor ligands.^{27,28} These different properties provided by both adjacent nitrogens to the carbene. Indeed, the adjacent σ -electron-withdrawing and π -electron-donating nitrogen atoms stabilize this structure by lowering the energy of the occupied σ -orbital and mesomerically by donating electron density in the unoccupied p -orbital at the C² carbon (**Figure 2**).

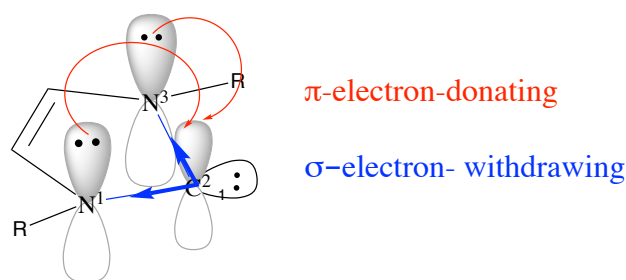


Figure 2: Ground-state electronic structure of imidazol-2-ylidenes

The ground-state electronic structure of NHCs provides a framework for understanding their reactivity.²⁹ In contrast to the typical electrophilicity of most transient carbenes, the lone pair located in the plane of the heterocyclic ring renders these compounds, good nucleophilic agents.^{30,31} NHCs form significantly stronger bonds than phosphines^{32,33,34} with the majority of metals owing to the strong σ -donation from the NHC to the metal center and the weak π -backbonding from the metal center to the NHC (**Figure 3**).^{35,36}

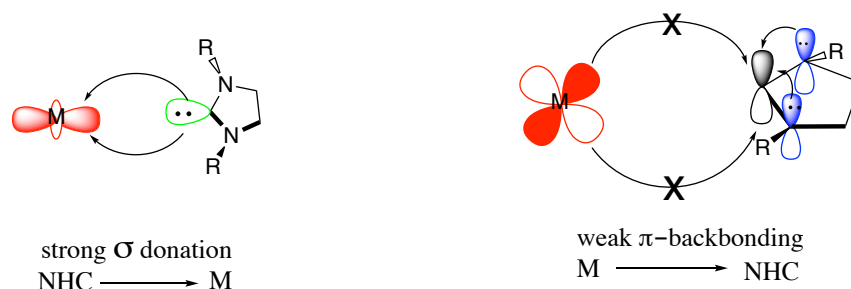


Figure 3: Orbital interactions representation in a free NHC and coordination

II. 2. Steric properties

From a geometric point of view, steric congestion around the metal center is essentially defined by the nature of the substituents on both nitrogen atoms. The heterocyclic plane containing the carbene is indeed not congested and the possible substituents in the C₄ or C₅ positions are distant from the metal coordination sphere. The size and substitution pattern of the nitrogen heterocycle can also have a large effect on the properties of the carbene.

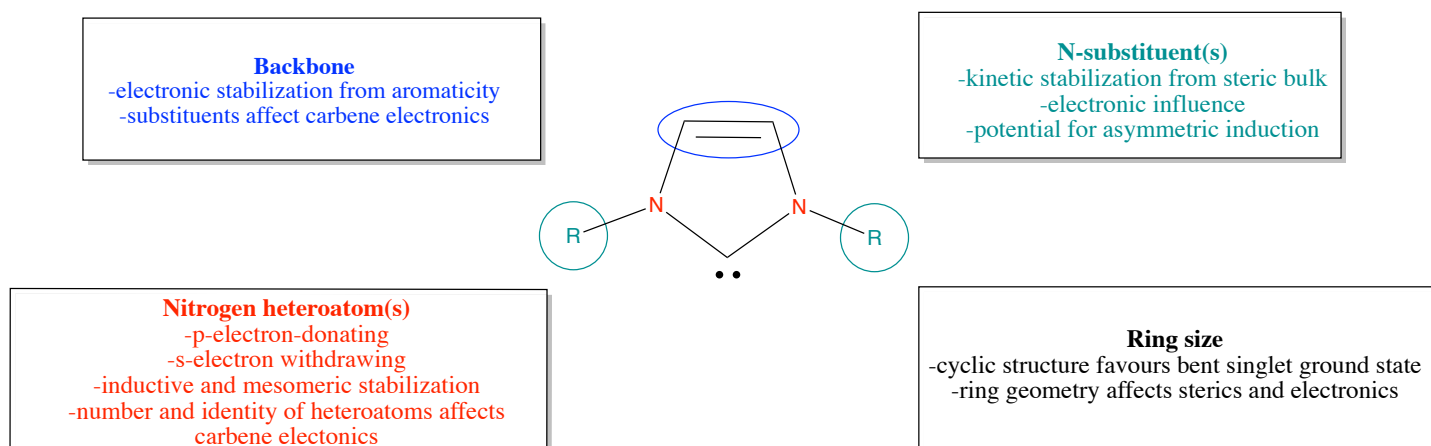


Figure 4: General structural features detailing the effects of the ring size, nitrogen heteroatoms, the ring backbone, and nitrogen-substituents

III. Metallic adduct synthesis supported by NHCs ligands

There are several methods for the synthesis of carbenic adducts (**Figure 5**).³⁷

- I. The best method to synthesize NHC complexes of oxophilic metals (*e.g.* group 13 metals) is the coordination of a free and stable carbene to the metal.
- II. Carbenes can be generated *in situ* with a metal, by introducing a base with which it will react.
- III. With a weak external base, carbenes can be generated *in situ* then reacted with the desired metallic precursor

IV. Another method is the transmetallation from silver complexes [AgX(NHC)], which are often formed *in situ* and then immediately reacted with the desired metallic precursor.³⁸

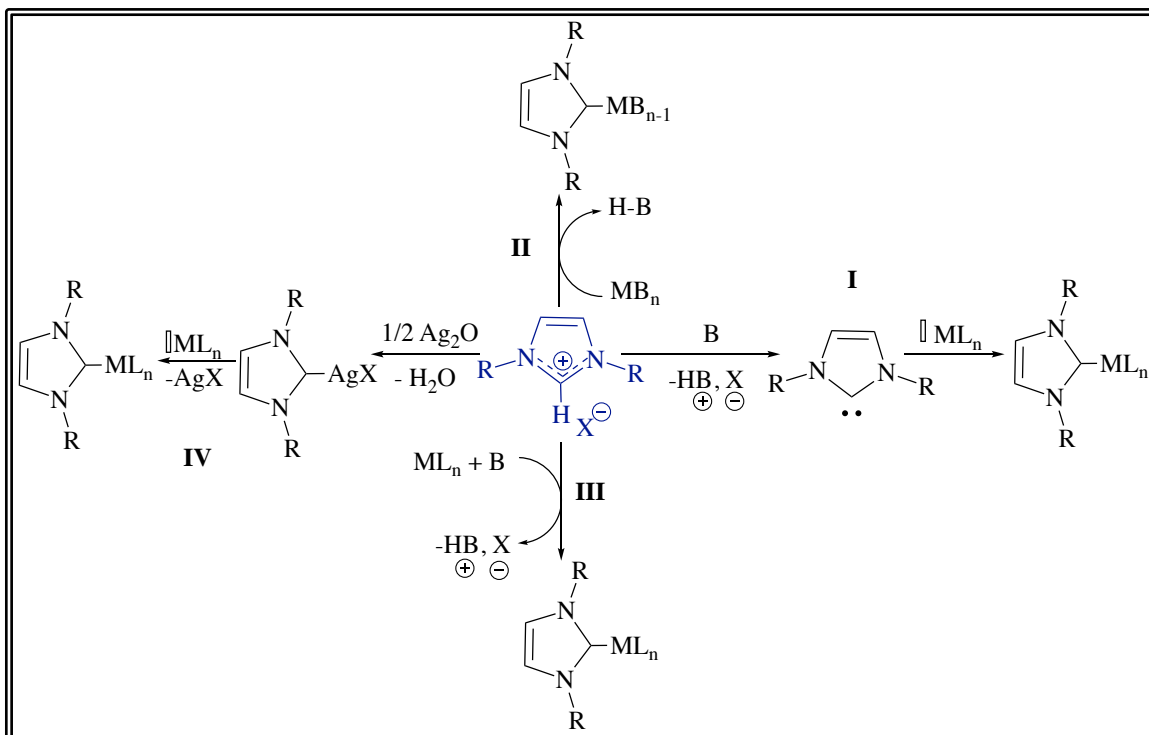


Figure 5: Different synthetic pathways for NHC-supported metal species

IV. Properties and applications of group 13 metals

The five elements of group 13 column from top to bottom are:

- Boron (B),³⁹
- Aluminium (Al),⁴⁰
- Gallium (Ga) and Indium (In),⁴¹
- Thallium (Tl).⁴²

5	B	10.81	Boron
13	Al	26.982	Aluminium
31	Ga	69.723	Gallium
49	In	114.82	Indium
81	Tl	204.38	Thallium

Figure 6: Boron to Thallium group 13 elements

Boron does not have the characteristic properties of a metal,⁴³ and thallium is highly toxic.⁴⁴ As a consequence, none of these elements will be studied or used in synthesis. Group 13 metals are relatively abundant, the aluminium in particular, which is the third most abundant element in the earth's crust, after oxygen and silicon.⁴⁵ Thus, aluminium metal is relatively inexpensive. On the contrary, gallium and indium are less abundant and have a considerably higher cost than aluminium (**Table 1**). Over the past ten years, Ga(III) and notably In(III) precursors have attracted a high interest in the ROP catalysis of cyclic esters such as lactide and may nowadays be considered as potentially efficient ROP initiators of cyclic esters. Despite the fact that Ga and In derivatives are more expensive than Al, they have very attractive features, including their biocompatible metal centers and their better stability than organoaluminium species in polar conditions.⁴⁶

	Aluminium	Gallium	Indium
Abundance (ppb)	10.2 x 10 ⁷	1.8 x 10 ⁴	2.5 x 10 ²
Minerals/Source	Bauxite	By-product during refinement of zinc and aluminium	By-product during refinement of zinc and lead
World production (Tonnes/year)	4 x 10 ⁷	1 x 10 ²	4.5 x 10 ²
Price ⁴⁷ (Purity)	140 €/Kg (99.9%)	700 €/50 g (99.99%)	230 €/50 g (99.99%)
Market price (June 2019)	1.75 \$/Kg	157.5 \$/Kg	162.5 \$/Kg

Table 1: Natural resources of group 13 metals⁴⁸

Group 13 metals have an electronic configuration $ns^2 np^1$ and usual oxidation state of (+III), so are high-oxidation-state metal centers. They are electropositive metals, with oxophilic character, very strong Lewis acids and their derivatives are well-established in organometallic chemistry.^{49,50} Notably, their Lewis acidic nature allows the coordination of various saturated or unsaturated organic substrates such as NHCs.

V. Results on the synthesis of new adducts

V. 1. Sterically bulky NHC group 13 adducts

The super-bulky IPr* NHC, first reported by Marko in 2010,⁵¹ is referred as “an exceptional bulky NHC with some flexible sterics”. This robust species is illustrated (**Figure 7**) and was considered as a good candidate for our studies because such a sterically hindered NHC may enhance the reactivity of the NHC–M bond (thanks to steric frustration) and thus favor monomer activation.⁵²

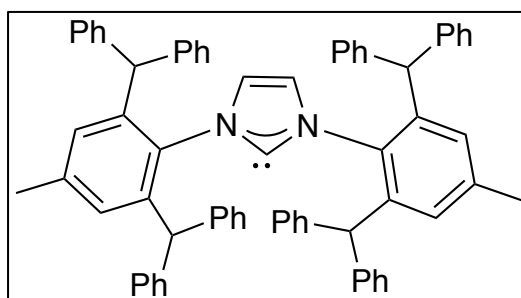


Figure 7: Structure of IPr* NHC

A number of IPr*-supported complexes of late transition metals are known, however, the coordination of IPr* to oxophilic metal centers is thus far unreported.⁵³ Different routes are available to prepare the imidazolium precursor salt. One of them is the one-pot synthesis starting from glyoxal, a primary amine, and formaldehyde.⁵⁴ In acidic conditions, the reaction proceeds through a coupling between amine and glyoxal and forms the corresponding Schiff base. Condensation with formaldehyde leads to the imidazolium salt. This reaction can be split into two distinct steps. Consequently, isolation of the diimine⁵⁵ allows the synthesis of symmetrically *N,N'*-substituted imidazolium salts with various aryl- or alkyl-groups for instance: 1,3-bis(cyclohexyl)imidazolium (ICy•HX) , 1,3-bis(adamantyl)imidazolium (IAd•HX).

IPr* carbene was prepared in four steps according to a literature procedure³⁰ (**Figure 8**). Then IPr* metal adducts were synthesized from AlMe₃, GaMe₃ and InMe₃ and their reactivity was studied.⁵⁶

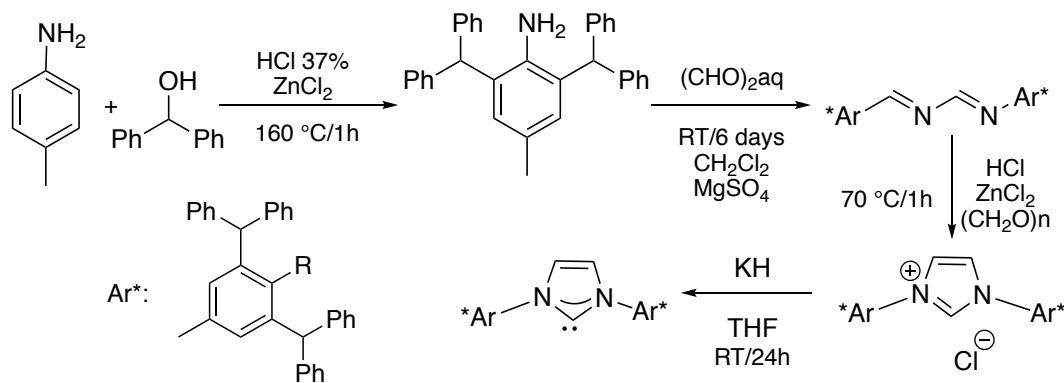
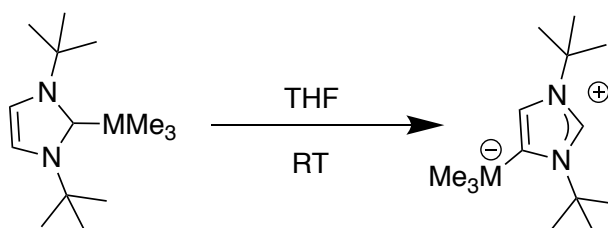


Figure 8: Preparation of IPr* carbene

The reaction between IPr* free carbene with a stoichiometric amount of MMe_3 (**1**, $M= Al$; **2**, $M= Ga$; **3**, $M= In$) in toluene during two hours led to the quantitative formation of the corresponding adducts. The NMR data are consistent with the coordination of IPr* to the $M(III)$ centers. Particularly the ^{13}C NMR $C_{carbene}$ chemical shifts (δ 179.0, 183.4 and 185.8 ppm for **1**, **2** and **3** respectively) lie in the expected range for NHC-Al, NHC-Ga, and NHC-In species and are considerably upfield shifted in comparison to the free IPr* (δ 220.0 ppm), in line with NHC coordination to the $M(III)$ center. Surprisingly, given the steric properties of IPr*, the three adducts are very stable species in solution at room temperature and do not coordinate to Lewis bases such as THF. A 1H NMR monitoring experiment for each adduct showed that these species are thermally robust, and retain their integrity upon extended heating (C_6D_6 , 2 days, 80 °C). The latter observation contrasts with the instability of the (tBu) MMe_3 counterparts which isomerize in minutes in THF at room temperature (**Figure 9**).^{57,58}

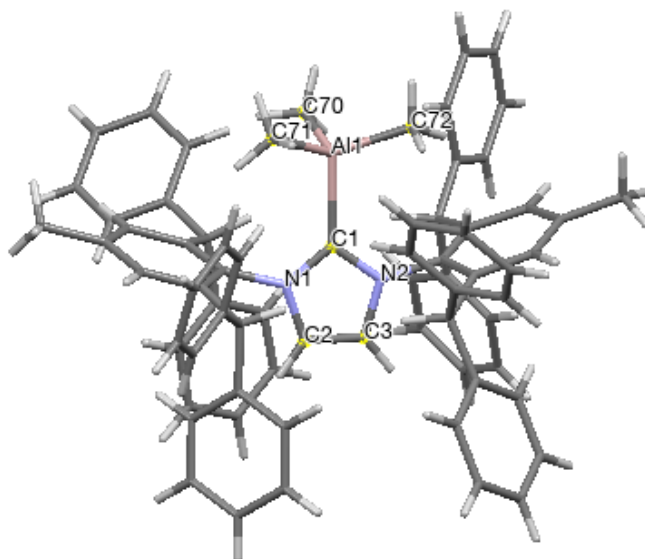


($M= Al, Ga, \text{ and } In$)

Figure 9: Isomerization of tBu NHC carbene adducts of group 13 complexes

The X-ray crystallographic studies of the solid-state molecular structures of **1** and **3** confirmed the effective coordination of IPr* carbene to AlMe₃ for **1** (**Figure 10**) and to InMe₃ for **3** (**Figure 11**). Both resulted in a four-coordinate M(III) with (M= Al, In) with a distorted tetrahedral geometry and the M(III) centers residing in the NHC heterocyclic ring plane.

(a)



(b)

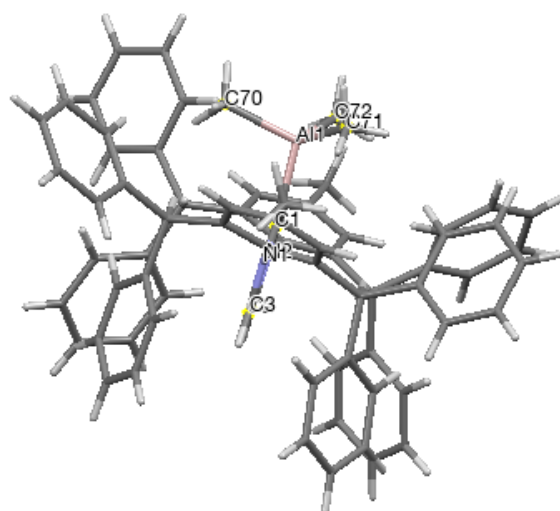
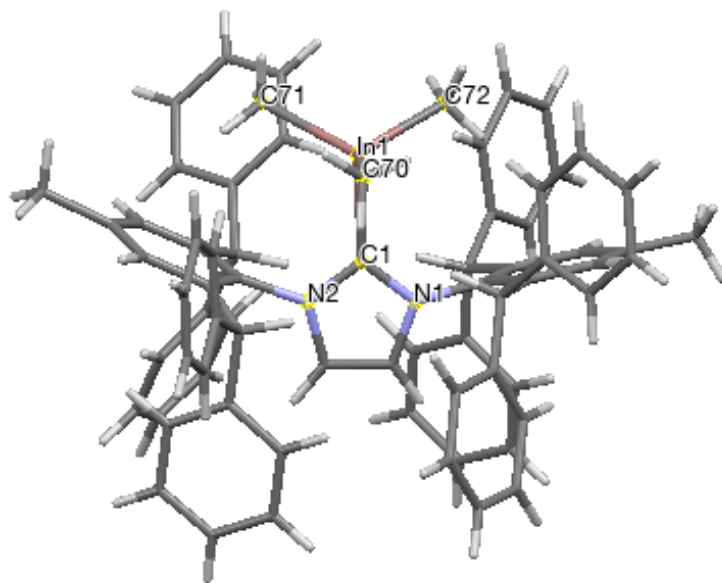


Figure 10: Molecular structure of adduct (IPr*)AlMe₃ (1). Hydrogen atoms are omitted for clarity. (a) Front view. (b) Side view. Selected bond distances (Å): Al(1)–C(1) = 2.129(2), C(1)–N(1) = 1.366(3), C(1)–N(2) = 1.358(6), C(2)–C(3) = 1.335(6).

(a)



(b)

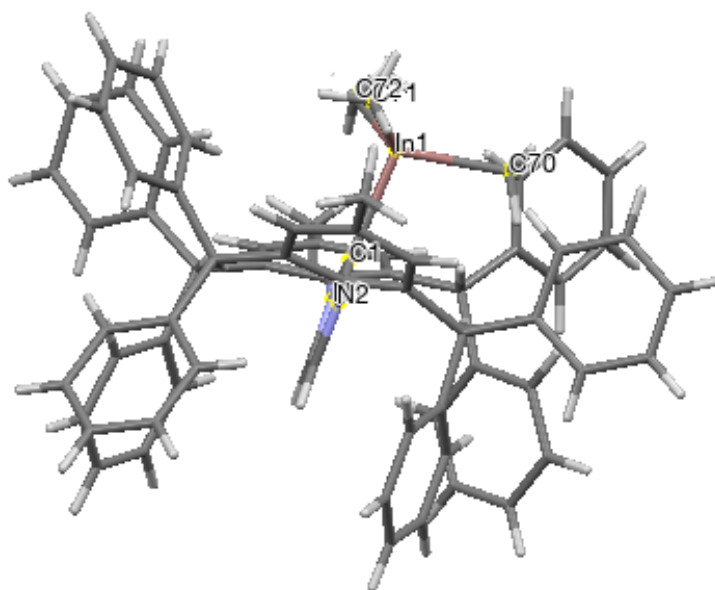


Figure 11: Molecular structure of adduct (IPr*)InMe₃ (3). Hydrogen atoms are omitted for clarity. (a) Front view. (b) Side view. Selected bond distances (Å): In(1)–C(1) = 2.330(5), C(1)–N(1) = 1.368(5), C(1)–N(2) = 1.355(6), C(2)–C(3) = 1.335(6).

Concerning the (IPr*)AlMe₃ adduct **1**, the Al–C_{carbene} bond (2.129(2) Å) is slightly longer than those in (IMes)InMe₃ and (IPr)InMe₃ (2.101(3) and 2.105(1) Å, respectively: IMes = 1,3-bis(2,4,6-trimethylphenyl)-1,3-dihydro-imidazol-2-ylidene; IPr = 1,3-bis{2,6-bis(1-methylethyl)phenyl}-1,3-dihydro-imidazol-2-ylidene), likely reflecting greater steric hindrance between the NHC and AlMe₃ in **1**.

Concerning the (IPr*)InMe₃ adduct, the In–C_{carbene} bond (2.330(5) Å) is also slightly longer than those in (IMes)InMe₃ and (IPr)InMe₃ (2.292(6) and 2.309(2) Å). These data reflect greater steric hindrance between the NHC and AlMe₃ in **1** and InMe₃ in **3**.^{59,60} However, the shortest contacts between IPr* and AlMe₃ (H···H = 2.334 Å and C···H = 2.7724 Å) and between IPr* and InMe₃ (H···H = 2.257 Å and C···H = 2.747 Å) remain close to the sum of the van der Waals (vdW) radii of the corresponding atoms, which is consistent with no severe steric congestion in **1** and **3** and matches with the observed stability of these adducts in solution.

As sterically bulky Lewis adducts, the reactivity of these NHC adducts with H₂ was studied. In line with their stability and robustness in solution, IPr* adducts were found to not react with H₂ even under prolonged heating (80 °C, C₆D₆, 48 h). Thus these adducts don't lead to FLPs.

VI. Synthesis of NHC-supported group 13 metal alkyl cations

Different NHC adducts were synthesized by reaction of the appropriate precursor MMe₃ (M= Al, Ga, In) with an equimolar amount of IMes free carbene in cold toluene (**Figure 12**).

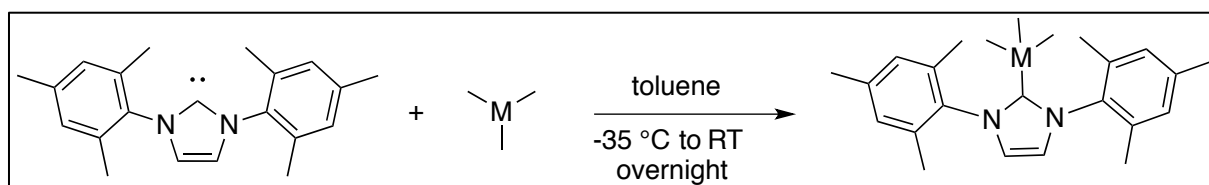


Figure 12: Adducts synthesis

Neutral IMesAlMe₃ precursor adduct was ionized via a methide abstraction at the Al(III) center with one equivalent of B(C₆F₅)₃ in the presence of two equivalents of Et₂O as an external Lewis base, leading to the quantitative formation of [IMesAlMe₂(OEt₂)]⁺ cation and [CH₃B(C₆F₅)₃]⁻ salt (**Figure 13, Figure 14**).⁶¹ The advantage of developing cationic complexes

stabilized by enveloping ligands is to increase the stability of the metal precursors while maintaining a good reactivity. Indeed, the increase of the Lewis acidity of the metal due to its cationic character allows a better activation of these polar substrates. The NMR data (**Figure 15**) agree with dissociated cation/anion entities in solution under the studied conditions (CD_2Cl_2 , RT) and with the effective coordination of Et_2O to the cationic aluminium center. The AlMe_2^+ singlet resonance ($\delta = -1.13$ ppm) is significantly downfield shifted relative to the AlMe_3 signal in the precursor ($\delta = -1.55$ ppm), which is consistent with a more-electron deficient metal center. The ^1H NMR signals for Et_2O ($\delta = 1.14$ and 3.75 ppm) are downfield shifted compared to those of free Et_2O , in agreement with an effective Et_2O coordination to the Al cationic center.

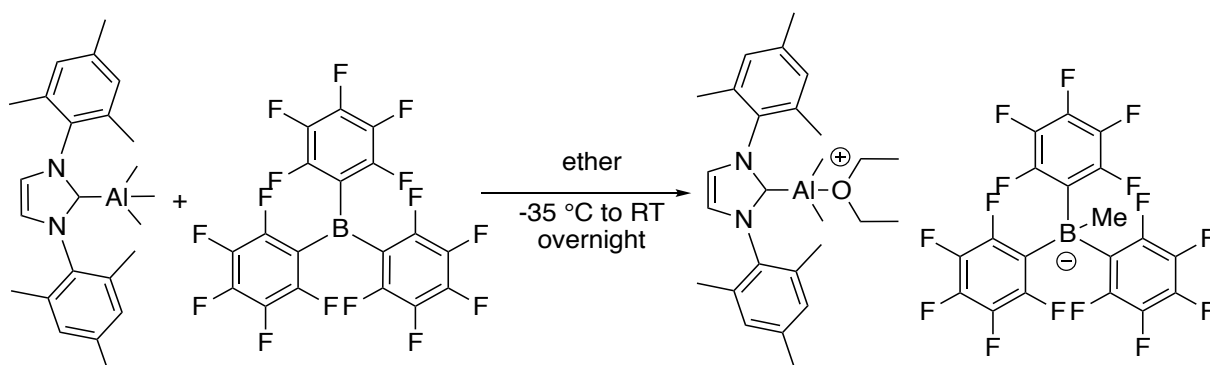
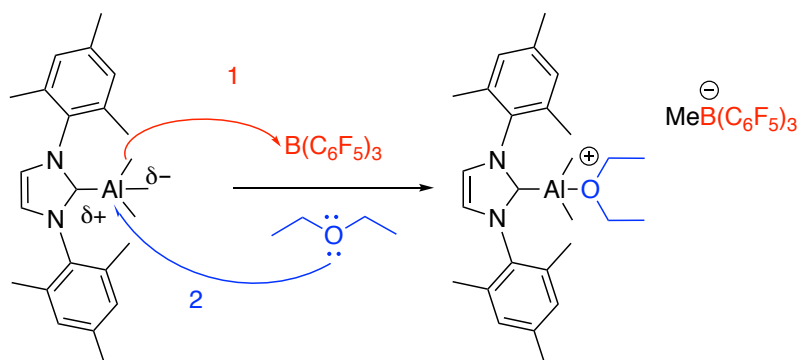


Figure 13: Ionization of IMesAlMe₃ adduct



1: Methide abstraction with $\text{B}(\text{C}_6\text{F}_5)_3$ Lewis acid. 2: Coordination of the external Lewis base Et_2O on the aluminium center.

Figure 14: Mechanism of aluminium cation formation

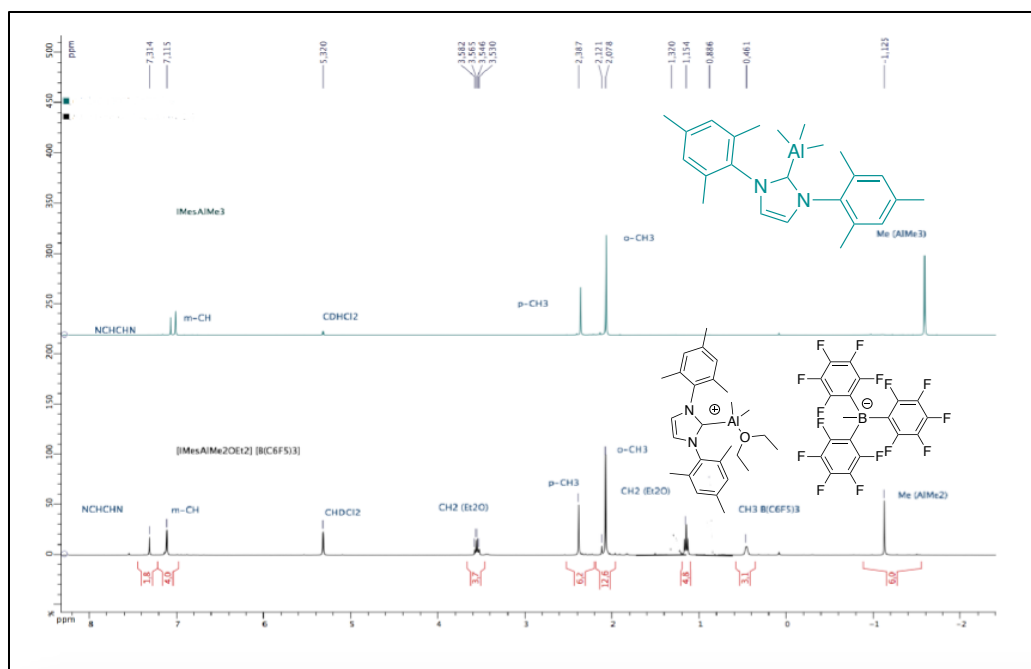


Figure 15: ^1H NMR (CD_2Cl_2 , 400 MHz): Comparison of the ^1H NMR spectrum of IMesAlMe_3 with the ^1H NMR spectrum $[\text{IMesAlMe}_2(\text{OEt}_2)][\text{MeB}(\text{C}_6\text{F}_5)_3]$

VII. ROP of *rac*-lactide with the IMesMMe_3 complexes.

The polar metal-NHC bond in the synthesized complexes may potentially be reactive in the presence of lactide, with the MMe_3 fragment acting as Lewis acid for monomer activation and the NHC moiety as a nucleophile able to ring-open the lactide monomer. Following propagation steps (successive insertions into the formed M-O alkoxide bond) may allow PLA chain growth from the metal center.

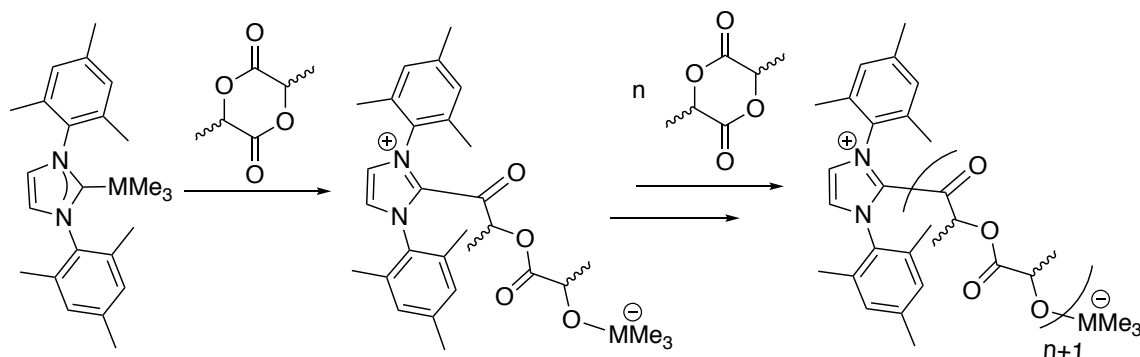


Figure 16: Proposed mechanism for the ROP of *rac*-lactide by the group 13 metal NHC adducts of the type IMesMMe_3 reported above.

All synthesized complexes were found to induce the ring-opening polymerization of *rac*-lactide. The polymerization results are compiled in **Table 2** for various conditions (dichloromethane, 25 °C, 0.33-83 h, with/without BnOH).

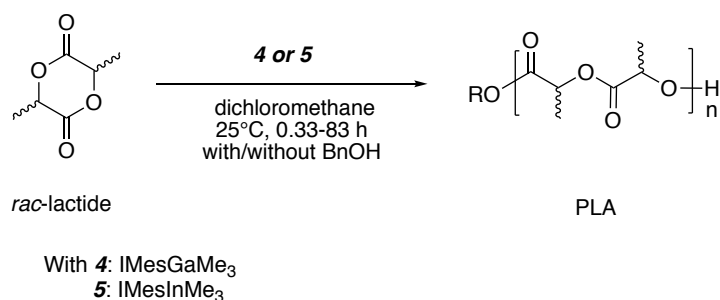


Figure 17: ROP of *rac*-lactide initiated by species **4 (IMesGaMe₃) or **5** (IMesInMe₃)**

Entry	Catalyst	<i>Rac</i> -LA ^a	BnOH ^a	Time ^b (h)	Conversion ^c (%)	M _n theo ^d (g/mol)	M _n GPC ^e (g/mol)	PDI
1	4	300	5	0.33	8	692	679	1.01
2	4	300	5	0.66	23	1989	2114	1.01
3	4	300	5	5.66	96	8302	7431	1.2
4	4	300	5	8.33	100	8648	9085	1.15
5	4	300	/	1	1	433	440	1.02
6	4	300	/	1.5	2	865	991	1.01
7	4	300	/	13.3	38	16430	16444	1.06
8	4	300	/	14.4	41	17727	17657	1.05
9	4	300	/	16.16	45	19457	19611	1.01
10	4	300	/	83	100	43238	43580	1.06
11	5	300	5	0.033	20	1729	1677	1.4
12	5	300	5	0.116	63	5448	6070	1.3
13	5	300	5	0.183	82	7091	7359	1.2
14	5	300	5	0.5	100	8647	8306	1.2
15	5	300	/	0.8	16	6918	2349	1.1
16	5	300	/	1.8	39	16863	5606	1.1
17	5	300	/	11.6	100	43275	23600	2.54

Polymerization conditions: [Monomer]₀ = 1 M. DCM, RT.

^a Equiv. versus initiator. ^b Reaction time. ^c Monomer conversion. ^d Calculated using M_n theo = number of equiv. of *rac*-LA × M_{rac-lactide} × conv.; in the presence of BnOH, M_n theo = [*rac*-LA]₀ × M_{rac-lactide} × conv.; without BnOH. ^e Measured by GPC in THF (30 °C) using PS standards and corrected by applying the appropriate correcting factor (0.58).

Table 2: Results of the ROP of *rac*-lactide initiated by all species **4 and **5****

VII. 1. ROP of lactide with IMesGaMe₃ (catalyst 4)

The IMes-supported GaMe₃ (**4**) was found to mediate the ROP of *rac*-lactide (300 equiv.) at room temperature in presence of BnOH (5 equiv.) as transfer agent (**entry 4, Table 2**) to produce atactic PLA with full conversion after 8.3 hours (as deduced from ¹H NMR spectrum and GPC data). The GPC trace of PLA derived from the ROP by species **4** features a monomodal trace, which agrees with a well-defined monodisperse (PDI: 1.15) polymer, (**Figure 18**).

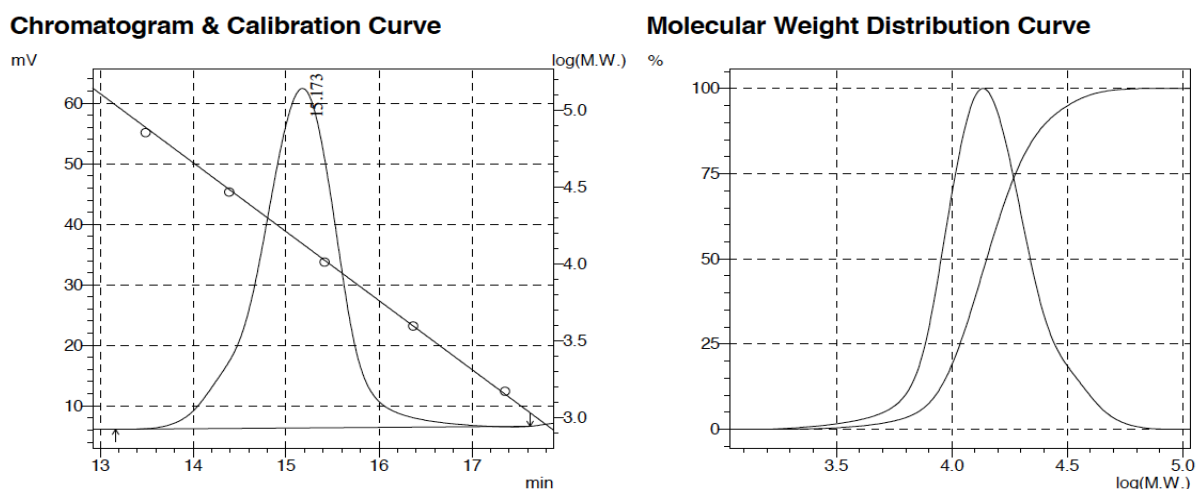


Figure 18: SEC traces of isolated PLA prepared via ROP of *rac*-lactide initiated by the *catalyst 4*/BnOH system. (Conditions: [*rac*-lactide]₀ = 1 M, 300 equiv. of *rac*-lactide, 5 equiv. of BnOH, 8.3 h, DCM, RT, 100% conv.).

Kinetic studies carried out for the ROP of *rac*-lactide by a **4**/BnOH system are consistent with a ROP proceeding in a controlled manner. The first order kinetic in *rac*-lactide ($K_{app} = 9.2 \times 10^{-3} \text{ min}^{-1}$) agrees with a controlled ROP process (**Figure 19**). Also, a linear correlation between the experimental M_n values of the formed PLA and the lactide monomer conversion during the polymerization reaction is observed, demonstrating that the polymer chain grows linearly with monomer conversion (**Figure 20**).

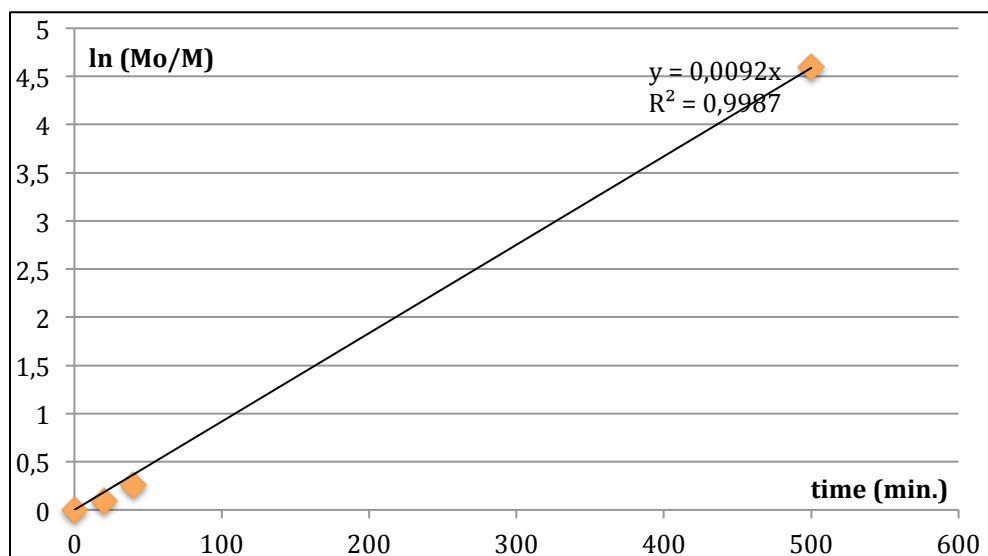


Figure 19: Plot of $\ln(Mo/M)$ vs. time of the ROP of *rac*-lactide using the gallium *catalyst 4*/BnOH system with BnOH as ROP initiator. (Conditions: $[rac\text{-lactide}]_0 = 1$ M, 300 equiv. *rac*-lactide, 5 equiv. BnOH, DCM, RT, 8.3 h, total conv.).

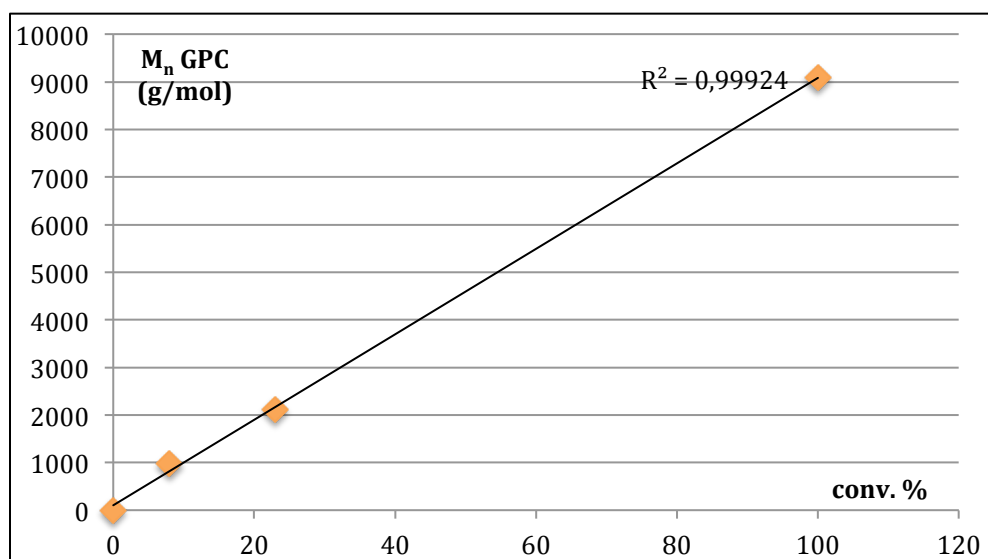


Figure 20: Plot of M_n as a function of the conv. in the ROP of *rac*-lactide using the *catalyst 4*/BnOH system. (Conditions: $[rac\text{-lactide}]_0 = 1$ M, 300 equiv. *rac*-lactide, 5 equiv. BnOH, RT, DCM, 8.3 h, total conv.).

The PLA sample was also analyzed by MALDI-TOF mass spectrometry to identify the nature of the chain-end. The PLA produced with the IMesGaMe₃/BnOH initiating mixture agrees with a linear PLA chain with a terminal OBn group at the ester end, indicating that BnOH acts as an effective chain transfer agent as the polymerization proceeds.

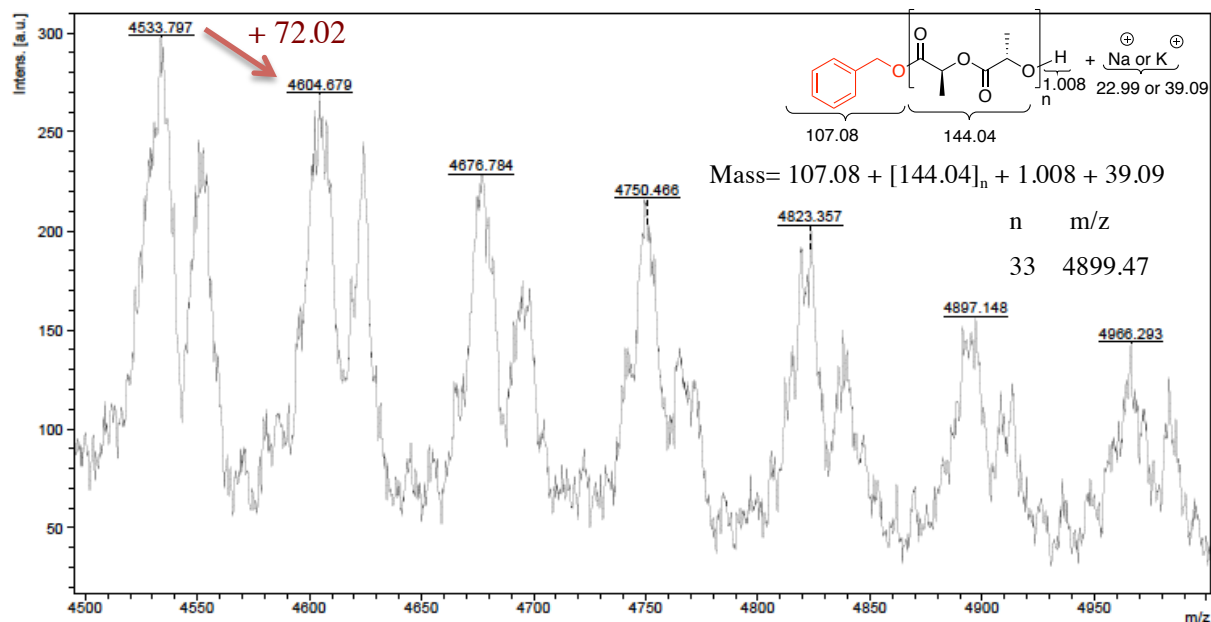


Figure 21: Zoom-in of the MALDI-TOF spectrum of the PLA prepared by ROP of *rac*-lactide initiated using the *catalyst 4*/BnOH system. (Conditions: [*rac*-lactide]₀ = 1 M, 300 equiv. *rac*-lactide, DCM, RT, polymer isolated at 100% conversion to PLA).

The lactide ROP activity of *catalyst 4* is considerably lower in the absence of an alcohol source (45% conversion to PLA of 300 equivalents of *rac*-lactide after 16 h at RT; **entry 9, Table 2**). Despite this fact, the total conversion in PLA is still achieved after a long reaction time of 83 hours (**entry 10, Table 2**). The SEC traces of the produced PLA for 300 equivalents in monomer is monomodal (**Figure 22**) with a narrow polydispersity (PDI: 1.06), and a good match between the theoretical value (43238 g/mol) and the experimental value (43580 g/mol) is observed. Kinetic data agree with a controlled ROP process (**Figures 23** and **24**).

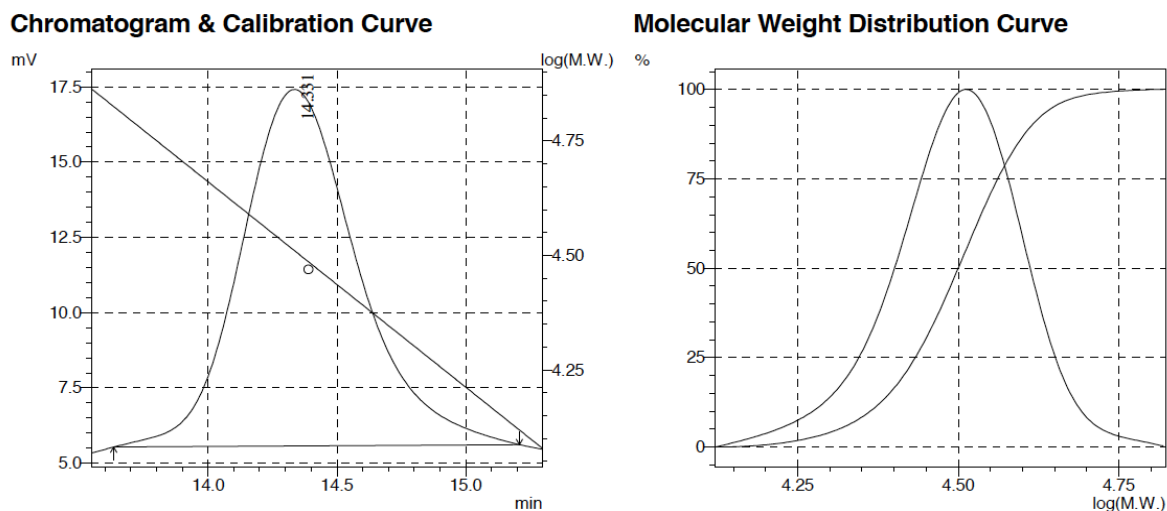


Figure 22: SEC traces of isolated PLA prepared via ROP of *rac*-lactide initiated by the *catalyst 4* system. (Conditions: $[rac\text{-lactide}]_0 = 1 \text{ M}$, 300 equiv. of *rac*-lactide, DCM, RT, 83 h, 100% conv.).

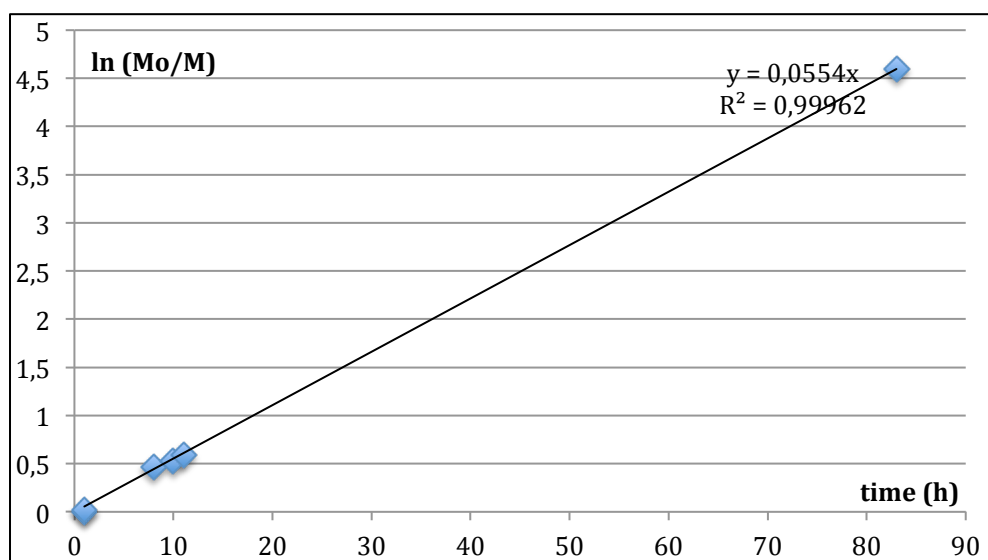


Figure 23: Plot of $\ln(M_0/M)$ vs. time of the ROP of *rac*-lactide using *catalyst 4* system. (Conditions: $[rac\text{-lactide}]_0 = 1 \text{ M}$, 300 equiv. of *rac*-lactide, RT, DCM, 83 h, total conv.).

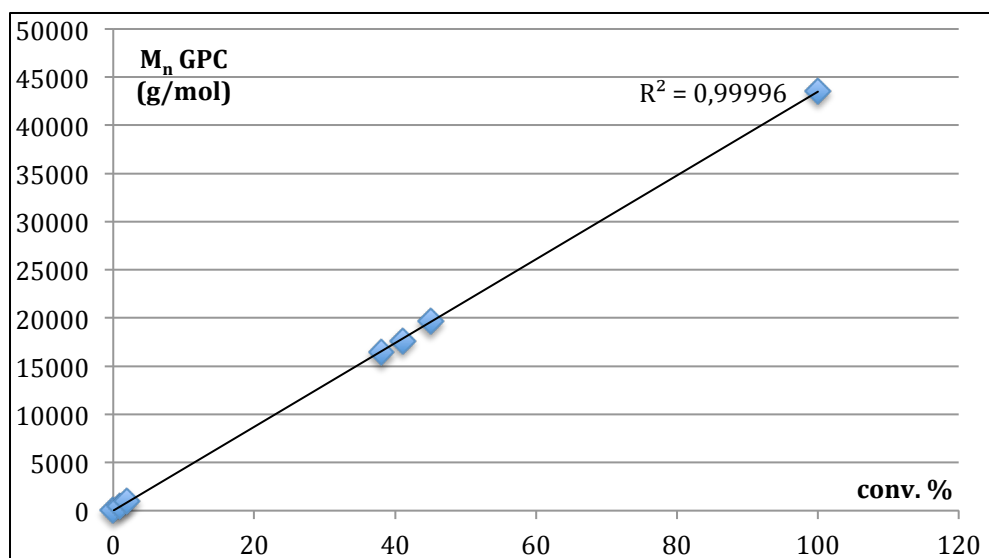


Figure 24: Plot of M_n as a function of *rac*-lactide conv. in the ROP of *rac*-lactide using the *catalyst 4* system. (Conditions: $[rac\text{-lactide}]_0 = 1$ M, 300 equiv. of *rac*-lactide, RT, DCM, 83 h, total conv.).

VII. 2. ROP of *rac*-lactide with IMesInMe₃ *catalyst 5*

The In(III)-NHC analog *catalyst 5* shows the quantitative conversion of 300 equivalents of *rac*-lactide to chain-length controlled PLA within 30 minutes at room temperature using BnOH initiating component (**entry 14, Table 2**). The good $M_{n\text{theo}}/M_{n\text{GPC}}$ match for the produced PLA chains, the monomodal SEC traces (**Figure 25**) and the narrow polydispersity (PDI: 1.2) suggest a well-behaved ROP process with BnOH acting as an effective chain transfer agent as the polymerization proceeds.

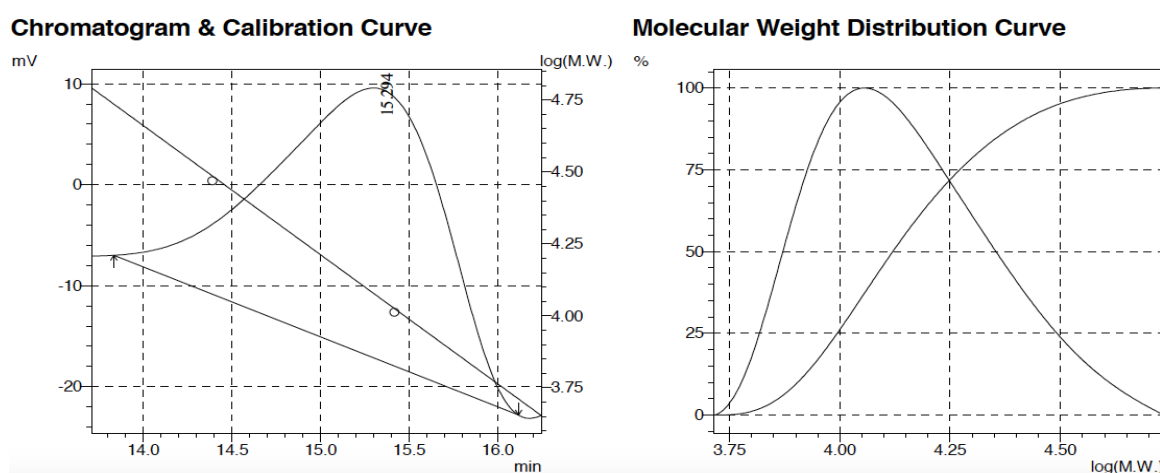


Figure 25: SEC traces of isolated PLA prepared via ROP of *rac*-lactide initiated by the *catalyst 5*/BnOH system. (Conditions: $[rac\text{-lactide}]_0 = 1$ M, 300 equiv in *rac*-lactide, 5 equiv. BnOH, DCM, RT, 30 min., 100% conv.).

The value of the apparent rate constant (k_{app}) for *rac*-lactide polymerization was evaluated from the slope of the straight line kinetic data (first-order reaction rate with $k_{app} = 1.535 \times 10^{-1} \text{ min}^{-1}$, **Figure 26**). This, combined with a linear correlation between the PLA M_n values and monomer conversion (**Figure 27**), further substantiates a controlled ROP process using the *catalyst 4*/BnOH initiating system.

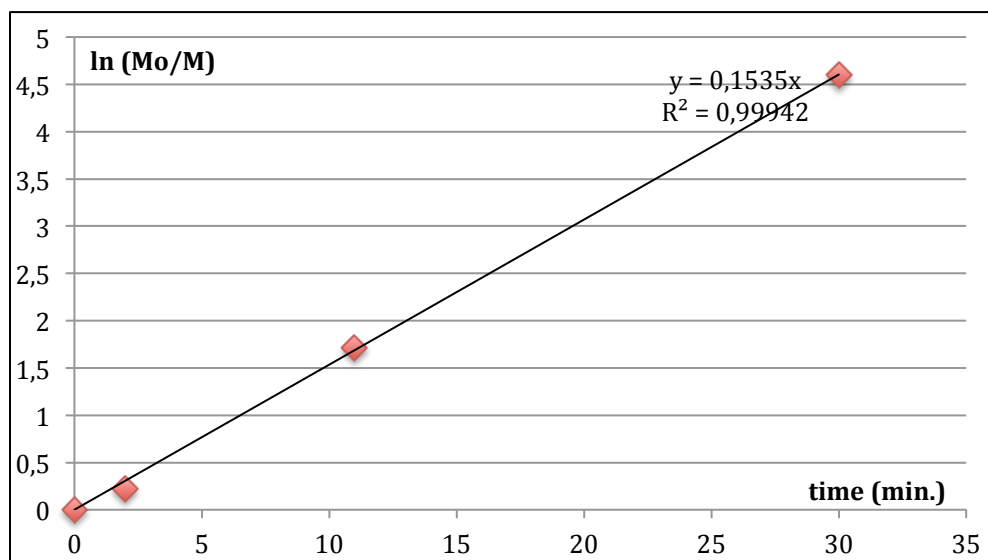


Figure 26: Plot of $\ln(Mo/M)$ vs. time of the ROP of *rac*-lactide using the indium *catalyst 5*/BnOH system. (Conditions: $[rac\text{-lactide}]_0 = 1 \text{ M}$, 300 equiv. of *rac*-lactide, 5 equiv. of BnOH, RT, DCM, 30 min., total conv.).

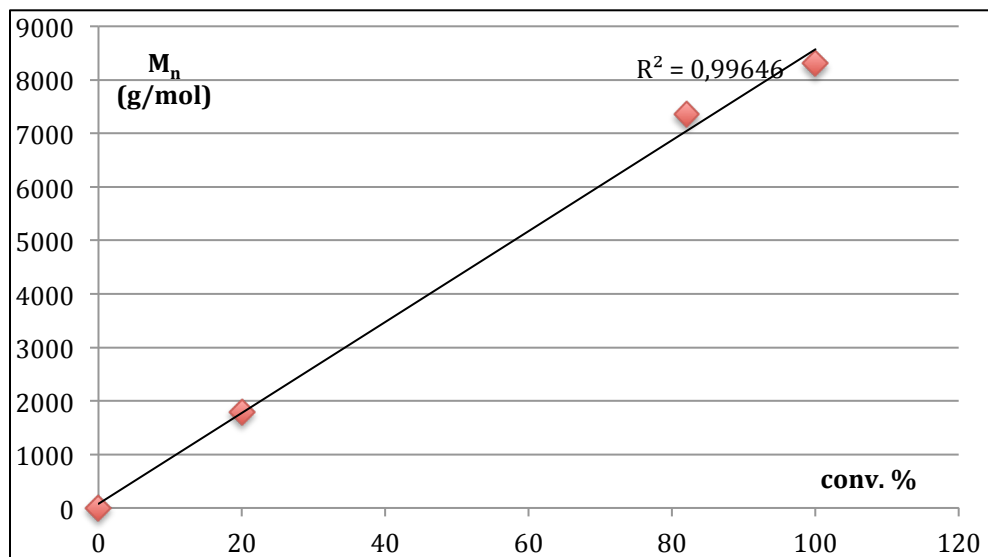


Figure 27: Plot of M_n as a function of the conversion in the ROP of *rac*-lactide using the *catalyst 5*/BnOH system. (Conditions: $[rac\text{-lactide}]_0 = 1 \text{ M}$, 300 equiv. of *rac*-lactide, 5 equiv. of BnOH, RT, DCM, 30 min., total conv.).

The MALDI-TOF spectrum of the prepared PLA produced with the *catalyst 5*/BnOH initiating system is in line with the production of linear PLA bearing a terminal OBn group, and the presence of transesterification reactions during the ROP process: presence of peaks that are equally separated by 72 a.u. (half the mass of lactide) (**Figure 28**).

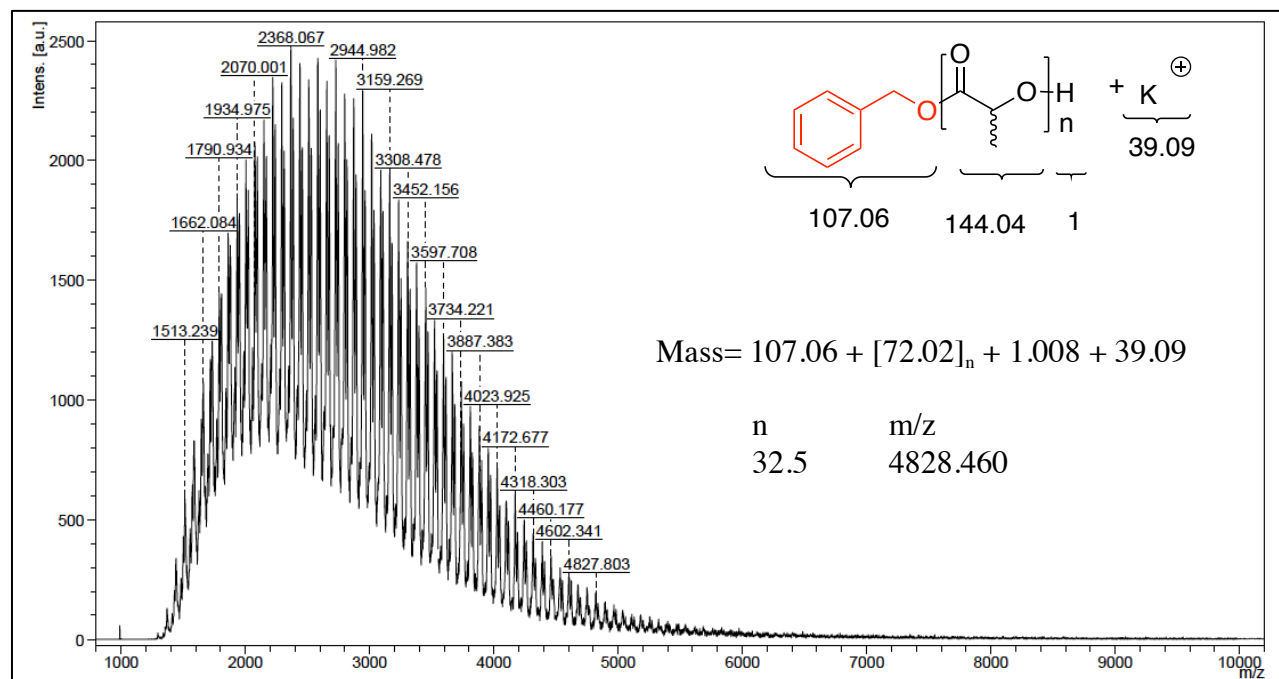


Figure 28: MALDI-TOF spectrum of the PLA prepared by ROP of *rac*-lactide initiated using the *catalyst 5*/BnOH system. (Conditions: [*rac*-lactide]₀ = 1 M, 300 equiv. of *rac*-lactide, 5 equiv. of BnOH, DCM, RT, 30 min.).

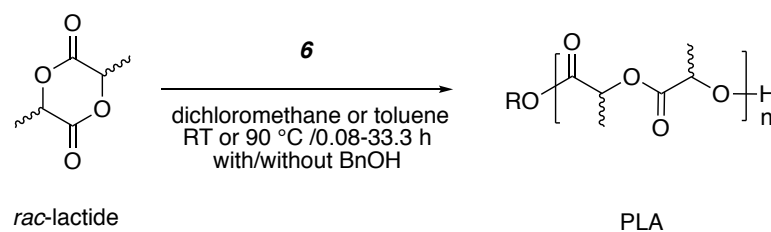
The use of the In(III)-NHC *catalyst 5* in the absence of any alcohol initiator led to an ill-controlled lactide ROP process at room temperature, as deduced from SEC data (300 equivalents of *rac*-lactide in DCM were completely converted in PLA with a duration close to 12 hours (**entry 17, Table 2**). The SEC traces of the produced PLA after total conversion is bimodal (**Supporting data: Figure 1**) with two different molecular weight distributions ($M_n = 7300$ g/mol, PDI = 1.05; $M_n = 16300$ g/mol, PDI = 1.03) resulting in a broad polydispersity (PDI: 2.54).

Overall, the addition of an alcohol source (such as BnOH), that can act as both a nucleophile and a chain transfer agent, was found to greatly improve the control and activity of the ROP catalysis mediated by these group 13 metal NHC adducts.⁶² Thus, both *catalysts 4* and *5* led

to a significantly more active and controlled ROP. In only 30 minutes, using 1/5: indium *catalyst 5*/BnOH initiating system, a complete conversion of 300 equivalents of *rac*-lactide to a well-defined and narrowly disperse PLA was produced.

VIII. [IMesAlMe₂(OEt₂)]⁺ *catalyst 6* for the ROP of *rac*-lactide

The synthesized NHC-supported Al alkyl cations are expected to behave as potent Lewis acidic and electrophilic entities and are able to polymerize many polar substrates. It can be noted that simple Al alkyl cations of the type AlR₂L⁺ have thus far not been reported as ROP initiators of cyclic esters. Therefore, the ROP of *rac*-lactide was tested with a new Al cation species.



With **6**: [IMesAlMe₂(OEt₂)][MeB(C₆F₅)₃]

Figure 31: ROP of *rac*-lactide initiated by species 6

Entry	catalyst	<i>rac</i> -lactide ^a	BnOH ^a	T (°C)	Time ^b (h)	Conversion ^c (%)	M _n ^{theo} ^d (g/mol)	M _n ^{GPC} ^e (g/mol)	PDI
1	6	300	5	RT	0.08	5	432	479	1
2	6	300	5	RT	0.16	18	1557	1581	1.09
3	6	300	5	RT	0.3	44	3805	3840	1.15
4	6	300	5	RT	0.66	100	7091	7275	1.08
5	6	300	/	90	0.8	1	433	561	1.03
6	6	300	/	90	1.6	3	1297	1014	1.02
7	6	300	/	90	12.5	41	17295	17727	1.02
8	6	300	/	90	33.3	88	38049	38047	1.06

Polymerization conditions: [Monomer]₀ = 1 M. DCM or toluene, RT or 90 °C.

^a Equiv. versus initiator. ^b Reaction time. ^c Monomer conversion. ^d Calculated using M_n^{theo} = number of equiv. of *rac*-LA × M_{*rac*-lactide} × conv.; in the presence of BnOH, M_n^{theo} = [*rac*-LA]₀ × M_{*rac*-lactide} × conv./[BnOH]₀. ^e Measured by GPC in THF (30 °C) using PS standards and corrected by applying the appropriate correcting factor (0.58).

Table 3: Results of the ROP of *rac*-lactide initiated by species 6.

As seen in the previous ROP, the addition of an external alcohol source such as BnOH considerably improves the activity and the control of the ROP process. Thus, in the presence of BnOH, species **6** effectively mediates the controlled ROP of *rac*-lactide at room temperature to produce controlled chain-length PLA with a narrowly disperse PLA (PDI: 1.2) (**entry 4, Table 3**).

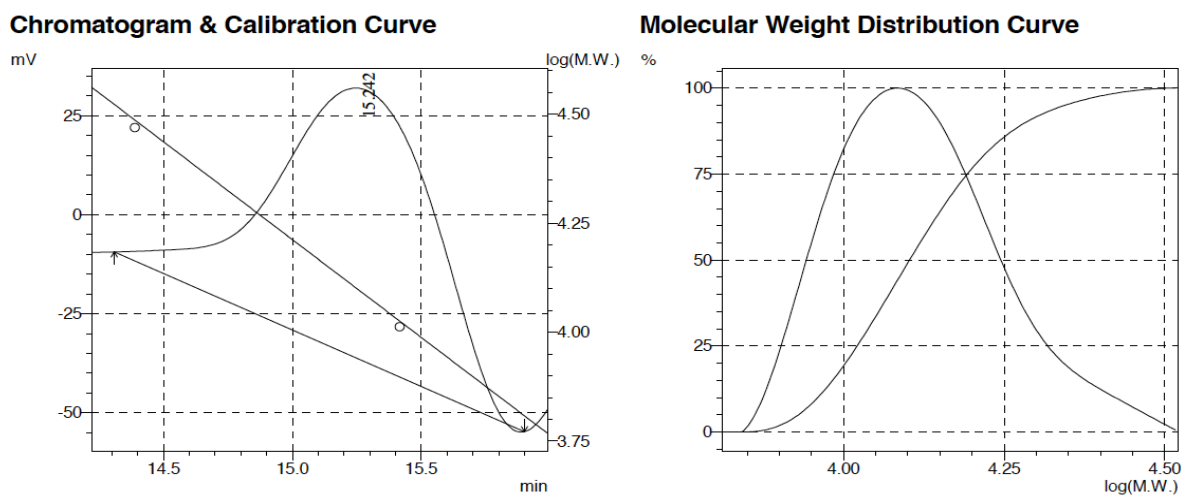


Figure 32: SEC traces of isolated PLA prepared via ROP of *rac*-lactide initiated by the aluminium cation *catalyst 6*/BnOH system. (Conditions: [*rac*-lactide]₀ = 1 M, 300 equiv. of *rac*-lactide, 5 equiv. of BnOH, DCM, RT, 40 min., 100% conv.).

Kinetic data also agree with a controlled ROP process. The reaction rate follows a first kinetic order ($k_{app} = 4.23 \times 10^{-2} \text{ min}^{-1}$) with respect to monomer (**Figure 33**) and a linear correlation between the PLA chain length (M_n values) and the monomer conversion is observed. The experimental M_n values of the formed PLA match well with theoretical ones, (lactide/alcohol ratio: 300/5) (**Figure 34**). BnOH appears to act as an effective chain transfer agent during the ROP reaction.

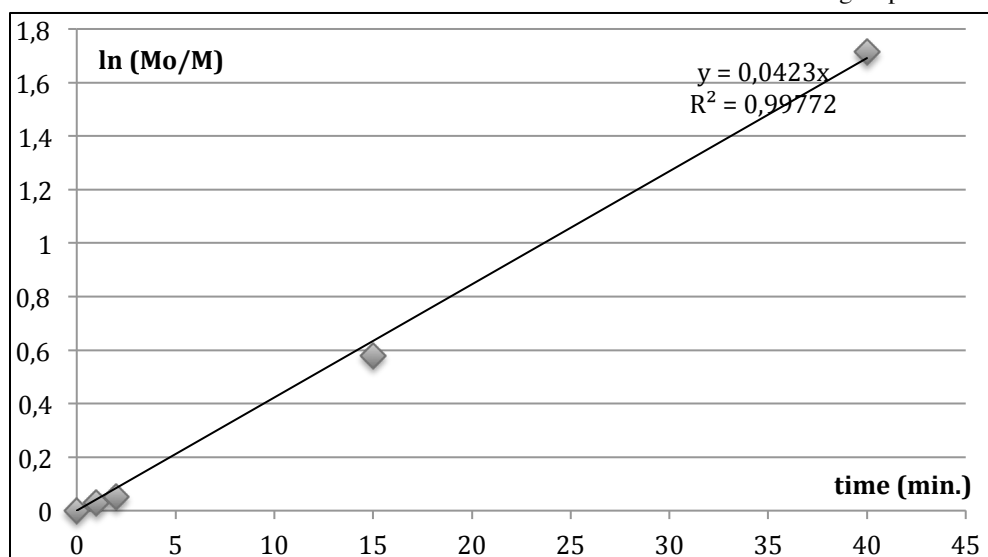


Figure 33: Plot of $\ln(Mo/M)$ vs. time of the ROP of *rac*-lactide using *catalyst 6*/BnOH system. (Conditions: $[rac\text{-lactide}]_0 = 1$ M, 300 equiv. of *rac*-lactide, 5 equiv. of BnOH, RT, DCM, 40 min., total conv.).

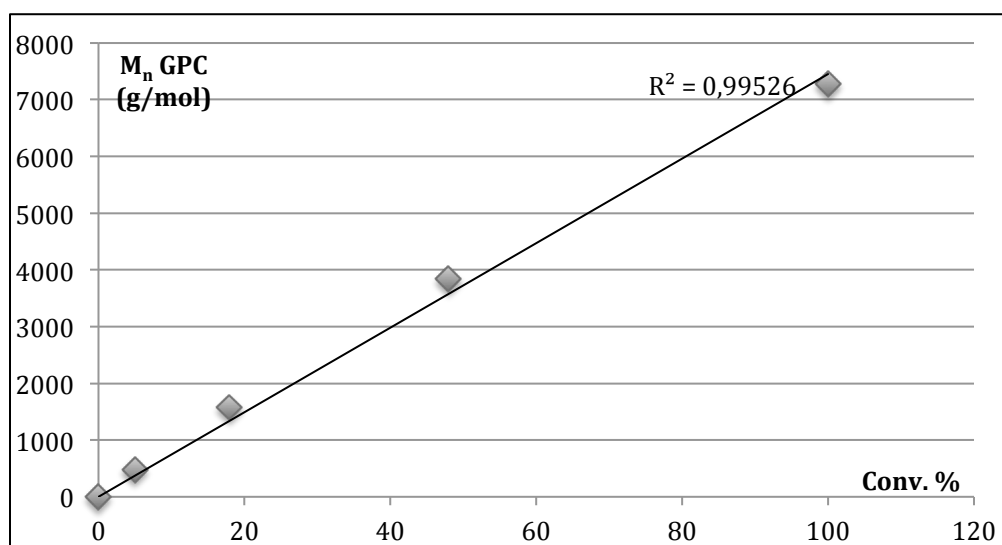


Figure 34: Plot of M_n as a function of the conv. in the ROP of *rac*-lactide using the *catalyst 6*/BnOH system. (Conditions: $[rac\text{-lactide}]_0 = 1$ M, 300 equiv. of *rac*-lactide, 5 equiv. of BnOH vs. *catalyst 6*, RT, DCM, 40 min., total conv.).

The MALDI-TOF spectrometric data of the produced PLA are consistent with the formation of a linear transesterified PLA bonded to a terminal OBn group, and as shown by $[M+Na]^+$ and $[M+K]^+$ peaks which are spaced by 72 a.u., the presence of transesterification reactions during the ROP process (**Figure 35**).

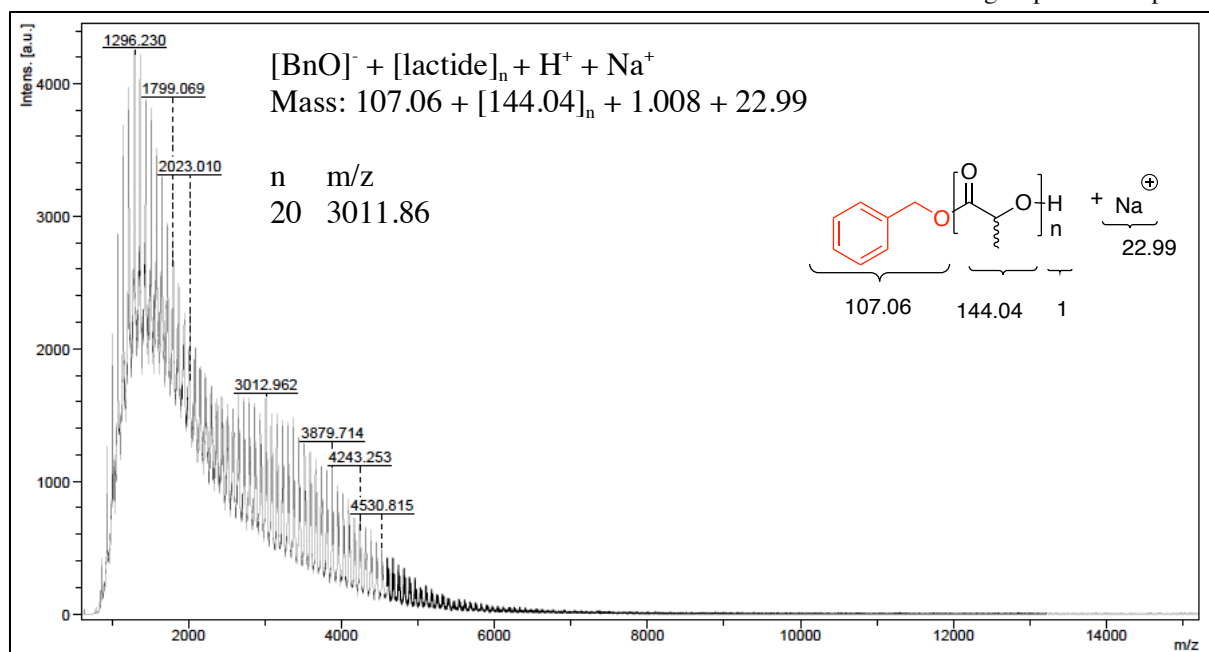


Figure 35: MALDI-TOF spectrum of the PLA prepared by ROP of *rac*-lactide initiated using Al cation *catalyst 6*/BnOH system. (Conditions: $[rac\text{-lactide}]_0 = 1$ M, 300 equiv. of *rac*-lactide, 5 equiv. of BnOH, DCM, RT, 40 min.).

Without any alcohol source, the Al cation **6** is inactive at room temperature. Thus, the ROP of *rac*-lactide was performed in toluene at 90 °C. Despite the fact that a long time of 33 hours was needed to obtain a conversion of 88% (**entry 8, Table 3**), the polymerization is controlled, as reflected by GPC data that is consistent with a narrow monodisperse PLA (PDI: 1.06) (**Figure 36**) and with PLA chain length matching the theoretical values (**Figure 38**).

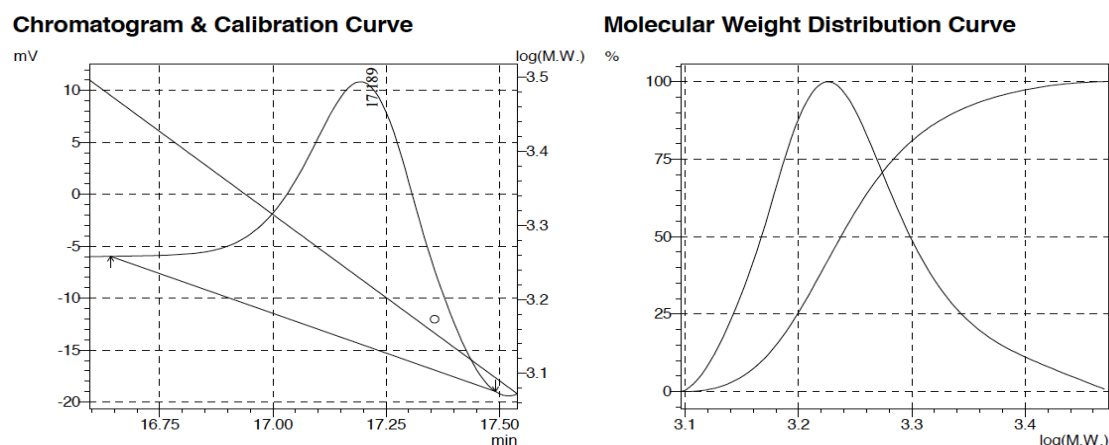


Figure 36: SEC traces of isolated PLA prepared via ROP of *rac*-lactide initiated by the *catalyst 6* system. (Conditions: $[rac\text{-lactide}]_0 = 1$ M, 300 equiv. of *rac*-lactide, toluene, 90 °C, 33 h, 88% conv.).

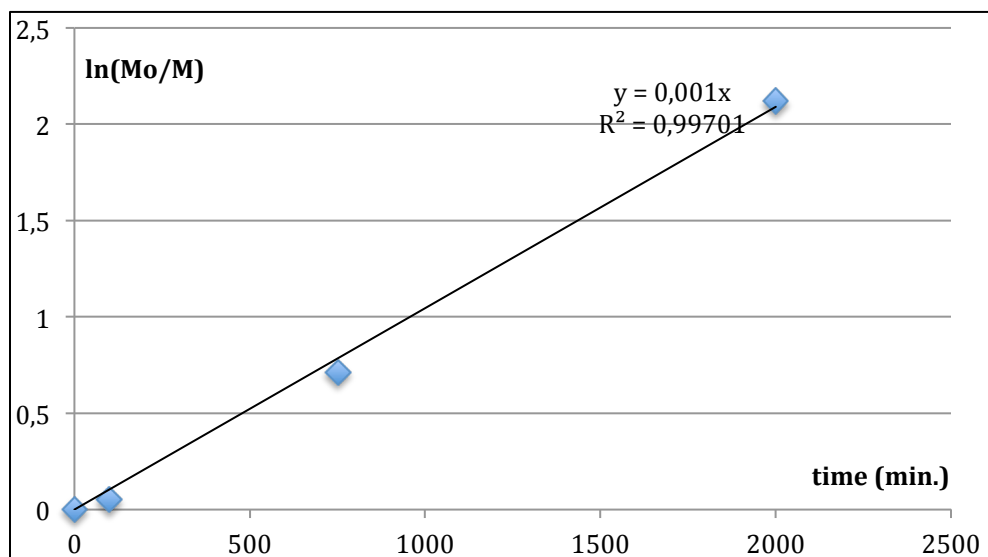


Figure 37: Plot of $\ln(Mo/M)$ vs. time of the ROP of *rac*-lactide using *catalyst 6* system. (Conditions: $[rac\text{-lactide}]_0 = 1$ M, 300 equiv. of *rac*-lactide, toluene, 90 °C, 33 h, 88%).

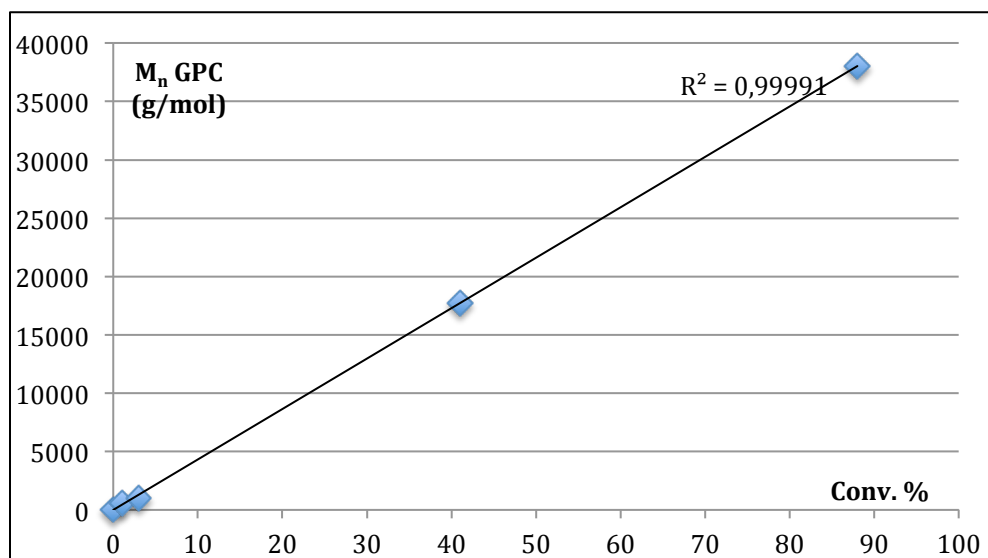


Figure 38: Plot of M_n as a function of the conv. in the ROP of *rac*-lactide using the *catalyst 6* system. (Conditions: $[rac\text{-lactide}]_0 = 1$ M, 300 equiv. of *rac*-lactide, 90 °C, toluene, 33 h, 88%).

IX. Conclusion

In summary, different group 13 metal (M= Al, Ga, In)/NHC complexes were synthesized according to a simple procedure. Different adducts (M= Ga, In) were found to promote the ROP of *rac*-lactide under a controlled ROP reaction with full conversion to PLA. Comparing the In species **5** with its Ga analog **4**, the In(III) derivative exhibits higher ROP performance. Indeed, In complexes are shown to be more reactive than their Ga analogs.⁶³ In³⁺ has lower Lewis acid character than Ga³⁺, thus the bond between the C_{carbene} and the In metal is more flexible than the C_{carbene}-Ga metal so more reactive toward the ROP of lactide.

Furthermore, the addition of an external alcohol source, like BnOH, acting as an effective chain transfer agent, was shown to improve the ROP control and activity. The mechanism first step is probably a ROP proceeding *via* activation/dissociation of the M-C_{carbene} (**Figure 39 (a)**) followed by a transesterification reaction with BnOH acting as a nucleophile and yielding in the release of the NHC, and finally the classical «coordination-insertion» mechanism. Without any chain transfer agent, the ROP occurs probably via an activated monomer mechanism where the NHC acts as the nucleophile and promotes the ROP while the metal derivatives M(Me)₃ operate as electrophiles (**Figure 39 (b)**).

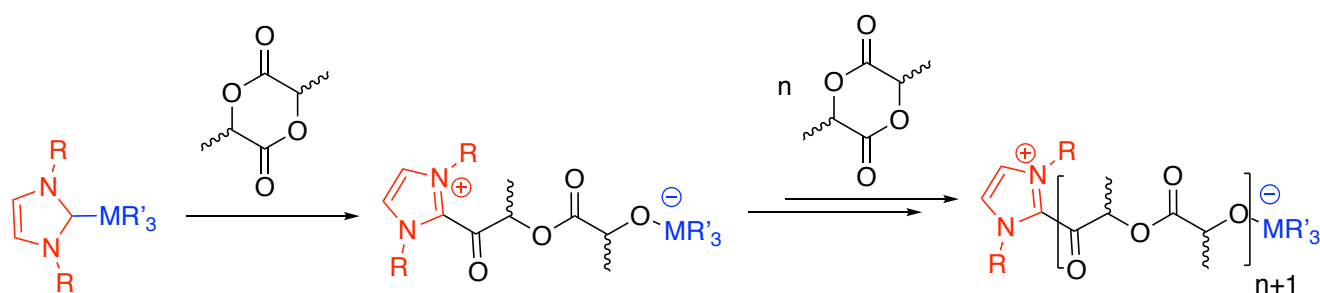


Figure 39: a) Proposed mechanism first step for the ROP of lactide by group 13 metal NHC adducts

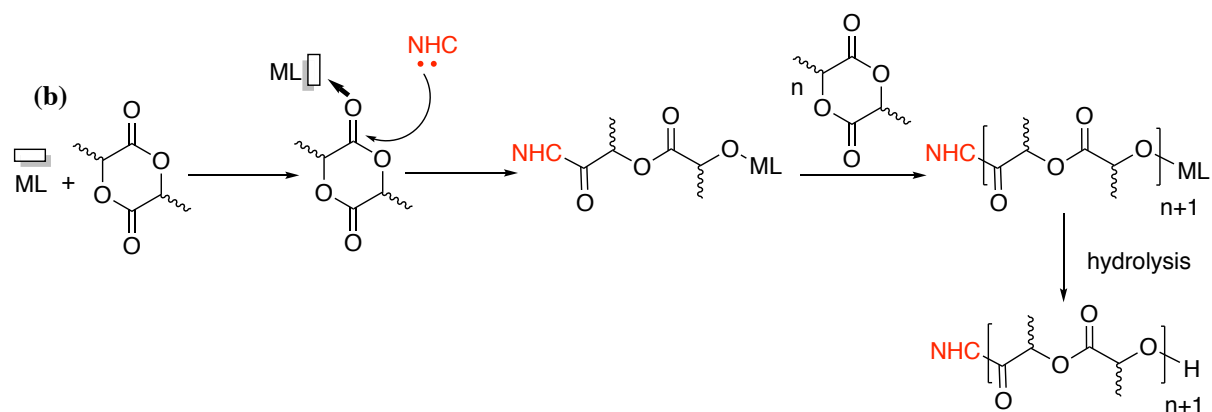


Figure 39: b) “Activated monomer” general mechanism for the ROP of *rac*-lactide

It was found that neutral Al-NHC adducts of the type (NHC)MMe₃ may be readily and quantitatively ionized by B(C₆F₅)₃ Lewis acid to produce, in the presence of a Lewis base (L) like Et₂O or THF, the corresponding cationic alkyls (NHC)MMe₂(L)⁺. The NHC-stabilized Al(III) alkyl cation **6** is stable in solution and is a very strong Lewis acid. Combined with BnOH, this species may mediate the controlled ROP of the lactide at room temperature affording a chain-length controlled PLA.

X. References

- [1]. H. W. Wanzlick, H. J. Schönherr, *Angew. Chem. Int. Ed.* **1968**, *7*, 141-142.
- [2]. H. W. Wanzlick, E. Fjedor, K. H. Jerg, *Chem. Ber.* **1963**, *96*, 1208-1212.
- [3]. K. Öfele, *J. Organomet. Chem.* **1968**, *12*, 42-43.
- [4]. A. J. Arduengo, M. Kline, R. L. Harlow, *J. Am. Chem. Soc.*, **1991**, *113*, 361-363.
- [5]. A. J. Arduengo, *Acc. Chem. Res.* **1999**, *32*, 913-921.
- [6]. P. Jerabek, P. Schwerdtfeger, G. Frenking, *J. Comput. Chem.* **2019**, *40*, 247-264.
- [7]. C. M. Crudden, D. P. Allen, *Coord. Chem. Rev.* **2004**, *248*, 2247-2273.
- [8]. L. Jafapour, S. P. Nolan, *Adv. Organomet. Chem.* **2001**, *46*, 181-222.
- [9]. I. Dragutan, V. Dragutan, L. Delaude, A. Demonceau, *Arkivoc*, **2005**, *10*, 206-252.
- [10]. F. E. Hahn, M. C. Jahnke, *Angew. Chem. Int. Ed.* **2008**, *47*, 3122-3172.
- [11]. P. De Frémont, N. Marion, S. P. Nolan, *Coord. Chem. Rev.* **2009**, *253*, 862-892.
- [12]. A. J. Arduengo, R. Krafczyk, R. Schmutzler, H. A. Craig, J. R. Goerlich, W. J. Marshall, M. Unverzagt, *Tetrahedron*, **1999**, *55*, 14523-14534.
- [13]. C. J. E. Davies, M. J. Page, C. E. Ellul, M. F. Mahon, M. K. Whittlesey, *Chem. Commun.* **2010**, *46*, 5151-5515.
- [14]. H. Türkmen, T. Pape, T. F. E. Hahn, B. Çetinkaya, *Organometallics*, **2008**, *27*, 571-575.
- [15]. W. A. Herrmann, C. Köcher, *Angew. Chem. Int. Ed.* **1997**, *36*, 2162-2187.
- [16]. M. N. Hopkinson, C. Richter, M. Schedler, F. Glorius, *Nature* **2014**, *510*, 485-496.
- [17]. (a) R. Lindner, C. Wagner, D. Steinborn, *J. Am. Chem. Soc.*, **2009**, *131*, 8861-8874. (b) D. G. Gusev, *Organometallics*, **2009**, *28*, 6458-6461. (c) S. K. Yen, L. L. Koh, H. V. Huynh, T. S. A. Hor, *Dalton Trans.*, **2007**, *35*, 3952-3958.
- [18]. (a) S. Bellemin-Laponnaz, *Polyhedron*, **2010**, *29*, 30-33. (b) D. C. Graham, K. J. Cavell, B. F. Yates, *Dalton Trans.*, **2007**, 4650-4658. (c) J. A. Cabeza, I. del Rio, D. Miguel, E. Perez-Carreno, M. G. Sanchez-Vega, *Organometallics*, **2008**, *27*, 211-217.
- [19]. E. Despagnet-Ayoub, R. H. Grubbs. *J. Am. Chem. Soc.*, **2004**, *126*, 10198-10199.
- [20]. E. Despagnet-Ayoub, R. H. Grubbs. *Organometallics*, **2005**, *24*, 338-340.
- [21]. V. Lavallo, Y. Canac, B. Donnadiou, W. W. Schoelle, G. Bertrand, *Science*. **2006**, *312*, 722-724.
- [22]. (a) J. Yun, E. R. Marinez, R. H. Grubbs, *Organometallics* **2004**, *23*, 4172-4173. (b) M. Mayr, K. Wurst, K. -H. Ongaria, M. R. Buchmeiser, *Chem. Eur. J.*, **2004**, *10*, 1256-1266.

- [23]. C. C. Scarborough, M. J. W. Grady, I. A. Guzei, B. A. Gandhi, E. E. Bunel, S. S. Stahl, *Angew. Chem. Int. Ed.* **2005**, *44*, 5269-5272.
- [24]. (a) R. W. Alder, M. E. Blake, *Chem. Commun.* **1997**, 1513-1514. (b) M. Otto, S. Conejero, Y. Canac, V. D. Romanenko, V. Rudzevitch, G. Bertrand, *J. Am. Chem. Soc.*, **2004**, *126*, 1016-1017. (c) W. A. Herrmann, K. Ofele, D. Preysing, E. Herdtweck, *J. Organomet. Chem.*, **2003**, *684*, 235-248. (d) K. Denk, P. Sirsch, W. A. Herrmann, *J. Organomet. Chem.*, **2002**, *649*, 219-224.
- [25]. M. -T. Lee, C. -H. Hu, *Organometallics* **2004**, *23*, 976-983.
- [26]. R. W. Alder, P. R. Allen, M. Murray, A. G. Orpen, *Angew. Chem., Int. Ed. Engl.* **1996**, *35*, 1121-1123.
- [27]. M. M. Rogers, S. S. Stahl, F. Glorius, *N-Heterocyclic Carbenes as Ligands for High-Oxidation-State Metal Complexes and Oxidation Catalysis, Vol. 21*, **2007**.
- [28]. W. A. Herrmann, *Angew. Chem. Int. Ed.* **2002**, *41*, 1291-1309.
- [29]. D. J. Nelson, S. P. Nolan, *Chem. Soc. Rev.* **2013**, *42*, 6723-6753.
- [30]. V. Nair, S. Bindu, V. Sreekuman, *Angew. Chem. Int. Edit*, **2004**, *43*, 5130-5135.
- [31]. V. César, S. Bellemin-Laponnaz, L. H. Gade, *Chem. Soc. Rev.* **2004**, *33*, 619-636.
- [32]. K. Ofele, K. W. A. Herrmann, D. Mihalios, M. Elison, E. Herdtweck, W. Sherer, J. J. Mink, *Organomet. Chem.* **1993**, *459*, 177-184.
- [33]. S. Diez-Gonzalez, S. P. Nolan, *Coord. Chem. Rev.*, **2007**, *251*, 874-883.
- [34]. D. J. D. Wilson, S. A. Couchman, J. L. Dutton, *Inorg. Chem.* **2012**, *51*, 7657-7668.
- [35]. D. Bourissou, O. Guerret, F. P. Gabbaï, G. Bertrand, *Chem. Rev.* **2000**, *100*, 39-91.
- [36]. C. Boehme, G. Frenking. *Organometallics* **1998**, *17*, 5801-5809.
- [37]. E. Peris, *Top. Organomet. Chem.* **2007**, *21*, 83-116.
- [38]. H. M. J. Wang, I. J. B. Lin, *Organometallics* **1998**, *17*, 972-975.
- [39]. E. Weintraub, *Ind. Eng. Chem.* **1913**, *5*, 106-115.
- [40]. For Aluminium: (a) A. J. Arduengo, H. V. Rasika Dias, J. C. Calabrese, F. Davidson, *J. Am. Chem. Soc.*, **1992**, *114*, 9724-9725. (b) M. L. Cole, D. E. Hibbs, C. Jones, P. C. Junk, N. A. Smithies, *Inorg. Chim. Acta*, **2005**, *358*, 102-108. (c) B. Bantu, G. M. Pawar, K. Wurst, U. Decker, A. M. Schmidt, M. R. Buchmeiser, *Eur. J. Inorg. Chem.*, **2009**, 1970-1976. (d) S. G. Alexander, M. L. Cole, C. M. Forsyth, *Chem. Eur. J.*, **2009**, *15*, 9201-9214. (e) R. S. Ghadwal, H. W. Roesky, R. Herbst-Irmer, P. G. Jones, *Z. Anorg. Allg. Chem.*, **2009**, 431-433. (f) R. J. Baker, A. J. Davies, C. Jones, M. Kloth, *J. Organomet. Chem.*, **2002**, *656*, 203-210.

- [41]. For Gallium and Indium: (a) S. J. Black, D. E. Hibbs, M. B. Hursthouse, C. Jones, K. M. Abdul Malik, N. A. Smithies, *J. Chem. Soc., Dalton Trans.*, **1997**, 4313-4320. (b) M. D. Francis, D. E. Hibbs, M. B. Hursthouse, C. Jones, N. A. Smithies, *J. Chem. Soc., Dalton Trans.*, **1998**, 3249-3254. (c) R. J. Baker, H. Bettentrup, C. Jones, *Eur. J. Inorg. Chem.*, **2003**, 2446-2451. (d) N. Marion, E. C. Escudero-Adan, J. Benet-Buchholz, E. D. Stevens, L. Fensterbank, M. Malacria, S. P. Nolan, *Organometallics*, **2007**, *26*, 3256-3259. (e) M. L. Cole, S. K. Furfari, M. Kloth, *J. Organomet. Chem.*, **2009**, *694*, 2934-2940.
- [42]. P. Cvjetko, I. Cvjetko, M. Pavlica, *Thallium Toxicity in Humans*, **2010**, *61*, 111-119.
- [43]. Y. Fang, X. Wang, *Angew. Chem. Int. Ed.* **2017**, *56*, 15506-15518.
- [44]. J. O. Nriagu, *Chem. Eng. News* **2003**, *81*, 153-164.
- [45]. A. Lubkowka, D. Chlubek, *Trace Elem. Electrolytes*. **2015**, *32*, 52-59.
- [46]. S. Dagorne, C. Fliedel, P. de Frémont, Gallium and Indium Compounds in Homogeneous Catalysis. In *Encyclopedia of Inorganic and Bioinorganic Chemistry*; Wiley, **2016**; 1-27.
- [47]. <http://www.sigmaaldrich.com/> (February 2019).
- [48]. *The group 13 metal aluminium, gallium indium and thallium, chemical pattern and peculiarities* (ed. S. Aldridge and A. J. Downs), A. J. Downs, H. J. Himmel, Wiley-VCH VerlagGmbH: Weinheim, **2011**, 1.
- [49]. C. Fliedel, G. Schnee, T. Avilés, S. Dagorne, *Coord. Chem. Rev.* **2014**, *275*, 63-86.
- [50]. S. Dagorne, R. Wehmschulte, *chemcatchem* **2018**, *10*, 1-13.
- [51]. G. Berthon-Gelloz, M. A. Siegler, A. L. Spek, B. Tinant, J. N. H. Reek, I. E. Marko, *Dalton Trans.* **2010**, *39*, 1444-1446.
- [52]. A. Gómez-Suárez, R. S. Ramón, O. Songis, A. M. Z. Slawin, C. S. J. Cazin, S. P. I. Nolan, *Organometallics* **2011**, *30*, 5463-5470.
- [53]. J. Balogh, A. M. Z. Slawin, S. P. Nolan, *Organometallics* **2012**, *31*, 3259-3263.
- [54]. (a) Arduengo, A. J. Patent: WO 9114678, **1992**. (b) A. A. Gridnev, I. M. Mihaltseva, *Synth. Commun.* **1994**, *24*, 1547-1555.
- [55]. (a) A. J. Arduengo, R. Krafczyk, R. Schmutzler, *Tetrahedron* **1999**, *55*, 14523-14534. (b) L. Jafarpour, E. D. Stevens, S. P. Nolan, *J. Organomet. Chem.* **2000**, *606*, 49-54.
- [56]. A. Bolley, G. Schnee, L. Thevenin, B. Jacques, S. Dagorne, *Inorganics* **2018**, *23*, 1-9.
- [57]. A. -L. Schmitt, G. Schnee, R. Welter, S. Dagorne, *Chem. Commun.* **2010**, *46*, 2480-2482.

- [58]. M. Uzelac, A. Hernán-Gómez, D. R. Armstrong, A. R. Kennedy, E. Hevia, *Chem. Sci.* **2015**, *6*, 5719–5728.
- [59]. G. Schnee, A. Bolley, F. Hild, D. Specklin, S. Dagorne, *Catal. Today.* **2017**, *289*, 204-210.
- [60]. M. Mantina, A. C. Chamberlin, R. Valero, C. J. Cramer, D. G. Truhlar, *J. Phys. Chem. A* **2009**, *113*, 5806-5812.
- [61]. G. Schnee, A. Bolley, C. Gourlaouen, R. Welter, S. Dagorne, *J. Organomet. Chem.* **2016**, *820*, 8-13.
- [62]. D. Specklin, F. Hild, L. Chen, L. Thévenin, M. Munch, F. Dumas, F. Le Bideau, S. Dagorne, *ChemCatChem* **2017**, *9*, 3041-3046.
- [63]. A. B. Kremer, R. J. Andrews, M. J. Milner, X. R. Zhang, T. Ebrahimi, B. O. Patrick, P. L. Diaconescu, P. Mehrkhodavandi, *Inorg. Chem.* **2017**, *56*, 1375-1385.

Chapter II

Synthesis of PEG-*co*-PLLA amphiphilic copolymers using different catalysts under mild conditions

I. Introduction

Polyethylene glycols (PEGs) are composed of polyether compounds repeating ethylene glycol units according to the constituent monomer or parent molecule¹ (**Figure 1**) and appear to be a neutral polyether available in a wide variety of molecular weights.^{2,3}

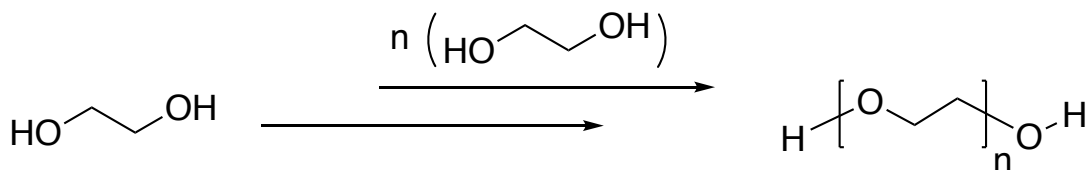


Figure 1: Polymerization of ethylene glycol

This polymer has the property to be soluble in water but also in many organic solvents.⁴ A very important feature of PEGs is their solubility in water, which is due to intermolecular *H*-bonds between PEG and water,⁵ as well as the intramolecular *H*-bonds between the end hydroxyl of PEG with the ether oxygens of the main chain.⁶ Thus, PEG is frequently described as an amphiphilic polymer.⁷ This non-toxic (approved by the FDA for use in drugs),⁸ hydrophilic with proven biocompatibility⁹ polymer is subject to allow chemical modifications on biodegradable polyesters, which are all strongly hydrophobic involving many limitations. Therefore, PEG attachment to other molecules or monomers allows adding hydrophilic character and modifies their physicochemical properties like solubility. Also, there is a modulation on the material's degradation rate.¹⁰ For example, if a covalent link is created, PEG solubility can be altered by attachment of hydrophobic tails including comonomers in the polymer backbone like polylactide. This hydrophilic polymer is used in a large field of applications; for example, we can highlight its importance in the pharmaceutical industry especially for the encapsulation of various drugs.¹¹ Indeed, amphiphilic blocks copolymers consisting of a hydrophilic block like PEG and a hydrophobic block, for instance, a polylactide chain, lead to the biodegradable PEG-co-PLA copolymer (**Figure 2**),¹² which can self-assemble forming spherical polymeric micelles in aqueous solution.¹³

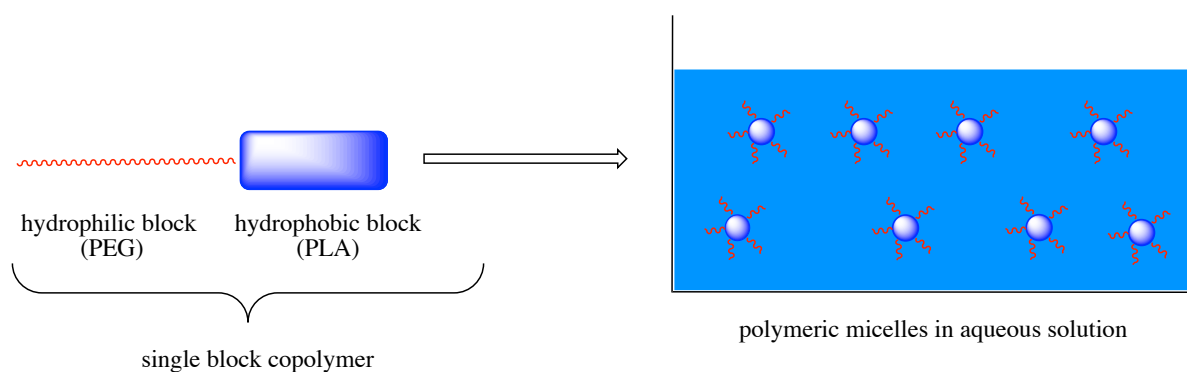


Figure 2: Self-assembly of amphiphilic block copolymers to a micellar structure in an aqueous solution

This molecular arrangement gives very important property for drug delivery vehicles¹⁴ such as nano-particles,¹⁵ micelles,² hydrogels,¹⁶ and injectable delivery systems.¹⁷ The polymeric micelle illustrated (**Figure 3**) shows how the hydrophobic block of the polymer inside the micelle surrounds a hydrophobic drug whereas the hydrophilic block is exposed to the hydrophilic solvent. It creates an environment where hydrophobic molecules can be dissolved in the hydrophobic core of the micelle.^{18,19,20}

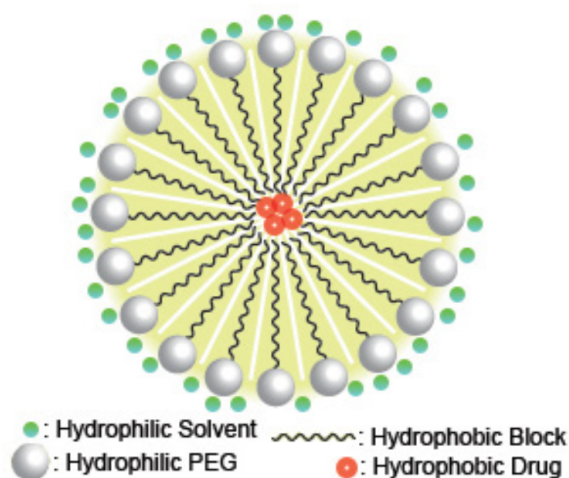


Figure 3: Drug-loaded polymeric micelle

PEG is commonly used as biocompatible hydrophilic polymer but isn't a bio-sourced polymer and allows the modulation of the degradation rate of materials.²¹ Bonded with PLA, a bio-sourced polyester, it degrades over time into acids that can be safely eliminated. Furthermore, PEG is currently used in cosmetics in Europe because of its interesting properties such as solubility, viscosity, and low toxicity properties. In this field, PEG has three main functions:

- Emollients in skin care emulsions^{22,23} that soften and lubricate the skin.
- Emulsifiers,²⁴ which are surface-active agents that stabilize emulsions²⁵ lowering the interfacial tension²⁶ between the phases.²⁷ They help water-based and oil-based ingredients to be mixed properly (**Figure 4**).
- Vehicles, delivering other ingredients deeper into the skin.²⁸

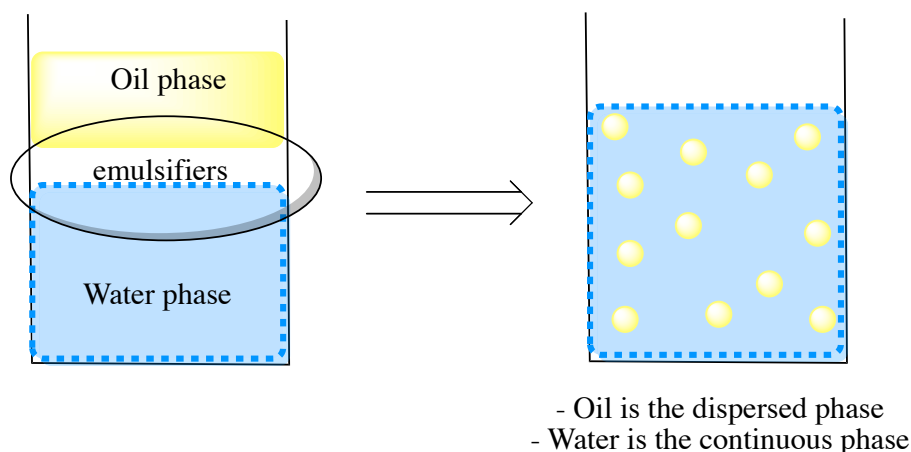


Figure 4: Basic components of an emulsion

The phase in which an emulsifier is more soluble constitutes the continuous phase like mentioned the Bancroft rule.^{29,30,31}

Our strategy for modifying the physicochemical properties of hydrophobic and biodegradable PLA has been to incorporate hydrophilic PEG segments. The different copolymer blocks were synthesized using several robust metal-based catalysts under mild conditions, incorporating Al(III), Ga(III), Zn(II) and Mg(II) in contrast to stannous octoate which is the catalyst of choice to perform the classical synthesis of PEG-PLA copolymer.^{32,33} Tin(II) leads to the contamination of soil, ground water and thus is released to the environment. It's important to mention the possible toxicity of tin^{34,35} along with the current limitations of the produced copolymer (limited thermal and mechanical properties, and excessive brittleness).³⁶

II. *N,O,N*-supported Al(III) and Ga(III) amido chelates **2** and **3**: synthesis and structure

We are interested in *N,O,N*-supported tetracoordinate amido aluminium κ^3 -*N,O,N*-[(C₆H₁₁)N-C₆H₄]₂OAlNMe₂ and amidogallium κ^3 -*N,O,N*-[(C₆H₁₁)N-C₆H₄]₂OGaNMe₂ complexes as ROP initiators of lactide.³⁷ They consist of a tetracoordinate group 13 metal in which the metal center adopts a distorted trigonal monopyramidal geometry and were demonstrated to be efficient catalysts of the ROP of cyclic esters and carbonates.³⁸ These complexes were exploited to access narrowly dispersed PEG-co-PLLA amphiphilic copolymers.

II. 1. Synthesis of *N,O,N* ligand **1**

N,O,N ligand bearing N-C₆H₅ substituents (**Figure 5**) was initially synthesized. The synthesis of the ligand consists of the condensation between commercially available 2,2'-oxydianiline and two equivalents of cyclohexanone in acetic acid at 70 °C during 40 hours under a nitrogen atmosphere. The ligand was isolated as a white solid in 74% yield.

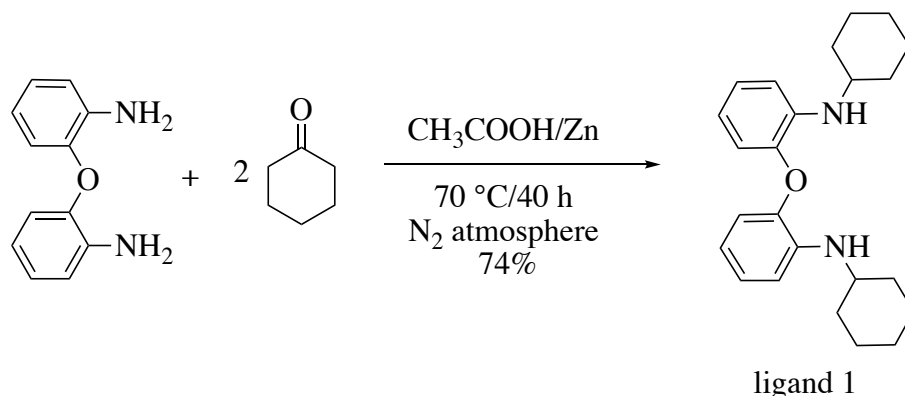
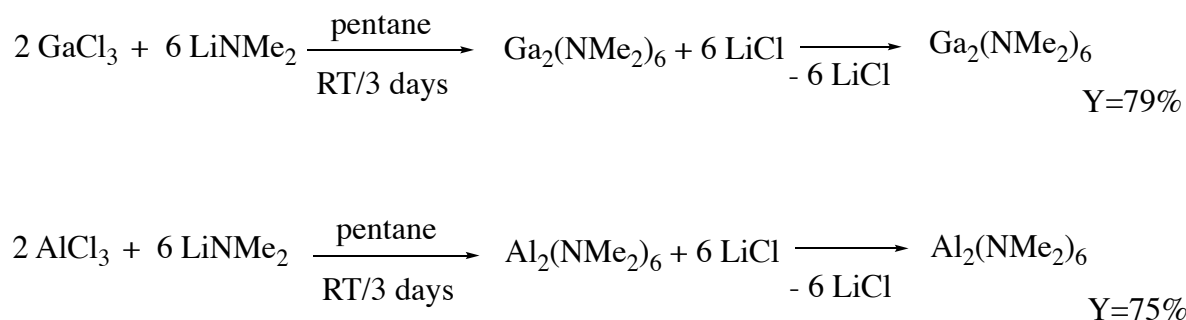


Figure 5: Synthesis of the *N,O,N* ligand **1**

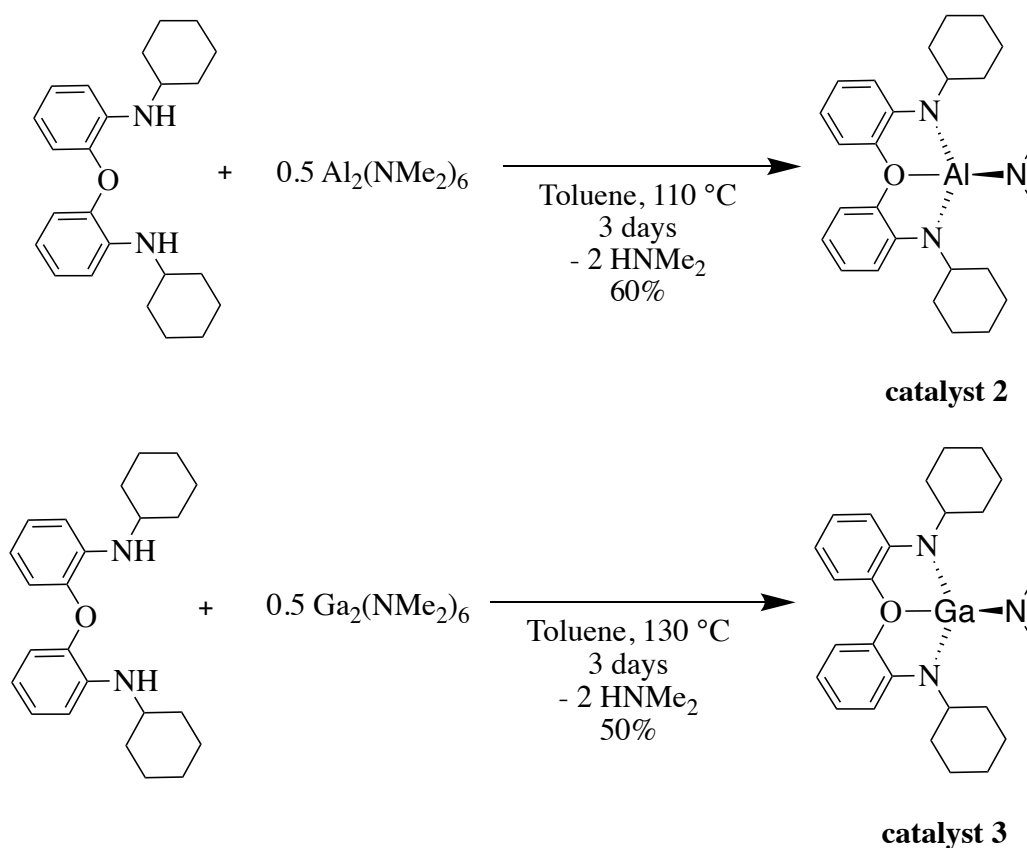
III. Synthesis and structural characterization of *N,O,N* group 13 complexes

III. 1. Synthesis of complexes

First, two amido Al(III) and Ga(III) precursors, Ga₂(NMe₂)₆ and Al₂(NMe₂)₆, were prepared for a subsequent amine elimination reaction with protio ligand **1**. Ga₂(NMe₂)₆ and Al₂(NMe₂)₆ were obtained by reaction of AlCl₃ and GaCl₃, respectively, with three equivalents of LiNMe₂ in pentane.

**Figure 6: Synthesis of Ga(NMe₂)₃ and Al(NMe₂)₃**

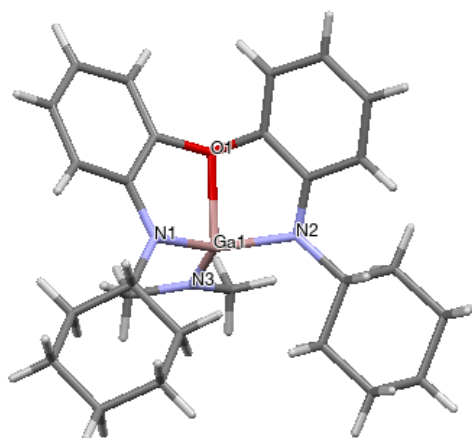
Then ligand **1** reacts with 1 equivalent of Ga(NMe₂)₃ or Al(NMe₂)₃ via amine elimination to produce well-defined *N,O,N*-supported Lewis acid chelate complexes **2** and **3** (**Figure 7**), which were isolated in reasonable yields.

**Figure 7: Synthesis of *N,O,N*-supported Al and Ga amido *catalyst 2* and *3***

Single crystals suitable for X-ray analyses were grown for *catalyst 3*. As illustrated, *catalyst 3* consists of a tetracoordinate Ga species effectively κ^3 -(*N,O,N*)-chelated by the dianionic diamido-amino ligand, forcing the Ga center to adopt a distorted trigonal-

monopyramidal geometry. The nitrogen atoms of the backbone and the Ga-NMe₂ moiety define the pyramidal base, nearly coplanar with the Ga ($\Sigma(\text{N-Ga-N})$ angles: 358.68 °. All bond lengths are as expected with the Ga-N amido bond distances lying between 1.81 to 1.89 Å.^{39,40,41} Similarly, the shorter bond distance is for Ga(1)-N(3): 1.818(1) Å by comparison to Ga(1)-N(1): 1.8927(9) Å and Ga(1)-N(2): 1.872(1) bonds, reflecting a stronger ionic character of the Ga(1)-N(3) bond.⁴²

(a)



(b)

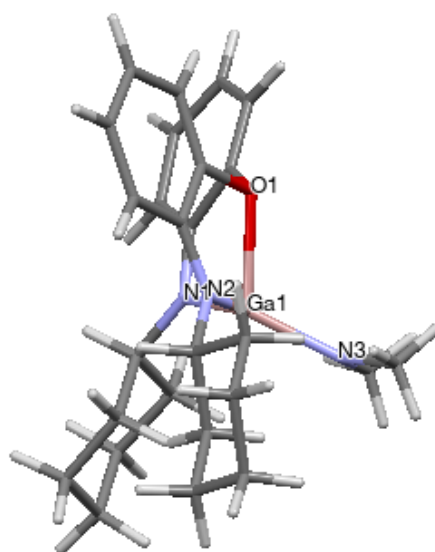


Figure 8: Molecular structure of κ^3 -*N,O,N*-[(C₆H₁₁)NH-C₆H₄]₂OGaNMe₂ (*catalyst 3*). (a) Front view. (b) Side view. Selected bond lengths (Å) and angles (deg): Ga(1)-N(1)= 1.8927(9), Ga(1)-N(2)= 1.872(1), Ga(1)-N(3)= 1.818(1), Ga(1)-O(1)= 2.1030(9); N(1)-Ga(1)-N(2)= 120.38(5), N(1)-Ga(1)-N(3)= 117.14(5), N(3)-Ga(1)-N(2)= 121.16(5), N(3)-Ga(1)-O(1)= 114.00(5).

III. 2. ROP of PEG-co-PLLA with *catalyst 2*

Commercial m-PEG-OH has a dual function in our polymerizations. On the one hand, it acts as an alcohol co-initiator and on the other hand, it constitutes a hydrophilic polymer block. *Catalysts 2* to *5* were tested for the ROP of *L*-lactide in the presence of m-PEG-OH to produce the PEG-co-PLLA amphiphilic copolymer.

Entry	catalyst	<i>L</i> -lactide ^a	PEG (1900) ^a	T (°C)	Time ^b (min.)	Conversion ^c %	M _n theo ^d (g/mol)	M _n GPC ^e (g/mol)	PDI
1	2	150	3	90	30	47	5290	5337	1.04
2	2	150	3	90	45	63	6444	6967	1.16
3	2	150	3	90	90	100	9112	9990	1.06
4	2	100	5	90	48	70	3919	4908	1.05
5	2	100	5	90	68	100	4785	7006	1.25
6	3	100	5	90	25	78	4150	6159	1.13
7	3	100	5	90	44	84	4324	6837	1.20
8	3	100	5	90	77	100	4785	7232	1.22
9	4	100	5	70	55	41	3083	2784	1.12
10	4	100	5	70	90	52	3400	3131	1.14
11	4	100	5	70	100	100	4785	6284	1.13
12	5	100	5	-35	0.8	57	3544	2568	1.11
13	5	100	5	-35	1	66	3804	3143	1.27
14	5	100	5	-35	4	100	4785	5315	1.20

Polymerization conditions: [Monomer]₀ for *catalyst 2, 3* and *4* = 1 M, [Monomer]₀ = 0.5 M for *catalyst 5*. Toluene, 90 °C, DCM, RT or -35 °C.

^a Equiv. versus initiator. ^b Reaction time. ^c Monomer conversion. ^d Calculated using $M_{n\text{theo}} = (([L\text{-Lactide}]_0/[PEG]_0 \times M_{L\text{-lactide}} \times \text{conv.}) + 1900)$. ^e Measured by GPC in THF (30 °C) using PS standards and corrected by applying the appropriate correcting factor (0.58).

Table 1: Results of the ROP of *L*-lactide initiated by species *2, 3, 4* and *5*

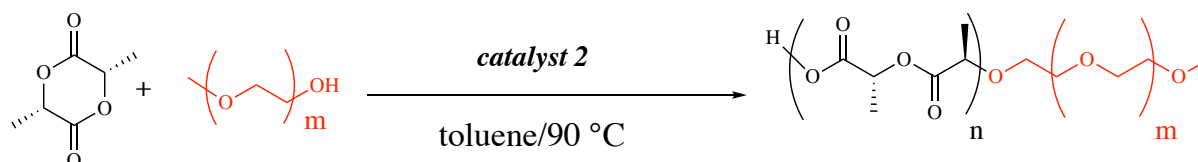


Figure 9: ROP of *L*-lactide by *2*/m-PEG-OH system

Using **2** as catalyst, the copolymerization effectively occurs with the quantitative polymerization of 150 equivalents of *L*-lactide in presence of 3 equivalents of PEG within 1h30 at 90 °C (**entry 3, Table 1**) to yield narrow disperse PEG-*co*-PLLA (PDI: 1.06) materials, as deduced from SEC data (**Figure 10**).

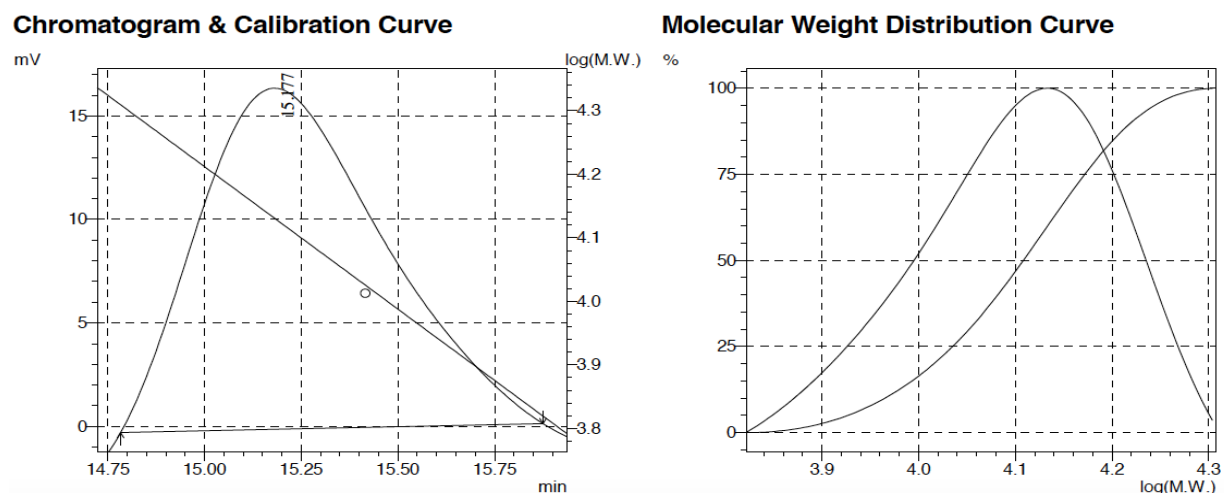


Figure 10: SEC traces of isolated PEG-*co*-PLLA prepared by polymerization of *L*-lactide initiated by the *catalyst 2*/PEG system. (Conditions: [Lactide]₀ = 1 M, 150 equiv. *L*-lactide, 3 equiv. PEG(1900), 90 °C, toluene, 1h30, total conv.).

The controlled character of the present ROP system is further demonstrated by kinetic data, with an observed first-order dependence in monomer ($k_{app} = 1.76 \times 10^{-2} \text{ min}^{-1}$) (**Figure 11**) and a linear correlation between the M_n value of the formed PEG-*co*-PLLA and *L*-LA conversion during the polymerization reaction (**Figure 12**).

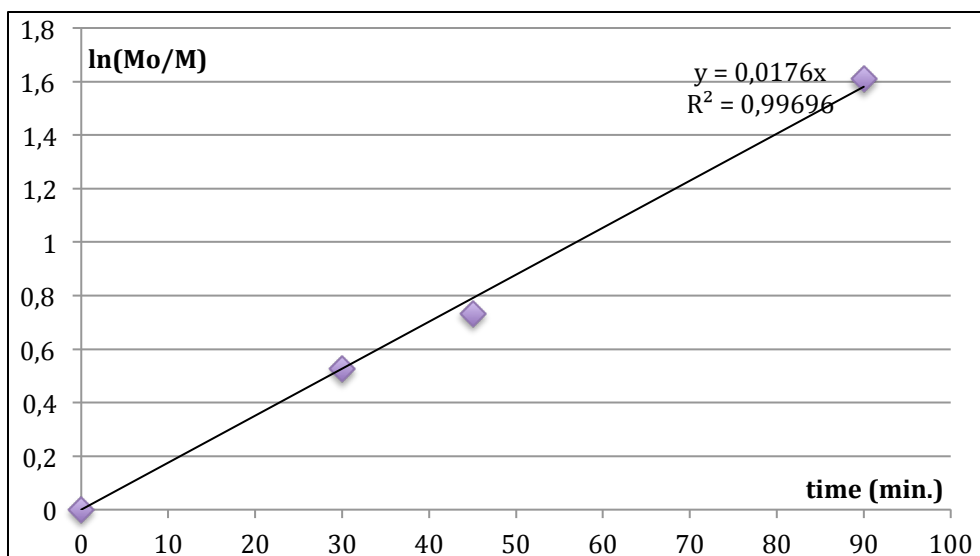


Figure 11: Plot of $\ln(M_0/M)$ as a function of time in the ROP of *L*-Lactide using *catalyst 2* and PEG as initiator. (Conditions: $[L\text{-lactide}]_0 = 1 \text{ M}$, 150 equiv. in *L*-lactide, 3 equiv. in PEG(1900) initiator, toluene, 90 °C, 1h30, total conv.).

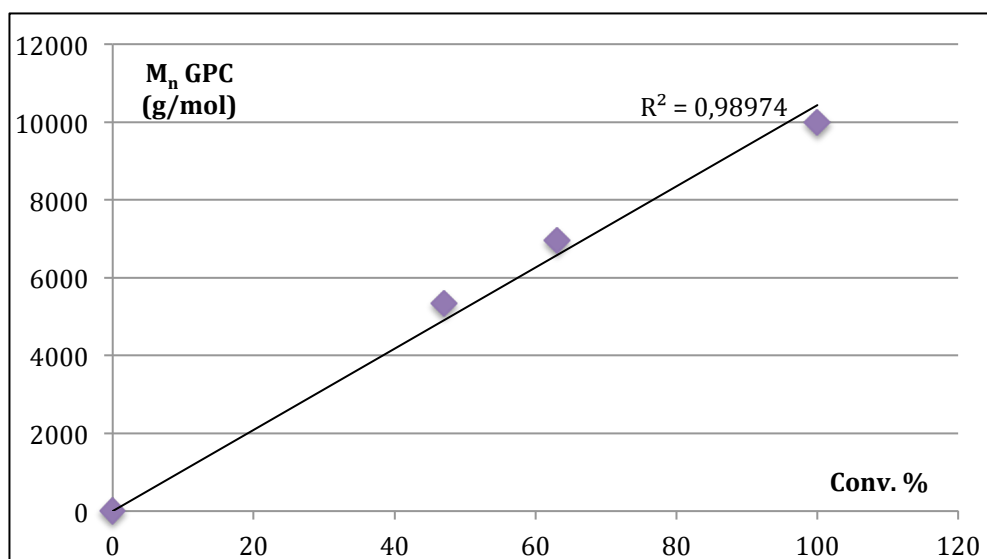


Figure 12: Plot of M_n as a function of the conv. in the ROP of *L*-lactide using *catalyst 2* and PEG(1900) as initiator. (Conditions: $[L\text{-lactide}]_0 = 1 \text{ M}$, 150 equiv. in *L*-lactide, 3 equiv. in PEG(1900), toluene, 90 °C, 1h30, total conv.).

The MALDI-TOF spectrum of the prepared PEG-co-PLLA with the Al(III) *catalyst 2* agrees with a linear copolymer confirming the presence of a PEG(1900) moiety covalently bonded to a PLLA segment in the final material (**Figure 13**).

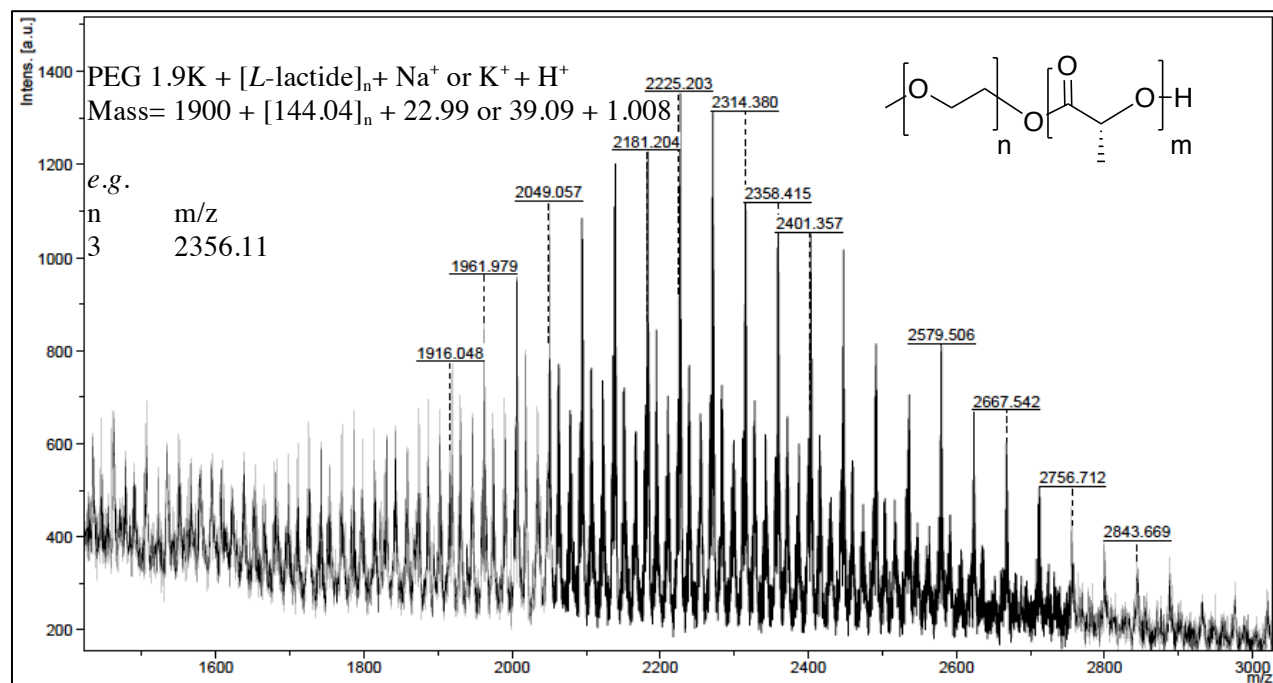


Figure 13: MALDI-TOF of the PLLA prepared by ROP of *L*-lactide initiated by PEG and *catalyst 2*. (Conditions: $[L\text{-lactide}]_0 = 1$ M, 150 equiv. *L*-lactide, 3 equiv. of PEG(1900), toluene, 90 °C, polymer isolated at 100% conv. to PEG-co-PLLA).

III. 3. ROP of PEG-co-PLLA with *catalyst 3*

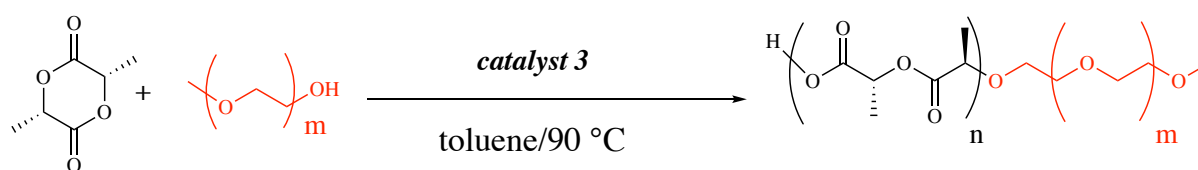


Figure 14: ROP of *L*-lactide by 3/*m*-PEG-OH system

The Ga amido *catalyst 3* was also found to be an active ROP initiator at 90 °C. The total conversion of 100 equivalents of *L*-lactide with 5 equivalents of PEG initiator was performed within 1h17 to produce narrow disperse PEG-co-PLLA copolymers (**entry 8**, **Table 1**). Kinetic studies carried out for *catalyst 3* are all consistent with a ROP proceeding in a controlled manner, with for instance an observed first-order dependence (in monomer) of

the reaction rate ($k_{app} = 4.2 \times 10^{-2} \text{ min}^{-1}$, **Figure 15**). In addition, the PEG-*co*-PLLA chain length growth correlates well with monomer conversion (**Figure 16**).

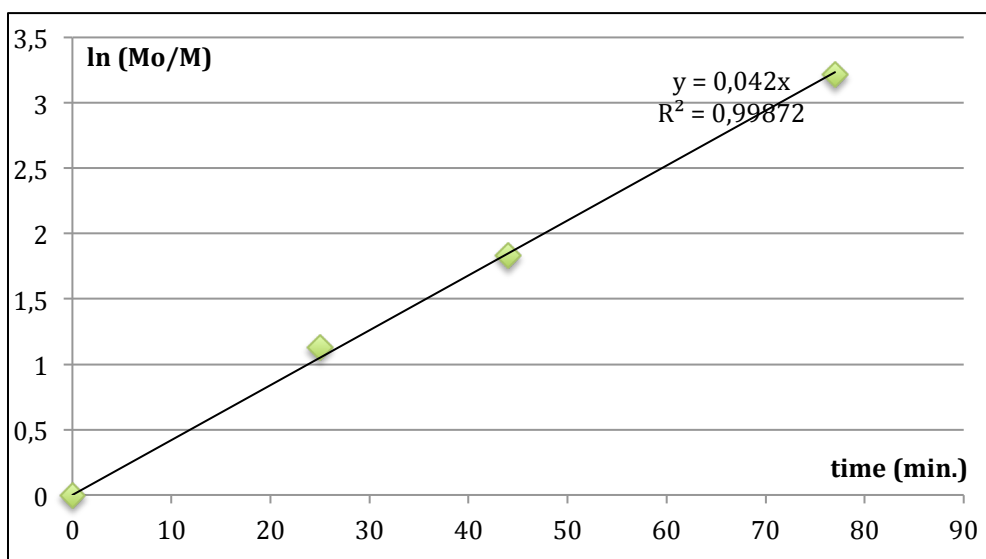


Figure 15: Plot of $\ln(M_0/M)$ as a function of time in the ROP of *L*-lactide using *catalyst 3* and PEG as initiator. (Conditions: $[L\text{-lactide}]_0 = 1 \text{ M}$, 100 equiv. in *L*-lactide, 5 equiv. in PEG(1900) initiator, toluene, 90 ° C, 1h17).

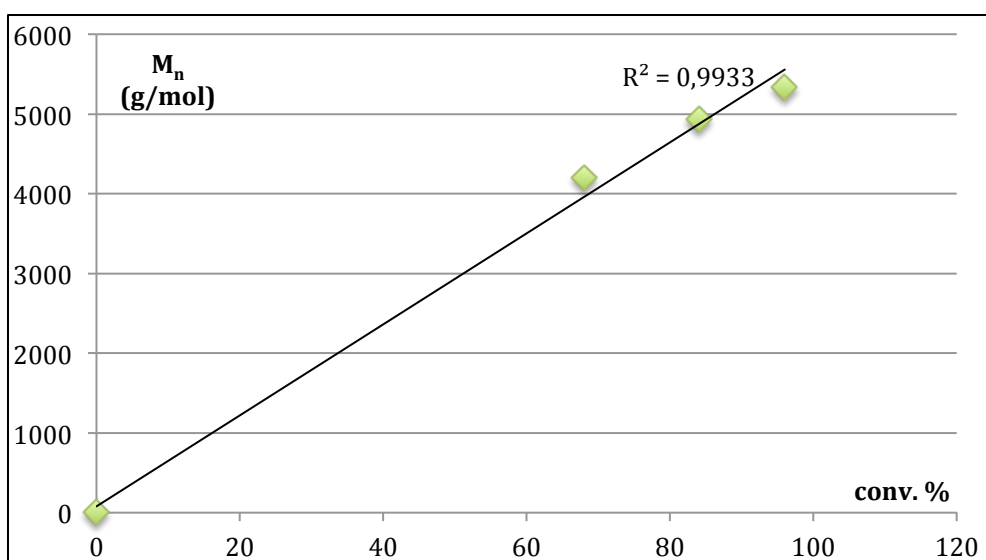


Figure 16: Plot of M_n as a function of the conv. in the ROP of *L*-lactide using *catalyst 3* and PEG(1900) as initiator. (Conditions: $[L\text{-lactide}]_0 = 1 \text{ M}$, 100 equiv. in *L*-lactide, 5 equiv. in PEG, toluene, 90 ° C, 1h17).

The MALDI-TOF spectrum of the prepared PEG-co-PLLA (with the initiating system *catalyst 3*/PEG(1900)) also agrees with a linear PEG-*b*-PLLA copolymer (**Figure 17**).

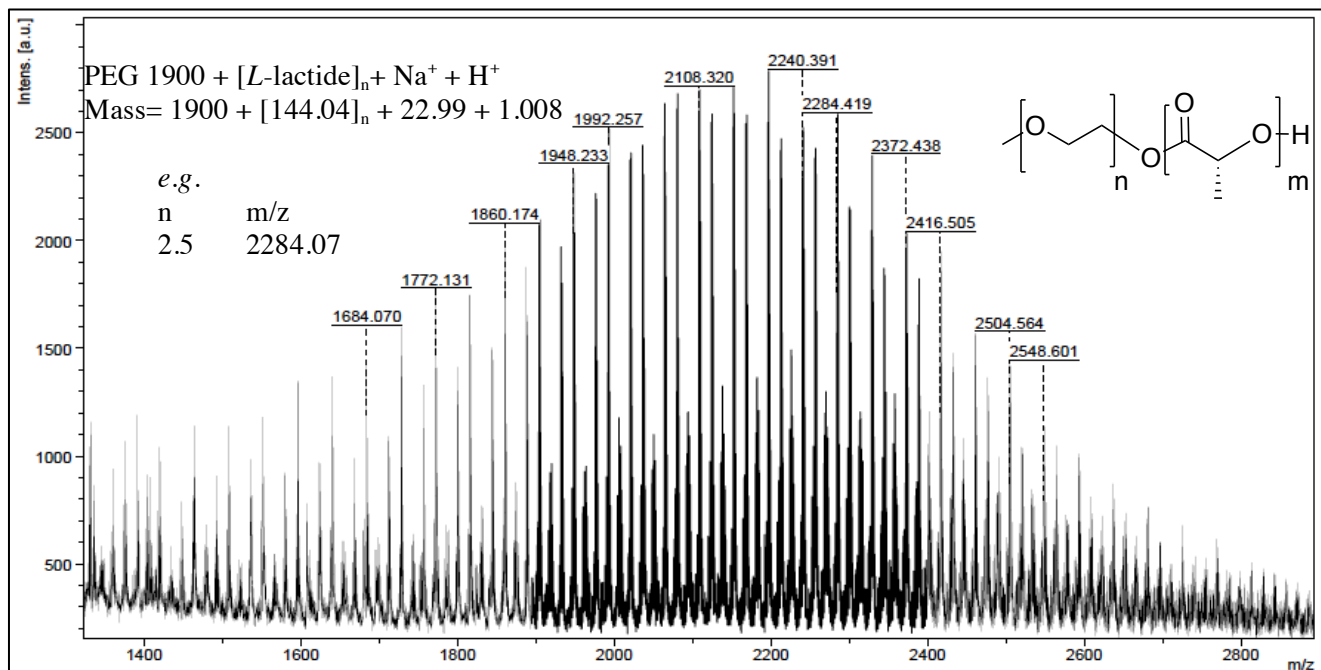


Figure 17: MALDI-TOF of the PEG-co-PLLA prepared by ROP of *L*-lactide initiated using PEG(1900) and *catalyst 3*. (Conditions: [Lactide]₀ = 1 M, 100 equiv. *L*-lactide, 5 equiv. PEG(1900), toluene, 90 °C, polymer isolated at 100% conv. to PEG-co-PLLA).

III. 4. Comparison of the activity of the metal center between the two κ^3 -*N,O,N* catalysts

To compare the influence of the metal center in the ROP of PEG-co-PLLA, the aluminium amido compound (*catalyst 2*) and the gallium amido compound (*catalyst 3*) were tested under identical conditions (toluene, 80 °C, 150 equivalents of *L*-lactide, 3 equivalents of PEG(1900), 130 min.). After 130 minutes of reaction, the polymerization is quantitative with κ^3 -*N,O,N*-[(C₆H₁₁)NH-C₆H₄]₂OGaMe₂ *catalyst 3* with an apparent rate constant found to be 2.46 x 10⁻² min⁻¹ whilst the same reaction in presence of the aluminium amido catalyst κ^3 -*N,O,N*-[(C₆H₁₁)NH-C₆H₄]₂OAlMe₂ *catalyst 2* led to a 89% conversion to PEG-PLLA within 130 min. with an apparent rate constant of 1.67 x 10⁻² min⁻¹ (**Figure 18**).

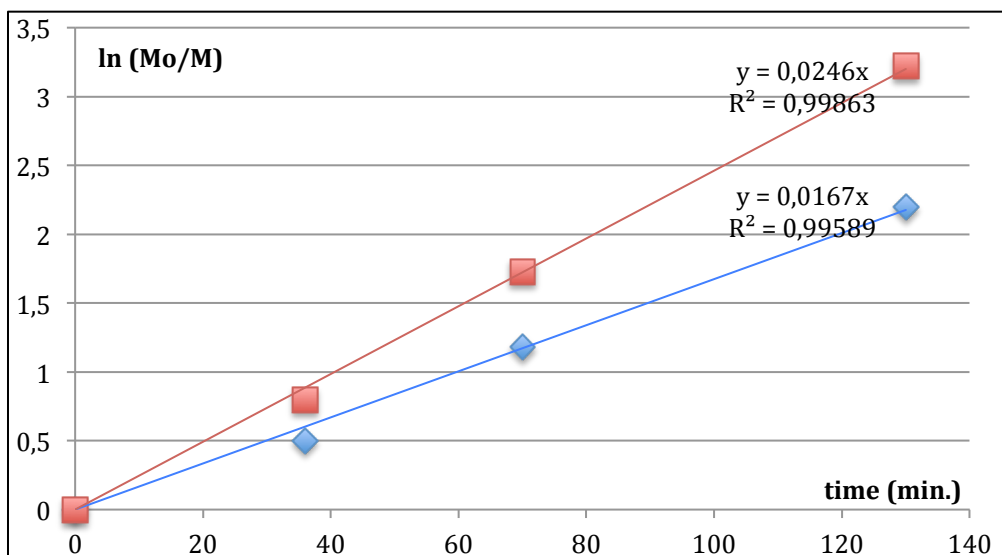


Figure 18: Kinetic comparison of *catalyst 2* vs. *3* for the ROP of *L*-lactide. (Conditions: $[\text{Lactide}]_0 = 1 \text{ M}$, 150 equiv. in *L*-lactide, 3 equiv. in PEG(1900) initiator, toluene, 80 °C, 130 min.). Plot of $\ln(M_0/M)$ as a function of time in the ROP of PLLA using *catalyst 2* (blue line), *catalyst 3* (red line) and PEG as initiator.

The ^1H NMR spectrum obtained with the *catalyst 3* is in agreement with a total conversion, confirmed by the integration of 5 protons for the PEG signal appearing as a singlet at 3.64 ppm versus protons of the PLLA polymer signals: the methyl doublet at 1.58 ppm and the CH multiplet between 5.14 and 5.19 ppm (**Figure 19**). Both GPC data agree with a monomodal and well-defined polymer of narrow polydispersity (PDI: 1.09) with *catalyst 3* (**Figure 20**) and (PDI: 1.16) with *catalyst 2* (**Figure 22**), consistent with a controlled ROP process.

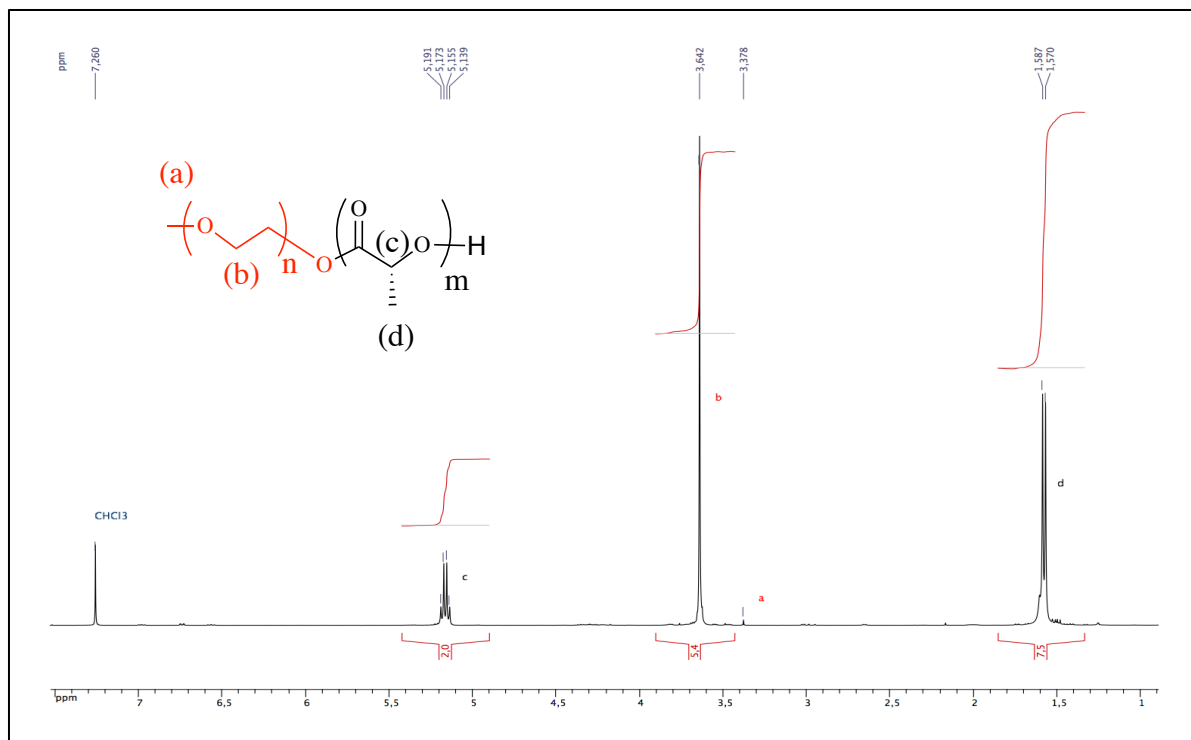


Figure 19: ^1H NMR (CDCl_3 , 400 MHz) spectrum of PEG-co-PLLA using *catalyst 3*/PEG system. (Conditions: $[\text{L-lactide}]_0 = 1 \text{ M}$, 150 equiv. *L*-lactide, 3 equiv. PEG(1900), 130 min., toluene, 80°C , total conv.).

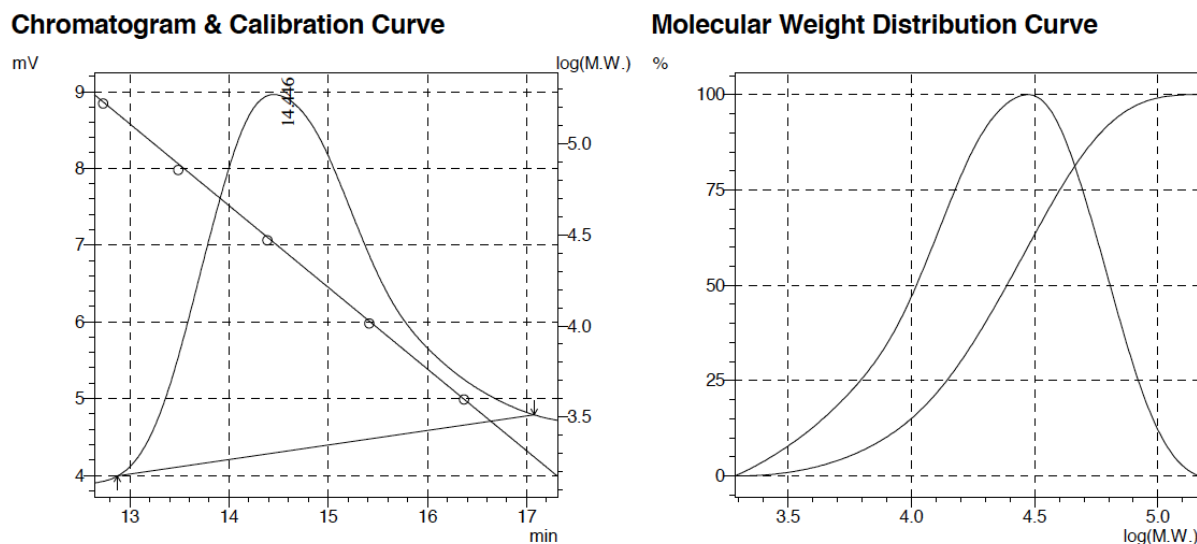


Figure 20: SEC traces of isolated PEG-co-PLLA prepared by ROP of *L*-lactide initiated by the *catalyst 3*/PEG system. (Conditions: $[\text{Lactide}]_0 = 1 \text{ M}$, 150 equiv. *L*-lactide, 3 equiv. PEG(1900), 80°C , toluene, 130 min., total conv.).

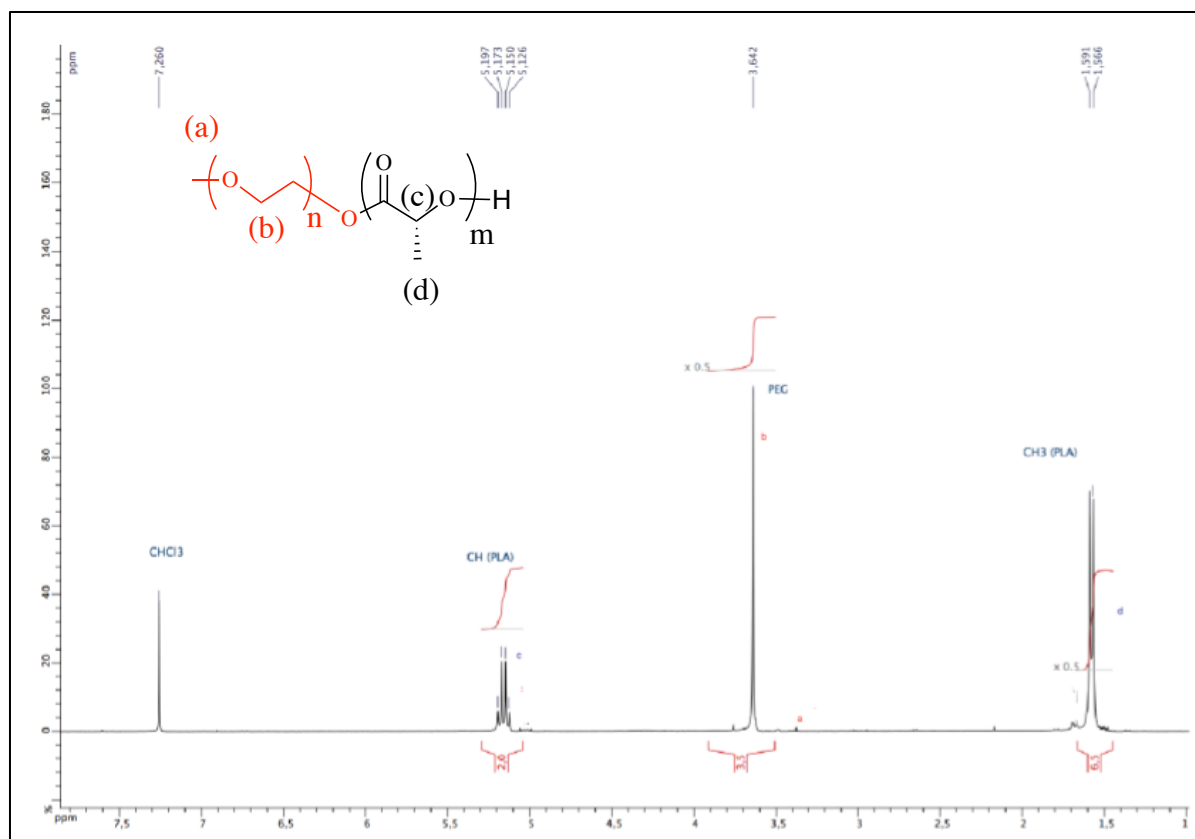


Figure 21: ^1H NMR (CDCl_3 , 400 MHz) spectrum of PEG-co-PLLA using *catalyst 2*/PEG system. (Conditions: $[\text{L-lactide}]_0 = 1 \text{ M}$, 150 equiv. *L*-lactide, 3 equiv. PEG(1900), 130 min., toluene, $80 \text{ }^\circ\text{C}$, 89% conv., isolated polymer).

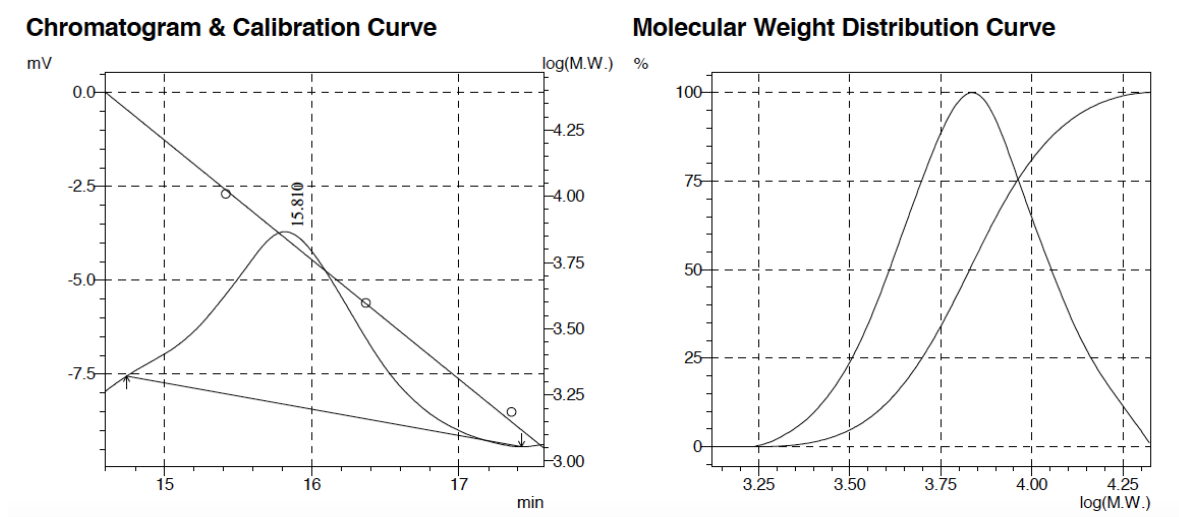


Figure 22: SEC traces of isolated PEG-co-PLLA prepared by ROP of *L*-lactide initiated by the *catalyst 2*/PEG system. (Conditions: $[\text{Lactide}]_0 = 1 \text{ M}$, 150 equiv. *L*-lactide, 3 equiv. PEG(1900), $80 \text{ }^\circ\text{C}$, toluene, 130 min., 89%).

The Ga amido species **3** is thus a more active *L*-lactide ROP (in presence of PEG(1900) initiator) than its Al(III) analog **2**, which can be explained by the soft nature of this metal.⁴³ It is important to point out however that the cost of gallium is much higher than that of aluminium (the price of aluminium: 140€/Kg (99.9%) whereas the price of gallium is 700€/50 g (99.99%)).^{44,45}

IV. Use of a biocompatible zinc catalyst for PEG-*co*-PLLA copolymerization

IV. 1. Zinc properties

Zinc is the 24th most abundant element in the crust of the Earth.⁴⁶ This common metal is naturally present in many natural materials such as air, water or soil⁴⁷ and it is one of the most abundant nutritionally essential elements in the human body (tissues, muscles, bones, skin and liver).⁴⁸ Zinc is one of the utilised metals that provides essential services at low cost in our society (*e.g.*: buildings, machinery, agriculture, chemicals, food in the pharmaceutical industry).⁴⁹ In biological systems, it has antioxidant properties⁵⁰ and is used as a pharmacologic agent under clinical controlled situations.⁵¹ Also, Zn(II) salts are interesting for their good biocompatible and environmentally friendly properties.⁵²

IV. 2. Synthesis of $\text{tol}\cdot\text{Zn}(\text{C}_6\text{F}_5)_2$ catalyst

The simple and discrete Zn^{II} Lewis acid $\text{Zn}(\text{C}_6\text{F}_5)_2$, a readily available compound,⁵³ was studied as ROP catalyst for the production of PEG-*co*-PLLA copolymers. $\text{Zn}(\text{C}_6\text{F}_5)_2(\text{toluene})$ was prepared according to a literature procedure by reaction between dimethylzinc and trispenta(fluorophenyl)borane in toluene at room temperature (**Figure 23**).⁵⁴

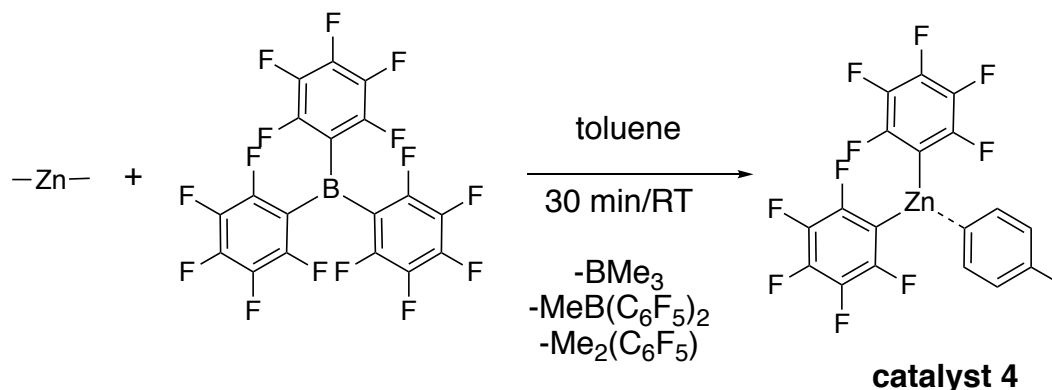
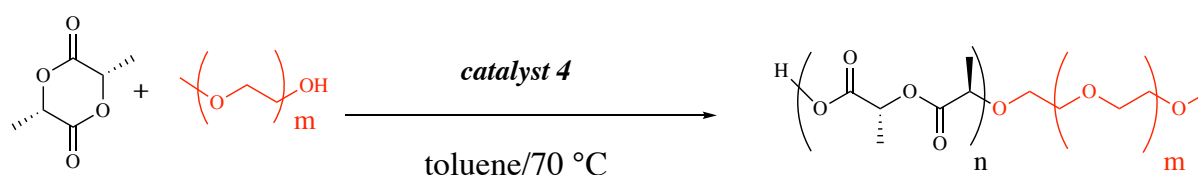


Figure 23: Preparation of $\text{tol}\cdot\text{Zn}(\text{C}_6\text{F}_5)_2$ catalyst

IV. 3. ROP of *L*-lactide in presence of PEG with $\text{tol}\cdot\text{Zn}(\text{C}_6\text{F}_5)_2$ catalyst **4**Figure 24: ROP of *L*-lactide by 4/*m*-PEG-OH system

Entry	catalyst	<i>L</i> -lactide ^a	PEG(1.9K) ^a	T (°C)	Time ^b (min.)	Conversion ^c %	$M_{n\text{theo}}$ ^d (g/mol)	$M_{n\text{GPC}}$ ^e (g/mol)	PDI
1	4	100	5	70	55	41	3083	2784	1.12
2	4	100	5	70	90	52	3400	3131	1.14
3	4	100	5	70	100	100	4785	6284	1.13

Polymerization conditions: $[\text{Monomer}]_0 = 1$ M. Toluene, 70 °C.

^a Equiv. versus initiator. ^b Reaction time. ^c Monomer conversion. ^d Calculated using $M_{n\text{theo}} = (([L\text{-Lactide}]_0/[PEG]_0 \times M_{L\text{-lactide}} \times \text{conv.}) + 1900)$. ^e Measured by GPC in THF (30 °C) using PS standards and corrected by applying the appropriate correcting factor (0.58).

Table 2: Summary of the ROP of *L*-lactide initiated by species **4**

$\text{Tol}\cdot\text{Zn}(\text{C}_6\text{F}_5)_2$ catalyst (**catalyst 4**) was found to be active at 70 °C in the ROP of 100 equivalents of *L*-lactide in the presence of 5 equivalents of PEG(1900) initiator. Monomodal SEC traces and narrow polydispersity (PDI: 1.13) agree with the formation of a well-defined material (**Figure 25**). Complete consumption of the monomer to PEG-*b*-PLLA was relatively fast in (100 min., 70 °C). Kinetic studies carried out for the Zn **catalyst 4** are consistent with a ROP proceeding in a controlled manner with an apparent first-order kinetic ($k_{\text{app}} = 4.54 \times 10^{-2} \text{ min}^{-1}$) towards *L*-lactide (**Figure 26**), with a linear correlation between the M_n obtained by GPC (corrected) and monomer conversion during the polymerization process (**Figure 27**).

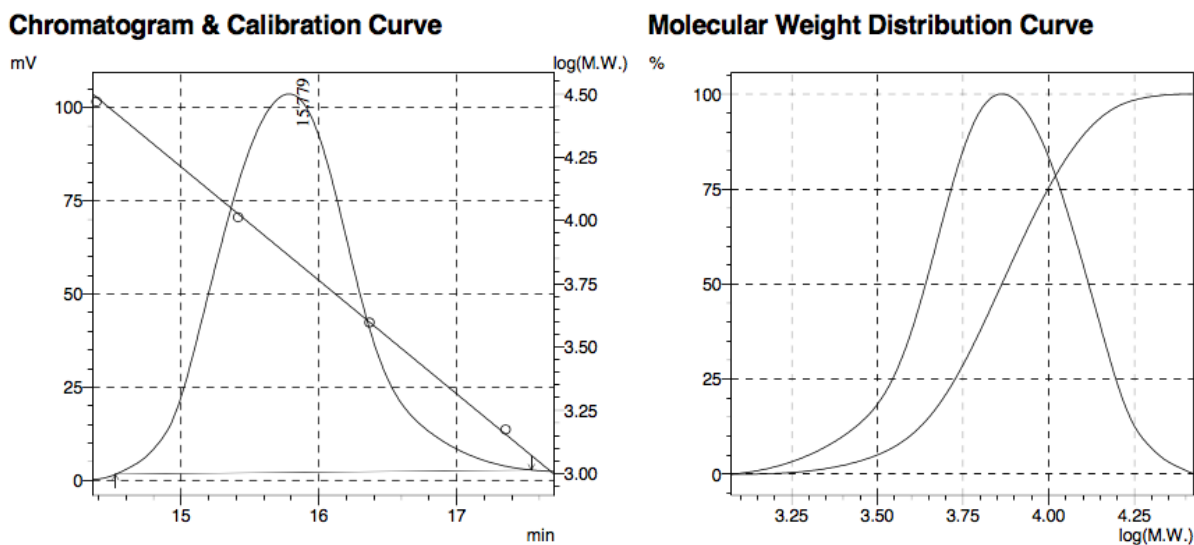


Figure 25: SEC traces of isolated PEG-co-PLLA prepared by ROP of *L*-lactide initiated by the system *catalyst 4*/PEG. (Conditions: $[L\text{-lactide}]_0 = 1 \text{ M}$, 100 equiv. *L*-lactide, 5 equiv. PEG(1900), toluene, 70 °C, 100 min., quantitative conv.).

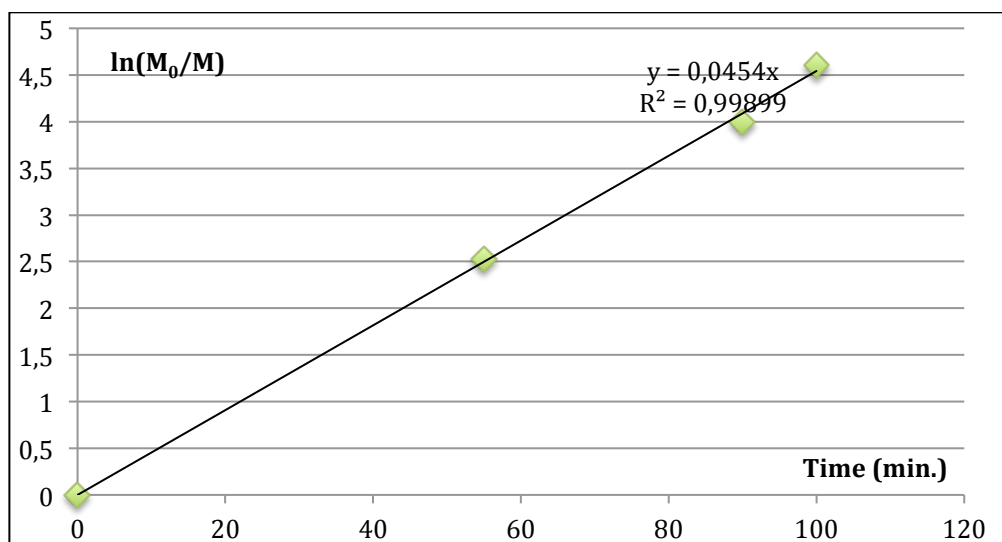


Figure 26: Plot of $\ln(M_0/M)$ as a function of time in the ROP of *L*-lactide using *catalyst 4* and PEG as initiator. (Conditions: $[Lactide]_0 = 1 \text{ M}$, 100 equiv. in *L*-lactide, 5 equiv. in PEG(1900) initiator, toluene, 70 °C, 100 min., total conv.).

V. Use of a magnesium catalyst for ROP of *L*-lactide in presence of PEG

V. 1. Magnesium properties

Magnesium is the eighth most abundant element in the earth's crust with a common tendency to +II oxidation states and it has a similar ionic radius as zinc.⁵⁵ Due to its low density, this element has been recognised for many years as the lightest structural metal currently available in the world (magnesium is 25% lighter than aluminum).⁵⁶ Therefore, it has very important applications in areas ranging from the automobile industry^{57,58} to biomedical applications⁵⁹, like resorbable metal implants.⁶⁰ In addition to being a biocompatible element,⁶¹ Mg(II) is non-toxic and inexpensive.⁶² Magnesium is an essential element to all life on earth, playing great roles in the human body.⁶³ Mg(II) is necessary for more than 300 metabolic reactions⁶⁴ and has an important role in the structure of the skeleton and muscles.⁶⁵

V. 2. Synthesis of Mg(THF)₂(C₆F₅)₂ catalyst **5**

Magnesium complexes are known to be very efficient catalysts for the ROP of lactide, though their limited stability towards protic impurities may seriously hinder their usefulness. They may allow the rapid immortal ROP of lactide (in the presence of an alcohol source) with high catalyst activity and remarkable catalyst efficiency.^{66,67}

By analogy with Zn(C₆F₅)₂, which has showed to be an effective ROP catalyst (*vide supra*), a Mg(II) analogue, *i.e.* the bis-THF adduct Mg(THF)₂(C₆F₅)₂ (**Figure 29**), was prepared as a potentially robust Mg-based lactide ROP catalyst. Thus, the stoichiometric reaction between 1-bromopentafluorophenylbenzene in THF and dibutylmagnesium (heptene solution) afforded Mg(THF)₂(C₆F₅)₂ (**5**) through a Br/Mg(II) exchange reaction. Species **5** was isolated in a quantitative yield (**Figure 29**).

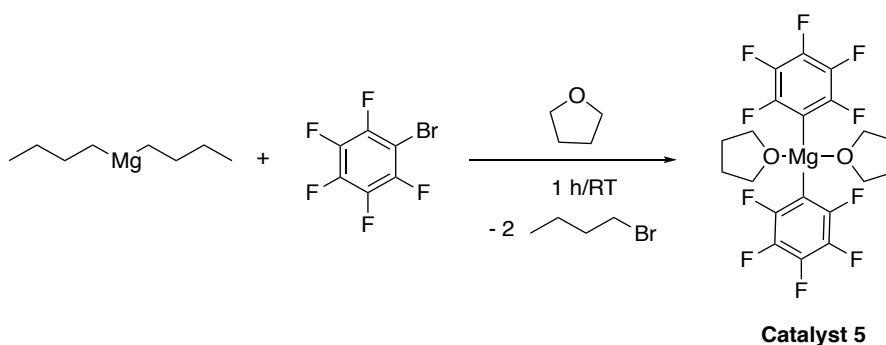


Figure 29: Preparation of Mg(THF)₂(C₆F₅)₂ catalyst **5**

V. 3. ROP of PEG-co-PLLA with Mg(THF)₂(C₆F₅)₂ catalyst 5

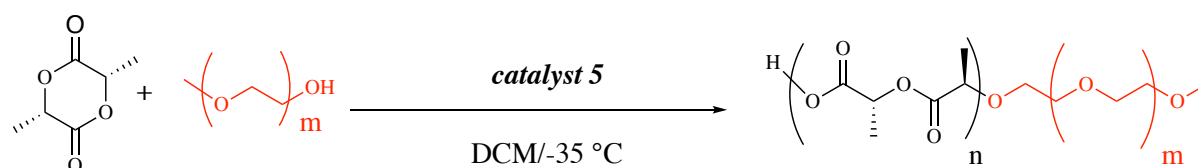


Figure 30: ROP of *L*-lactide by 5/*m*-PEG-OH system

Entry	catalyst	<i>L</i> -lactide ^a	PEG (1.9K) ^a	T (°C)	Time ^b (min)	Conversion ^c %	M _n theo ^d (g/mol)	M _n GPC ^e (g/mol)	PDI
1	5	100	5	-35	0.8	57	3544	2568	1.11
2	5	100	5	-35	1	66	3804	3143	1.27
3	5	100	5	-35	4	100	4785	5315	1.20

Polymerization conditions: [Monomer]₀ = 0.5 M, DCM, -35 °C.

^a Equiv. versus initiator. ^b Reaction time. ^c Monomer conversion. ^d Calculated using $M_{n \text{ theo}} = (([L\text{-Lactide}]_0/[PEG]_0 \times M_{L\text{-lactide}} \times \text{conv.}) + 1900)$. ^e Measured by GPC in THF (30 °C) using PS standards and corrected by applying the appropriate correcting factor (0.58).

Table 4: Summary of the ROP of *L*-lactide initiated by species 5

The Mg *catalyst 5* displays an extraordinarily high activity for the ROP of PEG-co-PLLA but it is essential to decrease the initial monomer concentration (to 0.5 M) and reaction temperature for a controlled ROP process. Indeed, with [L-LA]₀ = 1 M, the ROP of a 100/5 *L*-LA/*m*-PEG-OH mixture (1 equivalent of *catalyst 5*) was complete within a few seconds but SEC traces agree with a bimodal GPC (**Supporting data: Figure 2**), in line with a poorly controlled polymerization reaction. In addition, MALDI-TOF spectrometric data agree with the presence of cyclic PLLA, suggesting substantial intramolecular transesterifications during PLA chain growth. With [L-LA]₀ = 0.5 M, 100 equivalents of *L*-lactide with 5 equivalents of PEG(1900) are completely polymerized within four minutes in cold dichloromethane (-35 °C) (**entry 14, Table 1**) to yield PEG-*b*-PLA through a controlled ROP, as deduced from all data. In particular, SEC traces agree with the production of a chain-length controlled and narrowly disperse material (**Figure 31**).

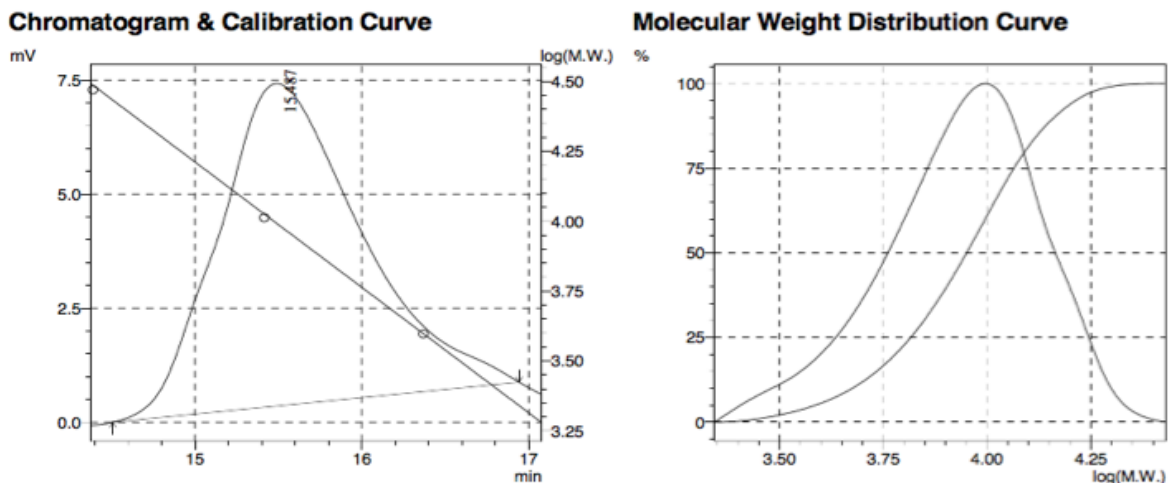


Figure 31: SEC traces of isolated PEG-co-PLLA prepared by ROP of *L*-lactide initiated by the system *catalyst 5*/PEG. (Conditions: $[L\text{-lactide}]_0 = 0.5$ M, 100 equiv. *L*-lactide, 5 equiv. PEG(1900), DCM, - 35 °C, 4 min., quantitative conv.).

Kinetic data also support a controlled ROP process: the reaction rate follows a pseudo first-order ($k_{app} = 1.1448 \text{ min}^{-1}$) with respect to monomer (**Figure 32**) and a linear correlation between the M_n chain length values and monomer conversion is observed as the ROP proceeds (**Figure 33**). The experimental M_n values of the formed PEG-co-PLLA match well the theoretical values (**entries 12, 13 and 14, Table 1**).

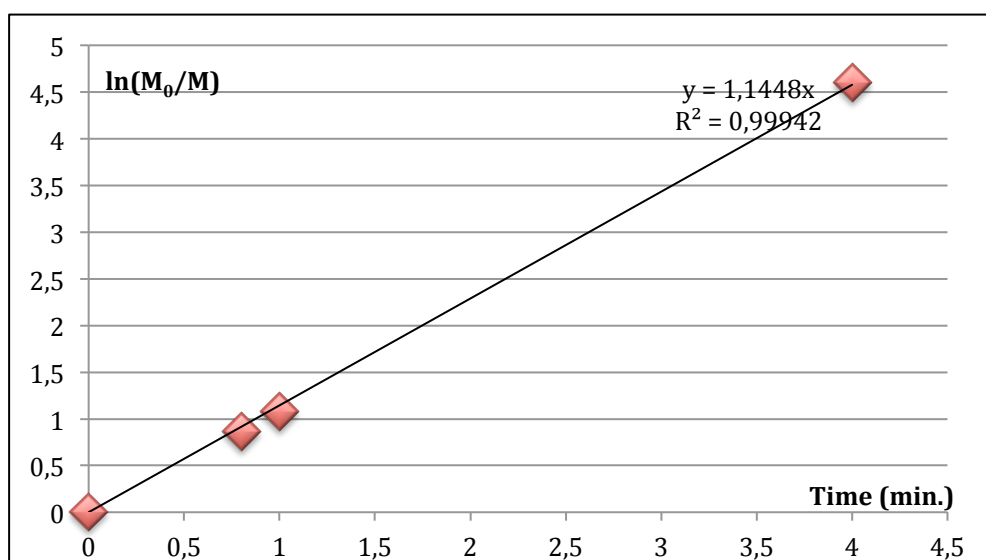


Figure 32: Plot of $\ln(M_0/M)$ as a function of time in the ROP of *L*-lactide using *catalyst 5* and PEG as initiator. (Conditions: $[Lactide]_0 = 0.5$ M, 100 equiv. in *L*-lactide, 5 equiv. in PEG(1900) initiator, DCM, - 35 °C, 4 min.).

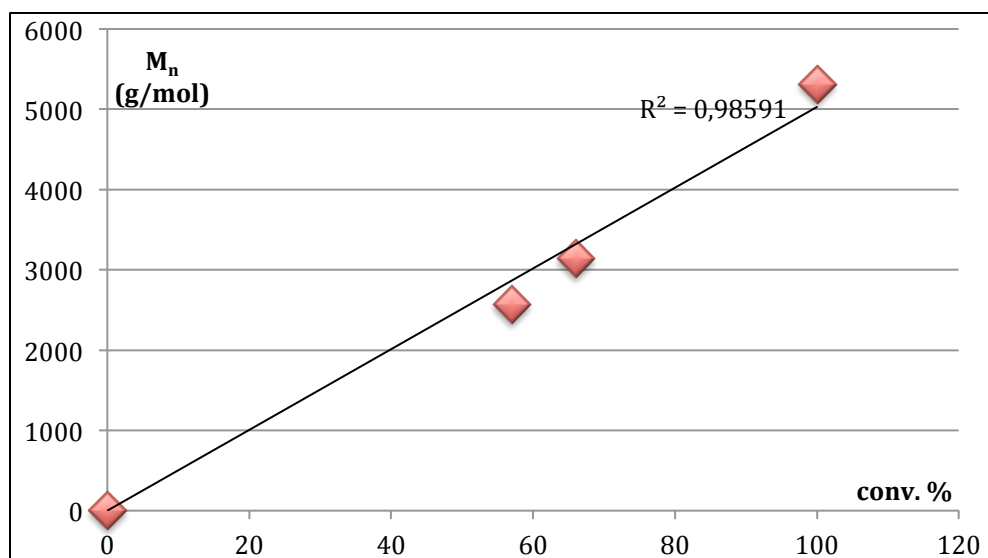


Figure 33: Plot of M_n as a function of the conv. in the ROP of *L*-lactide using *catalyst 5* and PEG(1900) as initiator. (Conditions: $[Lactide]_0 = 0.5$ M, 100 equiv. in *L*-lactide, 5 equiv. in PEG, DCM, - 35 °C, 4 min.).

Importantly, the MALDI-TOF spectrometric data confirmed the formation of a linear amphiphilic PEG-*b*-PLLA block copolymer (**Figure 34**).

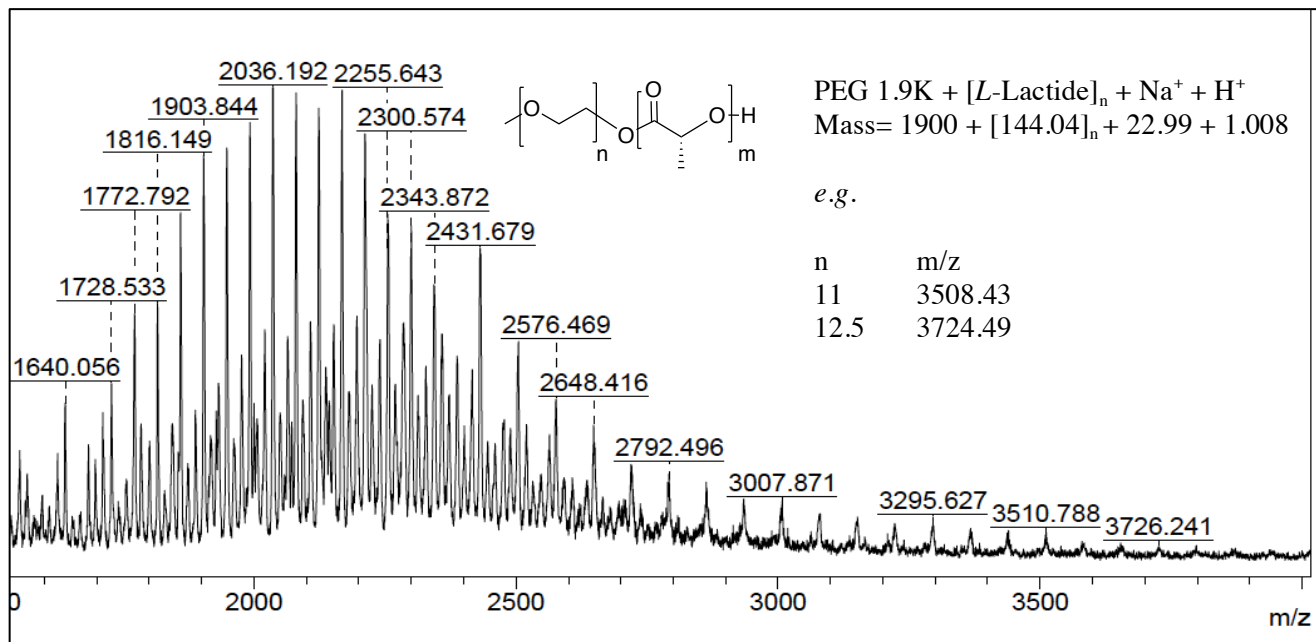


Figure 34: Zoom-in of the MALDI-TOF spectrum of the PEG-*co*-PLLA block prepared by ROP of *L*-lactide initiated using *catalyst 5*/PEG(1900). (Conditions: $[L-lactide]_0 = 0.5$ M, 100 equiv. *L*-lactide, PEG(1900): 5 equiv., DCM, - 35 °C, 4 min., copolymer isolated at 100% conv.).

Thus, the Al(III), Ga(III), Zn(II) and Mg(II)-based *catalysts 2-5* were all demonstrated to successfully mediate the ROP of PEG-*co*-PLLA under appropriate experimental conditions. The amphiphilic nature of the produced copolymers is also further indicated by NMR data of all prepared PEG-*co*-PLLA copolymers. In line with a biphasic medium, the ^1H NMR spectra in D_2O of all materials only exhibit the PEG signal at 3.75 ppm. An example of these NMR spectra is illustrated on **Figure 35**.

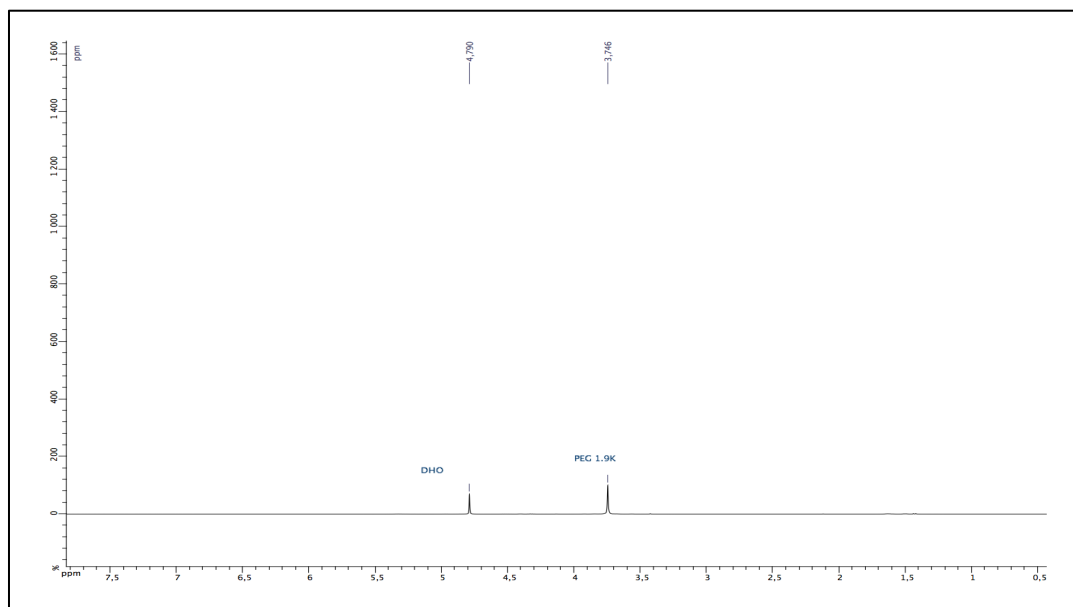


Figure 35: ^1H NMR (D_2O , 400 MHz) spectrum of PEG-*co*-PLLA using *catalyst 4*/PEG system. (Conditions: $[\text{L-lactide}]_0 = 1 \text{ M}$, 100 equiv. *L*-lactide, 5 equiv. PEG(1900), 100 min., toluene, 70 °C, total conv., isolated polymer).

VI. Bulk conditions

Bulk polymerization,⁶⁸ as implemented in industry for the production of PLLA via ROP of lactide, is carried out without any solvent or dispersant and is thus the simplest, cost-effective (and environmentally friendly) polymerization process in terms of formulation.⁶⁹ The reaction proceeds by heating the mixture in order to dissolve the initiator and catalyst in the melted monomer. The PEG-*co*-PLLA copolymerization was performed under bulk condition for each catalyst using 100 equivalents of *L*-lactide, 5 equivalents of PEG(1900) initiator and 1 equivalent of catalyst (130 °C, 2 h).

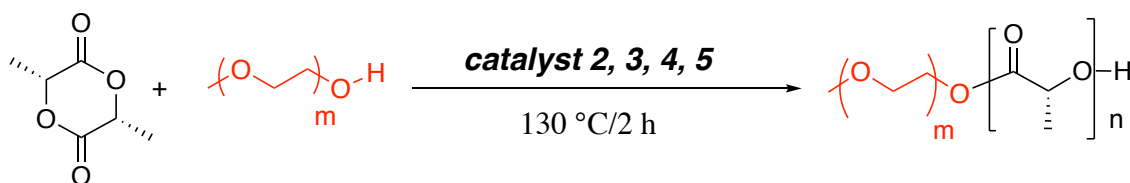


Figure 36: ROP of *L*-lactide using complexes 2, 3, 4 and 5/*m*-PEG-OH system

Entry	catalyst	Conversion ^a %	$M_{n \text{ theo}}^b$ (g/mol)	$M_{n \text{ GPC}}^c$ (g/mol)	PDI
1	2	100	4785	5084	1.38
2	3	80	4208	4927	1.31
3	4	100	4785	4928	1.56
4	5	85	4352	3955	1.36

Polymerization conditions: 130 °C, 2 h.

^a Monomer conversion. ^b Calculated using: $M_{n \text{ theo}} = ([L\text{-Lactide}]_0/[PEG]_0 \times M_{L\text{-lactide}} \times \text{conv.}) + 1900$. ^c Measured by GPC in THF (30 °C) using standards PS and corrected by the appropriate adjustment factor (0.58 for the lactide)

Table 2: Results of bulk ROP data for species 2, 3, 4 and 5.

The bulk conditions have successfully led to the different PEG-co-PLLA blocks. The molecular weights deduced from SEC data are close to theoretical values for all catalysts. We can note that, as typically observed, the polydispersities of the produced materials are a little bit broader than in solution polymerizations (approximately 1.3 for *catalysts 2, 3* and *5*) and larger for *catalyst 4* (PDI= 1.56).

VII. Conclusion

As a conclusion, block copolymers of the type PEG-*b*-PLA were synthesized using various metal catalysts under relatively mild conditions, but also in absence of solvent. The terminal hydroxyl groups of PEG have been used as the initiating groups to synthesize block copolymers while bringing an amphiphilic character to the copolymers. An aluminium amido (*catalyst 2*), one gallium amido (*catalyst 3*), and Zn(II) and Mg(II) centers supported by two electron-withdrawing C_6F_5 groups *4* and *5* were successfully used as ROP catalysts. The kinetic performances of aluminium amido (*catalyst 2*) and gallium amido (*catalyst 3*)

were compared, with the Ga derivative being more active than its Al(III) counterpart. However both **2** and **3** allow a highly controlled ROP process to afford narrow disperse PEG-functionalized PEG-*co*-PLLA amphiphilic copolymers. Overall, the different metal *catalysts* **2-5** tested herein show a combination of high activity (especially the Mg *catalyst* **5**) and an excellent level of chain control under mild conditions. Notably, as a comparison, many PEG-*co*-PLLA copolymers blocks are typically prepared via the ROP of lactide at 130 °C using a Sn(Oct.)₂/PEG initiator.⁷⁰

VIII. References

- [1]. H. -J. Jang, C. Y. Shin, K. -B. Kim, *Toxicol. Res.* **2015**, *31*, 105-136.
- [2]. <http://www.sigmaaldrich.com/> (April 2019)
- [3]. A. A. D'souza, R. Shegokar, *EXPERT OPIN DRUG DIS* **2016**, *13*, 1257-1275.
- [4]. C. Özdemir, A. Güner, *Eur. Polym. J.* **2007**, *43*, 3068-3093.
- [5]. (a) E. E. Dormidontova, *Macromolecules* **2002**, *35*, 987-1001. (b) Poly(ethylene oxide) (PEO) is also called (PEG): C. Ren, R. J. Nap, I. Szleifer, *J Phys Chem B.* **2008**, *112*, 16238-16248.
- [6]. O. E. Philippova, S. I. Kuchanov, I. N. Topchieva, V. A. Kabanov, *Macromolecules* **1985**, *18*, 1628-1633.
- [7]. S. Magazu, *Physica B Condens Matter.* **1996**, *226*, 92-106.
- [8]. F. Fuertges, A. Abuchowski, *J. Control. Release* **1990**, *11*, 139-148.
- [9]. X. Y. Liu, J. -M. Nothias, A. Scavone, M. Garfinkel, J. M. Millis, *ASAIO J.* **2010**, *56*, 241-245.
- [10]. D. Shiaw-Guang Hu, H.-J. Liu, *Polym. Bull.* **1993**, *30*, 669-676.
- [11]. H. Ho, J. Lee, *MACROMOL RES.* **2011**, *19*, 815-821.
- [12]. B. Jeong, Y. H. Bae, D. S. Lee, S. W. Kim, *Nature* **1997**, *388*, 860-862.
- [13]. H. Zhang, H. Xia, J. Wang, Y. Li, *J. Control. Release* **2009**, *139*, 31-39.
- [14]. V. G. Kadajji, G. V. Betageri, *Polymers* **2011**, *3*, 1972-2009.
- [15]. R. Z. Xiao, Z. W. Zeng, G. L. Zhou, J. J. Wang, F. Z. Li, A. M. Wang, *IJN* **2010**, *5*, 1057-1065.
- [16]. A. S. Hoffman, *Adv Drug Delivery Rev.* **2002**, *43*, 1-12.
- [17]. B. Jeong, Y. H. Bae, D. S. Lee, S. W. Kim. *Nature.* **1997**, *388*, 860-862. PEO: poly(ethylene oxide)= PEG: poly(ethylene glycol).
- [18]. V. P. Torchilin, *Adv. Drug Deliv. Rev.* **2002**, *54*, 235-252.
- [19]. A. Rösler, G. W. M. Vandermeulen, H. -A. Klok, *Adv. Drug Deliv. Rev.* **2001**, *53*, 95-108.
- [20]. M. -C. Jones, J. -C. Leroux, *Eur. J. Pharm. Biopharm* **1999**, *48*, 101-111.
- [21]. K. J. Zhu, L. Xiangzhou, Y. Shilin, *J. Appl. Polym. Sci.* **1990**, *39*, 1-9.
- [22]. J. C. Dederen, B. Chavan, A. V. Rawlings, *Int J Cosmet Sci* **2012**, *34*, 502-510.
- [23]. D. Vasiljevic, J. Parojcic, M. Primorac, G. Vuleta, *Int. J. Pharm* **2006**, *309*, 171-177.

- [24]. T. Kinyanjui, W. E. Artz, S. Mahungu, in *Encyclopedia of Food Sciences and Nutrition (Second Edition)* (Ed.: B. Caballero), Academic Press, Oxford, **2003**, pp. 2070-2077.
- [25]. J. T. Davies, *Proc. 2nd Int. Congr. Surface Activity*. **1957**, *1*, 426-438
- [26]. R. Zana, *Langmuir* **1995**, *11*, 2314-2315.
- [27]. Clariant Emulsifiers for personal care, **2009**: pdfs.semanticscholar.org
- [28]. C. Fruijtier-Pölloth, *Toxicology* **2005**, *214*, 1-38.
- [29]. W. D. Bancroft, *J. phys. Chem.* **1913**, *17*, 503-519.
- [30]. W. D. Bancroft, *J. Phys. Chem.* **1915**, *19*, 275-309
- [31]. J. Sjöblom, edited by Johan (**2001**). *Encyclopedic handbook of emulsion technology*. New York: Marcel Dekker. p. 97.
- [32]. G. Mhanna, Y. Bakkour, B. El Hamaoui, N. El-Ashi, C. A. Ghanem, J. H. El-Nakat, F. El-Omar. *IJPC* **2015**, *5*, 381-391.
- [33]. M. Alibolandi, F. Sadeghi, S. H. Sazmand, S. M. Shahrokhi, M. Seifi, F. Hadizadeh, *Int J Pharma Investig.* **2015**, *5*, 134-141.
- [34]. K. A. Winship, Adverse drug reactions and acute poisoning reviews, **1988**, *7*, 19-38.
- [35]. M. C. Tanzi, P. Verderio, M. G. Lampugnani, M. Resnati, E. Dejana, E. Sturani, *J. Mater Sci Mater Med: Materials in Medicine* **1994**, *5*, 393-396.
- [36]. Tin bis(2-Ethylhexanoate), CAS No. 301-10-0, U.S. High Production Volume (HPV) Chemical Challenge Program, Final Submittal, Metal Carboxylates Coalition, December **2007**, 1-67.
- [37]. F. Hild, L. BreLOT, S. Dagorne, *Organometallics* **2011**, *30*, 5457-5462.
- [38]. F. Hild, N. Neehaul, F. Bier, M. Wirsum, C. Gourlaouen, S. Dagorne, *Organometallics* **2013**, *32*, 587-598.
- [39]. I. Krossing, H. Nöth, H. Schwenk-Kircher, *EurJIC* **1998**, 927-939.
- [40]. R. J. Wehmschulte, P. P. Power, *Inorganic Chemistry* **1998**, *37*, 6906-6911.
- [41]. L. -C. Liang, M. -H. Huang, C. -H. Hung, *Inorganic Chemistry* **2004**, *43*, 2166-2174.
- [42]. P. P. Power, *Chem. Rev* **1999**, *99*, 3463-3504.
- [43]. T. -L. Ho, *Chem. Rev.* **1975**, *75*, 1-20.
- [44]. *The group 13 metal aluminium, gallium indium and thallium, chemical patterns and peculiarities* (ed. S. Aldridge and A. J. Downs), M. A. Malik, P. I'Brien, Wiley-VCH VerlagGmbH: Weinheim, Germany, **2011**, 519.
- [45]. <http://www.sigmaaldrich.com/> (April 2019).

-
- [46]. D. I. Bashmakov, A. S. Lukatkin, N. A. Anjum, I. Ahmad, E. Pereira, *Environ Sci Pollut Res* **2015**, *22*, 15443–15448.
- [47]. R. J. Irwin, M. VanMouwerik, L. Stevens, M.D. Seese, W. Basham, **1997**, *Environmental Contaminants Encyclopedia*, 6.
- [48]. H. Tapiero, K. D. Tew, *Biomed. Pharmacother* **2003**, *57*, 399-411.
- [49]. R. B. Gordon, R. J. Lifset, M. Bertram, B. Reck, T. E. Graedel, S. Spatari, *JOM* **2004**, *56*, 24-29.
- [50]. D. D. Marreiro, J. K. Cruz, B. J. Morais, B. J. Beserra, S. J. Severo, R. A. de Oliveira, *Antioxidants* **2017**, *6*, 1-9.
- [51]. S. R. Powell, *J. Nutr.* **2000**, *130*, 1447-1454.
- [52]. G. K. Levy, J. Goldman, E. Aghion, *Metals* **2017**, *7*, 402-420.
- [53]. G. Schnee, C. Fliedel, T. Avilés, S. Dagorne, *EurJIC* **2013**, *2013*, 3699-3709.
- [54]. D. A. Walker, T. J. Woodman, D. L. Hughes, M. Bochmann, *Organometallics* **2001**, *20*, 3772-3776.
- [55]. M. R. Kember, C. K. Williams, *J. Am. Chem. Soc.* **2012**, *134*, 15676-15679.
- [56]. M. Graf, M. Ullmann, R. Kawalla, *Materials Today: Proceedings* **2015**, *2*, S76-S84.
- [57]. M. K. Kulekci, *Int J Adv Manuf Technol*, **2008**, *39*, 851-865.
- [58]. S. K. Sah, M. A. Bawase, M. R. Saraf, *ARAI*, **2014**.
- [59]. W. H. Sillekens, D. Bormann, in *Advances in Wrought Magnesium Alloys* (Eds.: C. Bettles, M. Barnett), Woodhead Publishing, **2012**, 427-454.
- [60]. O. Charyeva, O. Dakischew, U. Sommer, C. Heiss, R. Schnettler, K. S. Lips, *J orthopaed traumato* **2016**, *17*, 63-73.
- [61]. Y. Yun, Z. Dong, N. Lee, Y. Liu, D. Xue, X. Guo, J. Kuhlmann, A. Doepke, H. B. Halsall, W. Heineman, S. Sundaramurthy, M. J. Schulz, Z. Yin, V. Shanov, D. Hurd, P. Nagy, W. Li, C. Fox, *Mater. Today* **2009**, *12*, 22-32.
- [62]. W. Wang, J. Han, X. Yang, M. Li, P. Wan, L. Tan, Y. Zhang, K. Yang, *Materials Science and Engineering: B* **2016**, *214*, 26-36.
- [63]. U. Gröber, J. Schmidt, K. Kisters, *Nutrients* **2015**, *7*, 8199-8226.
- [64]. (a) R. J. Wood, P. M. Suter, R. M. Russell. *Am. J. Clin. Nutr.* **1995**, *62*, 493–504. (b) Turnlund, J. R.; Betschart, A. A.; Liebman, M.; Kretsch, M. J.; Sauberlich, H. E. *Am. J. Clin. Nutr.* **1992**, *56*, 905–910.
- [65]. Livescience.com, The chemistry of life, **2016**.

- [66]. Y. Wang, W. Zhao, X. Liu, D. Cui, E. Y. X. Chen, *Macromolecules* **2012**, *45*, 6957-6965.
- [67]. L. Wang, H. Ma, *Macromolecules* **2010**, *43*, 6535-6537.
- [68]. A. Villalobos Marco, J. Debling, *Handbook of Polymer Synthesis, Characterization, and Processing* **2013**. Wiley ed.
- [69]. S. P. Parwe, S. D. Warkad, M. V. Mane, P. S. Shedage, B. Garnaik, *Polymer* **2017**, *111*, 244-251.
- [70]. M. Abdouss, S. Mehdi Hoseini, J. Mohammadi-Rovshandeh, M. Javanbakht, *Materialwiss. Werkstofftech.* **2009**, *40*, 676-683.

Chapter III

Synthesis of Poly(alpha-chloro-epsilon-caprolactone)

I. Introduction

The chemical modification of polyesters like PLA or PCL may be achieved through functionalization of the carbonyl CH/CH₂ α position.¹ For example, PCL can react with lithium diisopropylamide (LDA) base to form enolate function groups along the chain (**Figure 1**); this first way is the anionic functionalization. Then the enolate function can react with an electrophile group like CO₂ allowing the introduction of a carboxylic group.²

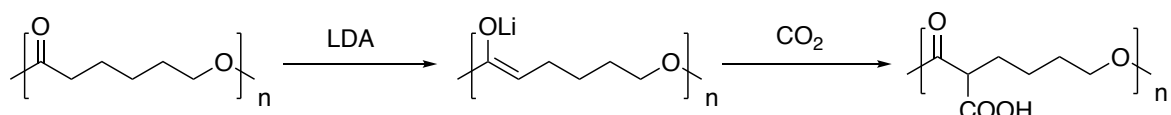


Figure 1: PCL functionalization by CO₂

Another way to access polyesters with pendant functional groups is through the ROP of a pre-functionalized cyclic ester such as α-chloro-ε-caprolactone (Cl-CL, **Figure 2**). It is interesting to introduce a halogen atom as it allows to chemically modify the synthesized polymer with various nucleophiles and consequently have access to a wide range of accessible polyesters. It should also be noted that the ROP of Cl-CL was only studied on one occasion under rather harsh conditions under a Sn-based ROP catalyst leading to the production of poly(Cl-CL) with a moderate control.³

II. Synthesis of α-chloro-ε-caprolactone (Cl-CL)

The synthesis of the α-chloro-ε-caprolactone monomer (Cl-CL) was performed by a Baeyer-Villiger oxidation at room temperature of 2-chlorocyclohexanone with *m*CPBA in dichloromethane.³

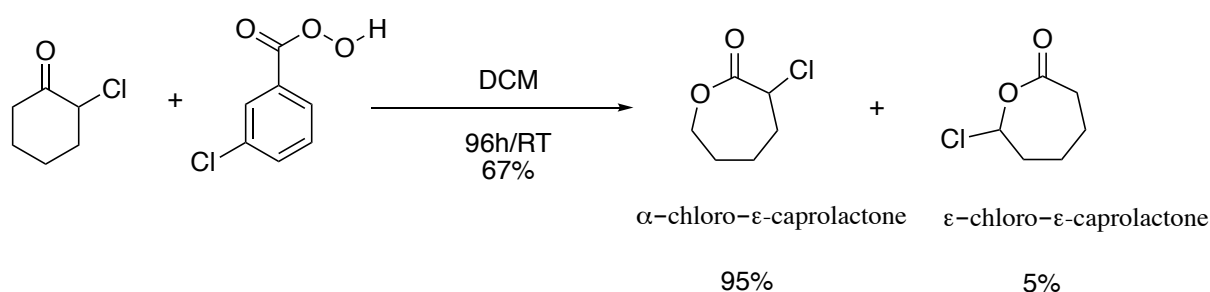


Figure 2: Oxidation of 2-chlorocyclohexanone

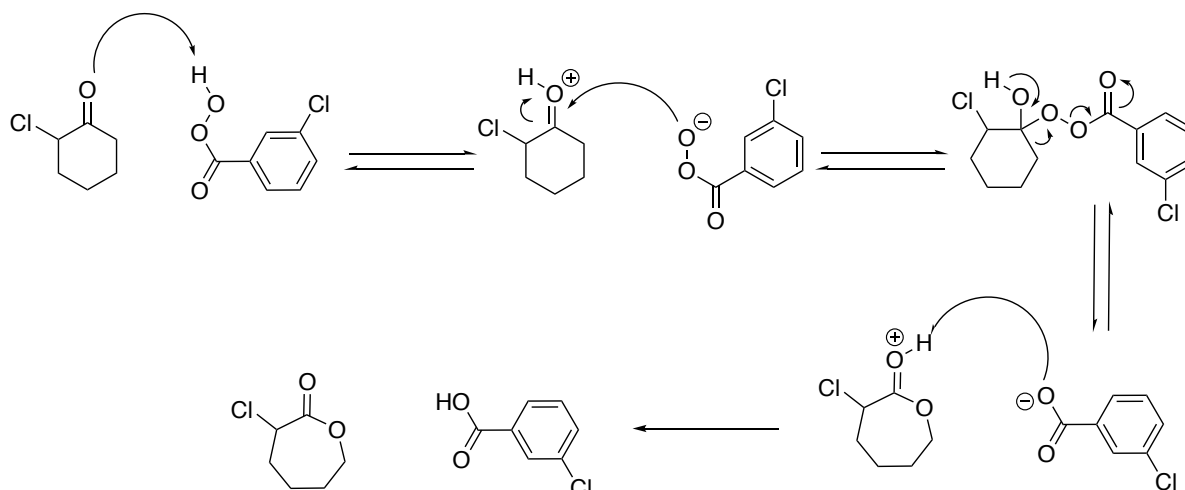


Figure 3: Mechanism of Bayer-Villiger oxidation for *rac*-(Cl-CL) formation

The ^1H NMR spectrum shows that the crude reaction mixture contains two isomers: Cl-CL (major) and ϵ -chloro- ϵ -caprolactone (minor) in a 95/5 ratio (**Figure 4**). The crude product was purified by chromatography in order to isolate the pure Cl-CL in 67% yield.

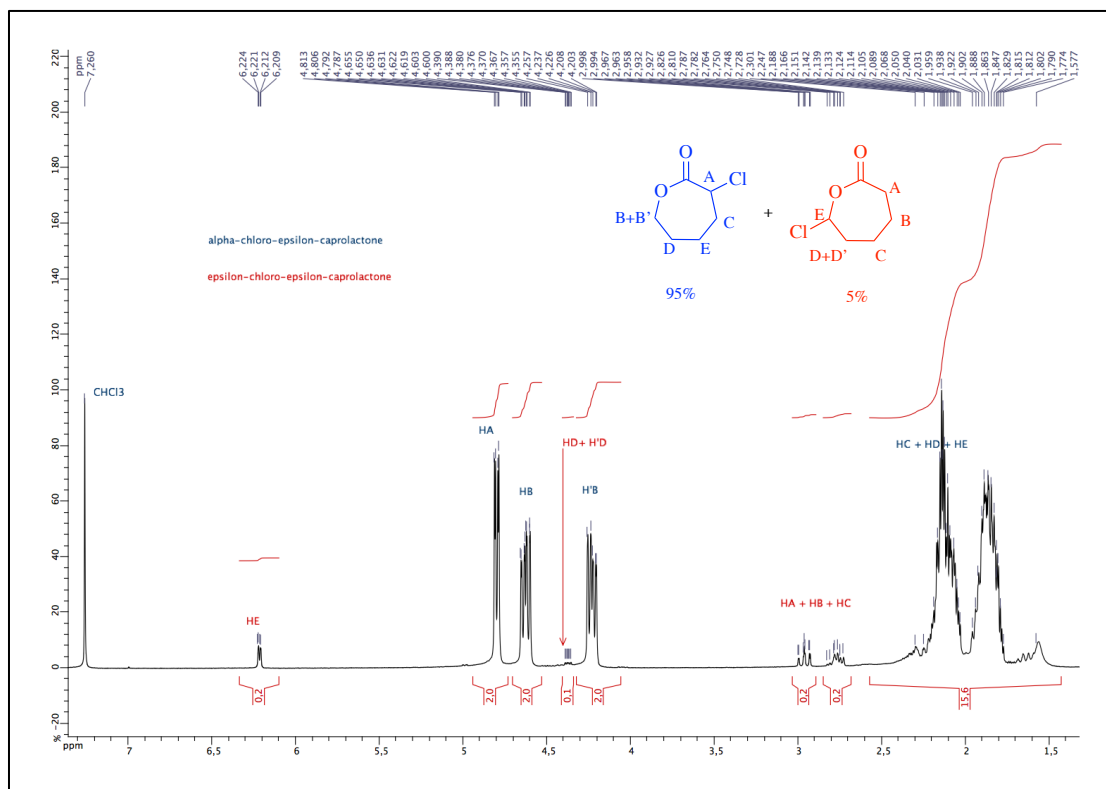


Figure 4: ^1H NMR (CDCl_3 , 400 MHz) spectrum of the crude reaction mixture

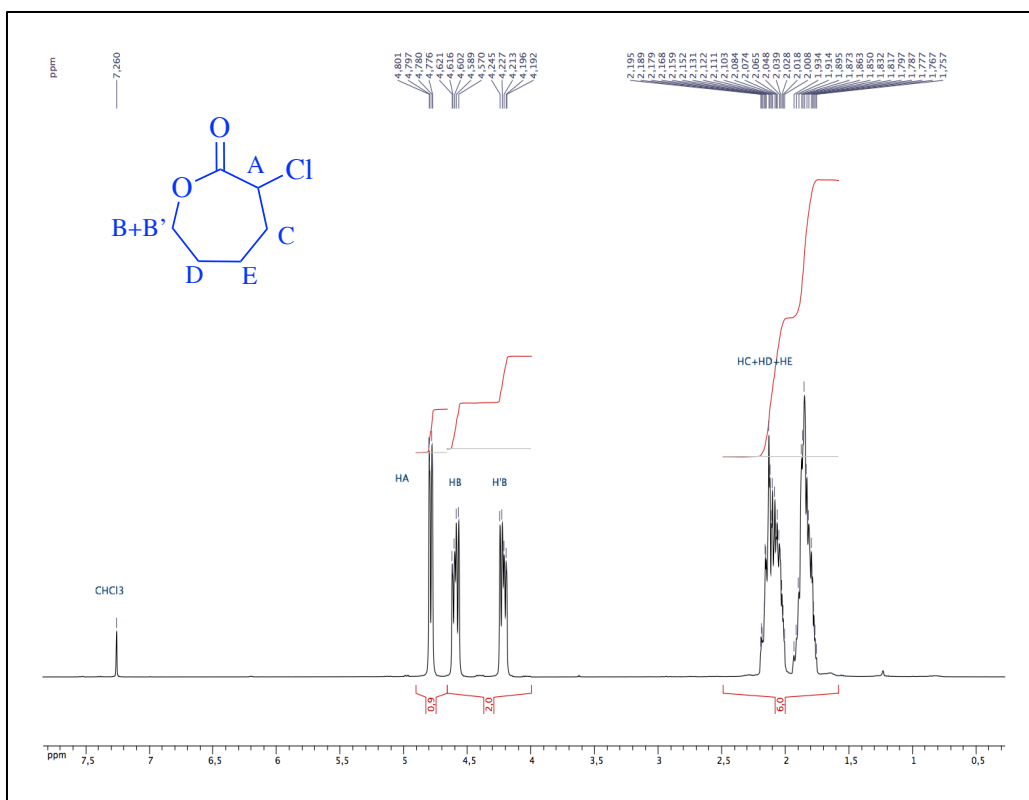


Figure 5: ¹H NMR spectrum (CDCl₃, 400 MHz) of isolated Cl-CL after purification by chromatography

Apart from purity issues, it should be pointed out that the removal of the minor product ϵ -chloro- ϵ -caprolactone is also important for an effective ROP of Cl-CL. Carrying out various ROP tests with crude Cl-CL were unsuccessful. An explanation could be that the presence of ϵ -chloro- ϵ -caprolactone would lead to an unstable alcoholate moiety (at the chain end) that may decompose through chloride elimination (**Figure 6**), thus precluding chain growth.

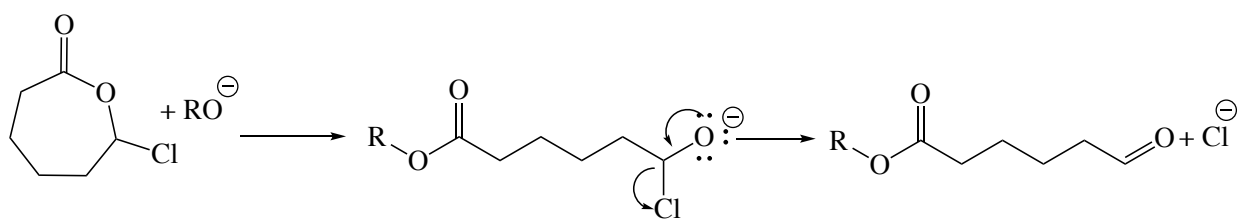


Figure 6: Elimination of the chlorine atom by the alcoholate

Single crystals of Cl-CL suitable for X-ray analysis were successfully grown in DCM/pentane mixture at -35 °C (**Figure 7**) and unambiguously confirmed the molecular structure of Cl-CL.

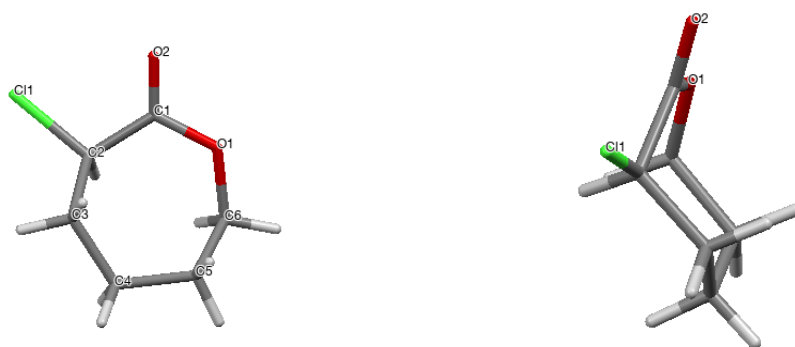


Figure 7: Molecular structure of Cl-CL species. Front and side views. Selected bond lengths (Å) and angles (deg): C(1)-O(1)=1.328(2), C(1)-C(2)= 1.517(2), C(2)-Cl(1)= 1.798(2); O(1)-C(1)-C(2)= 118.2(2).

III. ROP of chloro-caprolactone using a magnesium catalyst

III. 1. Polymerization of Cl-CL using $\text{Mg}(\text{THF})_2(\text{C}_6\text{F}_5)_2$ *catalyst 1*/BnOH system

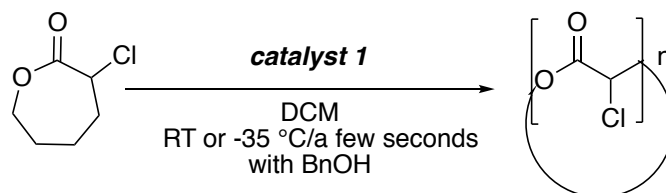


Figure 8: ROP of Cl-CL initiated by species 1 in presence of BnOH

The first catalyst used to perform the ROP of Cl-CL was the $\text{Mg}(\text{THF})_2(\text{C}_6\text{F}_5)_2$ complex (*catalyst 1*), whose synthesis is described in chapter II. The ROP results are compiled in **Table 1**.

Entry	Cl-CL ^a	BnOH ^a	T (°C)	Time ^b (sec)	Conversion ^c %	M _{n theo} ^d (g/mol)	M _{n GPC} ^e (g/mol)	M _{n corr} ^f (g/mol)	PDI
1	100	1	RT	1	100	14860	17044	14999	1.68
2	100	1	-35	1	27	3996	M _{n1} =5561 M _{n2} =1703 bimodal	M _{n1} =4894 M _{n2} =1499	PDI ₁ =1.10 PDI ₂ =1.03
3	100	1	-35	4	73	10804	15102	13290	1.03
4	100	1	-35	15	100	14860	20633	15615	1.47
5	100	/	-35	1	100	14860	M _{n1} =19638 M _{n2} =1118931 bimodal	M _{n1} =17281 M _{n2} =98466	PDI ₁ =1.25 PDI ₂ =1.08

Polymerization conditions: [Cl-CL]₀ = 1 M, DCM, RT or -35 °C

^a Equiv. of monomer versus initiator. ^b Reaction time. ^c Monomer conversion, ^d Calculated using $M_{n\text{theo}} = [\text{Cl-CL}]_0 \times M_{\text{Cl-CL}} \times \text{conv.} / [\text{BnOH}]_0$. ^e Measured by GPC in THF (30 °C) using PS standards. ^f $M_{n\text{GPC}} \times 0.88$ (0.88: correlation factor obtained in **section VIII**).

Table 1: Results of the ROP of Cl-CL initiated by species 1

The first polymerization was performed at room temperature with 100 equivalents of Cl-CL monomer in the presence of 1 equivalent of benzyl alcohol as a transfer agent *vs.* catalyst and the reaction mixture was quenched with MeOH after one second. The monomer was immediately and quantitatively converted into the corresponding P(Cl-CL) polymer as deduced from ¹H NMR spectrum (**Figure 9**).

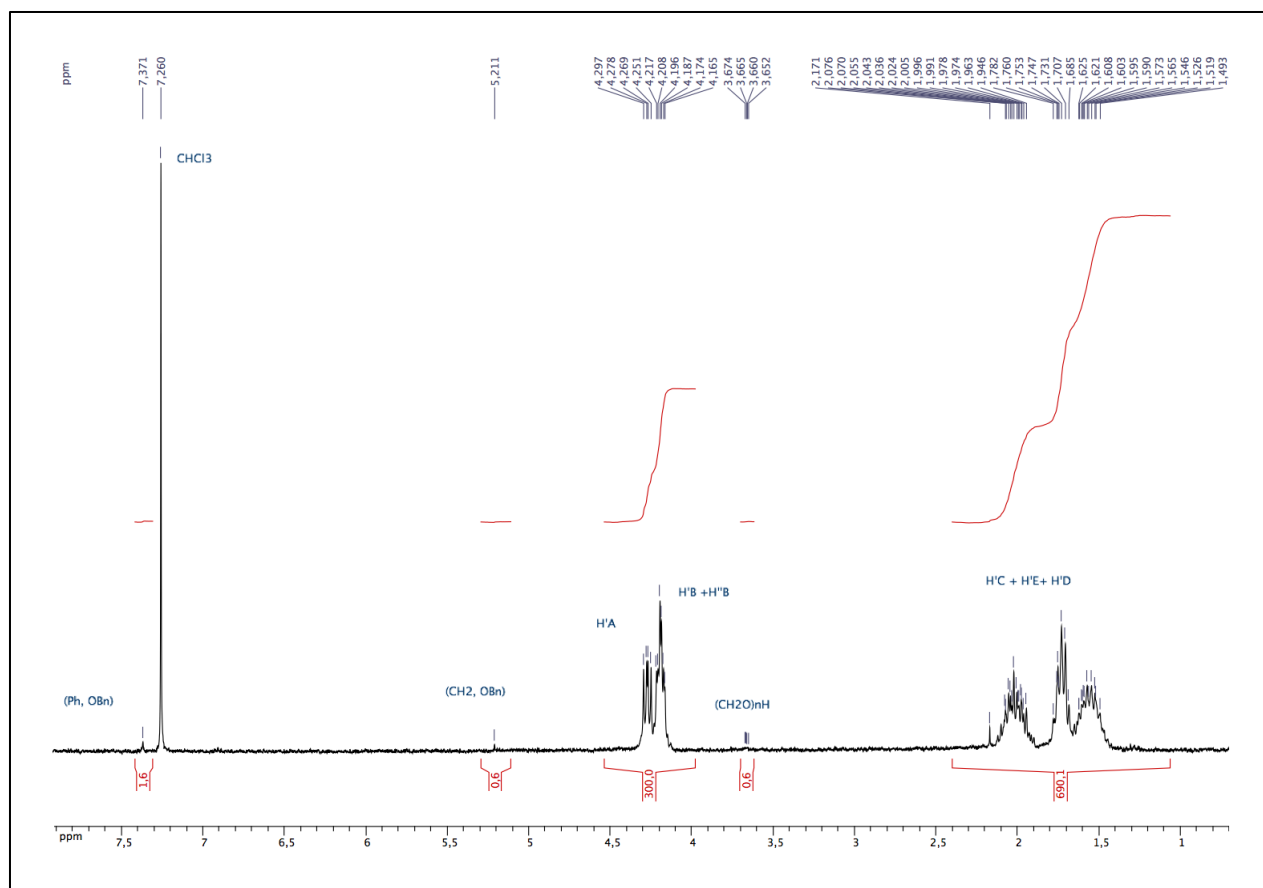


Figure 9: ^1H NMR (CDCl_3 , 400 MHz) of isolated P(Cl-CL) prepared by polymerization of 100 equiv. (vs. *catalyst 1*) of Cl-CL/1 equiv. BnOH, initiated by *catalyst 1*. (Conditions: $[\text{Cl-CL}]_0 = 1 \text{ M}$, DCM, RT, 1 second, quantitative yield).

The ^{13}C NMR spectrum of the isolated polymer samples (**Figure 10**) performed in CDCl_3 shows six different peaks. The upfield singlets at $\delta = 22.4$, 27.7 and 34.1 ppm are the different CH_2 groups of the aliphatic sequence. According to the DEPT (**Figure 11**), we can attribute the peaks at 57 ppm to the CHCl whereas the one at 65.5 ppm is the CH_2OH of the polymer end chain. The most downfield signal ($\delta = 169.6$ ppm) is, of course, the carbon of the carbonyl function.

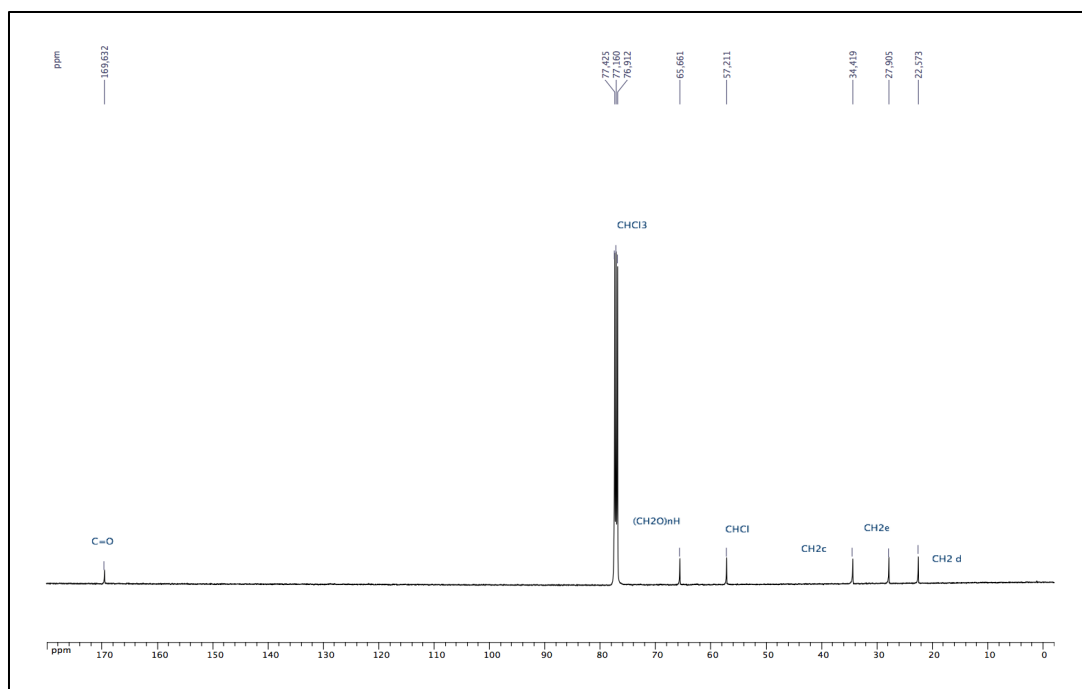


Figure 10: ^{13}C NMR (CDCl_3 , 500 MHz) of isolated P(Cl-CL) prepared by polymerization of 100 equiv. (vs. *catalyst 1*) of Cl-CL/1 equiv. BnOH, initiated by *catalyst 1*. (Conditions: $[\text{Cl-CL}]_0 = 1 \text{ M}$, DCM, RT, 1 second, quantitative yield).

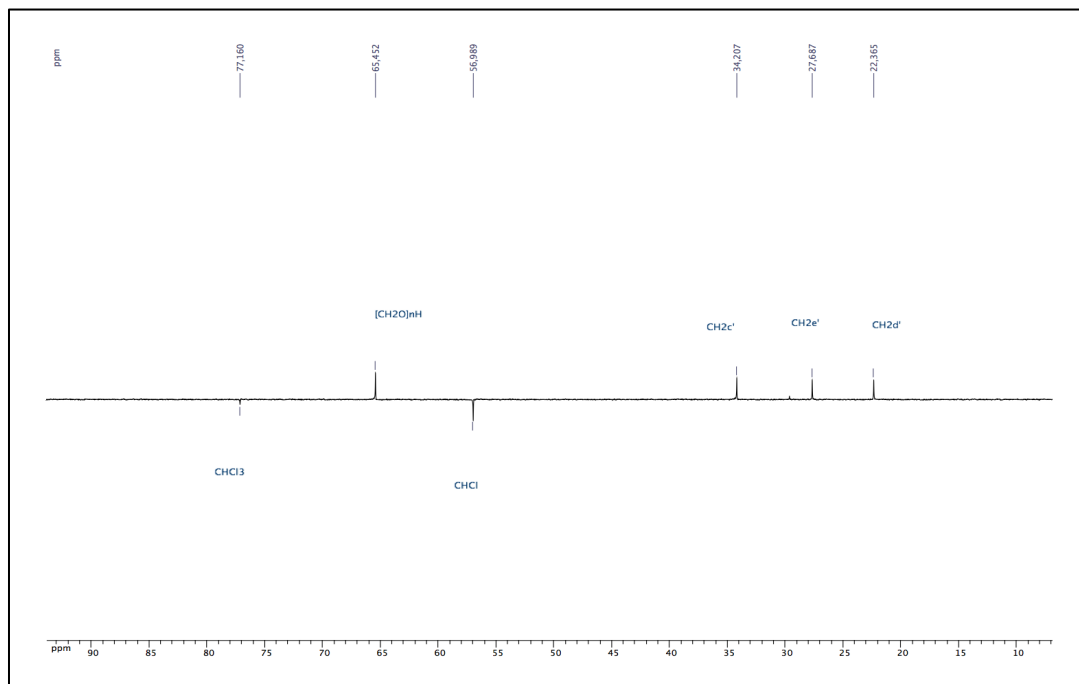


Figure 11: ^{13}C DEPT NMR (CDCl_3 , 500 MHz) of isolated P(Cl-CL) prepared by polymerization of 100 equiv. (vs. *catalyst 1*) of Cl-CL/1 equiv. BnOH, initiated by *catalyst 1*. (Conditions: $[\text{Cl-CL}]_0 = 1 \text{ M}$, DCM, RT, 1 second, quantitative yield).

For the ROP done at room temperature, GPC data indicate a broad polydispersity (PDI = 1.68; **Figure 12**). The MALDI-TOF spectrum analysis for this polymer shows the formation of a cyclic P(Cl-CL). Indeed, the difference between two peaks of the spectrum matches with an entity of Cl-CL (148.06 g/mol) (**Figure 13**). Nevertheless, ^1H NMR spectrum (**Figure 9**) shows the $\text{CH}_2\text{-Ph}$ peak at 5.21 ppm of the benzyloxy group and a singlet at 7.37 ppm corresponding to the $\text{CH}_2\text{-Ph}$ aromatic protons of the initiator, indicative of the presence of a PhCH_2O -ended linear polymer. The combination of MALDI-TOF and NMR data agree with the presence of both cyclic and linear P(Cl-CL) polymers, rationalizing the broad PDI of the produced material.

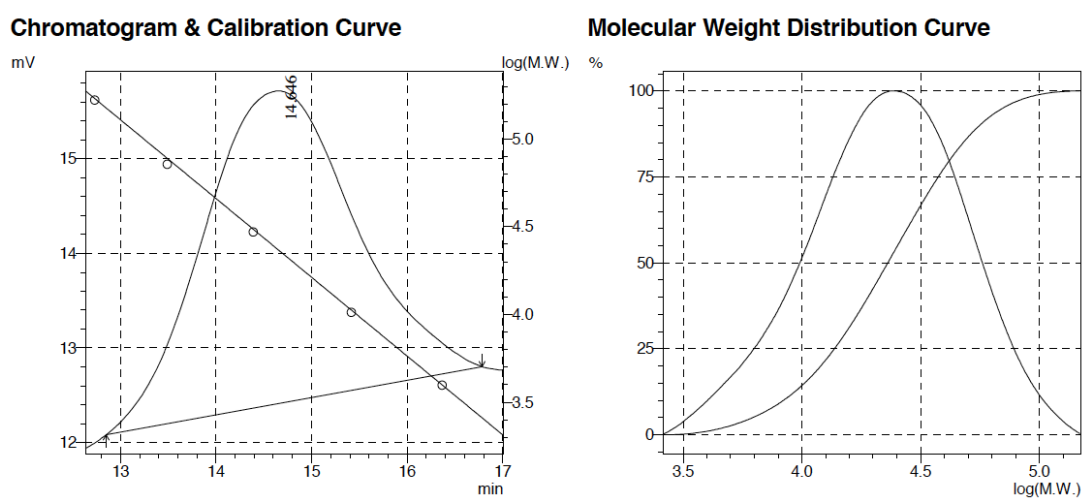


Figure 12: SEC traces of isolated P(Cl-CL) prepared via ROP of Cl-CL by the *catalyst 1*, with 1 equiv. of BnOH initiator (conditions: $[\text{Cl-CL}]_0 = 1 \text{ M}$, 100 equiv. of Cl-CL, 1 equiv. BnOH, RT, DCM, 100% conv., 1 second).

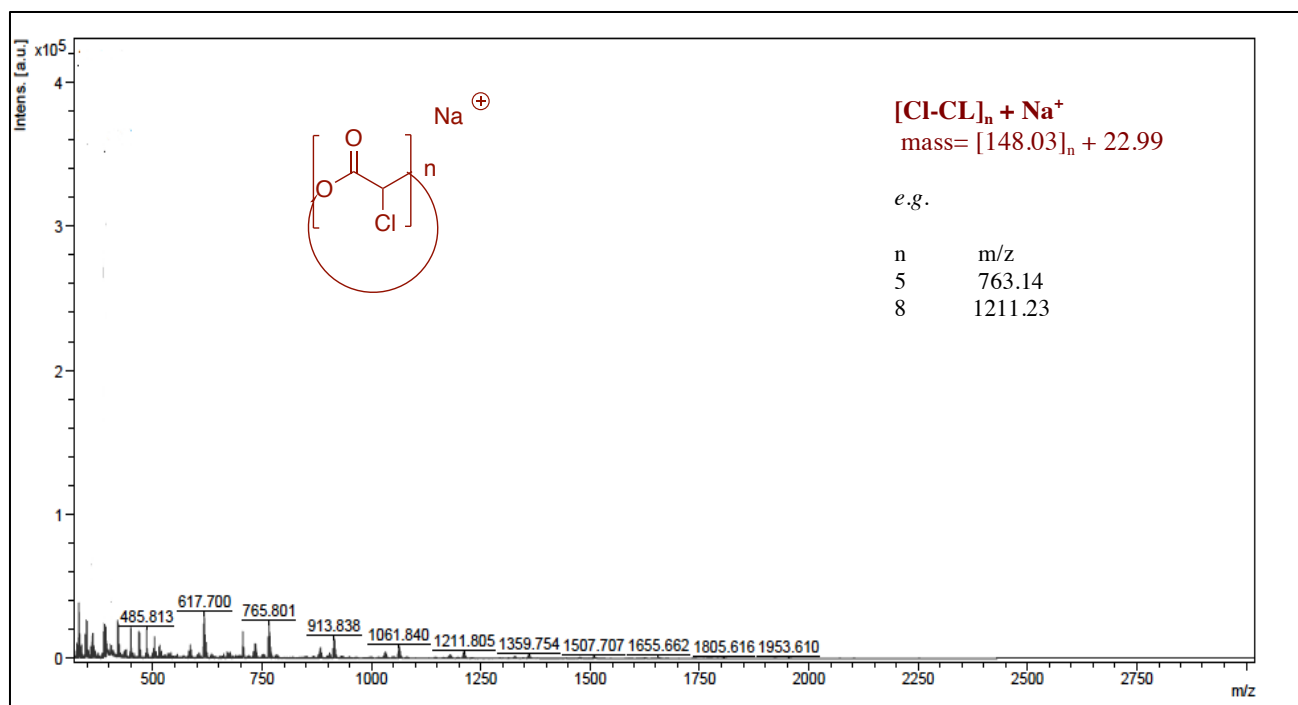


Figure 13: MALDI-TOF spectrum of the P(Cl-CL) prepared by ROP of Cl-CL initiated by the Mg *catalyst 1*/BnOH system. (Conditions: $[\text{Cl-CL}]_0 = 1 \text{ M}$, 100 equiv. of Cl-CL, 1 equiv. of BnOH, DCM, RT, polymer isolated at 100% conv. in P(Cl-CL)).

To decrease the extremely high reaction rate, the ROP temperature was decreased from room temperature to $-35 \text{ }^\circ\text{C}$ (**entries 2, 3 and 4, Table 1**), yet to afford the complete ROP of 100 equivalents of Cl-CL after 15 s at $-35 \text{ }^\circ\text{C}$. The GPC traces of P(Cl-CL) are monomodal with a moderately broad polydispersity (PDI: 1.47, **Figure 15**) and a reasonable level of chain length control. The ^1H NMR spectrum of the resulting polymer still shows benzyloxy signals at 5.21 ppm and 7.37 ppm (**Figure 14**), consistent with the presence of minor amount of BnO-ended linear P(Cl-CL). The MALDI-TOF spectrum of the P(Cl-CL) supports the same conclusion that for the previous ROP performed at RT (**Figure 13**) and the peaks present in the spectrum are assigned to the cyclic P(Cl-CL) (**Figure 18**). Thus, the ROP of Cl-CL mediated by **1**/BnOH (1/1) affords a mixture of cyclic and linear P(Cl-CL) material at room temperature and $-35 \text{ }^\circ\text{C}$.

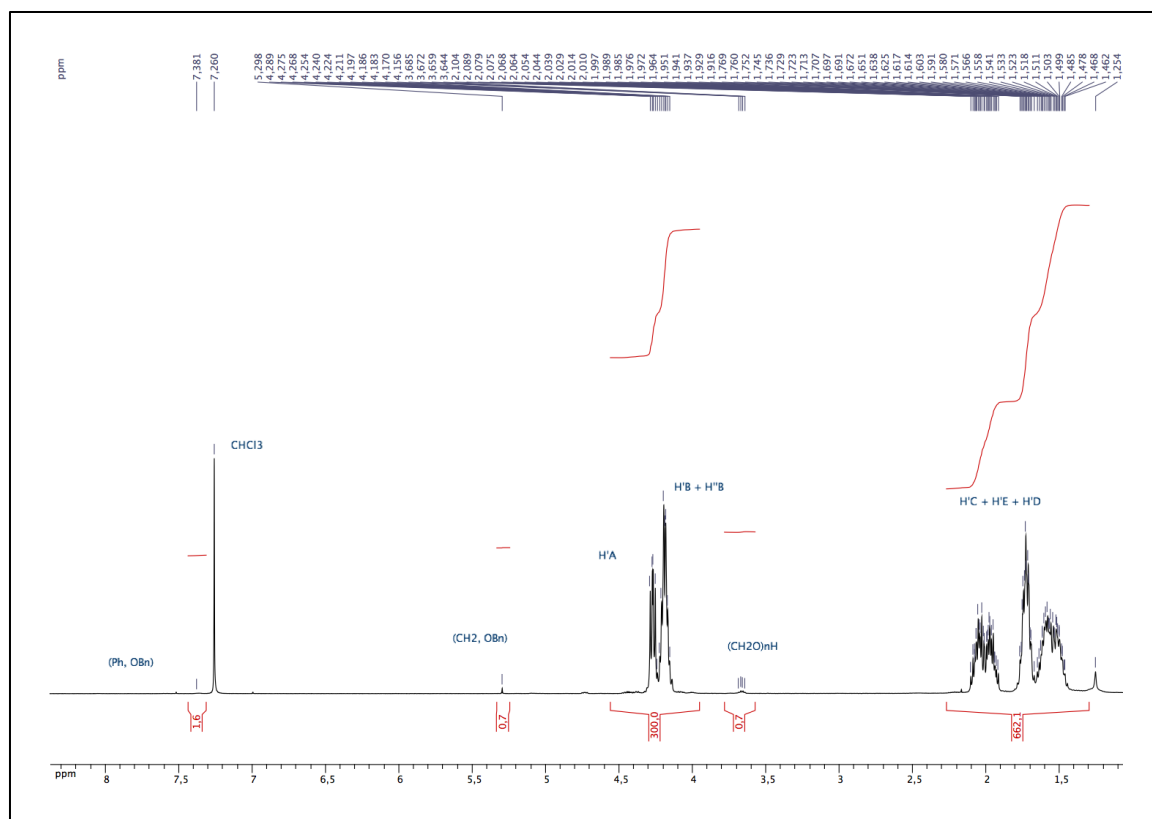


Figure 14: ^1H NMR (CDCl_3 , 400 MHz) of isolated P(Cl-CL) prepared via ROP of Cl-CL by *catalyst 1*/BnOH initiator. (Conditions: $[\text{Cl-CL}]_0 = 1 \text{ M}$, 100 equiv. of Cl-CL, 1 equiv. BnOH, -35°C , DCM, 100% conv., 15 s).

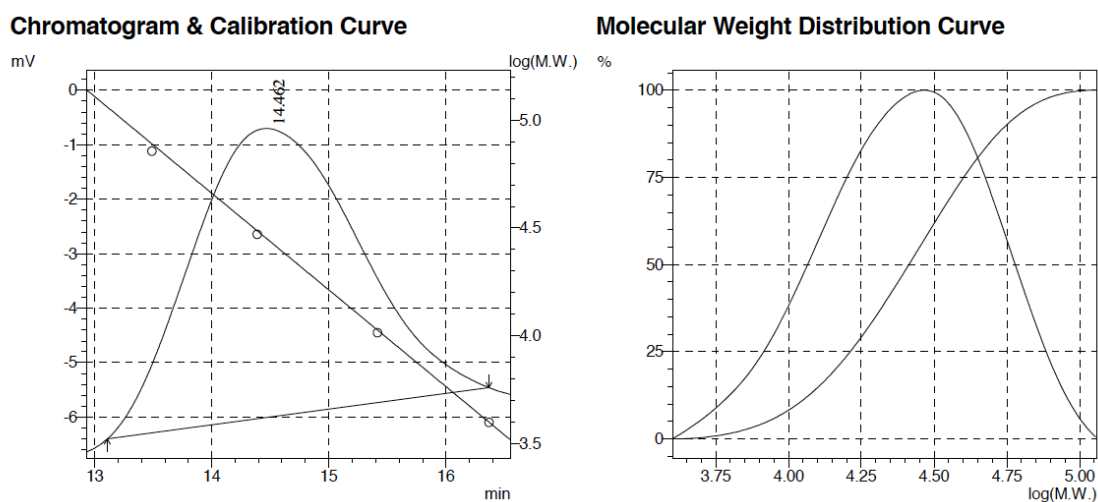


Figure 15: SEC traces of isolated P(Cl-CL) prepared via ROP of Cl-CL by *catalyst 1*, BnOH initiator. (Conditions: $[\text{Cl-CL}]_0 = 1 \text{ M}$, 100 equiv. of Cl-CL, 1 equiv. BnOH, -35°C , DCM, 100% conv., 15 s).

Kinetic studies carried out at $-35\text{ }^{\circ}\text{C}$ are consistent with a ROP proceeding in a rather controlled manner in the presence of BnOH. The plot of $\ln(M_0/M)$ versus time is linear (Figure 16) with an apparent rate constant found to be $3.067 \times 10^{-1} \text{ sec}^{-1}$. In addition, a linear correlation is observed between the M_n values of the formed P(Cl-CL) and monomer conversion during the polymerization process (Figure 17), which supports a controlled chain propagation.

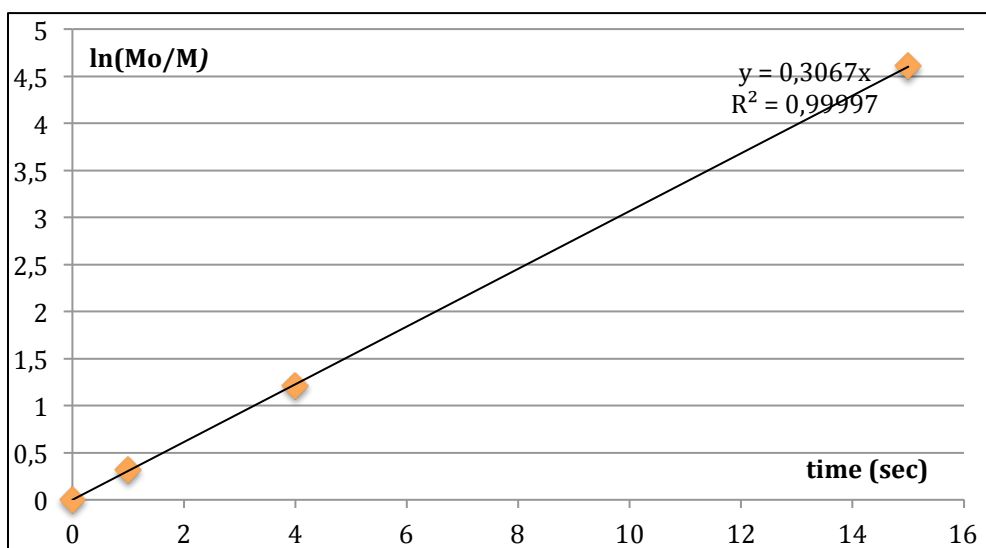


Figure 16: Plot of $\ln(M_0/M)$ as a function of time in the ROP of Cl-CL using *catalyst 1* and BnOH as initiator. (Conditions: $[\text{Cl-CL}]_0 = 1\text{ M}$, 100 equiv. in monomer, 1 equiv. BnOH, DCM, $-35\text{ }^{\circ}\text{C}$).

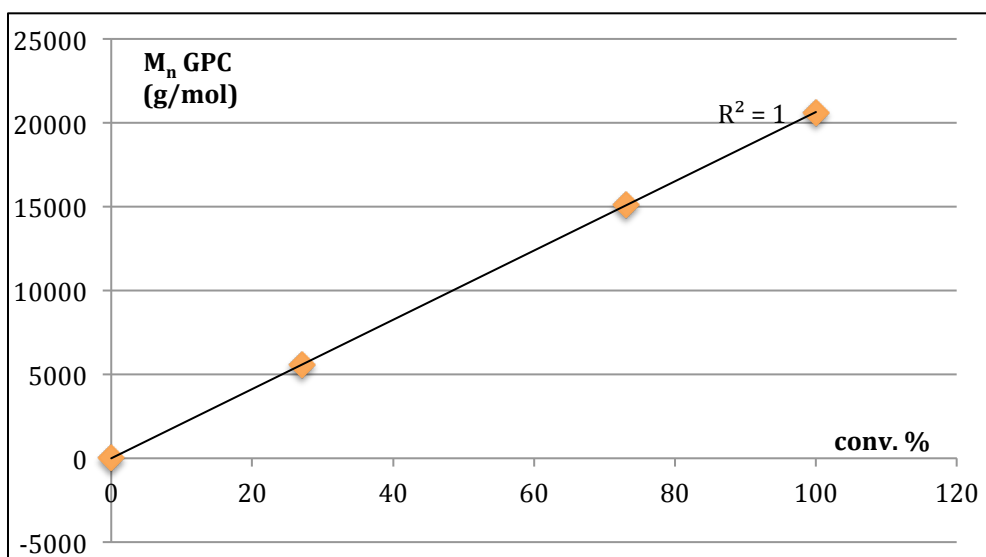


Figure 17: Plot of M_n as a function of the time in the ROP of Cl-CL using *catalyst 1* and BnOH as initiator (1 equiv.). (Conditions: $[\text{Cl-CL}]_0 = 1\text{ M}$, 100 equiv. in monomer, 1 equiv. BnOH, DCM, $-35\text{ }^{\circ}\text{C}$).

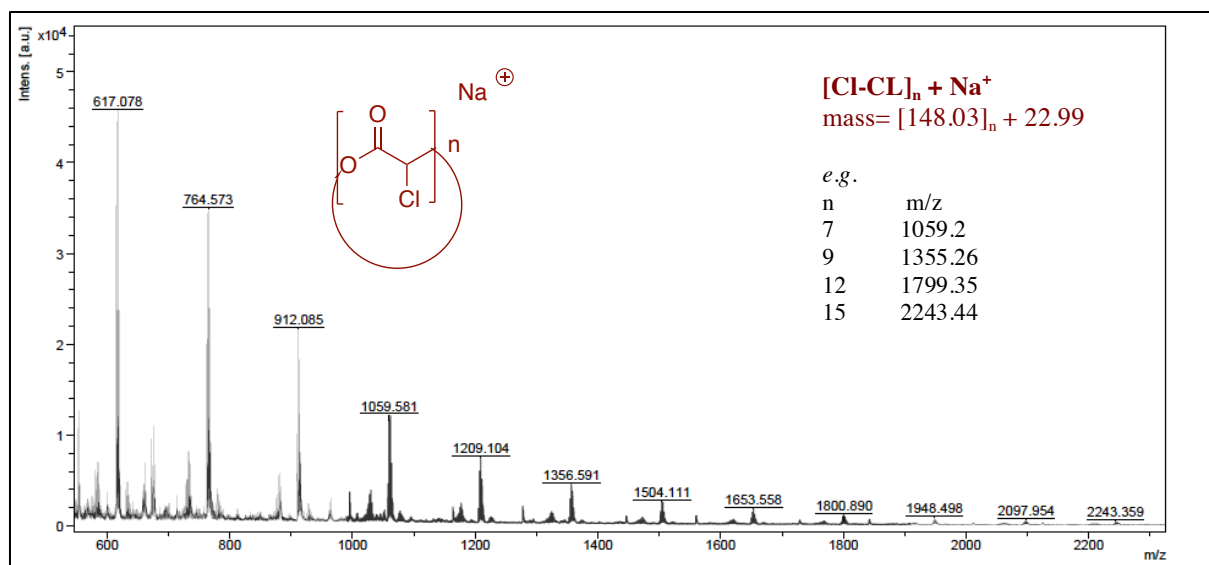


Figure 18: Zoom-in of the MALDI-TOF spectrum of the P(Cl-CL) prepared by ROP of Cl-CL initiated by the Mg catalyst 1/BnOH system. (Conditions: $[\text{Cl-CL}]_0 = 1 \text{ M}$, 100 equiv. of Cl-CL, 1 equiv. of BnOH, DCM, $-35 \text{ }^\circ\text{C}$, polymer isolated at 100% conv. in P(Cl-CL)).

When the polymerization was realized without any alcohol initiator at $-35 \text{ }^\circ\text{C}$ (**entry 5, Table 1**), the monomer was also immediately converted into the corresponding cyclic polymer as showed by the ^1H NMR spectrum (**Figure 20**). With regard to the GPC data, two different molecular weights were obtained: M_{n1} whose value is close to $M_{n \text{ theo}}$ with a rather narrow polydispersity (PDI: 1.25) and M_{n2} which has a very high molecular weight (1118931 g/mol) with a very fine polydispersity (PDI: 1.08). This latter could be obtained by a cationic polymerization directly initiated by the Mg Lewis acid.

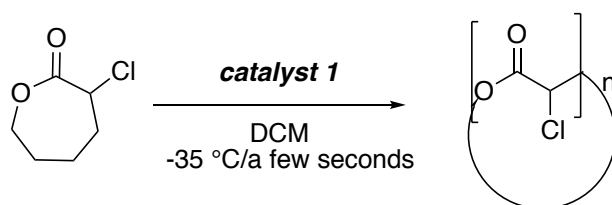


Figure 19: ROP of Cl-CL initiated by $\text{Mg}(\text{THF})_2(\text{C}_6\text{F}_5)_2$ species 1 without BnOH initiator

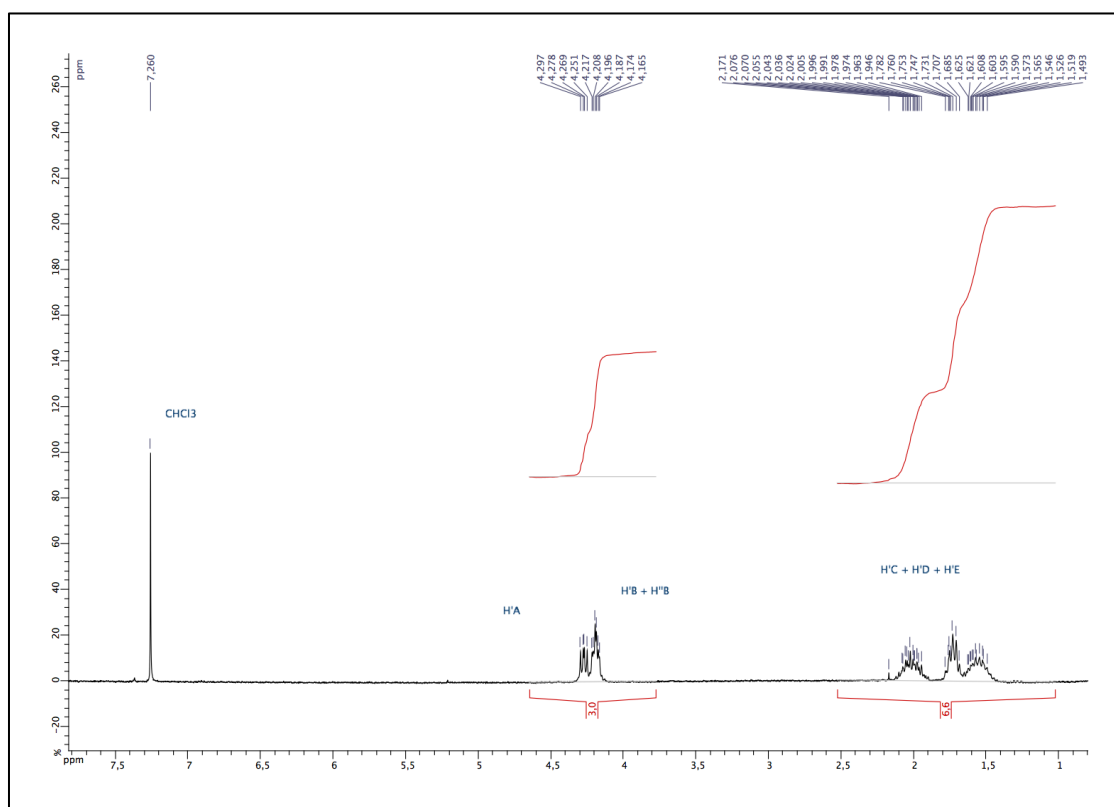


Figure 20: ^1H NMR (CDCl_3 , 400 MHz) of isolated P(Cl-CL) prepared by ROP of 100 equiv. of Cl-CL initiated by *catalyst 1*. (Conditions: $[\text{Cl-CL}]_0 = 1 \text{ M}$, DCM, $-35 \text{ }^\circ\text{C}$, a few seconds, 100% conv.).

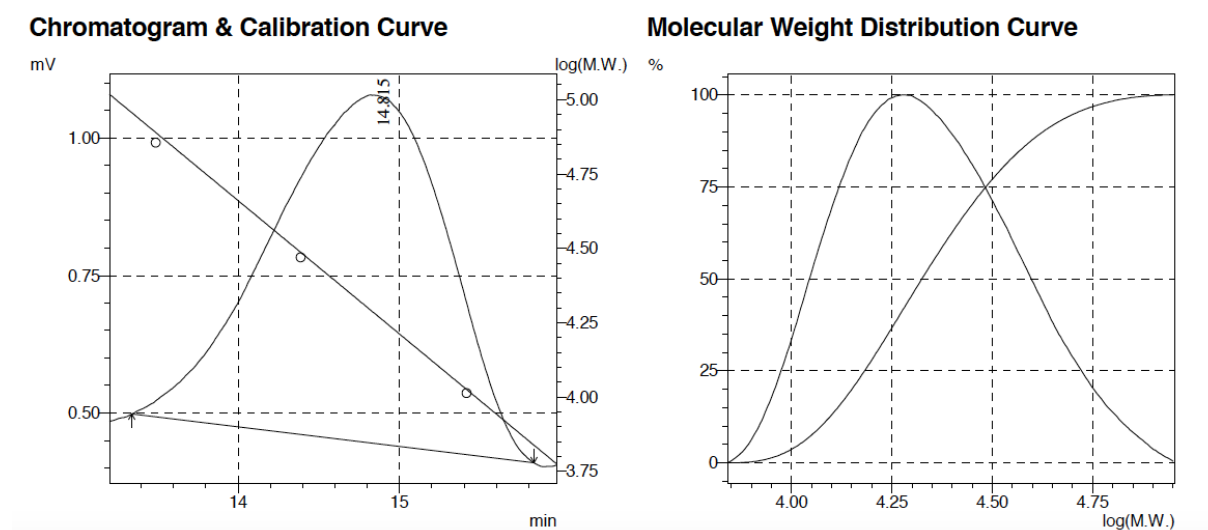


Figure 21: SEC traces of isolated P(Cl-CL) prepared via ROP of Cl-CL by *catalyst 1*. (Conditions: $[\text{Cl-CL}]_0 = 1 \text{ M}$, 100 equiv. of Cl-CL, $-35 \text{ }^\circ\text{C}$, DCM, 100% conv., a few seconds).

Entry	catalyst	Cl-CL ^a	BnOH ^a	T (°C)	Time (min.)	Conversion ^b %	M _{n theo} ^c (g/mol)	M _{n GPC} ^d (g/mol)	M _{n corr} ^e (g/mol)	PDI
1	2	100	1	90	120	10	1480	825	710	1.18
2	2	100	1	90	180	23	3404	3131	2693	1.15
3	2	100	1	90	300	40	5920	5561	4782	1.10
4	2	100	1	90	1320	100	14800	14029	12065	1.44
5	3	100	/	RT	11	100	14860	16421	14451	1.28
6	4	100	/	RT	1	40	6241	6945	6112	1.32
7	4	100	/	RT	2.7	82	12928	14431	12699	1.44
8	4	100	/	RT	4.3	93	13819	16465	14489	1.05
9	4	100	/	RT	6.9	100	14860	17719	15593	1.17
10	4	250	/	RT	10	33	12260	28955	25480	1.28
11	4	250	/	RT	15	42	18575	34241	30132	1.16
12	4	250	/	RT	35	64	26005	56896	50069	1.58
13	4	250	/	RT	130	100	37150	90500	79640	1.25
14	4	500	/	RT	420	100	74300	61357	53994	1.56
15	4	1000	5	RT	23	66	19615	16367	14403	1.02
16	4	1000	5	RT	40	83	24668	21047	18521	1.05
17	4	1000	5	RT	110	100	29720	25297	22261	1.10

Polymerization conditions: [Cl-CL]₀ = 1 M, toluene, 90 °C or DCM, RT.

^a Equiv. versus initiator. ^b Reaction time. ^c Monomer conversion, ^d Calculated using $M_{n \text{ theo}} = [\text{Cl-CL}]_0 \times M_{\text{Cl-CL}} \times \text{conv.} / [\text{BnOH}]_0$. ^e Measured by GPC in THF (30 °C) using PS standards. ^f Calculated using the correlation factor 0.88 (*vide infra*) obtained in **section VIII**.

Table 2: ROP of Cl-CL using species 2, 3, and 4

IV. Tol·Zn(C₆F₅)₂ as catalyst for the ROP of chloro-caprolactone (Cl-CL)

At room temperature, the tol·Zn(C₆F₅)₂⁴ *catalyst 2* was inactive for the ROP of Cl-CL and the reaction was thus performed at 90 °C.

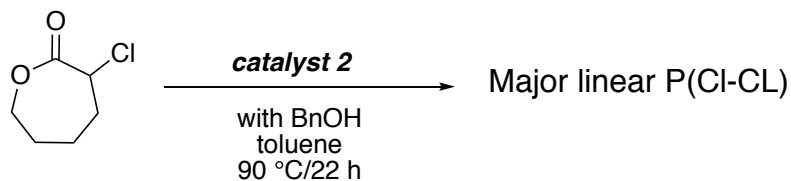


Figure 24: ROP of Cl-CL using species 2/BnOH system

The ROP of Cl-CL was performed using 100 equivalents of Cl-CL and 1 equivalent of BnOH (*vs.* catalyst) as chain transfer agent. The ¹H NMR spectrum (**Figure 25**) suggests the formation of a linear BnO-ended poly(Cl-CL). Despite a monomodal SEC traces (**Figure 26**), kinetic data of the ROP agree with a moderately controlled process (**Figures 27 and 28**). Total conversion to a relatively broadly disperse P(Cl-CL) (PDI: 1.44) is only achieved after 22 hours at 90 °C (**entry 4, Table 2**).

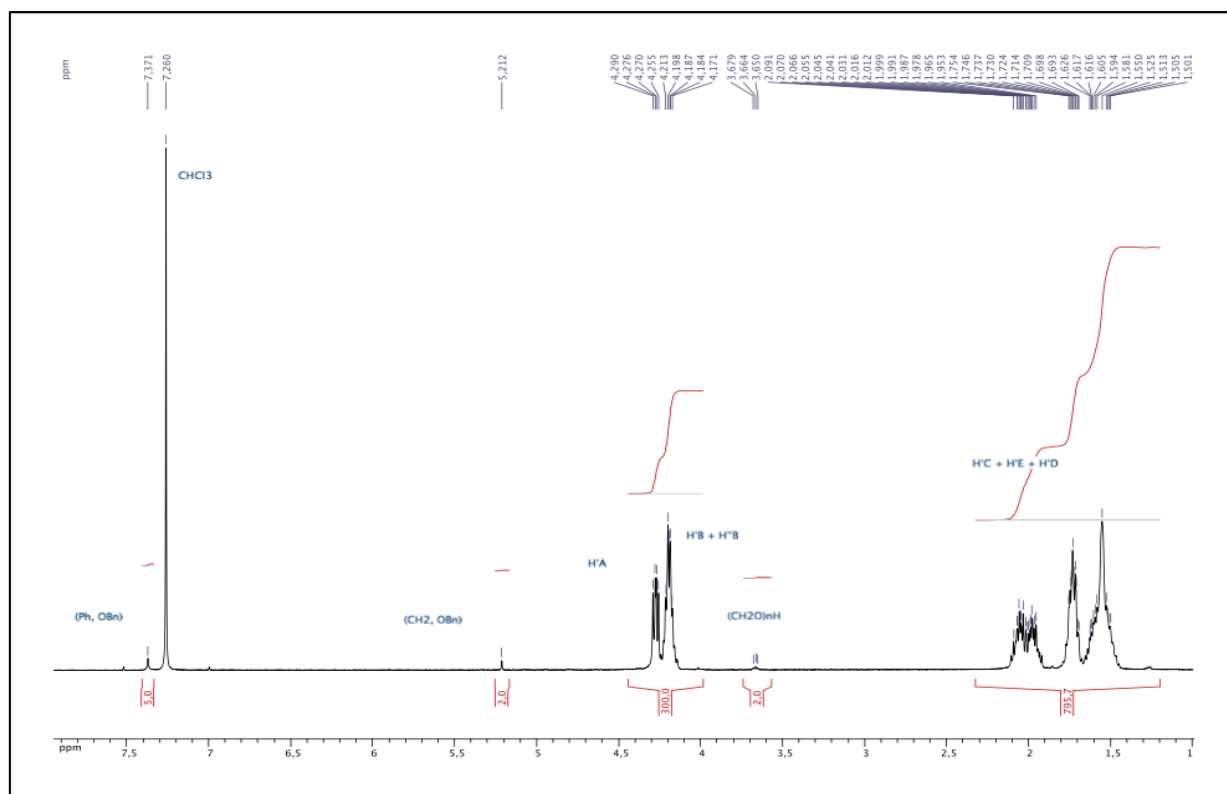


Figure 25: ¹H NMR (CDCl₃, 400 MHz) of isolated P(Cl-CL) prepared by ROP of 100 equiv. (*vs.* catalyst) of Cl-CL, 1 equiv. of BnOH, initiated by *catalyst 2*. (Conditions: [Cl-CL]₀ = 1 M, toluene, 90 °C, 22 h, 100% conv.).

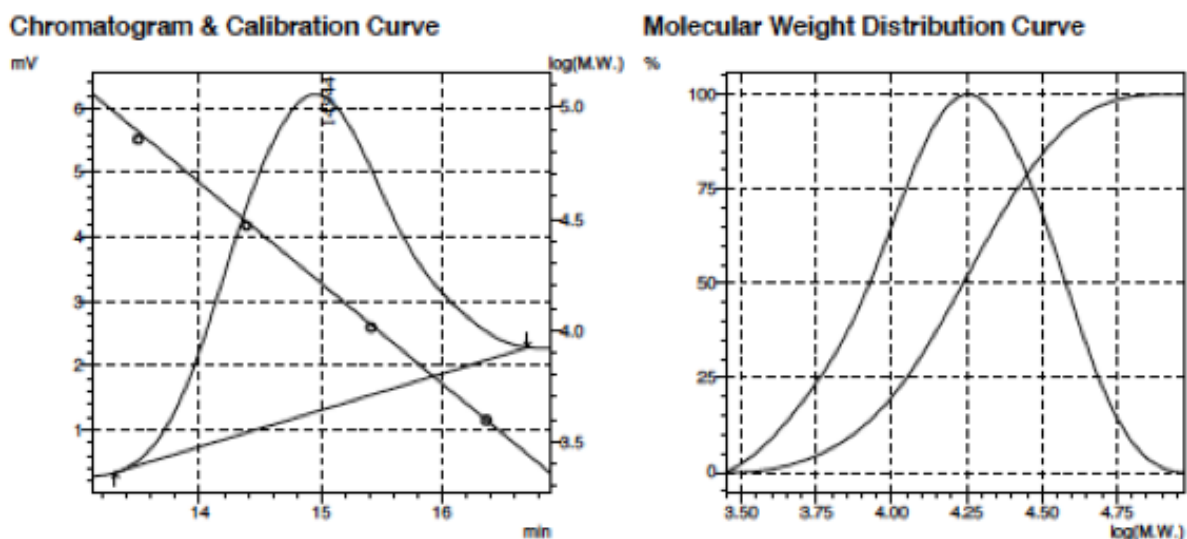


Figure 26: SEC traces of isolated P(Cl-CL) prepared via ROP of Cl-CL by the Zn catalyst 2. (Conditions: $[\text{Cl-CL}]_0 = 1 \text{ M}$, 100 equiv. of Cl-CL, 1 equiv. BnOH, $90 \text{ }^\circ\text{C}$, toluene, 22 h, 100% conv.).

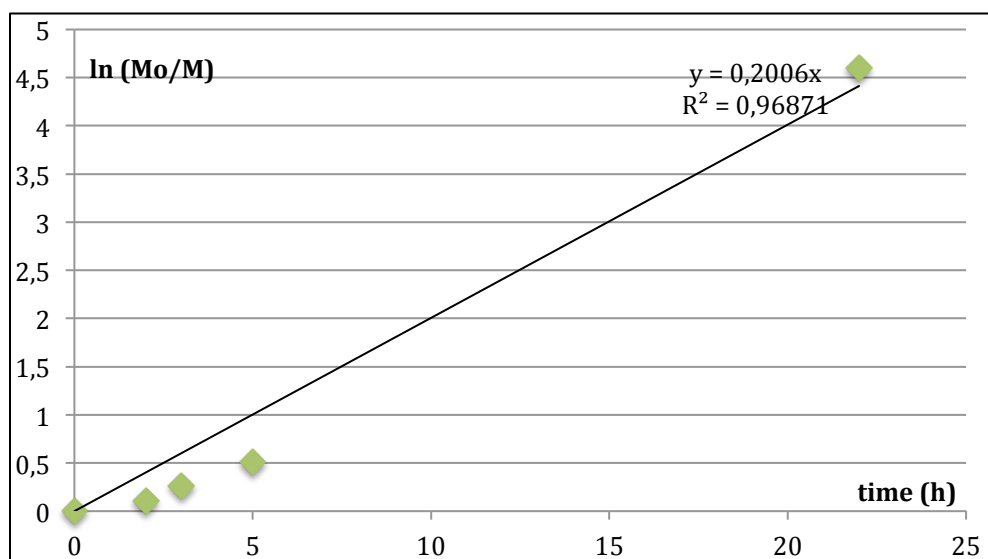


Figure 27: Plot of $\ln(M_0/M)$ as a function of time in the ROP of Cl-CL using $\text{tol}\cdot\text{Zn}(\text{C}_6\text{F}_5)_2$ catalyst 2. (Conditions: $[\text{Cl-CL}]_0 = 1 \text{ M}$, 1 equiv. BnOH, 100 equiv. in monomer, toluene, $90 \text{ }^\circ\text{C}$).

However, the M_n values for poly(Cl-CL) obtained from GPC data match well the theoretical value (entries 1 to 4, Table 2) as indicated by their linear correlation with monomer conversion (Figure 28).

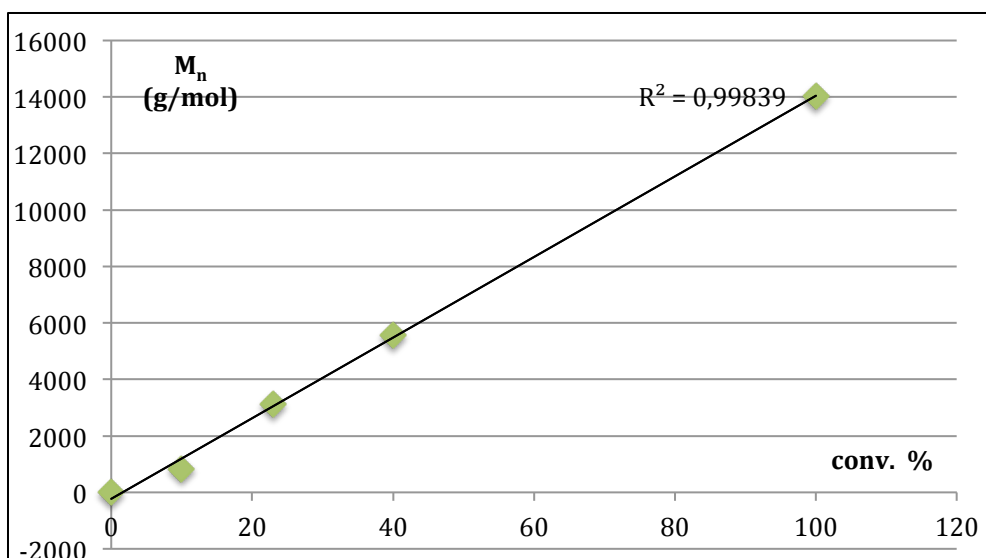


Figure 28: Plot of M_n as a function of the conv. in the ROP of Cl-CL using $\text{tol}\cdot\text{Zn}(\text{C}_6\text{F}_5)_2$ catalyst **2**. (Conditions: $[\text{Cl-CL}]_0 = 1 \text{ M}$, 1 equiv. BnOH, 100 equiv. Cl-CL, toluene, 90 °C).

According to the MALDI-TOF spectrometric data on isolated polymers (**Figure 29**), the produced material also contains unsaturated PCL. Indeed, the isotope pattern of MALDI-TOF signals agrees with the loss of chlorine pendant groups (with m/z peaks as triplets whereas the P(Cl-CL) shows massive m/z signals). It can be noticed that alkene signals are not visible in the NMR spectrum. So we could mention two hypotheses: we can have a very minor amount of this fragment in the polymer or some zinc catalyst impurity traces were still present in the polymer sample, and the chlorine elimination has occurred during the MALDI-TOF mass analysis (like reaction between the matrix and the sample).

Consequently, heating the reaction mixture probably promotes elimination reaction conditions, indicating the limited thermal stability of poly(Cl-CL). Based on these results, it appears crucial to mediate the ROP of Cl-CL under milder conditions (ideally at room temperature), thus requiring the choice of an appropriate catalyst.

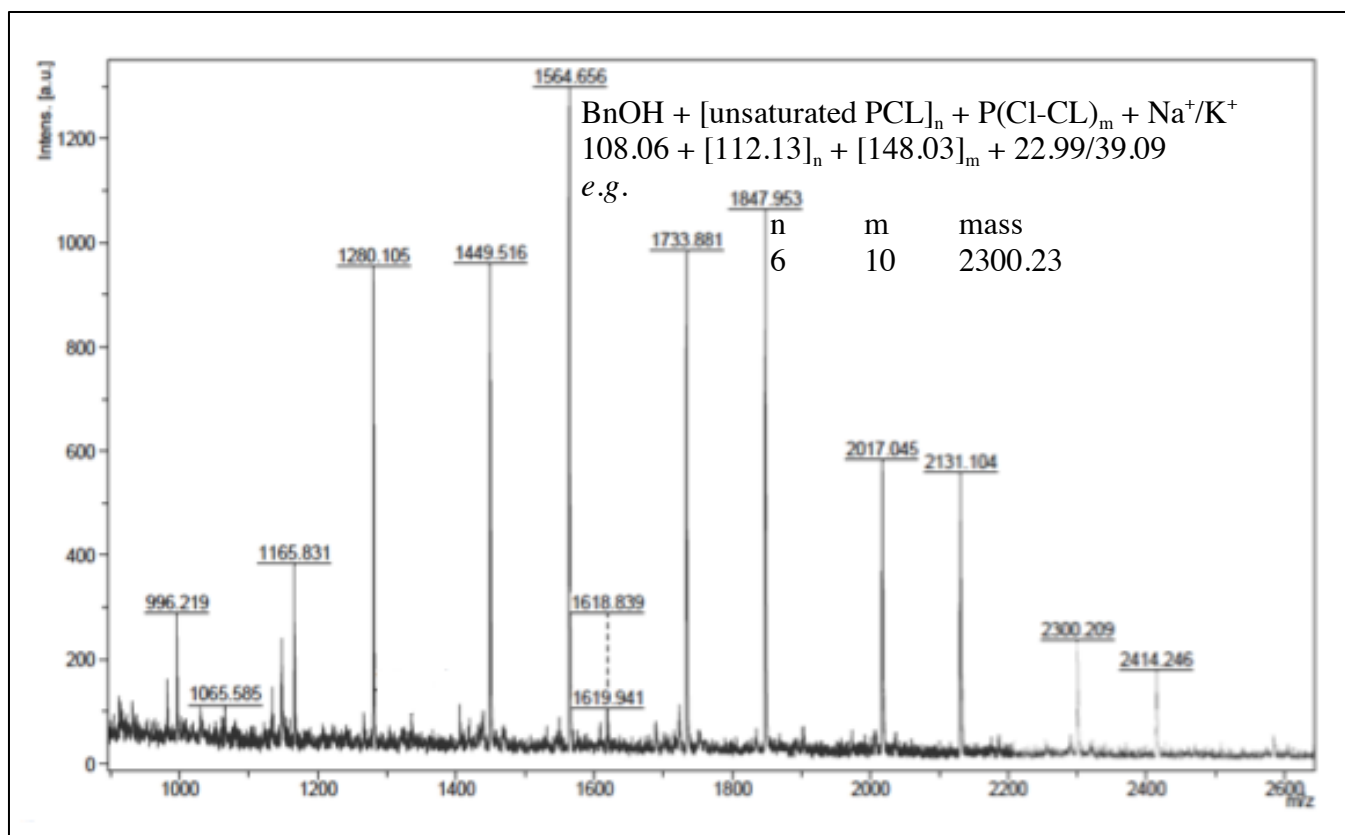


Figure 29: MALDI-TOF spectrum of the P(Cl-CL) prepared by ROP of Cl-CL initiated by *catalyst 2*/BnOH system. (Conditions: $[\text{Cl-CL}]_0 = 1 \text{ M}$, 100 equiv. of Cl-CL, 1 equiv. of BnOH, toluene, 90 °C, polymer isolated at 100% conv. in P(Cl-CL)).

V. Use of Salen catalysts for the ROP of alpha-chloro-epsilon-caprolactone

V. 1. Synthesis of two different salen-based catalysts

Aluminium salen catalysts are known to have a specifically high lactide ROP stereoselectivity⁵ and the ability to affect polymer's tacticity. Indeed, these complexes are employed as initiators for the ROP of *rac*-lactide and showed the formation of isotactic stereoblock.^{6,7,8} Such catalysts were used as ROP initiators for the ROP of P(Cl-CL).

Following a literature procedure,⁹ the reaction between salen ligand^{10,11,12} bearing ^tBu-substituted phenol rings, called “salen(^tBu)H₂”, and with 1 equivalent of AlMe₃ quantitatively yielded the corresponding Al-alkyl complex as a monomeric alkyl complex with a five-coordinate aluminium atom. Then, to produce the corresponding Al-OBn derivative, the alkyl complex was reacted with benzyl alcohol to afford the corresponding alkoxide complex in quantitative yield through an alcoholysis reaction.

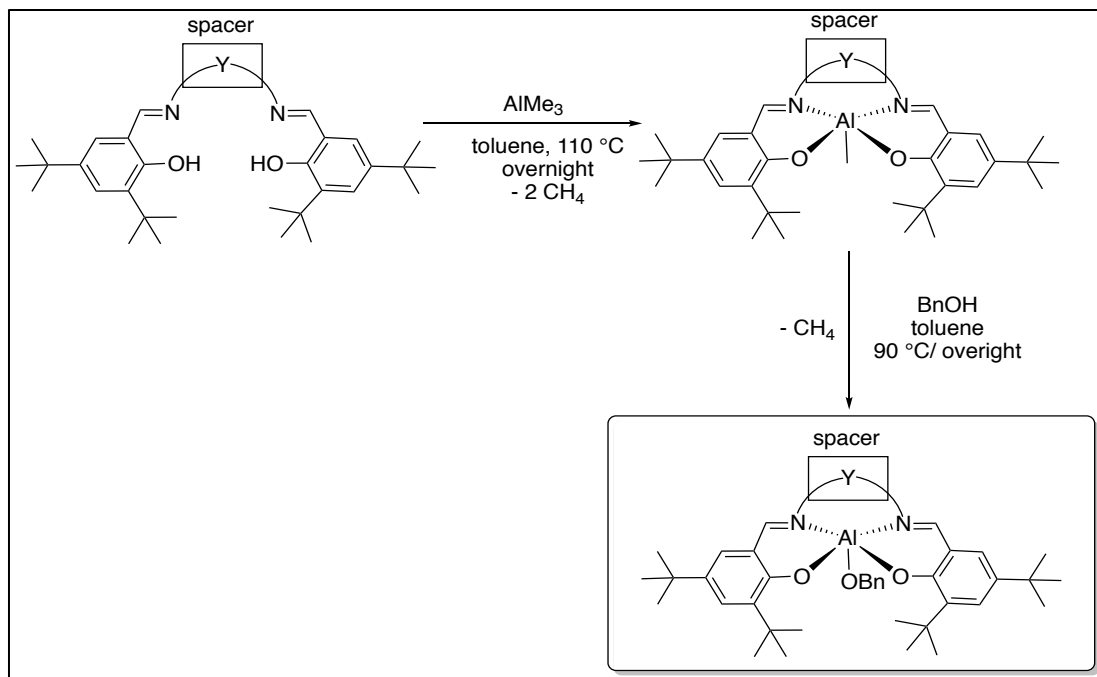
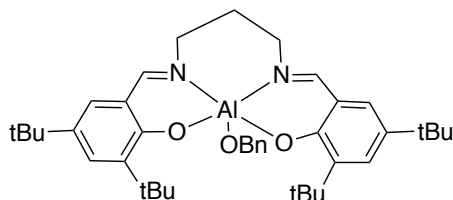


Figure 30: Complexation of “salen(^tBu)₂” ligands with aluminium

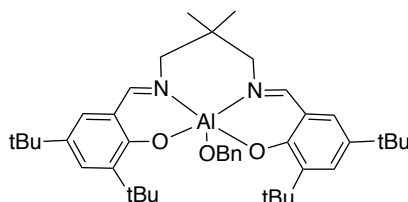
Hence, two different salen catalysts¹³ were synthesized for the ROP of Cl-CL:



[N,N'-bis(3,5-di-*tert*-butylsalicylidene)-1,3-diaminopropanato]aluminium(III) benzyloxyde¹⁴:

SalenAl1-OBn = catalyst 3

and



[N,N'-bis(3,5-di-*tert*-butylsalicylidene)-1,3-diamino-2,2'-dimethylpropanato]aluminium(III)

benzyloxyde¹⁵: *SalenAl2-OBn* = catalyst 4

Figure 31: Two different Al-salen complexes synthesized and tested in the ROP of Cl-CL

V. 2. Kinetic comparison of *catalyst 3* vs. *catalyst 4*

To determine the best catalyst between *catalyst 3* and *4*, kinetic analyses for ROP of Cl-CL were performed at RT using 100 equivalents of Cl-CL. Both plots of $\ln[(M_0/M)]$ versus time are linear. The values of the apparent rate constant were evaluated from the slope and were found to be $4.155 \times 10^{-1} \text{ min}^{-1}$ and $6.564 \times 10^{-1} \text{ min}^{-1}$ respectively (**Figure 32**). Indeed, *catalyst 4* has shown a polymerization rate of only 6.9 minutes for the conversion of 100 equivalents of Cl-CL whereas *catalyst 3* has obtained a total conversion for 100 equivalents of monomer (only) after 11 minutes at room temperature. Therefore, *catalyst 4* is more reactive than *catalyst 3* for the ROP of Cl-CL and consequently was chosen to perform subsequent ROP studies.

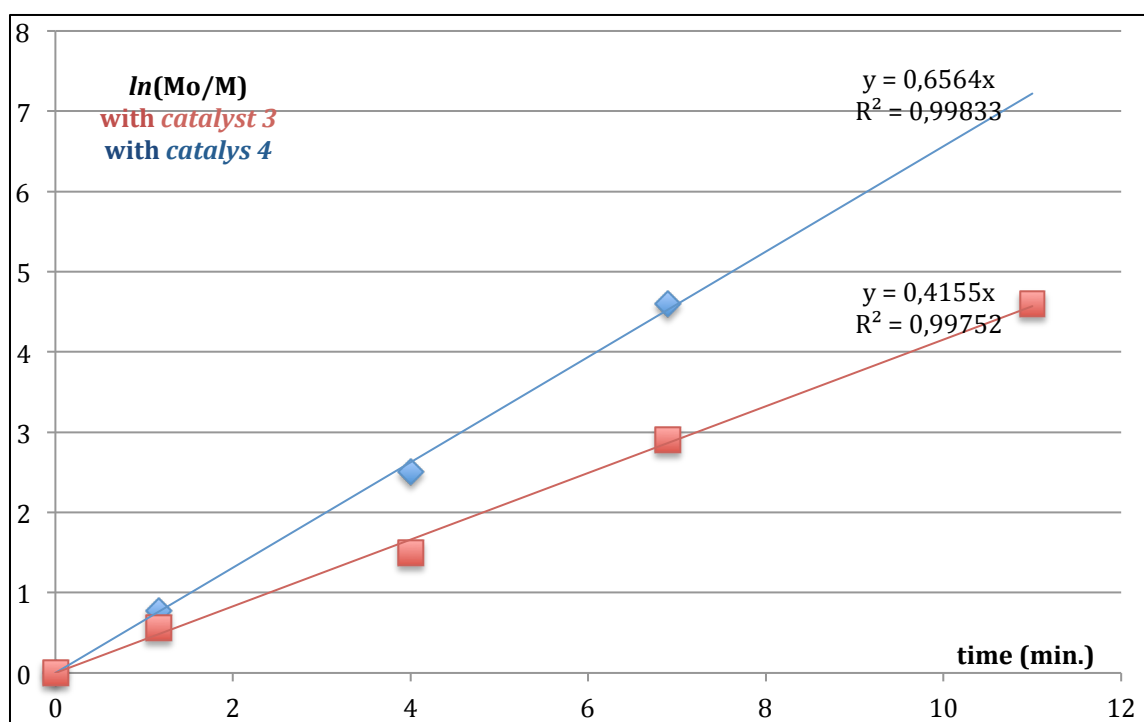


Figure 32: Plot of $\ln(M_0/M)$ as a function of time in the ROP of Cl-CL using first *catalyst 3* then *catalyst 4*. (Conditions: $[\text{Cl-CL}]_0 = 1 \text{ M}$, 100 equiv. in monomer, DCM, RT).

The data obtained by GPC (**Figures 34** and **36**) show both catalysts lead to approximately the same M_n GPC but the P(Cl-CL) obtained with *catalyst 4* exhibits a narrower PDI than that using *catalyst 3* (**entry 2, Table 3**). The ^1H NMR spectra (**Figures 33** and **35**) confirm the linear BnO-ended poly(Cl-CL) formation using both catalysts, (the high singlet peak in Figure

35 corresponds to water signal which probably comes from deuterated chloroform) which is in line with a ROP catalysis proceeding via a classical coordination-insertion mechanism.

Entry	Catalyst	Cl-CL ^a	T (°C)	Time (min.)	Conversion ^b %	M _n theo ^c (g/mol)	M _n GPC ^d (g/mol)	M _n corr ^e (g/mol)	PDI
1	3	100	RT	11	100	14860	16421	14451	1.28
2	4	100	RT	6.9	100	14860	17719	15593	1.17

Polymerization conditions: [Cl-CL]₀ = 1 M, DCM, RT.

^a Equiv. versus initiator. ^b Monomer conversion. ^c Calculated using $M_{n\text{ theo}} = [\text{Cl-CL}]_0 \times M_{\text{Cl-CL}} \times \text{conv.}$ ^d Measured by GPC in THF (30 °C) using PS standards. ^e $M_{n\text{ GPC}} \times 0.88$ (0.88: correlation factor obtained **section VIII**).

Table 3: Comparison of GPC data for *catalyst 3* versus *catalyst 4* in the ROP of 100 equivalents of Cl-CL (conditions: [Cl-CL]₀ = 1 M, 100 equivalents of Cl-CL, DCM, RT).

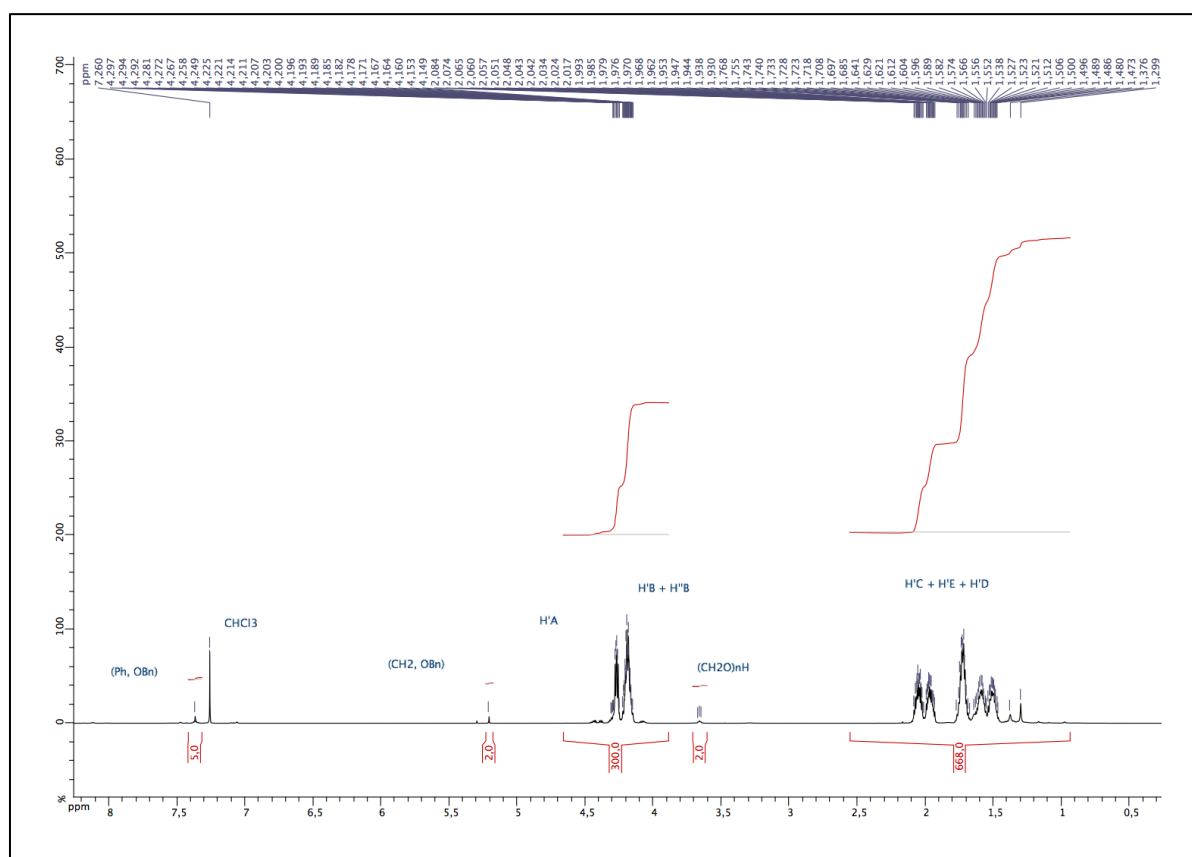


Figure 33: ¹H NMR (CDCl₃, 400 MHz) of isolated P(Cl-CL) prepared via ROP of Cl-CL by *catalyst 3*. (Conditions: [Cl-CL]₀ = 1 M, DCM, RT, 11 min., 100% conversion).

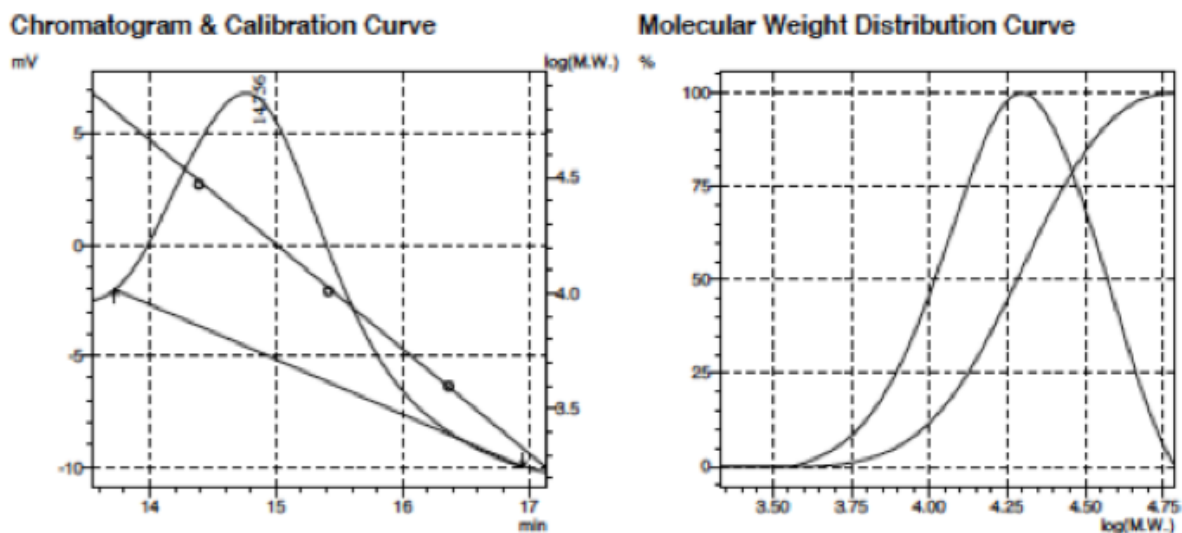


Figure 34: SEC traces of isolated P(Cl-CL) prepared via ROP of Cl-CL by *catalyst 3*. (Conditions: $[\text{Cl-CL}]_0 = 1 \text{ M}$, DCM, RT, 11 min., 100% conv.).

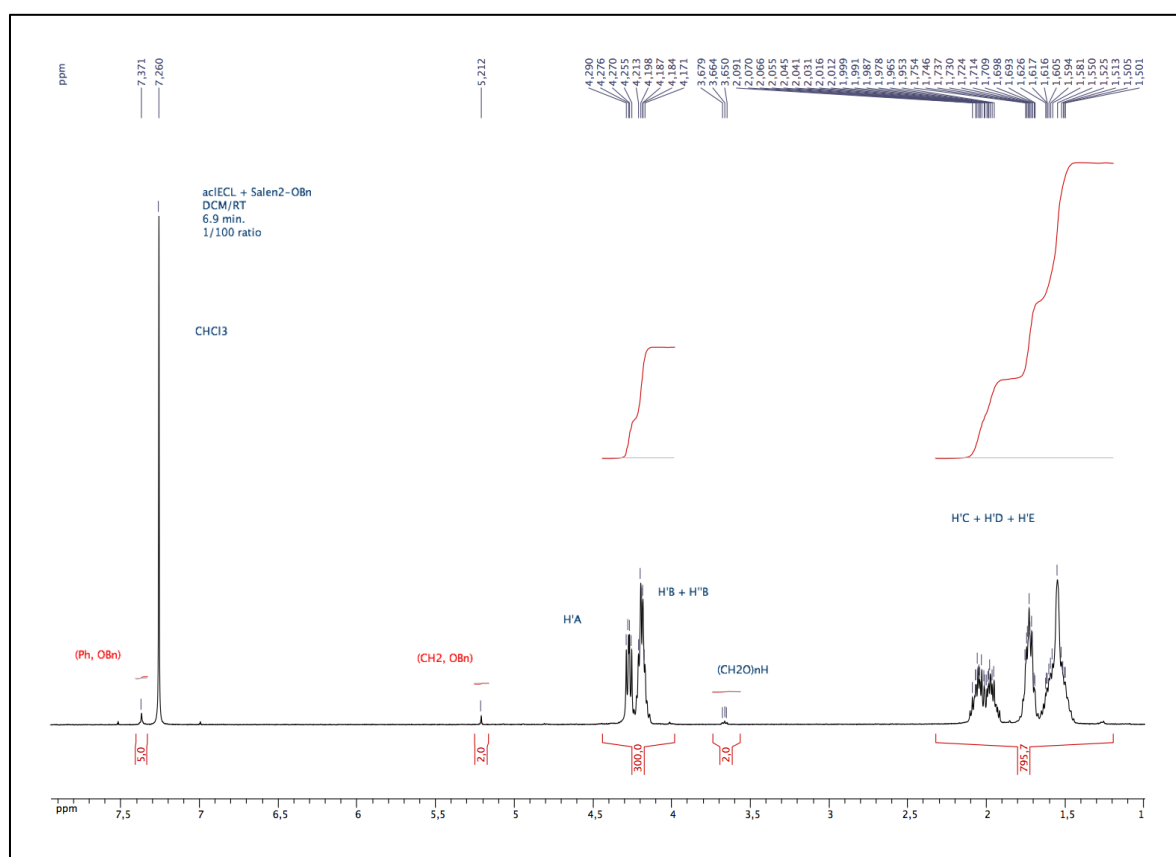


Figure 35: ^1H NMR (CDCl_3 , 400 MHz) of isolated P(Cl-CL) prepared via ROP of Cl-CL by *catalyst 4*. (Conditions: $[\text{Cl-CL}]_0 = 1 \text{ M}$, DCM, RT, 6.9 min., 100% conv.).

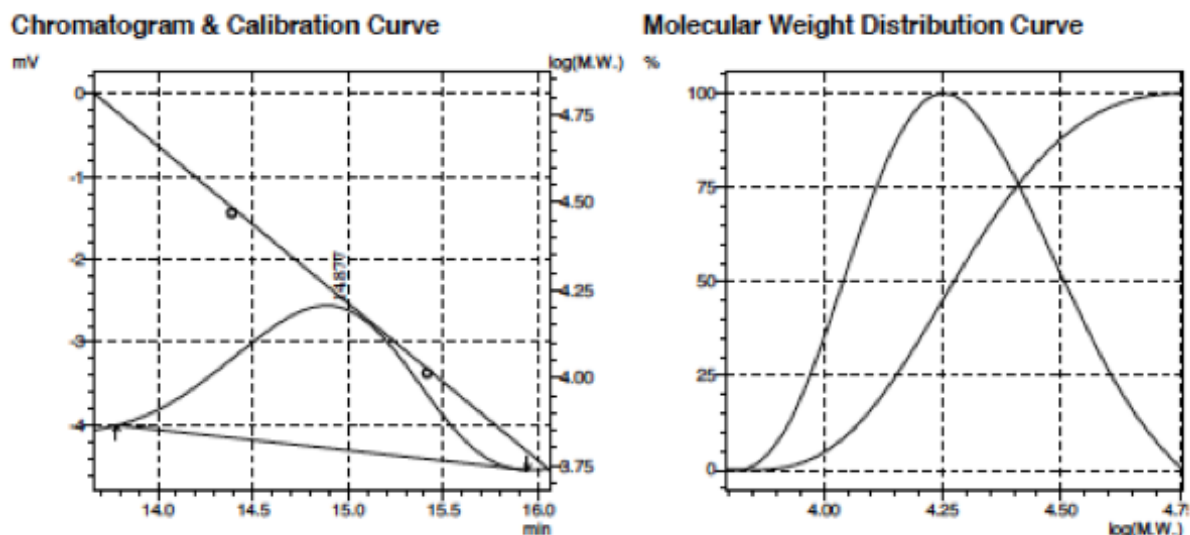


Figure 36: SEC traces of isolated P(Cl-CL) prepared via ROP of 100 equiv. of Cl-CL by *catalyst 4*. (Conditions: $[\text{Cl-CL}]_0 = 1 \text{ M}$, DCM, RT, 6.9 min., 100% conv.).

V. 3. Stability of Cl-CL' ROP above RT

Given the current industrial ROP of cyclic esters under bulk conditions (the melted monomer acts as a solvent and reagent), the ROP of 100 equivalents of Cl-CL was performed under bulk conditions (heating a mixture of Cl-CL and *catalyst 4* at 55 °C over 15 minutes).

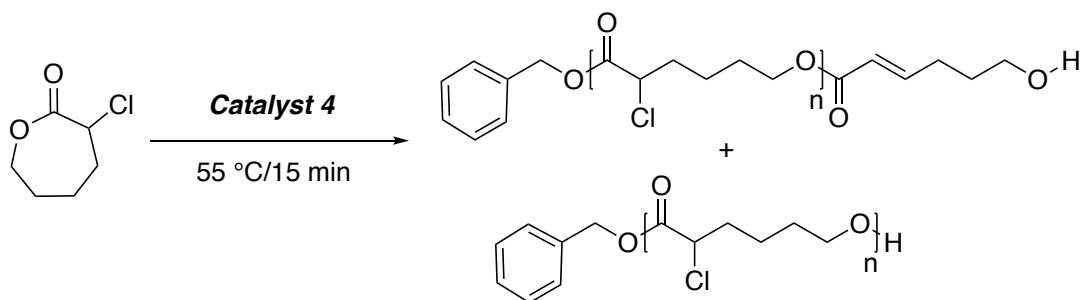


Figure 37: ROP of Cl-CL performed in bulk condition. (Conditions: 100 equivalents of Cl-CL vs. *catalyst 4*, 55 °C, 15 min., 99% conv.).

In the ^1H NMR spectrum (**Figure 38**), the presence of two new multiplets at 4.94 and 5.07 ppm is noticeable with identical integration, probably meaning the formation of a chloride elimination by-product during the ROP. Indeed, the chlorine pendant group is a leaving group and heating it during the ROP favors an elimination reaction. These data further confirm the limited stability of linear poly(Cl-CL).

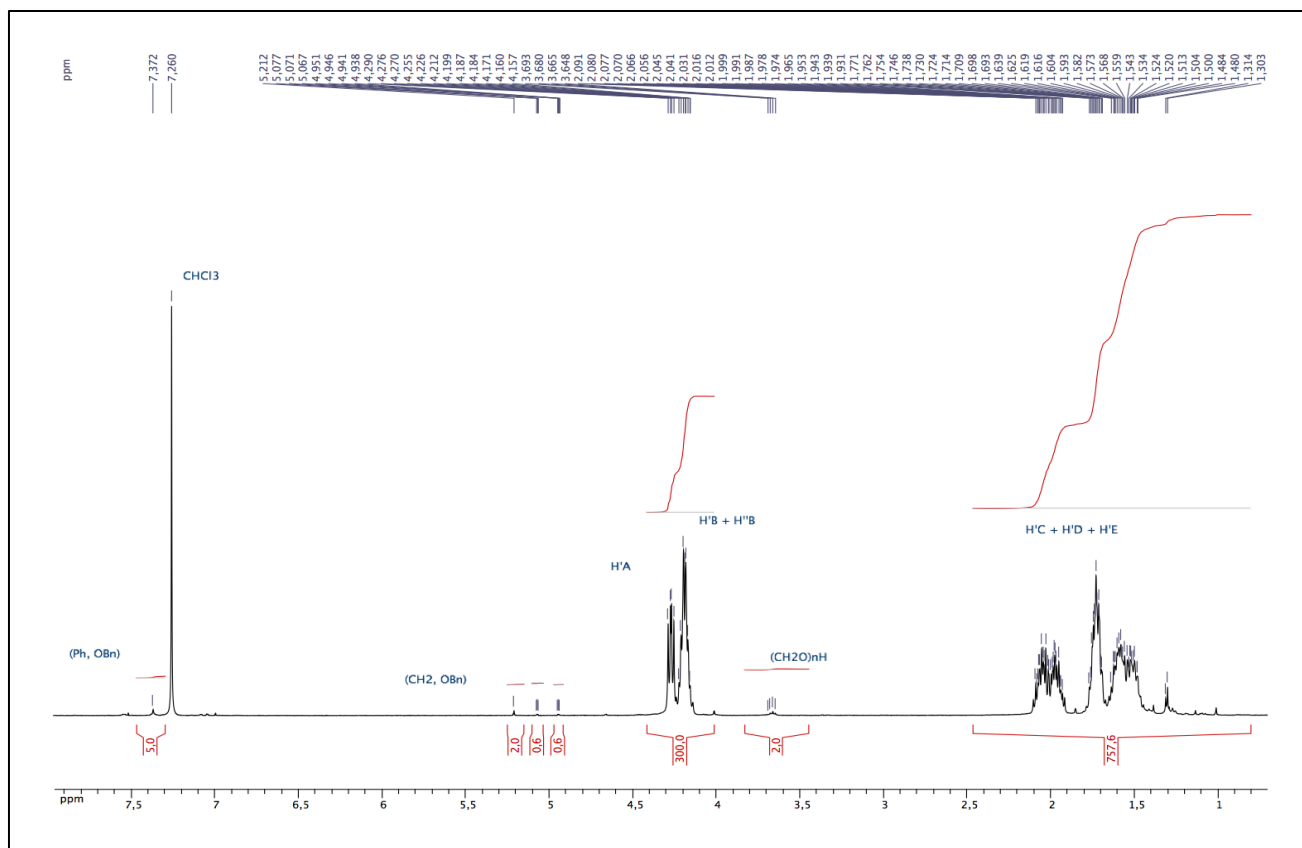


Figure 38: ^1H NMR (CDCl_3) of isolated P(Cl-CL) using 100 equiv. of Cl-CL, 1 equiv. of catalyst **4**. (Conditions: bulk, 55°C , 15 min., polymer isolated at 99% conv.).

In addition, the SEC traces for the obtained polymer (notably the molecular weight distribution curve) are bimodal (**Figure 39**) with a broad polydispersity (PDI: 1.54). These data allow one to conclude about the formation of a polymer mixture.

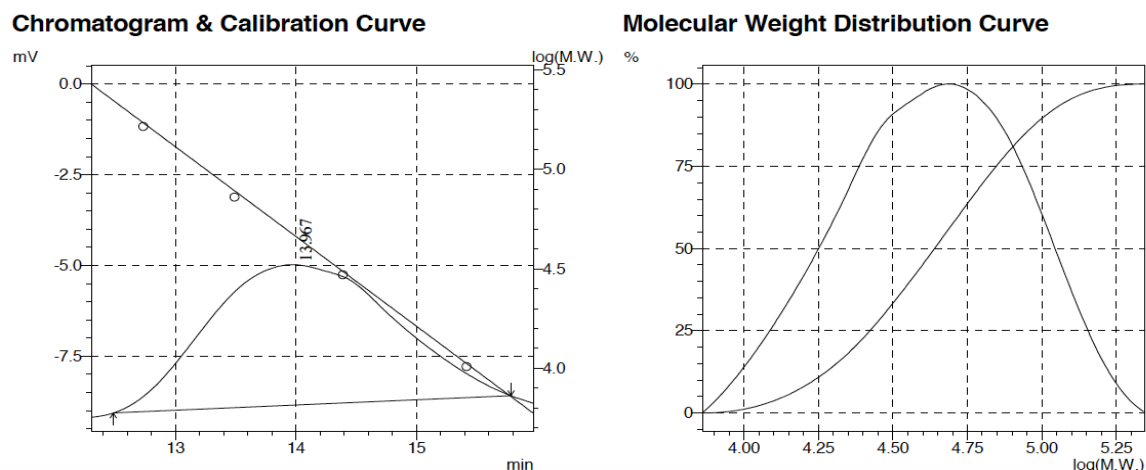


Figure 39: SEC traces of isolated polymer prepared via ROP of Cl-CL by the *catalyst 4*. (Conditions: bulk, 100 equiv. of Cl-CL, 55 °C, 15 min., polymer isolated at 99% conv.).

The MALDI-TOF obtained for this bulk polymerization (**Figure 40**) also supports the same conclusion than the ^1H NMR and SEC traces. Two different sets of peaks are identified and agree with the presence of linear BnO-ended poly(Cl-CL) along with degraded polymer material due to elimination reactions. Consequently, the ROP under bulk conditions confirms the results obtained while using the Zn(II) *catalyst 2* and shows the necessity to perform the ROP of Cl-CL at room temperature or even at a lower temperature.

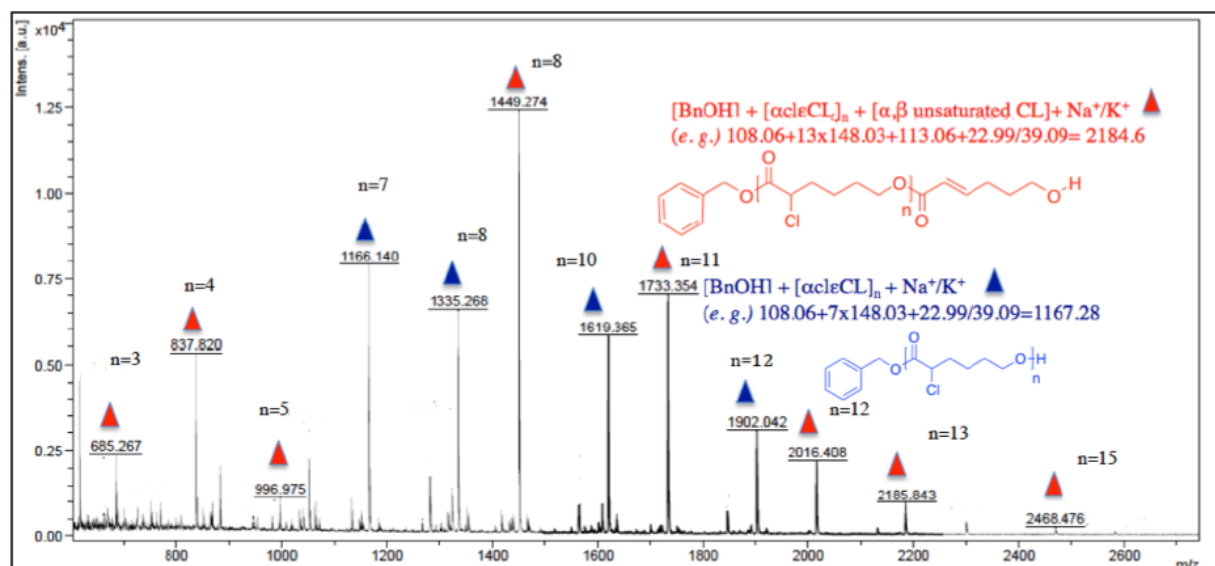


Figure 40: Zoom-in of the MALDI-TOF spectrum of the polymer prepared by ROP of Cl-CL initiated by the *catalyst 4*. (Conditions: bulk, 100 equiv. of Cl-CL, 55 °C, 15 min. polymer isolated at 99% conv.).

V. 4. Use of salen aluminium alkoxide **4** as ROP initiator of Cl-CL at RT

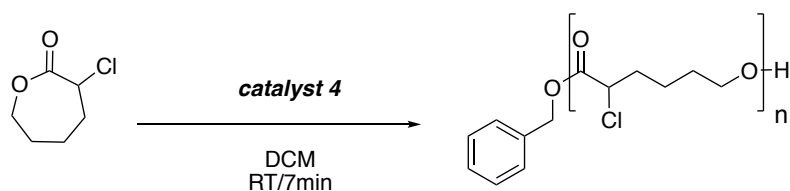


Figure 41: ROP of 100 equivalents of Cl-CL initiated by species **4**

catalyst	Cl-CL ^a	BnOH ^a	T (°C)	Time (min.)	Conversion ^b %	M_n theo ^c (g/mol)	M_n GPC ^d (g/mol)	M_n corr ^e (g/mol)	PDI
4	100	/	RT	1	40	6241	6945	6112	1.32
4	100	/	RT	2.7	82	12928	14431	12699	1.44
4	100	/	RT	4.3	93	13819	16465	14489	1.05
4	100	/	RT	6.9	100	14860	17719	15593	1.17

Polymerization conditions: [Cl-CL]₀ = 1 M, DCM, RT.

^a Equiv. versus initiator. ^b Monomer conversion. ^c Calculated using $M_{n \text{ theo}} = [\text{Cl-CL}]_0 \times M_{\text{Cl-CL}} \times \text{conv.}$ ^d Measured by GPC in THF (30 °C) using PS standards. ^e $M_n \text{ GPC} \times 0.88$ (0.88: correlation factor obtained **section VIII**).

Table 4: ROP of 100 equivalents of Cl-CL using the alkoxide aluminium salen catalyst **4**

At room temperature, the total conversion of 100 equivalents of Cl-CL in P(Cl-CL) was performed within seven minutes using the *catalyst 4* and a narrow polydispersity was observed (PDI: 1.17) (**entry 9, Table 2**). The ¹H NMR spectrum of the polymer clearly shows the presence of the benzyloxy group (δ ($\text{CH}_2\text{-Ph}$): 5.21 ppm and δ ($\text{CH}_2\text{-Ph}$): 7.37 ppm) (**Figure 42**): the NMR data are thus consistent with a linear BnO-ester-ended poly(Cl-CL) material.

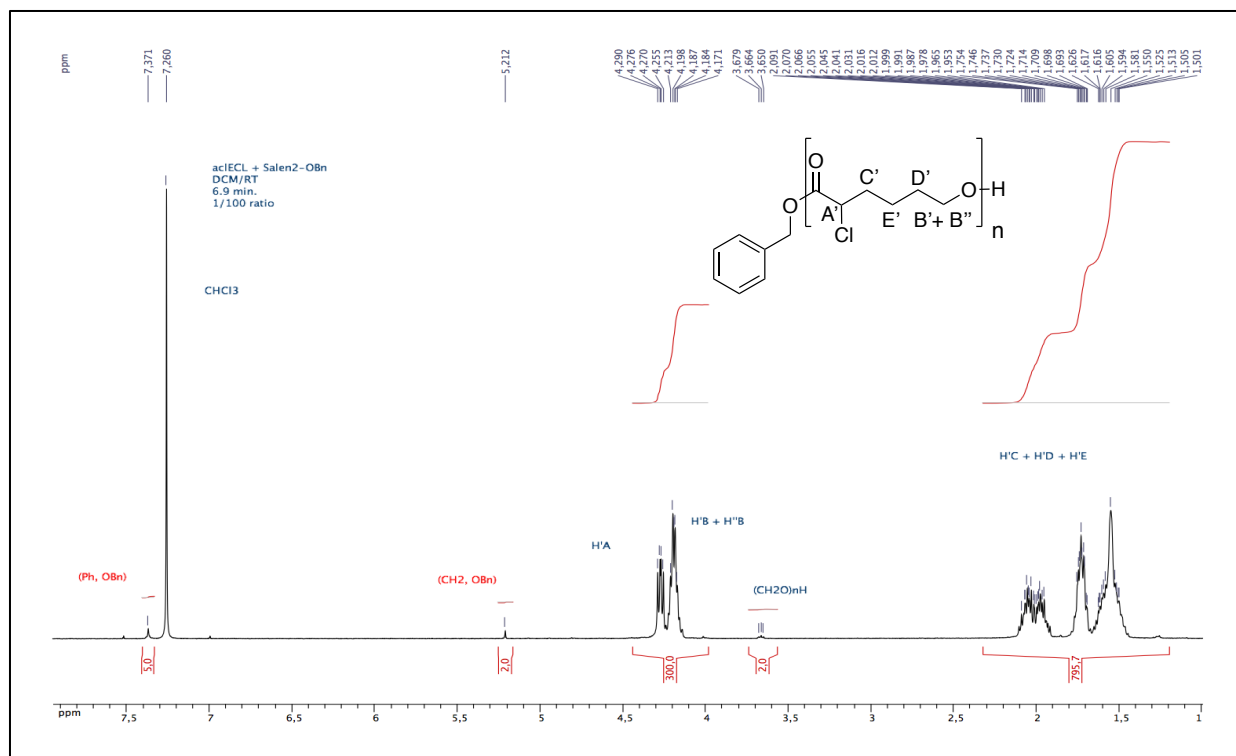


Figure 42: ^1H NMR (CDCl_3 , 400 MHz) of isolated P(Cl-CL) prepared by ROP of 100 equiv. of Cl-CL (vs. catalyst) initiated by *catalyst 4*. (Conditions: $[\text{Cl-CL}]_0 = 1 \text{ M}$, DCM, RT, 6.9 min., 100% conv.).

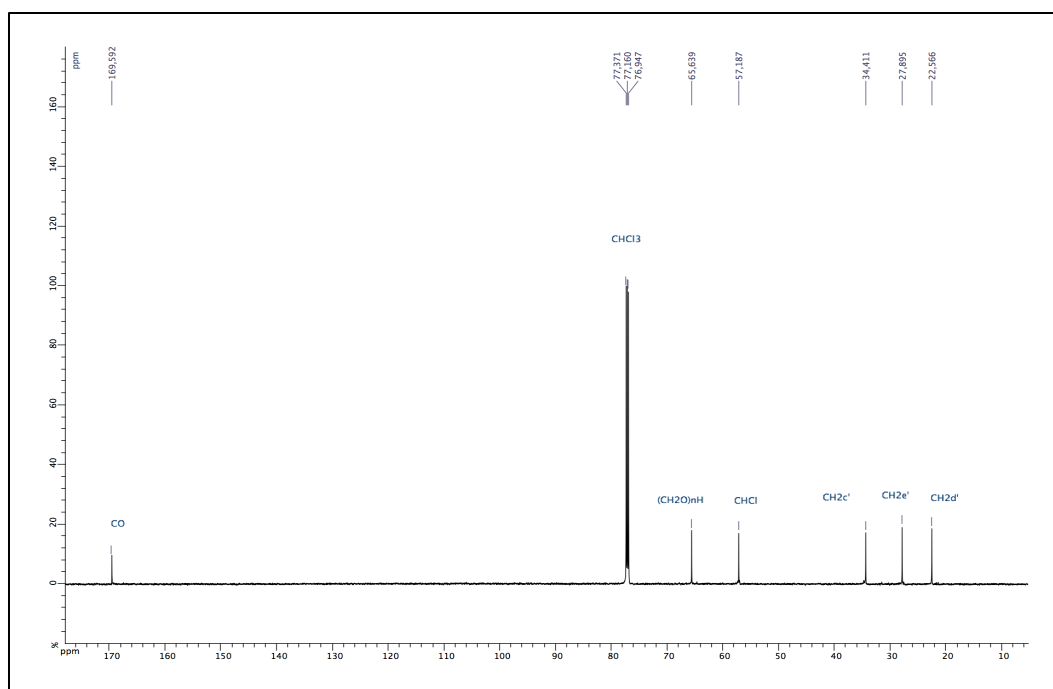


Figure 43: ^{13}C NMR spectrum (CDCl_3 , 500 MHz) of isolated P(Cl-CL) prepared by ROP of 100 equiv. of Cl-CL (vs. catalyst) initiated by *catalyst 4*. (Conditions: $[\text{Cl-CL}]_0 = 1 \text{ M}$, DCM, RT, 6.9 min., 100% conv.).

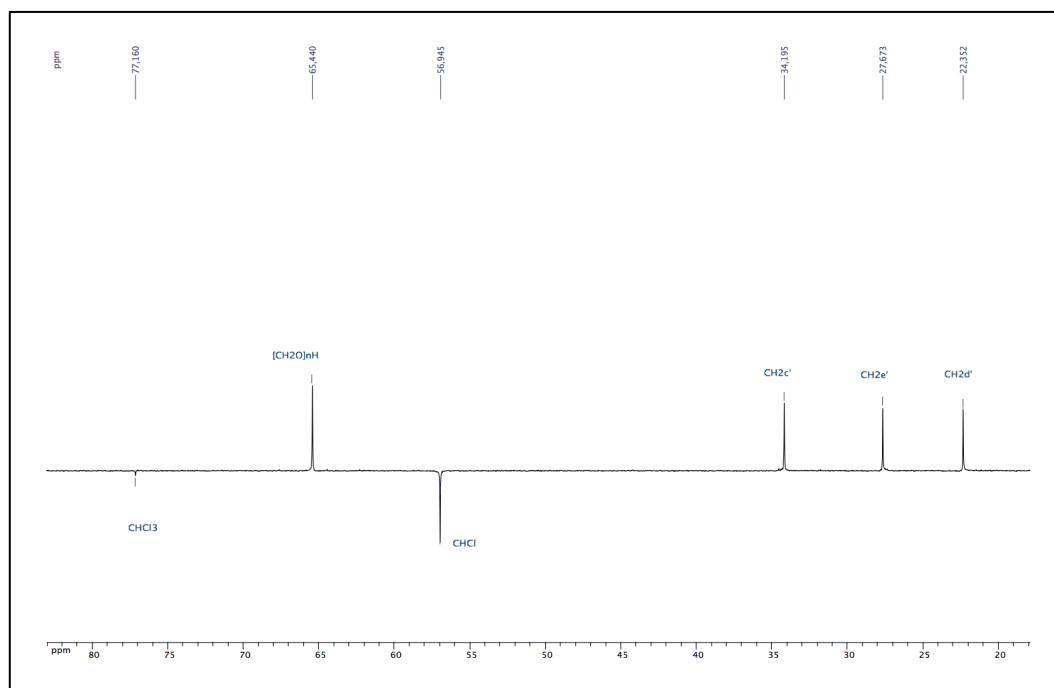


Figure 44: DEPT NMR spectrum (CDCl₃, 500 MHz) of isolated P(Cl-CL) prepared by ROP of 100 equiv. of Cl-CL (vs. catalyst) initiated by *catalyst 4*. (Conditions: [Cl-CL]₀= 1 M, DCM, RT, 6.9 min., 100% conv.).

Moreover, the SEC traces for the obtained P(Cl-CL) are monomodal (**Figure 45**) which allows one to conclude about the formation of a well-defined linear polymer.

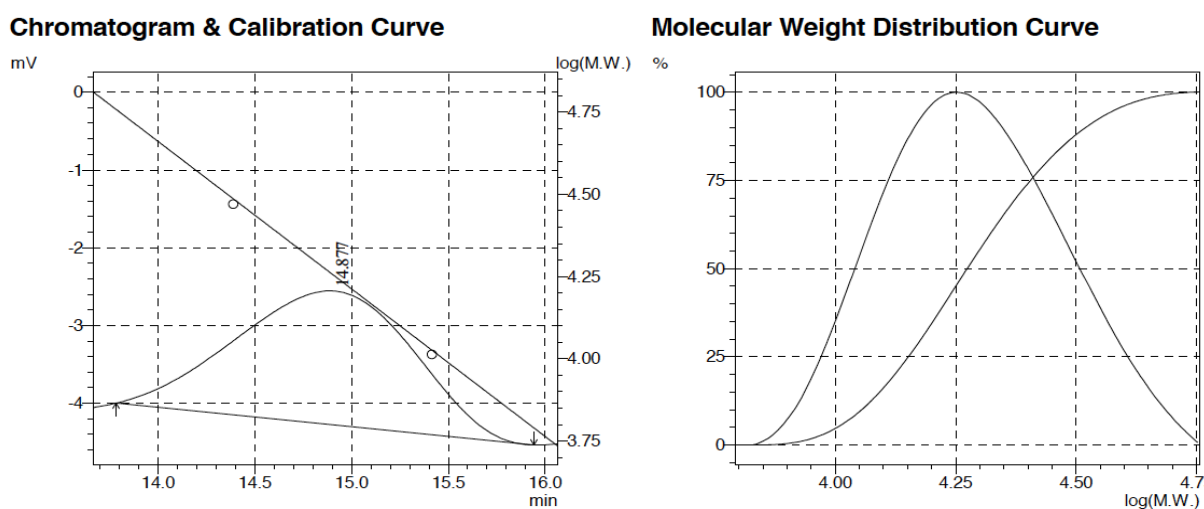


Figure 45: SEC traces of isolated P(Cl-CL) prepared via ROP of Cl-CL initiated by the *catalyst 4* system. (Conditions: [Cl-CL]₀= 1 M, 100 equiv. of Cl-CL vs. *catalyst 4*, RT, DCM, 100% conv., 6.9 min.).

Kinetic studies carried out for the *catalyst 4* system are consistent with a ROP proceeding in a controlled manner. Indeed, the plot of $\ln[(M_0/M)]$ vs. time is linear indicating a first-order kinetic (**Figure 46**), and the value of the apparent rate constant for Cl-CL polymerization initiated by **4** was found to be $6.499 \times 10^{-1} \text{ min}^{-1}$. Moreover, the plot of M_n vs. monomer conversion (**Figure 47**) depicts M_n values that linearly correlate with monomer conversion, which supports a controlled chain propagation.

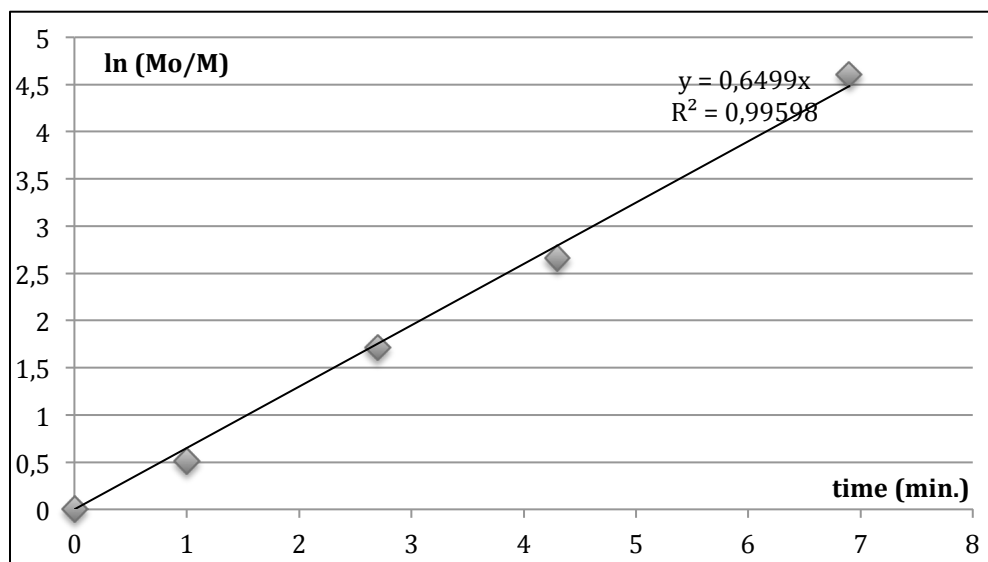


Figure 46: Plot of $\ln(M_0/M)$ as a function of time in the ROP of Cl-CL using *catalyst 4*. (Conditions: $[Cl-CL]_0 = 1 \text{ M}$, 100 equiv. in monomer, DCM, RT, quantitative conv.).

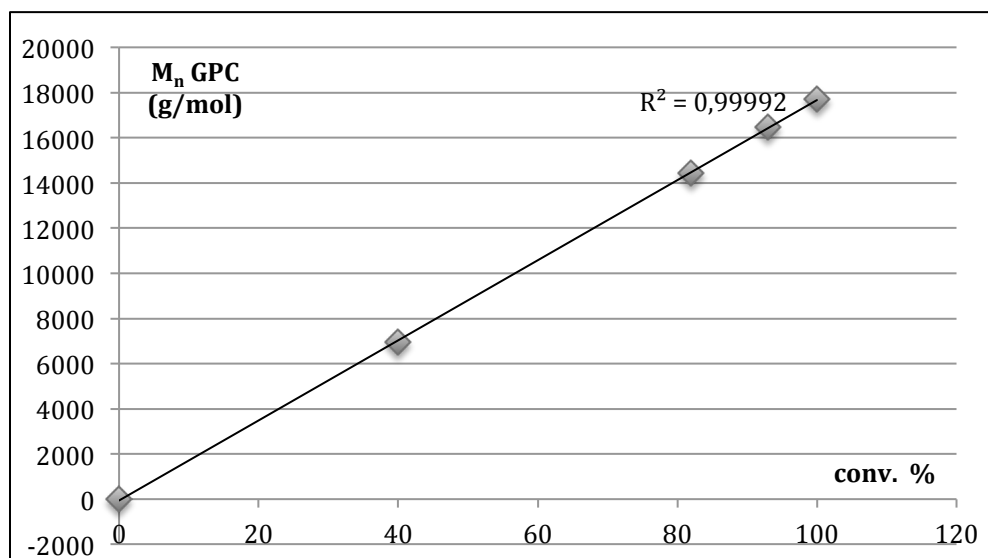


Figure 47: Plot of M_n as a function of the conv. in the ROP of Cl-CL using *catalyst 4*. (Conditions: $[Cl-CL]_0 = 1 \text{ M}$, 100 equiv. in monomer, DCM, RT, quantitative conv.).

The resulting polymer was characterized using MALDI-TOF spectrometry (**Figure 48**) further confirming the formation of BnO-ended linear poly(Cl-CL). Note that the MALDI-TOF apparatus isn't a powerful enough tool to only show the monoisotopic masses (**Supporting data: Figure 1**). The data match with the presence of a benzyloxy moiety at the ester end chain with equally spaced peaks by 148.03 g/mol (corresponding to a monomer unit).

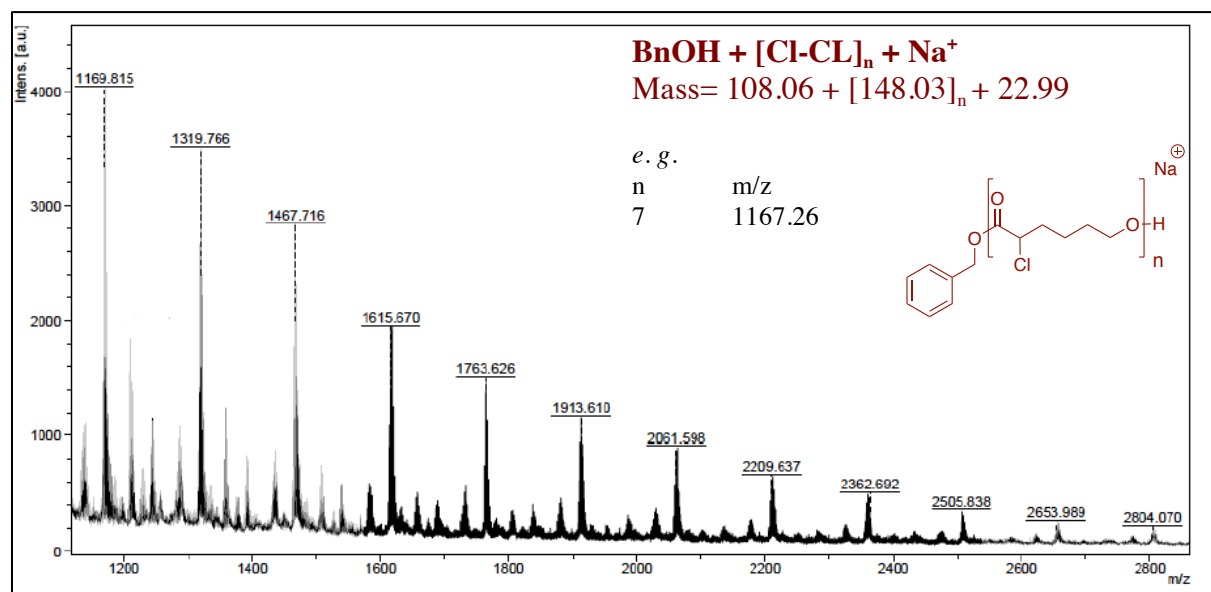


Figure 48: Zoom-in of the MALDI-TOF spectrum of the P(Cl-CL) prepared by ROP of Cl-CL initiated by the *catalyst 4* system. (Conditions $[\text{Cl-CL}]_0 = 1 \text{ M}$, 100 equiv. of Cl-CL, DCM, RT, polymer isolated at 100% conv. in P(Cl-CL)).

Thus, contrasting with the production of primarily cyclic polymers using the Mg(II) *catalyst 1* and a rather ill-defined material using Zn(II) *catalyst 2* as ROP catalyst, the salen *catalyst 4* leads to a successful formation of a well-defined linear P(Cl-CL).

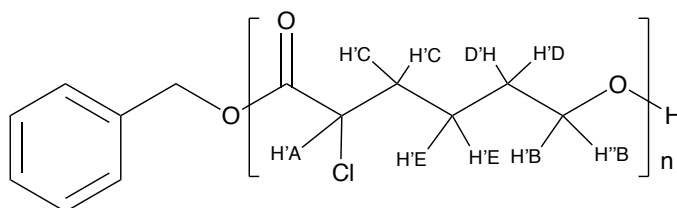


Figure 49: Attribution of the different protons on P(Cl-CL)

To further explore the well-controlled nature of the ROP of Cl-CL by *catalyst 4*, materials with longer chain length were prepared using 250 equivalents and also 500 equivalents of Cl-CL.

VI. Extension of the P(Cl-CL) chain length

VI. 1. 250 equivalents of P(Cl-CL)

catalyst	Cl-CL ^a	BnOH ^a	T (°C)	Time (min.)	Conversion ^b %	M _n theo ^c (g/mol)	M _n GPC ^d (g/mol)	M _n corr ^e (g/mol)	PDI
<i>4</i>	250	/	RT	10	33	12260	28955	25480	1.28
<i>4</i>	250	/	RT	15	42	18575	34241	30132	1.16
<i>4</i>	250	/	RT	35	64	26005	56896	50069	1.58
<i>4</i>	250	/	RT	130	100	37150	90500	79640	1.25

Polymerization conditions: [Cl-CL]₀ = 1 M, DCM, RT.

^a Equiv. versus initiator. ^b Monomer conversion. ^c Calculated using $M_{n\text{ theo}} = [\text{Cl-CL}]_0 \times M_{\text{Cl-CL}} \times \text{conv.}$ ^d Measured by GPC in THF (30 °C) using PS standards. ^e $M_{n\text{ GPC}} \times 0.88$ (0.88: correlation factor obtained **section VIII**).

Table 5: ROP of 250 equivalents in Cl-CL using the alkoxide aluminium salen *catalyst 4*

With a ratio of 250 equivalents of Cl-CL vs. *catalyst 4*, the ROP was longer than using 100 equivalents in monomer and was completed within 2h10 at RT leading a linear polymer as well. Indeed, the ¹H NMR spectrum features the same benzyloxy signals (**Figure 50**) as seen for the polymerization of 100 equivalents of monomer and the MALDI-TOF spectrometric data (**Figure 54**) also lead to the same conclusion (**Supporting data: Figure 2**).

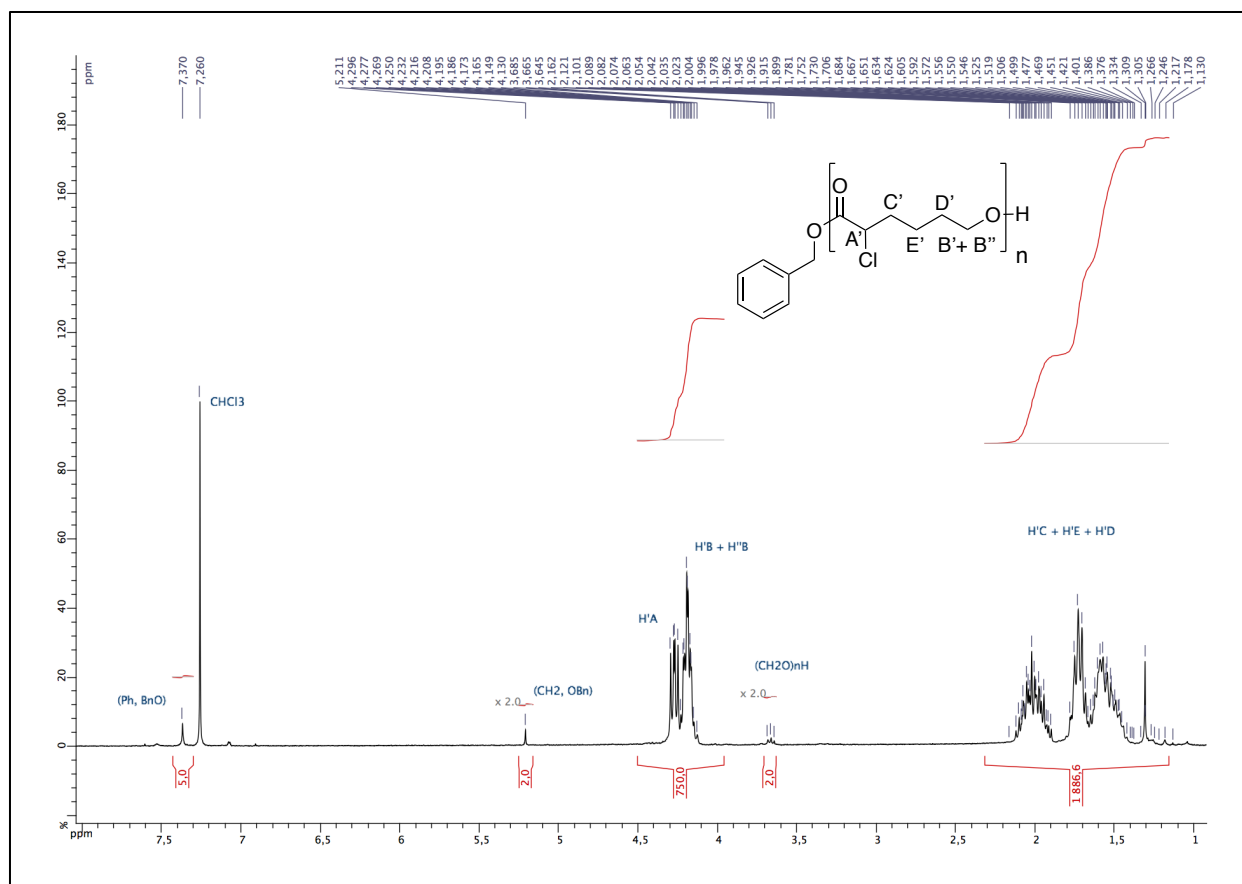


Figure 50: ^1H NMR spectrum (CDCl_3 , 400 MHz) of isolated P(Cl-CL) prepared by ROP of 250 equiv. of Cl-CL vs. *catalyst 4*. (Conditions: $[\text{Cl-CL}]_0 = 1 \text{ M}$, 250 equiv. of Cl-CL, DCM, RT, 130 min., quantitative conv.).

Similarly to the P(Cl-CL) made with 100 equivalents of Cl-CL, the GPC data for the obtained P(Cl-CL) are monomodal and agree with a narrow disperse material (PDI: 1.25) (**Figure 51**).

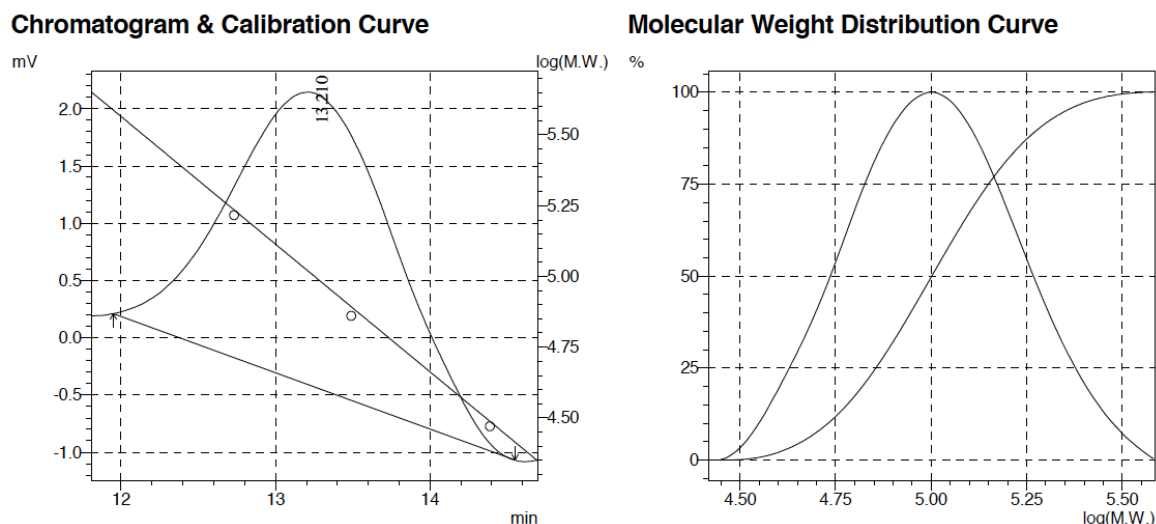


Figure 51: SEC traces of isolated P(Cl-CL) prepared via ROP of Cl-CL by the *catalyst 4* system. (Conditions: $[\text{Cl-CL}]_0 = 1 \text{ M}$, 250 equiv. of Cl-CL, DCM, RT, 100% conv., 130 min.).

As seen previously with 100 equivalents of Cl-CL, the kinetic studies carried out for the ROP of 250 equivalents in Cl-CL by *catalyst 4* match with a ROP proceeding in a controlled manner. The first-order kinetic in Cl-CL agrees with a controlled ROP process with $k_{\text{app}} = 3.52 \times 10^{-2} \text{ min}^{-1}$ (**Figure 52**) and a linear correlation between the M_n value of the formed P(Cl-CL) and the monomer conversion during the polymerization reaction is observed (**Figure 53**), demonstrating that the polymer chain grows linearly with monomer conversion even if the M_n GPC values are higher than the theoretical ones (**entry 13, Table 2**).

This molecular weight values could be explained by an initiation step consequently slower than the propagation step. Also, it is possible that repulsion between the polymer's backbone segments brings the polymer chains to contract and that it leads to their formation. The size and density of this material led to a partial insolubility of poly(Cl-CL) in THF. The solubility dramatically influences the polymers' functional properties and that could be a likely explanation for the obtained molecular weight values.

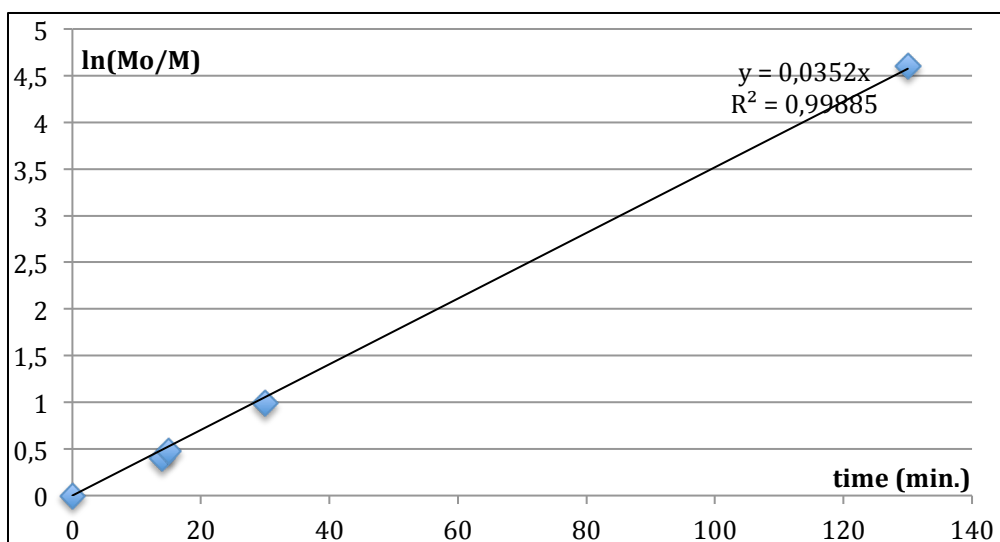


Figure 52: Plot of $\ln(M_0/M)$ as a function of time in the ROP of Cl-CL using the *catalyst 4* system. (Conditions: $[Cl-CL]_0 = 1$ M, 250 equiv. in monomer, DCM, RT).

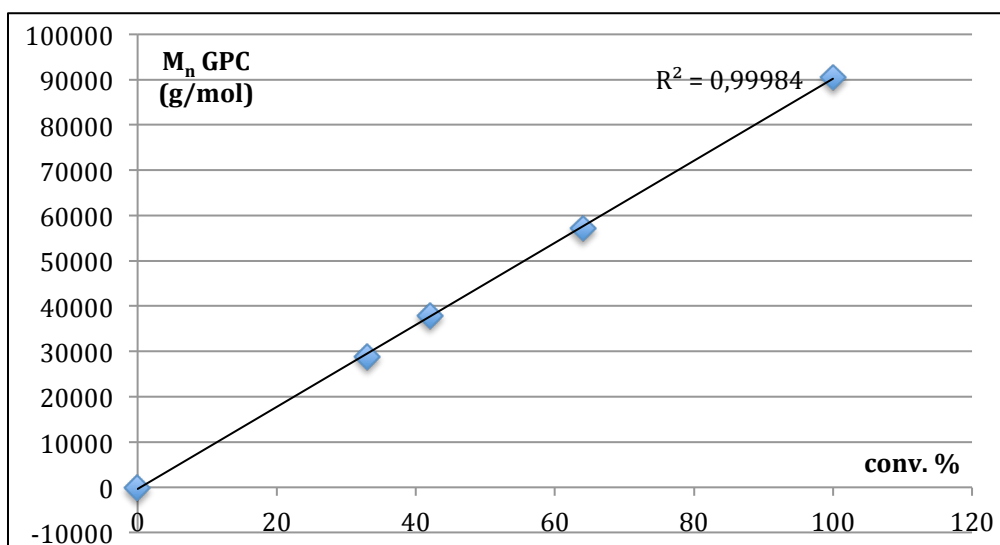


Figure 53: Plot of M_n as a function of the conv. in the ROP of Cl-CL using *catalyst 4*. (Conditions: $[Cl-CL]_0 = 1$ M, 250 equiv. in monomer, DCM, RT).

The MALDI-TOF spectrum of the obtained P(Cl-CL) prepared with *catalyst 4* initiator agrees with a linear P(Cl-CL) bonded to a benzyloxy moiety at the ester chain end such as for the ROP performed with 100 equivalents of Cl-CL. The difference between two successive peaks on the spectrum is 148.03 (the mass of one Cl-CL unit) (**Figure 54**).

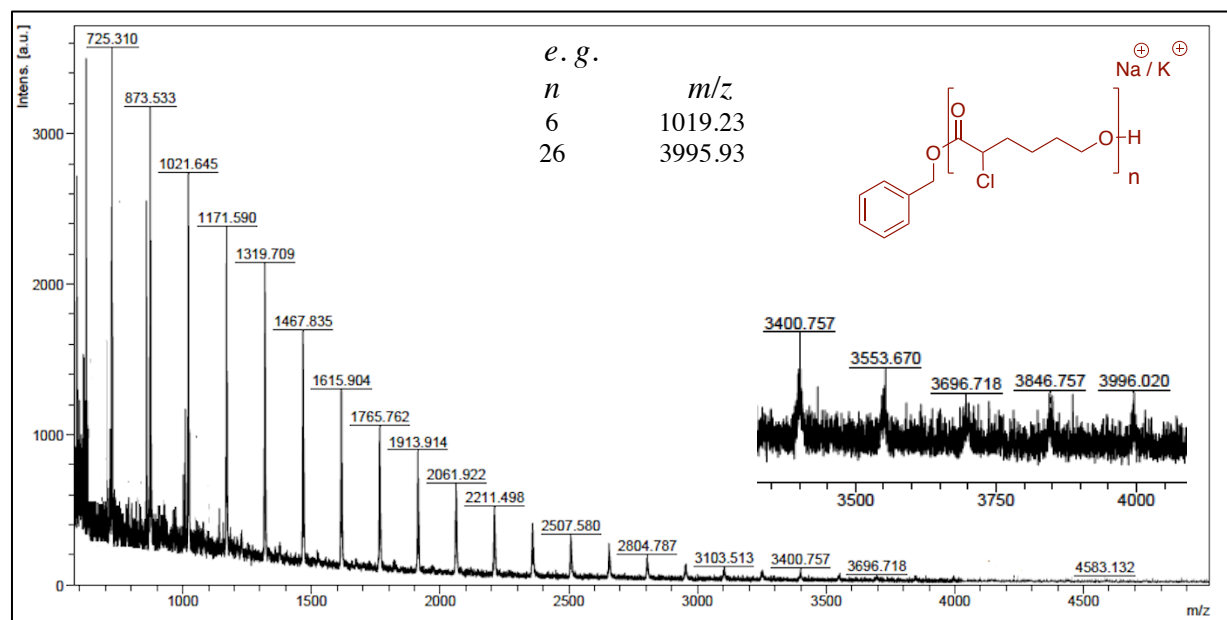


Figure 54: MALDI-TOF spectrum and zoom-in from m/z : 3400.757 to m/z : 3996.020 of the P(Cl-CL) prepared by ROP of Cl-CL initiated by the *catalyst 4* system. (Conditions $[\text{Cl-CL}]_0 = 1 \text{ M}$, 250 equiv. of Cl-CL, DCM, RT, isolated P(Cl-CL) at 100% conv.).

The ROP using 250 equivalents of Cl-CL appears to be a well-controlled process despite the higher than expected M_n values, as mentioned above, the latter presumably reflecting a higher propagation *vs.* initiation rate for Cl-CL ROP by species **4** under the studied conditions.

VI. 2. 500 equivalents of P(Cl-CL)

catalyst	Cl-CL ^a	BnOH ^a	T (°C)	Time (min.)	Conversion ^b %	M _n theo ^c (g/mol)	M _n GPC ^d (g/mol)	M _n corr ^e (g/mol)	PDI
4	500	/	RT	420	100	74300	61357	53994	1.56

Polymerization conditions: [Cl-CL]₀ = 1 M, DCM, RT.

^a Equiv. versus initiator. ^b Monomer conversion. ^c Calculated using $M_{n \text{ theo}} = [\text{Cl-CL}]_0 \times M_{\text{Cl-CL}} \times \text{conv.}$ ^d Measured by GPC in THF (30 °C) using PS standards. ^e $M_{n \text{ GPC}} \times 0.88$ (0.88: correlation factor obtained **section VIII**).

Table 6: ROP of 500 equivalents in Cl-CL using the alkoxide aluminium salen *catalyst 4*

Performing the ROP of 500 equivalents of Cl-CL with *catalyst 4* led to a surprisingly longer polymerization time (7 hours) for complete monomer conversion. Unlike previous ROP performed with 100 equivalents then 250 equivalents of Cl-CL monomer vs. *catalyst 4*, the SEC traces feature a bimodal signal leading to an overall broad polydispersity (PDI: 1.56) (**Figure 55**) and indicating the formation of two polymeric materials with different chain length.

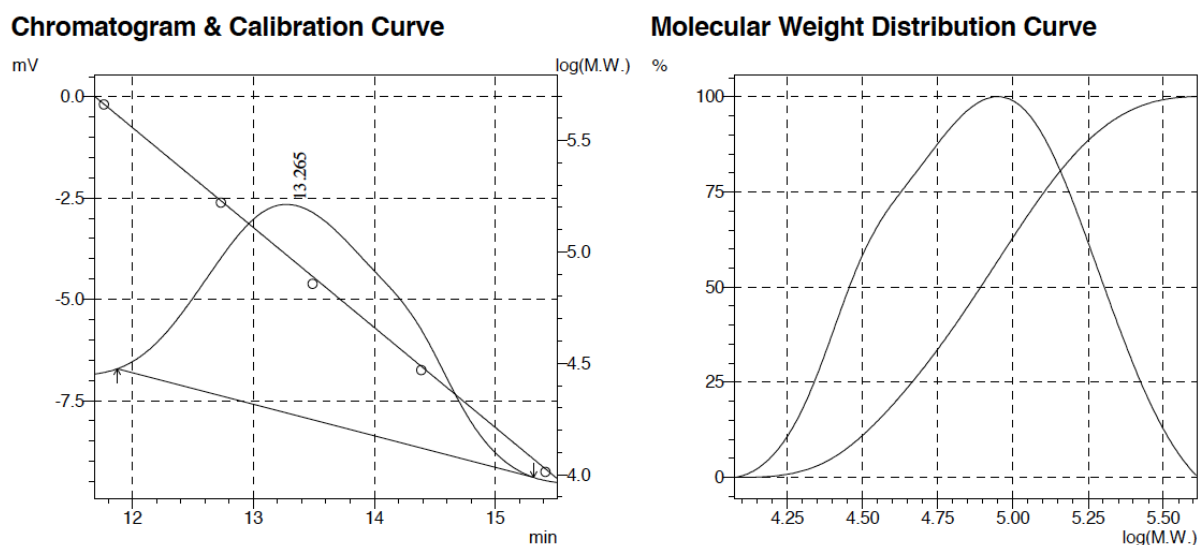


Figure 55: SEC traces of isolated P(Cl-CL) prepared via ROP of Cl-CL by the *catalyst 4*. (Conditions: [Cl-CL]₀ = 1 M, 500 equiv. of Cl-CL, RT, DCM, 7 h, 100% conv., bimodal).

The ^1H NMR spectrum (**Figure 56**) shows clearly the presence of the benzyloxy signals which is an indication of the linear P(Cl-CL) in the polymer mixture.

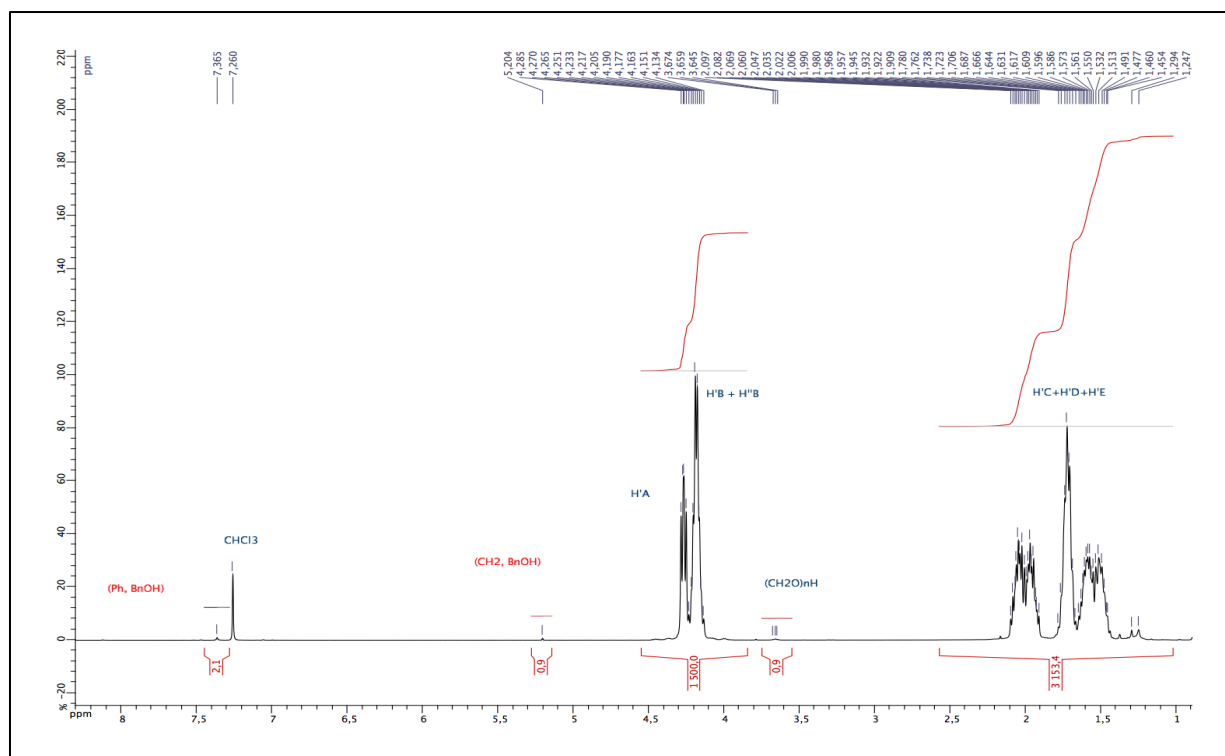


Figure 56: ^1H NMR (CDCl_3 , 400 MHz) of isolated P(Cl-CL) prepared by ROP of 500 equiv. of Cl-CL initiated by *catalyst 4* system. (Conditions: $[\text{Cl-CL}]_0 = 1 \text{ M}$, RT, DCM, 7 h, quantitative conv.).

The MALDI-TOF spectrometric data (**Figure 57**) for the P(Cl-CL) formed with initiator **4** allow one to conclude about the presence of a second polymer that would be cyclic P(Cl-CL). All high intensity peaks present in the spectrum are identified to cyclic poly(Cl-CL) and the lower intensity peaks correspond to the linear P(Cl-CL) bearing a benzyloxy at the end of its chain (**Supporting data: Figure 3**). The presence of cyclic poly(Cl-CL) with low M_n values is consistent with overall lower than theoretically expected M_n values obtained by GPC (61357 g/mol, **entry 14, Table 2**). In fact, the M_n values of the produced polymer with 500 equivalents of Cl-CL are lower than those of the poly(Cl-CL) material produced from 250 equivalents of Cl-CL (**entry 13, Table 2**).

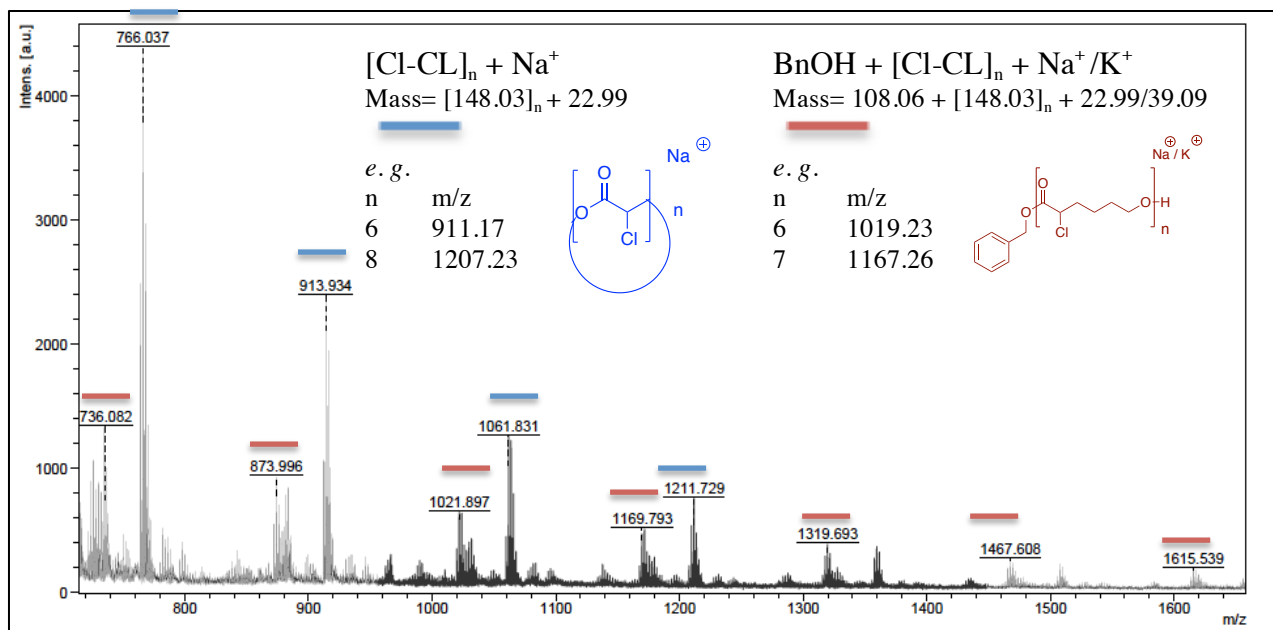


Figure 57: MALDI-TOF spectrum of the P(Cl-CL) prepared by ROP of Cl-CL initiated by the *catalyst 4* system. (Conditions: $[\text{Cl-CL}]_0 = 1 \text{ M}$, 500 equiv. of Cl-CL, DCM, RT, polymer isolated at 100% conv. in P(Cl-CL)).

The formation of a polymer mixture upon going to 500 indicates a threshold limit of polymeric units. Up to 250 equivalents, a very good and fast polymerization control is achieved leading to well-defined linear poly(Cl-CL). The polymerization is considerably slower with 500 equivalents of P(Cl-CL) which could explain the undesirable formation of cyclic P(Cl-CL) as side-products through intramolecular back-biting of the propagating chain.

VII. Coordination-insertion mechanism

The ^1H NMR spectra analyses imply that the polymerization proceeds via a «coordination-insertion» mechanism¹⁶ according to the noticeable signal of the polymer end chain: $-\text{CH}_2\text{OH}$. This signal is a multiplet which appears at 3.66 ppm in the NMR spectra of all linear P(Cl-CL) in deuterated chloroform (for instance **Figure 58**).

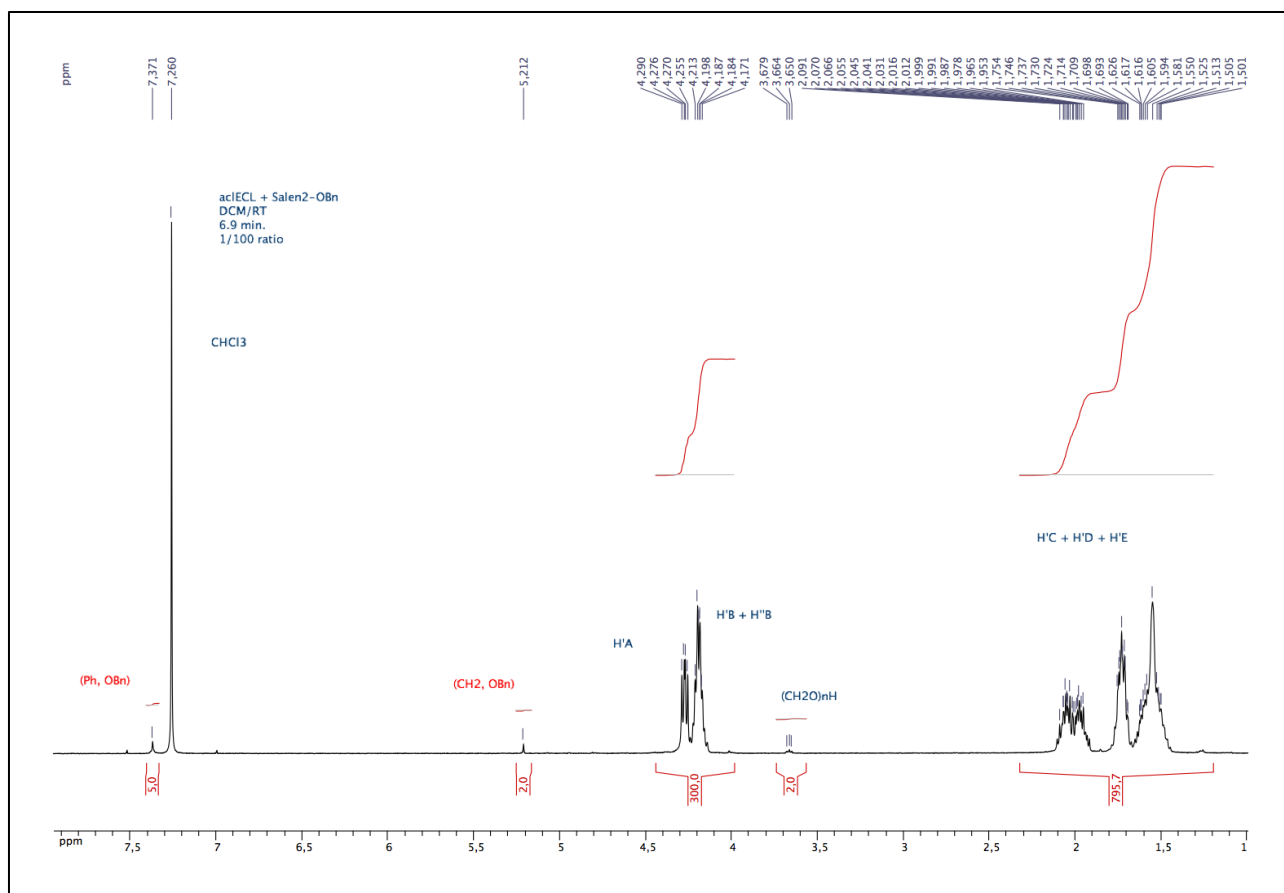


Figure 58: ^1H NMR (CDCl_3 , 400 MHz) of isolated P(Cl-CL) prepared by ROP of 100 equiv. of Cl-CL initiated by *catalyst 4* system. (Conditions: $[\text{Cl-CL}]_0 = 1 \text{ M}$, RT, DCM, 6.9 min., quantitative conv.).

All data on the ROP of Cl-CL by *catalyst 4* agree with a coordination-insertion mechanism. Thus, first, Cl-CL monomer coordinates to the aluminium metal center then it is followed by the acyl-oxygen bond cleavage of the monomer. Finally, polymerization will be initiated and the chain propagation will proceed (**Figure 59**).

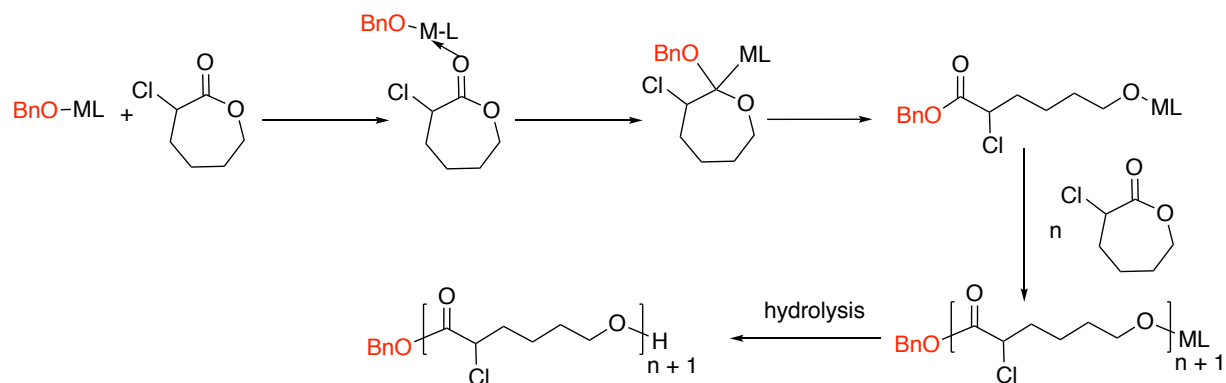


Figure 59: Coordination-insertion mechanism polymerization for the ROP of Cl-CL

VIII. Calibration curve obtained by ^1H NMR and by GPC as a function of different Cl-CL equivalents.

The data collected by GPC are relative to standard PS without any correction factor applied to the final results because, prior to the present study, the correction factor for poly(Cl-CL) was not known. For determination of the correction factor to be applied for poly(Cl-CL), several P(Cl-CL) with different chain lengths: 75, 100, 150 and 170 equivalents were synthesized and analyzed by GPC (**Figure 60**).



Figure 60: ROP of P(Cl-CL) initiated by species 4

On the one hand, the M_n was calculated from ^1H NMR spectra based on the comparison of the multiplets between 4.16 to 4.24 ppm (signals: A': CHCl , B'+ B'': $(\text{CH}_2\text{O})_n\text{H}$) and the signal of the phenyl group at 7.37 ppm providing from the benzyloxy moiety. On the other hand, the M_n for each polymer was measured by GPC in THF (30 °C) using PS standards. The polymerization results and the calculations for the M_n estimated by ^1H NMR are compiled in **Table 7**.

Entry	Cl-CL ^a	T (°C)	Time ^b (min.)	I (Ph, OBn) ^c δ=7.37ppm	M _n theo ^d (g/mol)	M _n ^e ¹ H NMR (g/mol)	M _n GPC ^f (g/mol)	PDI
1	75	RT	4	0.066	11145	11258	12119	1.06
2	100	RT	6.9	0.05	14860	14869	17719	1.17
3	150	RT	30	0.033	22290	22515	25376	1.03
4	170	RT	50	0.030	25262	25272	28111	1.02

Polymerization condition: [Cl-CL]₀ = 1 M, DCM, RT.

^a Equiv. versus initiator. ^b Reaction time. ^c Based on $\Sigma I (H'a + H'b + H''b) = 3 H$.

^d Calculated using $M_{n \text{ theo}} = [Cl-CL]_0 \times M_{Cl-CL} \times \text{conv.}$ ^e $M_n \text{ } ^1H \text{ NMR} = [(\Sigma I (H'a + H'b + H''b)) / 3] / [(I H_{Ph, OBn}) / 5] \times M_{Cl-CL} = [(3/3) / (I H_{Ph, OBn}) / 5] \times 148.6$. ^f Measured by GPC in THF (30 °C) using PS standards.

I = ¹H NMR integration of the corresponding polymer signals

Table 7: Results of the ROP of Cl-CL initiated by species 4

VIII. 1. 75 equivalents of Cl-CL

The GPC data (**entry 1, Table 7**) feature a monomodal and well-defined P(CL-CL) traces consistent with a fine polydispersity (PDI: 1.06) (**Figure 61**).

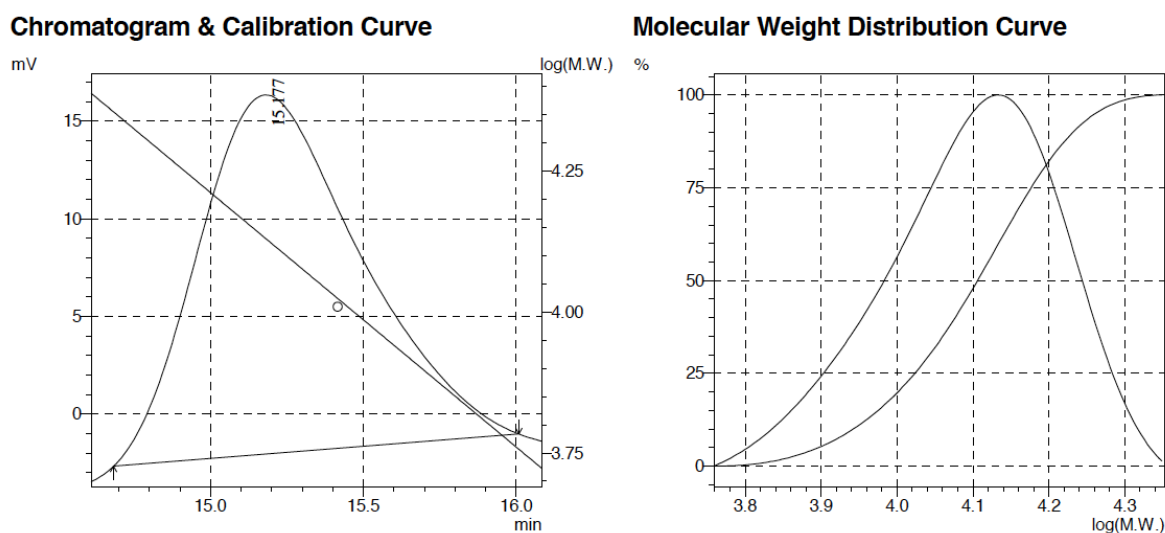


Figure 61: SEC traces of isolated P(Cl-CL) prepared via ROP of Cl-CL initiated by the catalyst 4 system. (Conditions: [Cl-CL]₀ = 1 M, 75 equiv. of Cl-CL vs. catalyst 4, RT, DCM, 100% conv., 4 min.).

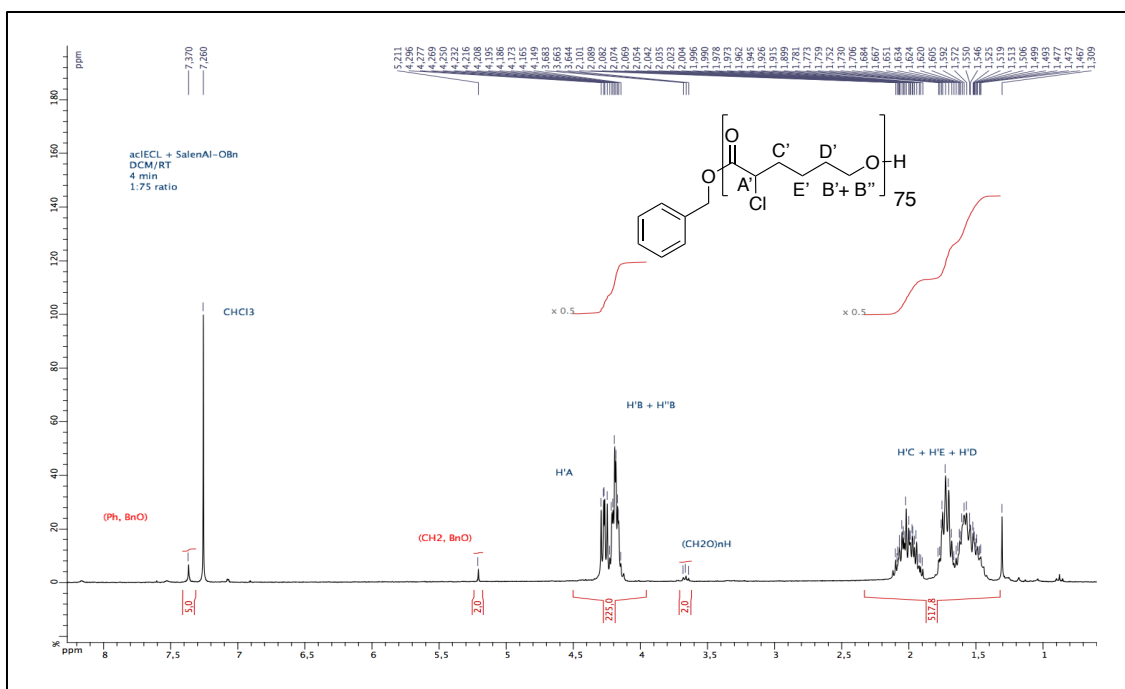


Figure 62: ^1H NMR (CDCl_3 , 400 MHz) of isolated P(Cl-CL) prepared via ROP of Cl-CL initiated by the *catalyst 4* system. (Conditions: $[\text{Cl-CL}]_0 = 1 \text{ M}$, 75 equiv. of Cl-CL vs. *catalyst 4*, RT, DCM, 100% conv., 4 min.).

VIII. 2. 100 equivalents of Cl-CL

For 100 equivalents in Cl-CL, the GPC data (**entry 2, Table 7**) agree with a monomodal and well-defined P(Cl-CL). The polymer has a narrow polydispersity (PDI: 1.17) (**Figure 63**).

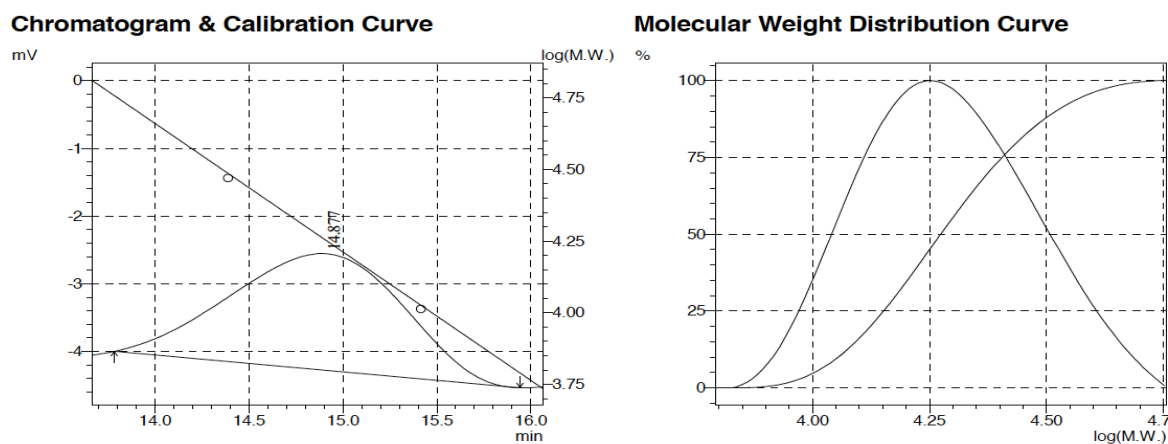


Figure 63: SEC traces of isolated P(Cl-CL) prepared via ROP of Cl-CL initiated by the *catalyst 4* system. (Conditions: $[\text{Cl-CL}]_0 = 1 \text{ M}$, 100 equiv. of Cl-CL vs. *catalyst 4*, RT, DCM, 100% conv., 6.9 min.).

The ^1H NMR spectrum agrees with the theoretical values as illustrated (**Figure 64**).

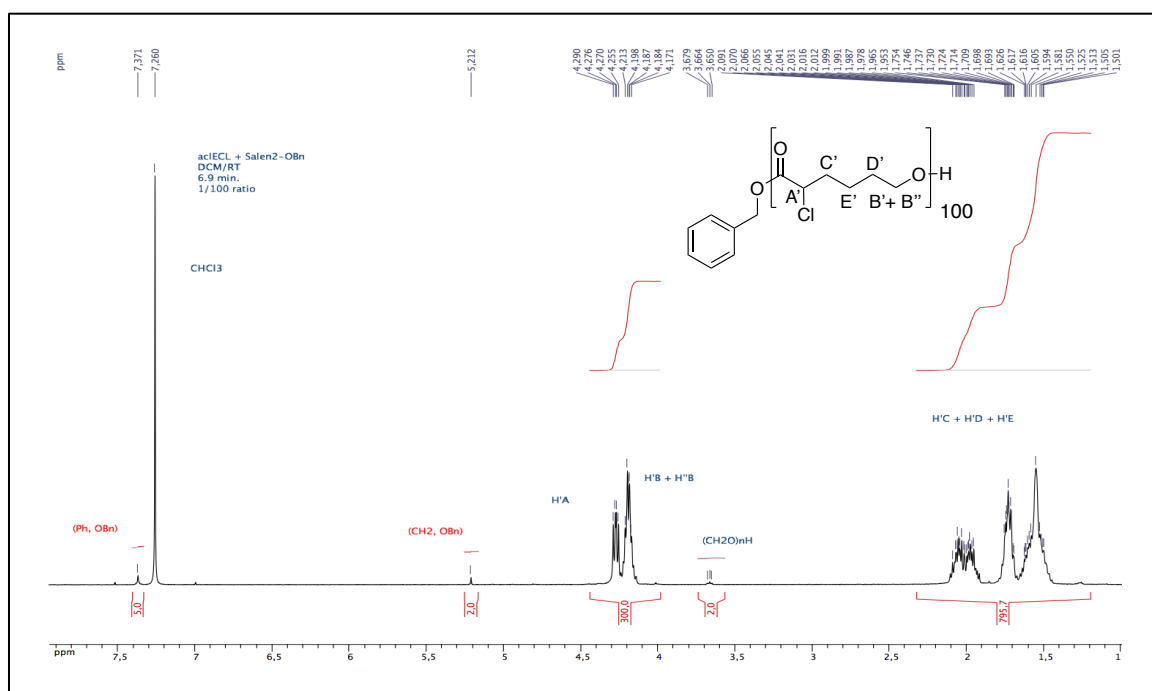


Figure 64: ^1H NMR (CDCl_3 , 400 MHz) of isolated $\text{P}(\text{Cl-CL})$ prepared via ROP of Cl-CL initiated by the *catalyst 4* system. (Conditions: $[\text{Cl-CL}]_0 = 1 \text{ M}$, 100 equiv. of Cl-CL vs. *catalyst 4*, RT, DCM, 100% conv., 6.9 min.).

VIII. 3. 150 equivalents of Cl-CL

The GPC data (**entry 3, Table 7**) match with a monomodal and well-defined polymer. The SEC traces are consistent with a narrow polydispersity (PDI: 1.03) (**Figure 65**) and the ^1H NMR spectrum is consistent with the 5H of the benzyloxy's phenyl and the 2H of its CH_2 (**Figure 66**).

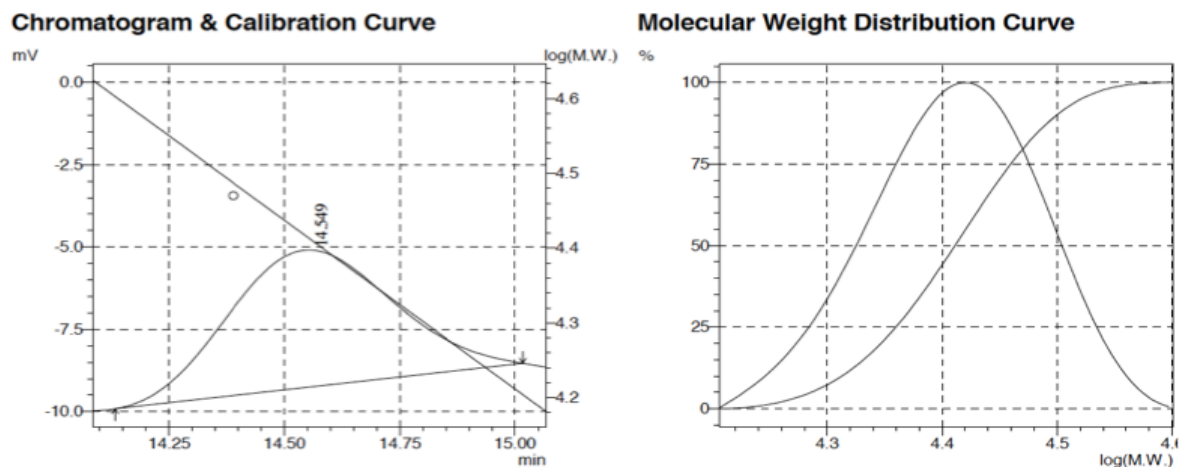


Figure 65: SEC traces of isolated P(Cl-CL) prepared via ROP of Cl-CL initiated by the *catalyst 4* system. (Conditions: $[\text{Cl-CL}]_0 = 1 \text{ M}$, 150 equiv. of Cl-CL vs. *catalyst 4*, RT, DCM, 100% conv., 30 min.).

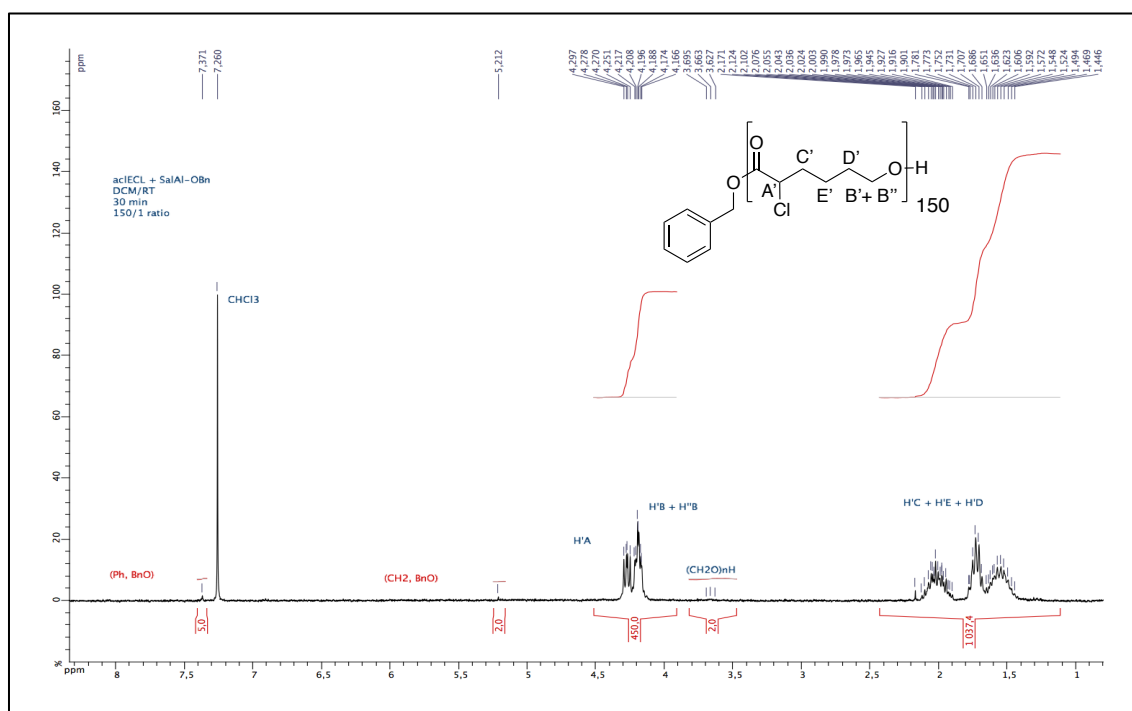


Figure 66: ^1H NMR (CDCl_3 , 400 MHz) of isolated P(Cl-CL) prepared by ROP of 150 equiv. of Cl-CL initiated by *catalyst 4*. (Conditions: $[\text{Cl-CL}]_0 = 1 \text{ M}$, DCM, RT, 30 min., 100% conv.).

VIII. 4. 170 equivalents of Cl-Cl

The GPC data (**entry 4, Table 7**), the SEC traces (**Figure 67**) and the ^1H NMR spectrum (**Figure 68**) are in agreement with the three previous data.

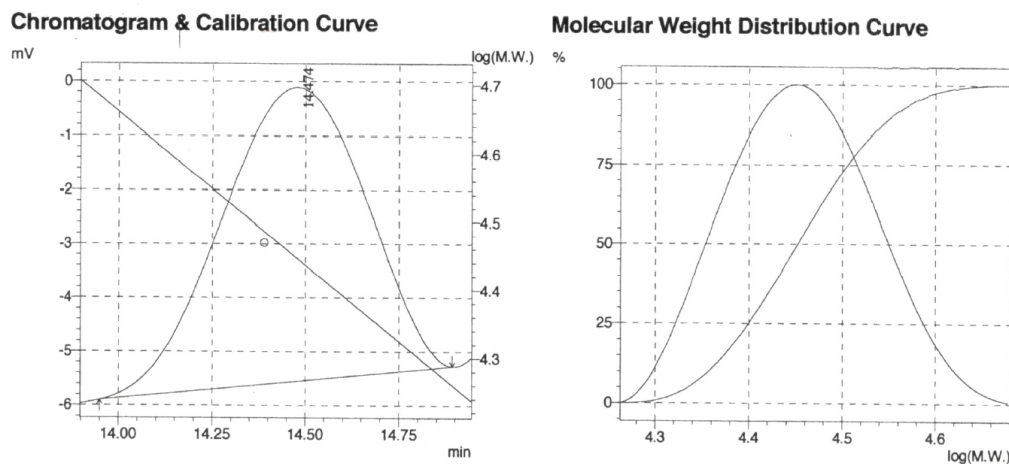


Figure 67: SEC traces of isolated P(Cl-CL) prepared via ROP of Cl-Cl initiated by the *catalyst 4* system. (Conditions: $[\text{Cl-Cl}]_0 = 1 \text{ M}$, 170 equiv. of Cl-Cl vs. *catalyst 4*, RT, DCM, 100% conv., 50 min.).

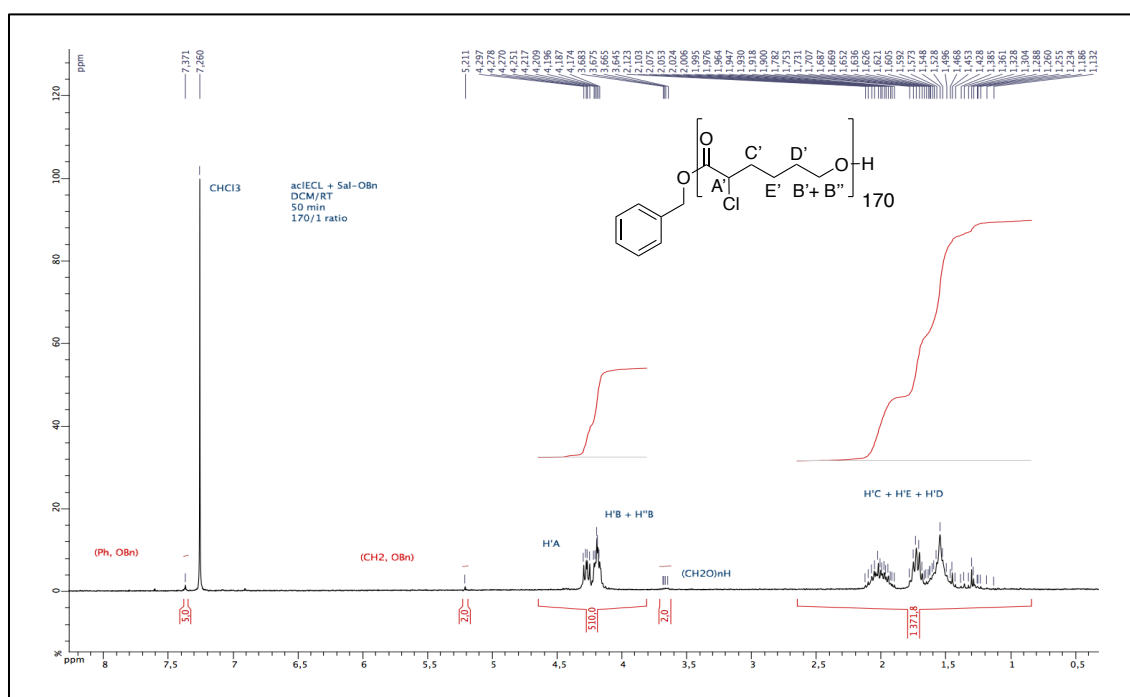


Figure 68: ^1H NMR (CDCl_3 , 400 MHz) of isolated P(Cl-CL) prepared via ROP of Cl-Cl initiated by the *catalyst 4* system. (Conditions: $[\text{Cl-Cl}]_0 = 1 \text{ M}$, 170 equiv. of Cl-Cl vs. *catalyst 4*, RT, DCM, 100% conv., 50 min.).

VIII. 5. Calibration curve plot

According to these different values, the M_n obtained according to the ^1H NMR spectra, and the M_n obtained by GPC can be plotted as a function of the Cl-CL equivalents (**Figure 69**). The ratio between the slope of the NMR-derived M_n values and the PS standards GPC data is the correcting factor.

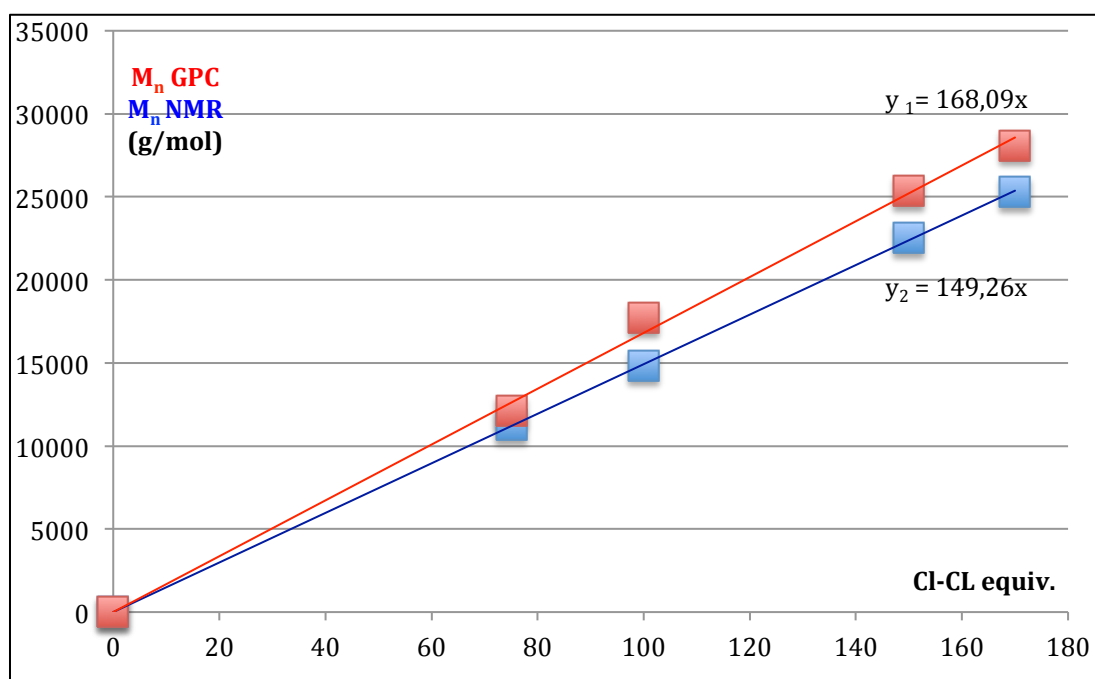


Figure 69: Plot presented the M_n GPC, the M_n obtained by ^1H NMR as a function of the Cl-CL equiv.

The correlation value between both straight lines is calculated thanks to the director factors:
 $(y_2/y_1) = 149.626/169.43 = 0.88$

In conclusion, the correlation value (0.88) between M_n ^1H NMR and M_n GPC with the standard PS is close to 1 meaning the hydrodynamic radius of the P(Cl-CL) is relatively close to the hydrodynamic radius of polystyrene.¹⁷

IX. Immortal ROP

The use of a cheap protic source (typically an alcohol) in the polymerization process allows it to act as a reversible chain transfer agent allowing a better control on the molecular masses and polydispersity of the produced polymers and, importantly, the use of a smaller amount of catalyst.¹⁸ At every step of the polymerization, there is an equilibrium between the active and the dormant chain,^{19,20} which allows eliminating termination reactions and lead to the production of many macromolecules per catalyst.

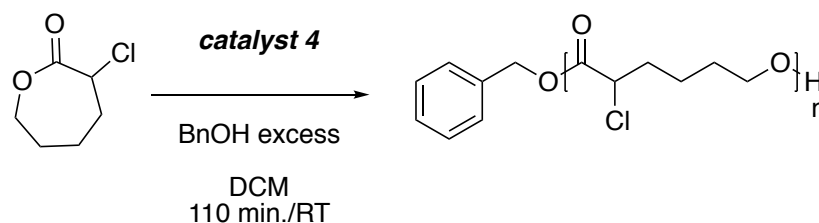


Figure 70: Immortal ROP of Cl-CL initiated by *catalyst 4*/BnOH excess system

An immortal ROP was performed on 1000 equivalents of Cl-CL using 5 equivalents of benzyl alcohol (*vs.* *catalyst 4*). The results are compiled in **Table 2**. Carrying out the ROP catalysis using 1000 equivalents of Cl-CL in the presence of 5 equivalents of BnOH (*vs.* species **4**) yields a total conversion to P(Cl-CL) within 110 minutes at room temperature with the production of narrowly disperse polymer (PDI: 1.10), as deduced from SEC data (**Figure 72**), thereby showing the excellent activity of the present **4**/BnOH system. The ¹H NMR spectrum for the isolated polymer (**Figure 71**) agrees with a linear poly(Cl-CL) with a BnO moiety at the ester end.

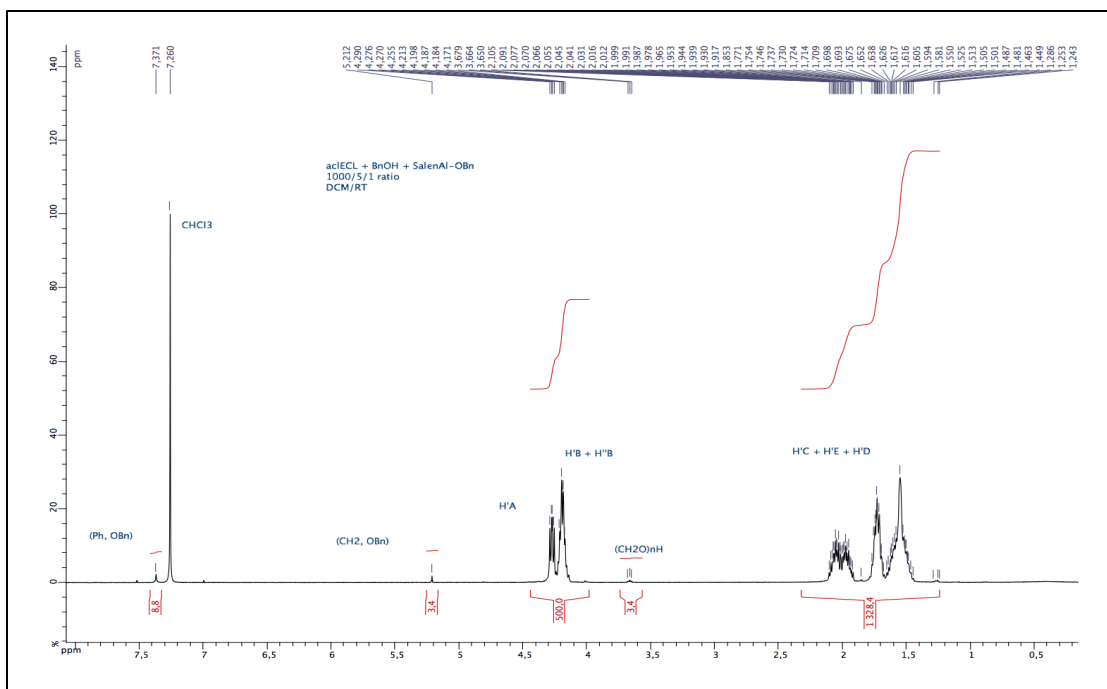


Figure 71: ^1H NMR spectrum (CDCl_3 , 400 MHz) of isolated P(Cl-CL) prepared by immortal ROP of 1000 equiv. of Cl-CL vs. *catalyst 4*/excess BnOH. (Conditions: $[\text{Cl-CL}]_0 = 1 \text{ M}$, 1000 equiv. of Cl-CL, 5 equiv. BnOH, DCM, RT, 110 min., quantitative conv.).

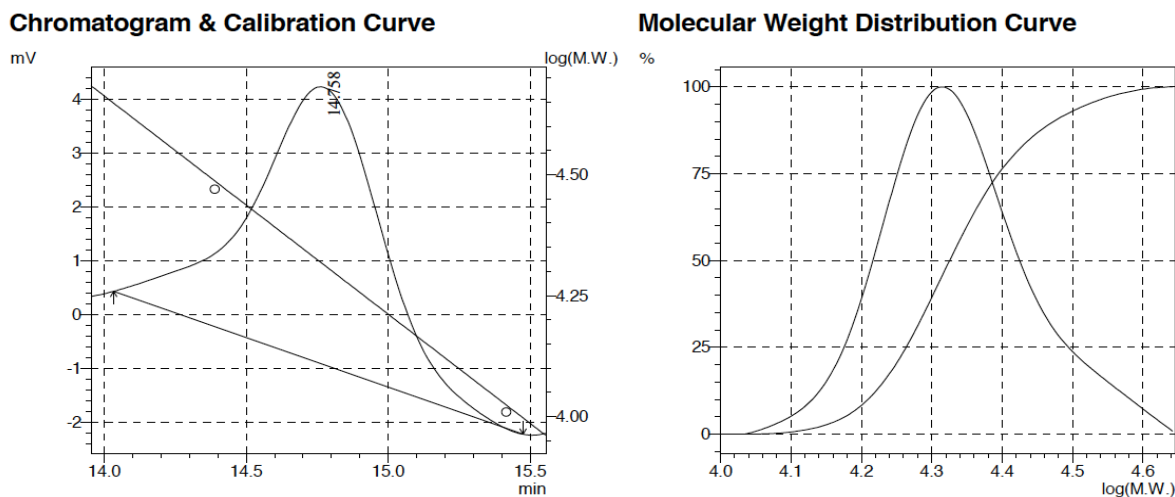


Figure 72: SEC traces of isolated P(Cl-CL) prepared by immortal ROP of 1000 equiv. of Cl-CL vs. *catalyst 4*/excess BnOH. (Conditions: $[\text{Cl-CL}]_0 = 1 \text{ M}$, 1000 equiv. of Cl-CL, 5 equiv. BnOH, DCM, RT, 110 min., quantitative conv.).

All data support that the ROP polymerization by **4**/BnOH proceeds in an immortal manner, with BnOH acting as chain transfer agent. Indeed, a first-order kinetic in Cl-CL with $k_{app} = 4.23 \times 10^{-2} \text{ min}^{-1}$ is observed (**Figure 73**).

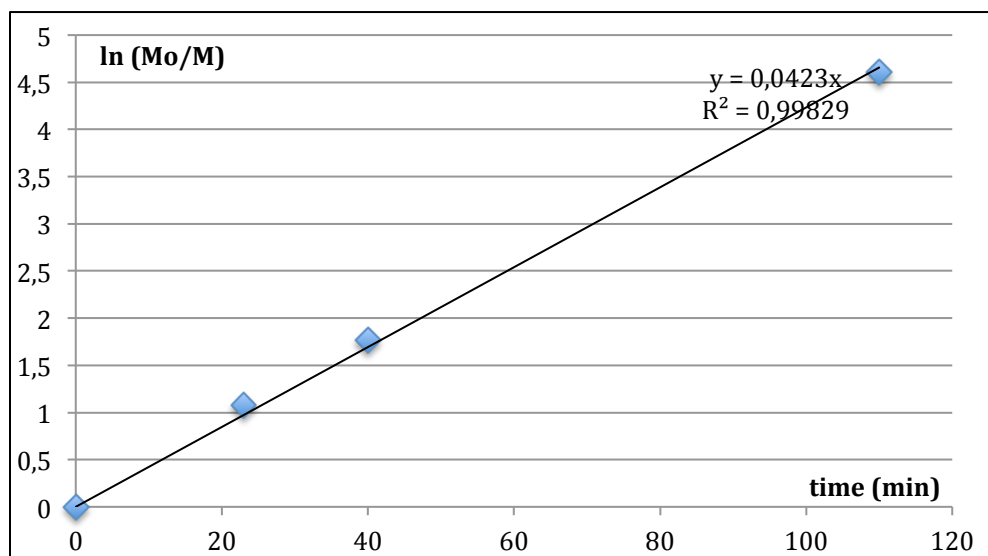


Figure 73: Plot of $\ln(M_0/M)$ as a function of the time in the ROP of Cl-CL using complex **4**/BnOH system. (Conditions: $[\text{Cl-CL}]_0 = 1 \text{ M}$, 1000 equiv. of Cl-CL, 5 equiv. of BnOH, DCM, RT, 110 min. total conv.).

Kinetic studies are also consistent with a linear correlation between the P(Cl-CL) M_n and monomer conversion during the polymerization reaction (**Figure 74**).

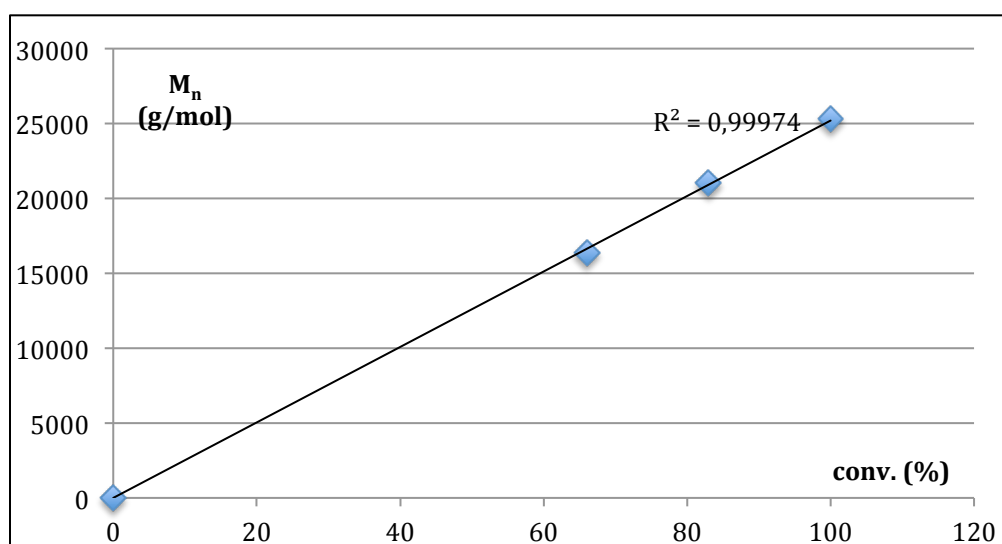


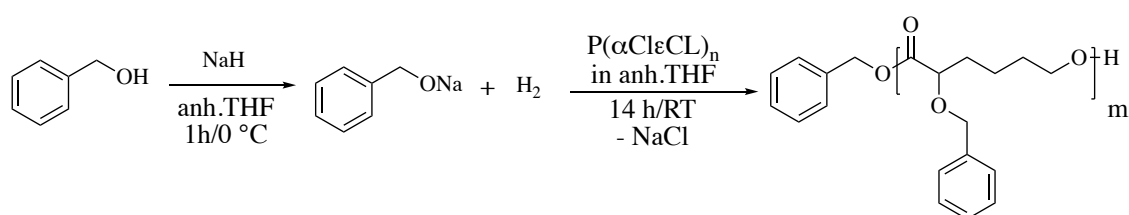
Figure 74: Plot of M_n as a function of the conv. in the immortal ROP of Cl-CL using *catalyst 4*/BnOH system. (Conditions: $[\text{Cl-CL}]_0 = 1 \text{ M}$, 1000 equiv. in monomer, 5 equiv. BnOH, DCM, RT, 110 min.).

Moreover, in particular as shown in **Table 2**, all observed M_n values closely match the initial $[\text{Cl-CL}]_0/[\text{BnOH}]_0$ ratio, with, for instance 5 polymer chains being generated per Al salen center. The MALDI-TOF spectrum of the prepared polymer (**Supporting data: Figures 4, 4a, 4b and 4c**) agrees with the formation of macromolecules with a linear P(Cl-CL) bearing an OBn group at the end of their chain. In consequence, the equivalent amount of Cl-CL was increased to 1000 with a monomodal and narrowly disperse P(Cl-CL) (1.02 to 1.10) and a fast and quantitative polymerization process. This result compares very favorably with the living ROP of 500 equivalents of Cl-CL, that led to a slow and poorly controlled ROP process and bimodal polymer, as previously discussed.

X. Functionalization of the poly(α -chloro- ϵ -caprolactone)

Chlorine is known to be a good leaving group which opens the way to functionalization of poly(Cl-CL) by a nucleophilic agent to, for instance, modify the hydrophobic nature of the polymer. To this end, the Williamson method was performed on P(Cl-CL) using benzyl alcohol as nucleophilic reagent and carried out under mild conditions. This synthetic pathway could allow access after hydrogenation of the benzyloxy group to hydrophilic alcohol pendant group according to the procedure illustrated below (**Figure 75**). The resulting polymeric material should exhibit solubility in water while incorporating a biodegradable and hydrophobic polyester backbone.

1. Williamson reaction:



2. Hydrogenation:

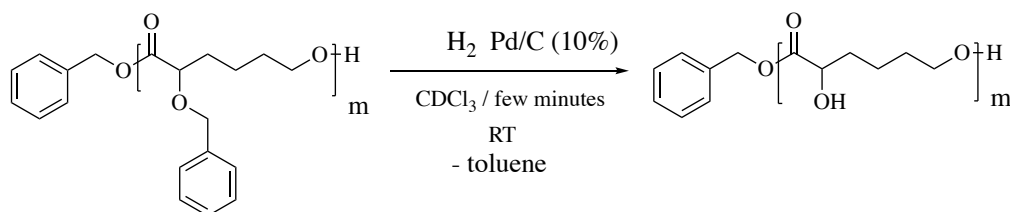


Figure 75: Two steps pathways for the formation of P(α OH ϵ CL)

X. 1. Substitution of the chlorine pendant group according to Williamson reaction

The incorporation of one benzyloxy group per monomer unit leads to high steric hindrance because of its voluminous benzyl ring. Indeed, in a long polymeric chain, it was observed in initial trials that all chlorine groups were not substituted using 1 equivalent of BnOH per monomeric unit in P(Cl-CL). In order to mitigate this impact, the nucleophilic amount choice was below or equal to 0.7 equivalents per monomeric unit in P(Cl-CL). We have chosen to discuss the optimal results in this part.

Entry	P(Cl-CL) ^a	BnOH ^b	T (°C)	M _n theo ^c (g/mol)	M _n GPC ^d (g/mol)	PDI
1	100	0.7	RT	19877	22889	1.38

^a P(Cl-CL) chain length. ^b Equiv. versus P(Cl-CL). ^c Calculated using $M_{n\text{theo}} = \text{equiv. [Cl-CL]}_0 \times M_{(\text{Cl-CL})} \times \text{conv.} + \text{equiv. [BnOH]}_0 \times \text{equiv.} \times M_{(\text{BnOH})} \times \text{conv.}$ ^d Measured by GPC in THF (30 °C) using PS standards. (Conditions: BnOH + NaH in anhydrous THF, 1 h, 0 °C, then P(Cl-CL) in anhydrous THF, RT, overnight).

Table 8: Results of the Williamson reaction

The Williamson substitution²¹ was performed on a P(Cl-CL) with a chain length of 100 monomer units with 0.7 equivalents of BnOH per monomeric unit in P(Cl-CL) (**entry 1, Table 8**). The ¹H NMR spectrum (**Supporting data: Figure 5**) shows the effective BnO-functionalization of poly(Cl-CL) but also the breakage of the P(αOBnεCL) into smaller oligomers based on ¹H NMR and GPC data. The ¹H NMR spectrum of the crude product contains two CH₂-Ph signals and the larger amount of -CH₂OH end chains (δ = 3.6 ppm) indicates the cleavage of the P(αOBnεCL) in smaller oligomers. The latter are probably produced by transesterification of the P(αOBnεCL) polyester with BnONa or by reaction of residual NaH (used in excess) with the polymer chain. The SEC traces of the isolated product is bimodal (**Supporting data: Figure 6**) with a fairly broad polydispersity (PDI: 1.39), in line with cleavage of poly(Cl-CL) to several oligomers. The MALDI-TOF spectrum (**Supporting data: Figures 7, 7a and 7b**) shows the presence of several polymers with a majority of BnO-functionalized P(αBnOεCL) polymer with an OBn ester end and (Cl-CL)P(αBnOεCL) material.

X. 2. Hydrogenation of the polymer mixture obtained after the Williamson reaction

In order to obtain the alcohol functions, the deprotection of the BnO to OH groups was studied through hydrogenation. The polymer mixture was dissolved in deuterated chloroform and the corresponding amount of Pd/C (10%) was added to the solution then the mixture was pressurized with H₂ (1 atm.). The reaction was monitored by ¹H NMR and was stopped when the intensity of toluene by-product (arising from BnO hydrogenation) didn't increase anymore. The resulting material was analyzed by GPC (**Table 9**).

Entry	P(Cl-CL) ^a	BnOH ^b	T (° C)	M _n theo ^c (g/mol)	M _n GPC ^d (g/mol)	PDI
1	100	0.7	RT	13568	16213	1.30

^a Chain length. ^b Equiv. versus P(Cl-CL). ^c Calculated using $M_{n\text{ theo}} = \text{equiv. BnOH} \times M_{(\alpha\text{OH}\epsilon\text{CL})} + \text{equiv. P(Cl-CL)} \times M_{(\text{Cl-CL})}$: $70 \times 220.27 + 30 \times 148.6$. ^d Measured by GPC in THF (30 °C) using PS standards. (Conditions: H₂, Pd/C (10%), CDCl₃, 15 min.).

Table 9: Hydrogenation on the mixture obtained after the Williamson reaction

In the ¹H NMR spectrum, after 15 minutes at RT, the reaction mixture does not evolve anymore. Only the signals of the OBn ester end bond were estimated because the benzyloxy group is not hydrogenated. A broad singlet corresponding to the OH function is visible between 2.24 and 2.84 ppm (**Supporting data: Figure 8**). The MALDI-TOF spectrometric data (**Supporting data: Figure 10, 10a, 10b, and 10c**) show a mixture composed of linear and cyclic P(αOHεCL) including some P(αOBnεCL) units, and a minority of polymer with the Cl-CL fragment. Consequently, the hydrogenation reaction only led to a partially deprotected polymer with an amount difficult to quantify given the presence of several by-products.

The starting hydrophobic P(Cl-CL) isn't soluble in water. In contrast, the introduction of alcohol groups onto the polymer chains mixture clearly provides a better hydrophilicity, as reflected by the water solubility of the OH-functionalized material. ¹H and ¹³C NMR spectra could be recorded in D₂O. Thus, even if the deprotection wasn't quantitative, the resulting material (after hydrogenation of the BnO group) displays an enhanced hydrophilicity vs. poly(Cl-CL).

XI. Conclusion

Using Al-salen ROP *catalysts 3* and *4*, a linear P(Cl-CL) was synthesized under very mild conditions through a classical coordination-insertion ROP mechanism leading to a well-controlled polymerization allowing access to chain-length controlled poly(Cl-CL). In contrast, the use of Mg(II) and Zn(II)-based ROP catalysts, $(\text{THF})_2\text{Mg}(\text{C}_6\text{F}_5)_2$ and $\text{Zn}(\text{C}_6\text{F}_5)_2$, led to ill-defined polymeric materials. Also, the hydrodynamic radii of various samples of P(Cl-CL) was estimated and revealed to be very close to that of polystyrene. An important part of this chapter is the functionalization of the produced poly(Cl-CL) through nucleophilic substitution of the chlorine group in order to get a hydrophilic material. The two steps synthesis from the substitution by benzyloxy groups via a Williamson reaction followed by the hydrogenation, known to convert benzyloxy into hydroxy group, have yielded a material partially functionalized with hydroxy pendant groups, which revealed to be significantly more hydrophilic than poly(Cl-CL), thus validating the developed approach for the production of biodegradable and hydrophilic polyester-based polymers.

XII. References

- [1]. J. Baran, A. Duda, A. Kowalski, R. Szymanski, S. Penczek, *Macromol. symp.* **1997**, *123*, 93-101.
- [2]. Y. W. Chun, D. A. Balikov, T. K. Feaster, C. H. Williams, C. C. Sheng, J. -B. Lee, T. C. Boire, M. D. Neely, L. M. Bellan, K. C. Ess, A. B. Bowman, H.-J. Sung, C. C. Hong, *Biomaterials* **2015**, *67*, 52-64.
- [3]. S. Lenoir, R. Riva, X. Lou, C. Detrembleur, R. Jérôme, P. Lecomte, *Macromolecules* **2004**, *37*, 4055-4061.
- [4]. G. Schnee, C. Fliedel, T. Avilés, S. Dagorne, *Eur. J. Inorg. Chem.* **2013**, *2013*, 3699-3709.
- [5]. Z. Wen, D. Li, J. Qi, X. Chen, Y. Jiang, C. Li, B. Gao, Y. Cui, Q. Duan, *Colloid Polym. Sci.* **2015**, *293*, 3449-3457.
- [6]. Y. Cui, D. Li, B. Gao, Y. Zhou, L. Chen, B. Qiu, Y. Li, Q. Duan, N. Hu, *J. Coord. Chem.* **2016**, *69*, 656-667.
- [7]. C. P. Radano, G. L. Baker, M. R. Smith, *J. Am. Chem. Soc.* **2000**, *122*, 1552-1553.
- [8]. T. M. Ovitt, G. W. Coates, *J. Am. Chem. Soc.* **1999**, *121*, 4072-4073.
- [9]. D. A. Atwood, M. J. Harvey, *Chem. Rev.* **2001**, *101*, 37-52.
- [10]. S. J. Dzuga, V. L. Goedken, *Inorg. Chem.* **1986**, *25*, 2858-2864.
- [11]. C. P. Radano, G. L. Baker, M. R. Smith, *J. Am. Chem. Soc.* **2000**, *122*, 1552-1553.
- [12]. T. M. Ovitt, G. W. Coates, *J. Am. Chem. Soc.* **1999**, *121*, 4072-4073.
- [13]. P. Hormnirun, E. L. Marshall, V. C. Gibson, R. I. Pugh, A. J. P. White, *Proc Natl Acad Sci USA* **2006**, *103*, 15343-15348.
- [14]. D. J. A. Cameron, M. P. Shaver, *Journal of Polymer Science Part A: Polymer Chemistry* **2012**, *50*, 1477-1484.
- [15]. N. Nomura, R. Ishii, Y. Yamamoto, T. Kondo, *Chem. Eur. J* **2007**, *13*, 4433-4451.
- [16]. K. Nakano, N. Kosaka, T. Hiyama, K. Nozaki, *Dalton Trans.* **2003**, 4039-4050.
- [17]. S. Park, T. Chen, *Macromolecules* **1991**, *24*, 5729-5731.
- [18]. S. Asano, T. Aida and S. Inoue, *J. Chem. Soc., Chem. Commun.*, **1985**, 1148-1149.
- [19]. N. Ajellal, J. -F. Carpentier, C. Guillaume, S. M. Guillaume, M. Hérou, V. Poirier, Y. Sarazin, A. Trifonov, *Dalton Trans.* **2010**, *39*, 8363-8376.
- [20]. B. Liu, T. Roisnel, L. Maron, J. -F. Carpentier, Y. Sarazin, *Chem. Eur. J.* **2013**, *19*, 3986-3994.

[21]. *Comprehensive Organic Name Reactions and Reagents, Vol. 3* (Eds.: Z. Wang), John Wiley & Sons, Inc., Hoboken, **2009**.

Chapter IV

Copolymers, diblocks and stereocomplex formation and their physicochemical properties

I. Introduction

Polymer properties can be easily modified via copolymerization. Indeed, the interest in copolymers lies on their physicochemical and mechanical properties, which are intermediate with those of the corresponding homopolymers. Based on our previous studies on P(Cl-CL) homopolymers described in the previous chapter, different copolymers and blocks were synthesized with the goal to introduce desirable properties such as hydrophilic properties and/or provide crystallinity to an amorphous polymeric material. In the polymer field, the physicochemical measurements are powerful tools to understand the behavior of the final material, which by the way can be useful for many applications.

II. Synthesis of PEG-co-P(Cl-CL)

Using a PEG initiator mono-capped methoxy end group, a hydrophilic polymer, ¹ polymerization with Cl-CL was performed in order to combine the properties of each component, and thus to obtain amphiphilic PEG-*b*-P(Cl-CL) copolymers. Three copolymers were synthesized using the Al(III) *catalyst 4* (**Figure 1**) and the polymerization results are compiled in **Table 1**. First, aluminium salen *catalyst 4* was reacted with PEG(1900) in toluene at 80 °C overnight to quantitatively convert species **4** to the corresponding Al-PEG derivative. The latter reacts with Cl-CL in DCM at RT until the total conversion as illustrated below (**Figure 1** and **Table 1**).

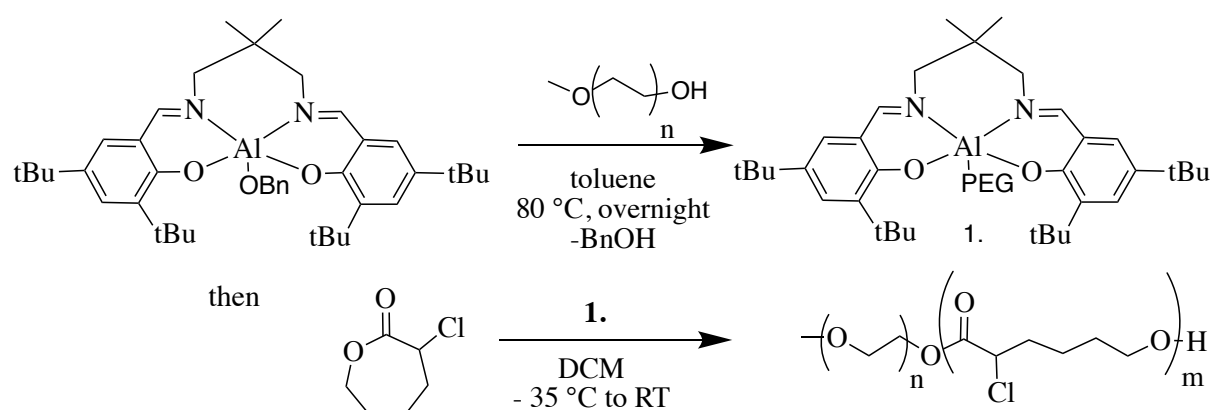


Figure 1: General procedure for PEG-co-P(Cl-CL) copolymer

Entry	Cl-CL ^a	PEG(1900) ^a	T (°C)	Time ^b (hours)	Conversion ^c (%)	M _n theo ^d (g/mol)	M _n GPC ^e (g/mol)	M _n corr ^f (g/mol)	PDI
1	70	5	RT	3.5	100	3980	4812	4463	1.15
2	100	5	RT	6	100	4872	5584	5142	1.27
3	500	5	RT	9	100	16706	20832	18560	1.39

Polymerization conditions: [Monomer]₀ = 1 M, DCM, RT. Species **4** as ROP catalyst.

^a Equiv. versus catalyst. ^b Reaction time. ^c Monomer conversion. ^d Calculated using $M_{n\text{theo}} = [\text{Cl-CL}]_0 / [\text{PEG}]_0 \times M_{\text{Cl-CL}} \times \text{conv.}$ ^e Measured by GPC in THF (30 °C) using PS standards.

^f $(M_{n\text{GPC}} - 1900) \times 0.88 + 1900$ (0.88: correlation factor obtained **section VIII, Chapter III.**)

Table 1: Results of the ROP of PEG-co-P(Cl-CL) copolymers initiated by species 4

A highly hydrophilic PEG-*b*-P(Cl-CL) was synthesized using 70 equivalents of Cl-CL, 5 equivalents of PEG(1900) and 1 equivalent in *catalyst 4* (**entry 1, Table 1**). The polymerization was successful as deduced from GPC data which agree with a monomodal and well-defined copolymer of narrow polydispersity (PDI: 1.15) and a $M_{n\text{GPC}}$ close to the $M_{n\text{theo}}$ (**entry 1, Table 1**) and (**Figure 2**). The ¹H NMR data are consistent with the formation of a PEG-*b*-P(Cl-CL) copolymer with the expected chain length for the P(Cl-CL) block (14 monomer units per PEG moiety, **Figure 3**).

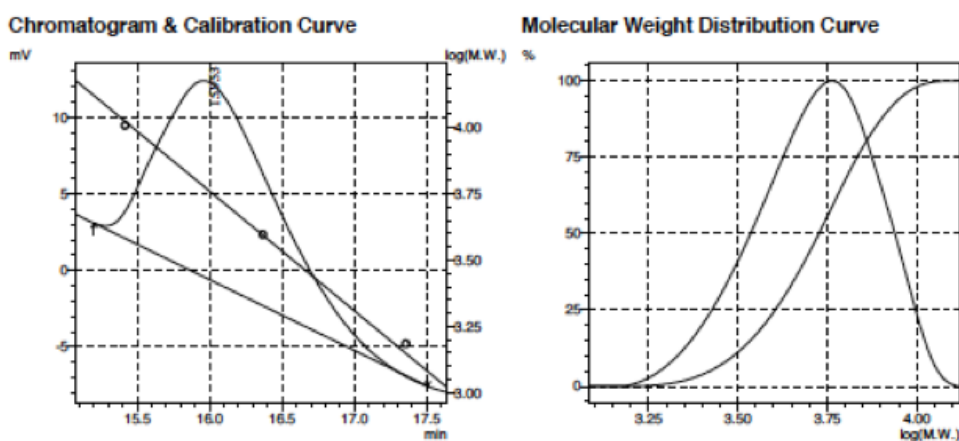


Figure 2: SEC traces of isolated PEG-co-P(Cl-CL) prepared via ROP of Cl-CL initiated by the *catalyst 4*/PEG(1900) system. (Conditions: 70 equiv. of Cl-CL, 5 equiv. of PEG (1900), RT, DCM, 3.5 h, 100% conv.).

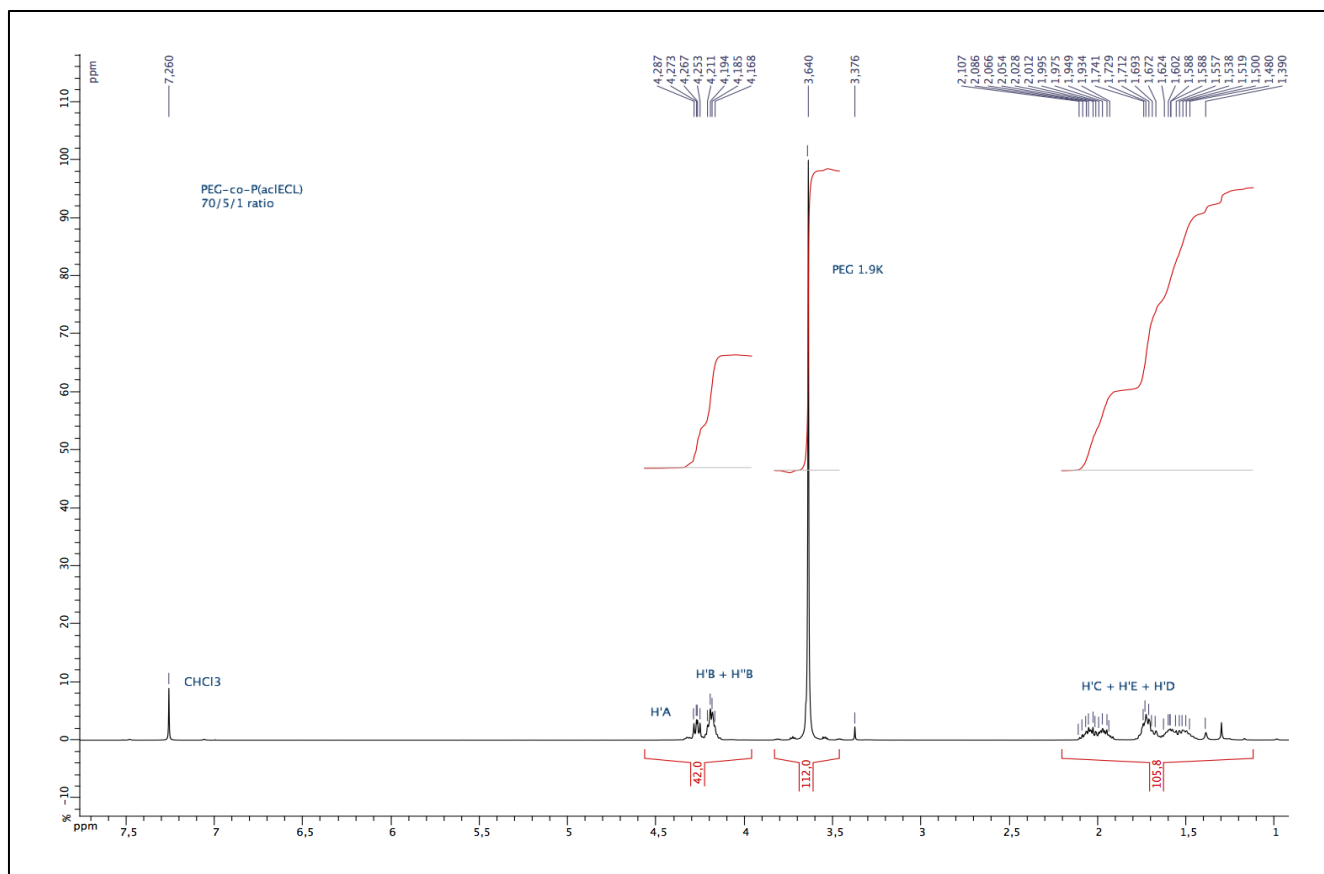


Figure 3: ^1H NMR (CDCl_3 , 400 MHz) of isolated PEG-*co*-P(Cl-CL) prepared by ROP of Cl-CL initiated by *catalyst 4*/PEG system. (Conditions: $[\text{Cl-CL}]_0 = 1 \text{ M}$, 70 equiv. of Cl-CL, 5 equiv. of PEG vs. catalyst, RT, DCM, 3.5 h, quantitative conv.).

A second PEG-*co*-P(Cl-CL) was synthesized using 100 equivalents of Cl-CL. The total conversion was obtained after 6 hours with the P(Cl-CL) chain length matching the theoretical value (**entry 2, Table 1**). The SEC traces feature a monomodal signal and agree with a fairly narrow polydispersity (PDI: 1.27) (**Figure 4**). The ^1H NMR spectrum (**Figure 5**) agrees with copolymer formation and the attachment of 20 equivalents of Cl-CL per PEG unit.

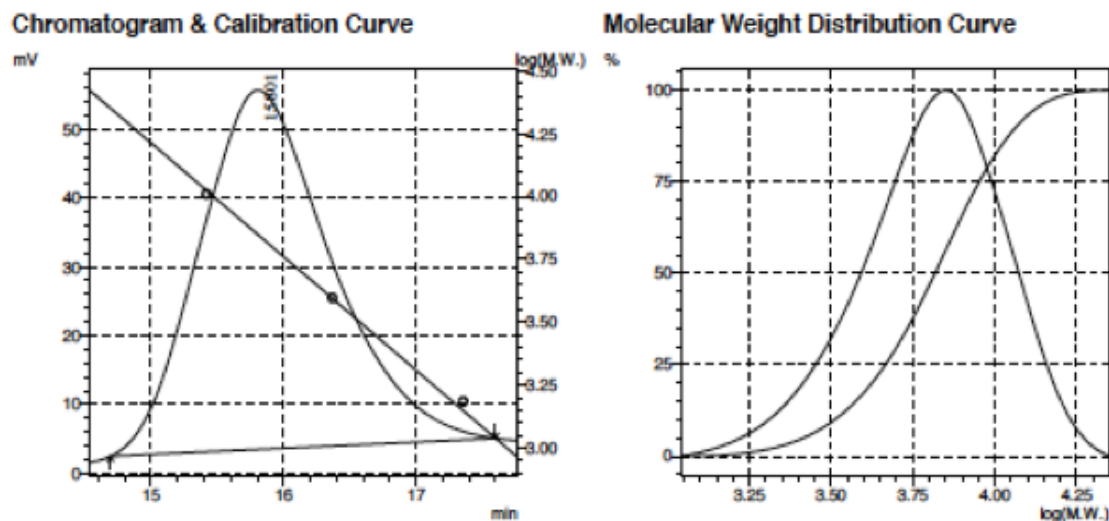


Figure 4: SEC traces of isolated PEG-*co*-P(Cl-CL) prepared via ROP of Cl-CL initiated by the *catalyst 4*/PEG(1900) system. (Conditions: 100 equiv. of Cl-CL, 5 equiv. of PEG (1900), RT, DCM, 6 h, 100% conv.).

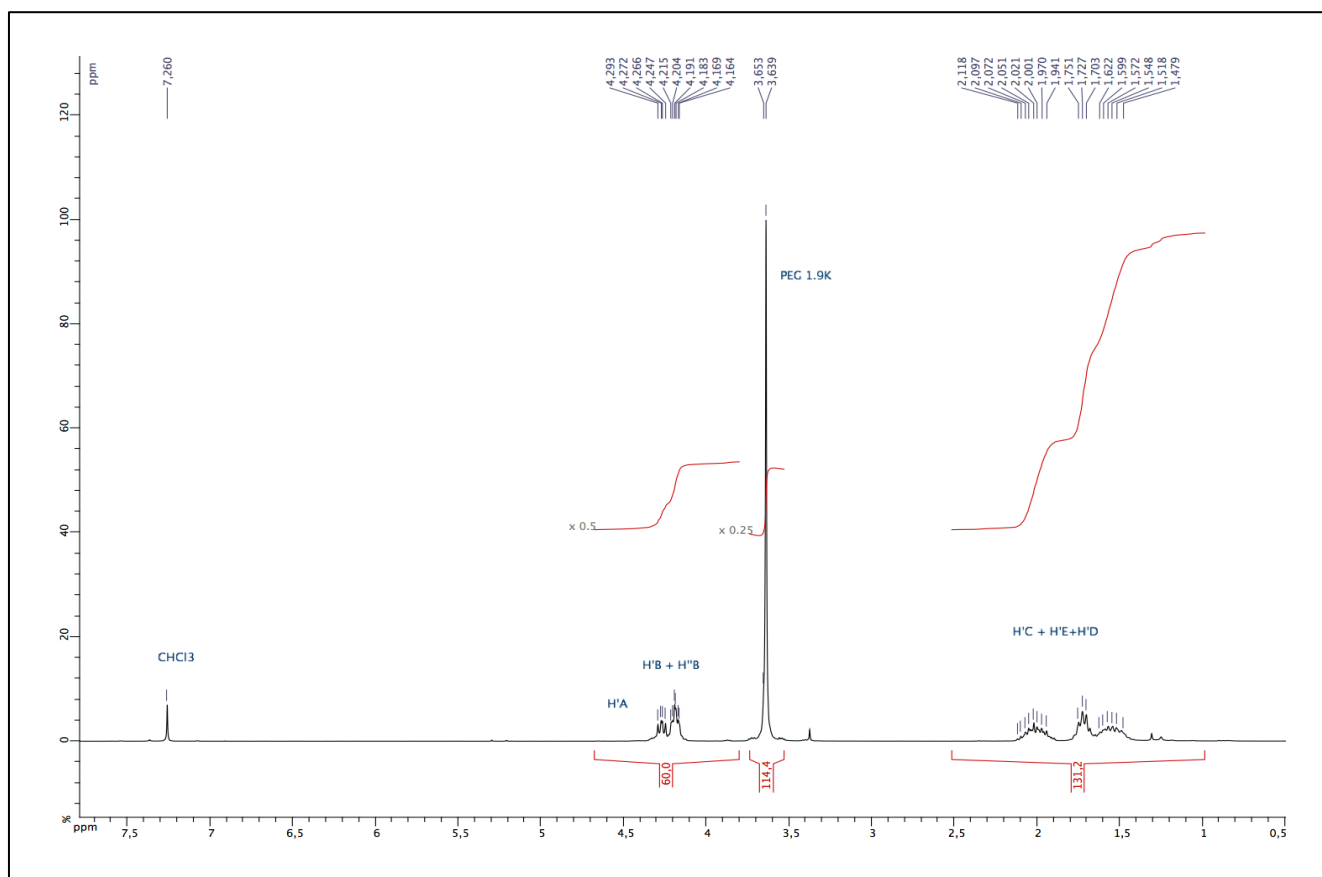


Figure 5: ¹H NMR (CDCl₃, 400 MHz) of isolated PEG-*co*-P(Cl-CL) prepared by ROP of Cl-CL initiated by *catalyst 4*/PEG system. (Conditions: [Cl-CL]₀ = 1 M, 100 equiv. of Cl-CL, 5 equiv. of PEG vs. catalyst, RT, DCM, 6 h, quantitative conv.).

A PEG-*b*-P(Cl-CL) sample was synthesized with 500 equivalents of Cl-CL, 5 equivalents of PEG and 1 equivalent of *catalyst 4*. The total conversion was obtained after 9 hours. The chain length matches the theoretical value (**entry 3, Table 1**), despite a broader polydispersity (PDI: 1.39) (**Supporting data: Figure 1**). ¹H NMR spectrum agrees with copolymer formation. The PEG signal intensity has considerably decreased and is in agreement with the 500 equivalents of P(Cl-CL) *vs.* the 5 equivalents of PEG.

¹H NMR spectra of all copolymers were also collected in D₂O and show the hydrophilic character of the first two copolymers with the sole presence of a PEG singlet at 3.74 ppm confirming the hydrophobicity of the P(Cl-CL) segment and the biphasic nature of the material in water (**Figure 6 and supporting data: Figures 2-4**).

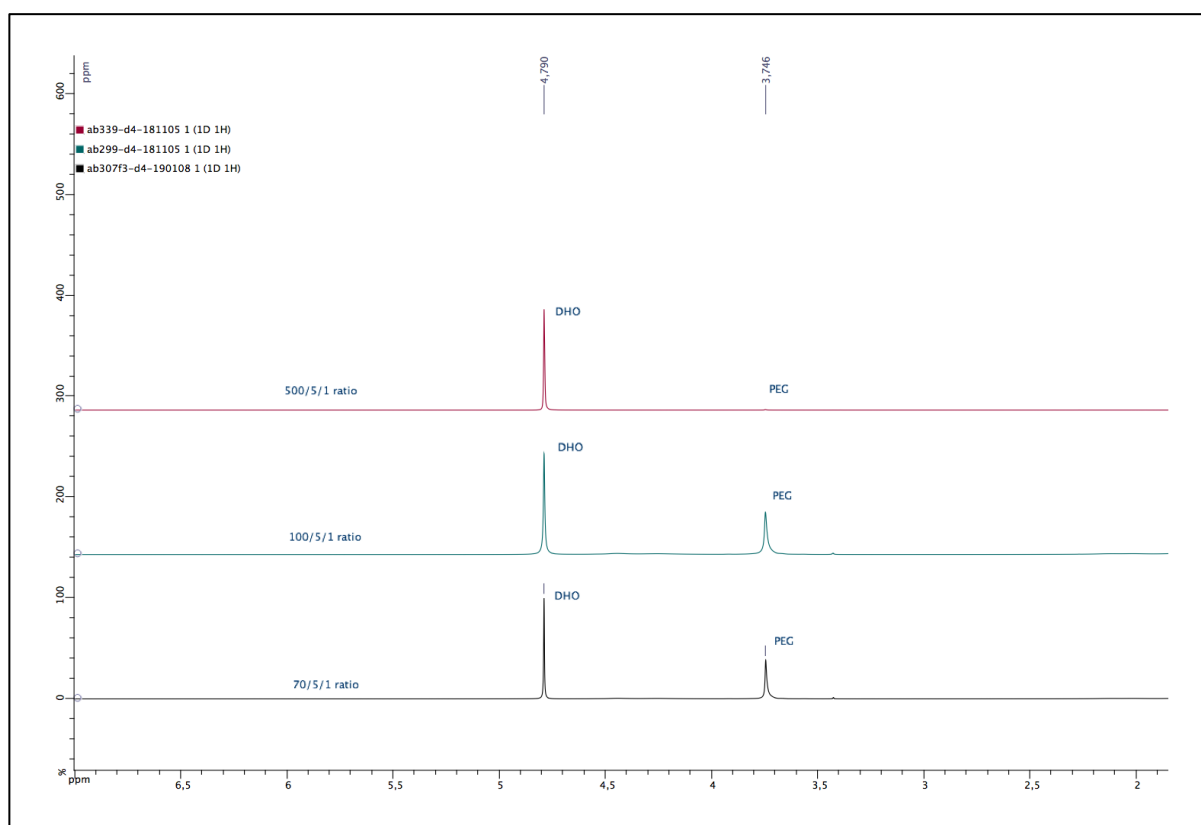


Figure 6: Superimposition of ¹H NMR (D₂O, 400 MHz) of isolated PEG-*co*-P(Cl-CL) copolymers prepared by ROP of Cl-CL initiated by *catalyst 4*/PEG system. a.) (Conditions: black spectrum [Cl-CL]₀ = 1 M, 70 equiv. of Cl-CL, 5 equiv. of PEG *vs.* catalyst, RT, DCM, 3.5 h, quantitative conv.). b.) Green spectrum: [Cl-CL]₀ = 1 M, 100 equiv. of Cl-CL, 5 equiv. of PEG *vs.* catalyst, RT, DCM, 6 h, quantitative conv.). c.) Red spectrum: [Cl-CL]₀ = 1 M, 500 equiv. of Cl-CL, 5 equiv. of PEG *vs.* catalyst, RT, DCM, 9 h, quantitative conv.).

II. 2. IFT measurements.

II. 2. a. IFT explanation and measurements principle

The physical phenomenon between water and oil is called interfacial tension (IFT) and results from the attractions due to intermolecular forces. A molecule at the surface of two immiscible liquids is subject to molecular attraction balanced by the fluid's resistance to compression (**Figure 7**).

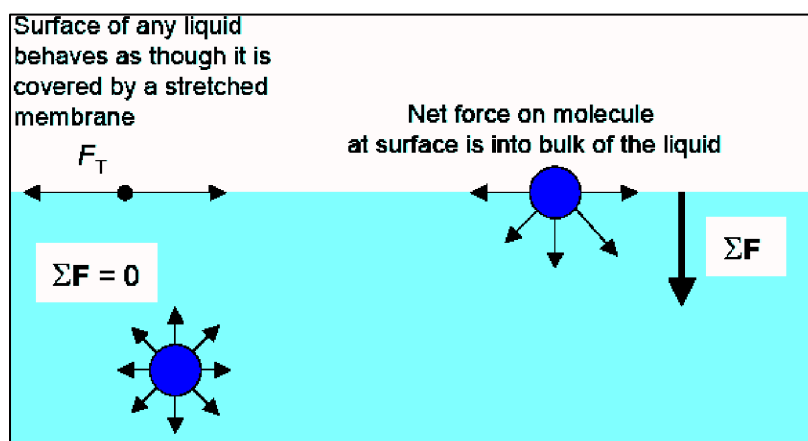


Figure 7: Attractive force on water molecule in a drop and on the surface

Many techniques have been proposed to measure interfacial tension.^{2,3}

The spinning drop method⁴ (**Figure 8**) was chosen for the calculation of the copolymers' IFT. This method is convenient in comparison to others because the contact angle measurement isn't required. Also, using this method, it is not necessary to know the curvature at the interface involving often some complexities due to the shape of the fluid drop.

The measurement was carried out a rotating horizontal tube, which contains a dense fluid (in these measurements aqueous solution of copolymer with water density: $\rho_2 = 0.998 \text{ g/mL}$) and a drop of a less dense liquid (dodecane which has a density $\rho_1 = 0.750 \text{ g/mL}$). The tube rotates about its longitudinal axis at a constant speed (5000 rpm) creating a centrifugal force. The liquid begins to deform into an elongated shape until the balance between the interfacial tension and the pressure difference at the interface occurs.⁵

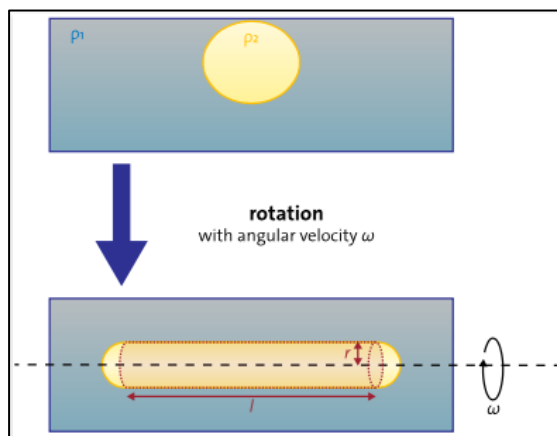


Figure 8: Drop deformation with the spinning drop principle

The shape of the drop is directly linked to the interfacial tension according to the Vonnegut's equation⁶ (**Figure 9**):

$$\sigma = \frac{\Delta\rho \omega^2 r^3}{4}$$

With $(\rho_2 - \rho_1) = \Delta\rho$

ω = rotation velocity

r = radius of the cylinder

Figure 9: Illustration of the Vonnegut's equation

II. 2. b. IFT Results on the different copolymers

Entry	Cl-CL ^a	PEG(1900) ^a	T (°C)	$M_{n, \text{corr}}^b$ (g/mol)	Concentration (ppm)	IFT ^c (mN/m)
1	70	5	RT	4463	1500	16
2	100	5	RT	5142	1500	16
3	500	5	RT	18560	1500	/

^a Equiv. versus initiator. ^b $((M_{n, \text{GPC}} - 1900) \times 0.88) + 1900$ (0.88: correlation factor obtained section VIII, Chapter III). ^c Obtained with a spinning drop tensiometer in a [dodecane/water] mixture.

Table 2: Results of the IFT data

IFT measurements ⁷ were performed in a (water/dodecane) mixture with the IFT (water/dodecane)= 31mN/m. The PEG-*co*-P(Cl-CL) using 70 equivalents of Cl-CL and 100 equivalents of Cl-CL (with 5 equivalents of PEG) have the same IFT value of 16 mN/m (**entries 1 and 2, Table 2**). This same value is due to the difference of only 30 equivalents between the hydrophobic chain length which is not significant enough to impact the IFT value. The decrease of the IFT value from 31 to 16 mN/m is in agreement with the amphiphilic character of these copolymers as shown in **Figures 6a**, and **6b**, (**Supporting data: Figures 2 and 3**). However, the PEG-*co*-P(Cl-CL) performed with 500 equivalents of Cl-CL and 5 equivalents of PEG wasn't soluble in water as seen on the same Figure (**Figure 6c** and **supporting data: Figure 4**) and, thus no IFT value was determined. As a consequence, it could be deduced that the ratio of hydrophobic polymer chain *vs.* PEG ratio is too high for significant amphiphilic property into the copolymer and the overall copolymers can be considered as hydrophobic.

The Cl-CL polymerization with an Al-PEG catalyst have allowed providing amphiphilic properties to the P(Cl-CL) hydrophobic homopolymer. Next, the introduction of a PLA segment onto P(Cl-CL) was studied to access more crystalline PLA-*b*-P(Cl-CL) copolymers.

III. Synthesis of P(*L/D*)LA-*b*-P(Cl-CL) diblocks and stereocomplex

III. 1. Diblocks synthesis

L- or *D*-lactide and then Cl-CL monomers were polymerized with **catalyst 4** as ROP initiator to give corresponding diblocks PLA-*b*-P(Cl-CL) copolymers.

The «living» nature of the ROP of Cl-CL and lactide allows the preparation of well-defined block copolymers by the sequential monomer addition method.⁸ After the full conversion of the lactide monomer (toluene, 80 °C, 9 h) to PLA, Cl-CL monomer was then introduced and stirred at RT during the appropriate time, resulting in the formation of diblock copolymers (**Figure 10**). The different diblocks were subsequently characterized by means of NMR, GPC, TGA, and DSC.

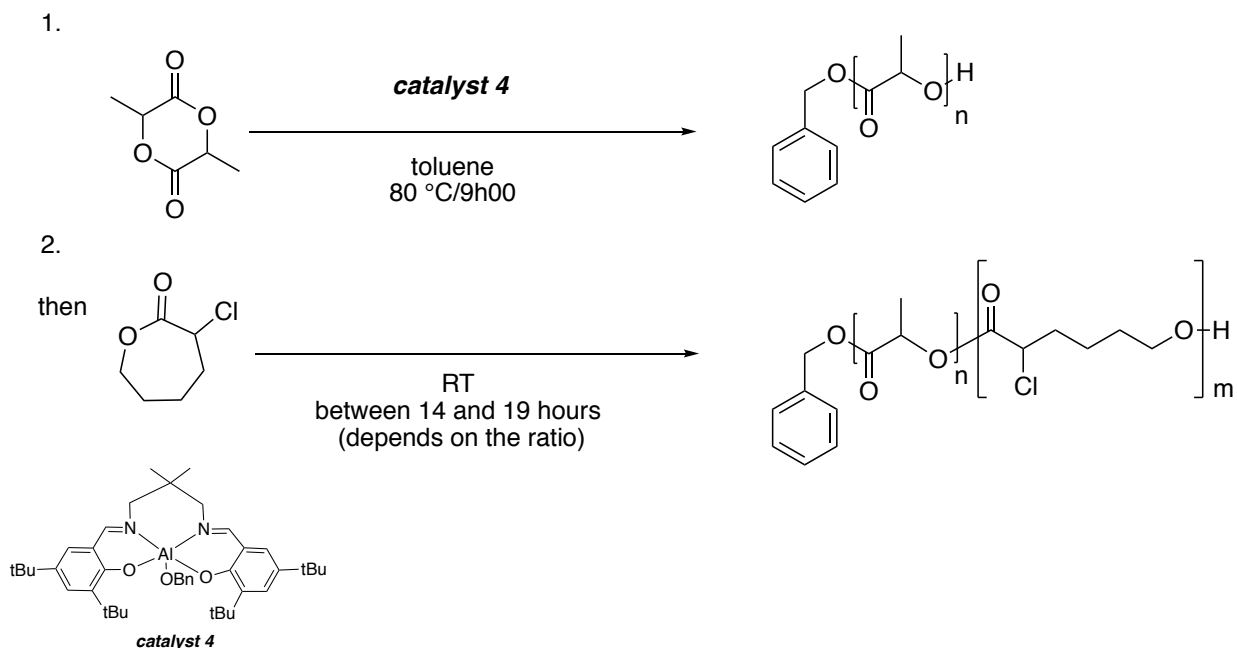


Figure 10: Synthesis of PLA-*b*-P(CI-CL) diblocks by the sequential monomer addition method

Five different PLA-*b*-P(CI-CL) diblocks were thus synthesized according to the procedure described above. Abbreviation of each diblock sample, ratio, corresponding percentage, $M_{n, \text{theo}}$, $M_{n, \text{GPC}}$ and PDI are summarized in **Table 3**.

Entry	diblocks Abbreviation	PLA/ P(CI-CL) ^a	PLA/ P(CI-CL) %	$M_{n, \text{theo}}$ ^b (g/mol)	$M_{n, \text{GPC}}$ ^c (g/mol)	PDI
1	PLLA- <i>b</i> -P(CI-CL) AB287f1	100/100	50/50	29272	33116	1.50
2	PDLA- <i>b</i> -P(CI-CL) AB302bis	100/100	50/50	29272	33741	1.45
3	PLLA- <i>b</i> -P(CI-CL) AB306	150/150	50/50	43928	62203	1.08
4	PLLA- <i>b</i> -P(CI-CL) AB318	200/100	67/33	43710	53290	1.09
5	PLLA- <i>b</i> -P(CI-CL) AB303bis	100/30	77/23	18883	22309	1.48

^a Equiv. versus initiator. ^b Calculated using lactide equiv. $\times M_{\text{lactide}} \times \text{conv.} + (\text{Cl-CL}) \text{equiv.} \times M_{\text{Cl-CL}} \times \text{conv.}$ ^c Measured by GPC in THF (30 °C) using PS standards.

Table 3: Results of the data obtained for the different diblocks

- A diblock with 100 equivalents of *L*-lactide and 100 equivalents of Cl-CL (**entry 1, Table 3**). Then the enantiomeric copolymer using 100 equivalents of *D*-lactide and 100 equivalents of Cl-CL (**entry 2, Table 3**). Both diblocks were performed in order to make a new stereocomplex.
- To compare the properties of PLA-*b*-P(Cl-CL) diblocks as a function of material chain length, 300 equivalents amount of total monomers with blocks of 150 equivalents of *L*-lactide and 150 equivalents of Cl-CL (**entry 3, Table 3**). A second diblock copolymer was prepared by increasing the lactide amount to 200 equivalents and using 100 equivalents of Cl-CL (**entry 4, Table 3**).
- A diblock resulting from the sequential ROP of a 100/30 *L*-lactide/Cl-CL mixture (**entry 5, Table 3**)

In all cases, the ROP of *L*- or *D*-lactide was performed within 9 hours at 80 °C in toluene (from 100 to 200 equivalents) initiated by *catalyst 4* and followed by the ROP of Cl-CL (30 to 150 equivalents) at room temperature during 14-19 hours to yield PDLA-*b*-P(Cl-CL) and PLLA-*b*-P(Cl-CL) diblocks with M_n GPC values in agreement with the theoretical values as deduced from ¹H NMR spectra and monomodal SEC traces (with polydispersities ranging from 1.08 to 1.50).

For the two PLLA/PDLA-*b*-P(Cl-CL) diblocks, the ¹H NMR spectra (**Figure 11**) match on the one hand with the presence of 100 equivalents of P(Cl-CL) and on the other hand with the presence of 100 equivalents of PLA. Also, the ¹H NMR spectrum agrees with the presence of a CH₂-*Ph* benzyloxy chain end signal while the CH₂-Ph resonance is hidden under the quadruplet of the CH of PLLA signal. Finally, the -CH₂OH chain end multiplet appears between 3.63 and 3.67 ppm.

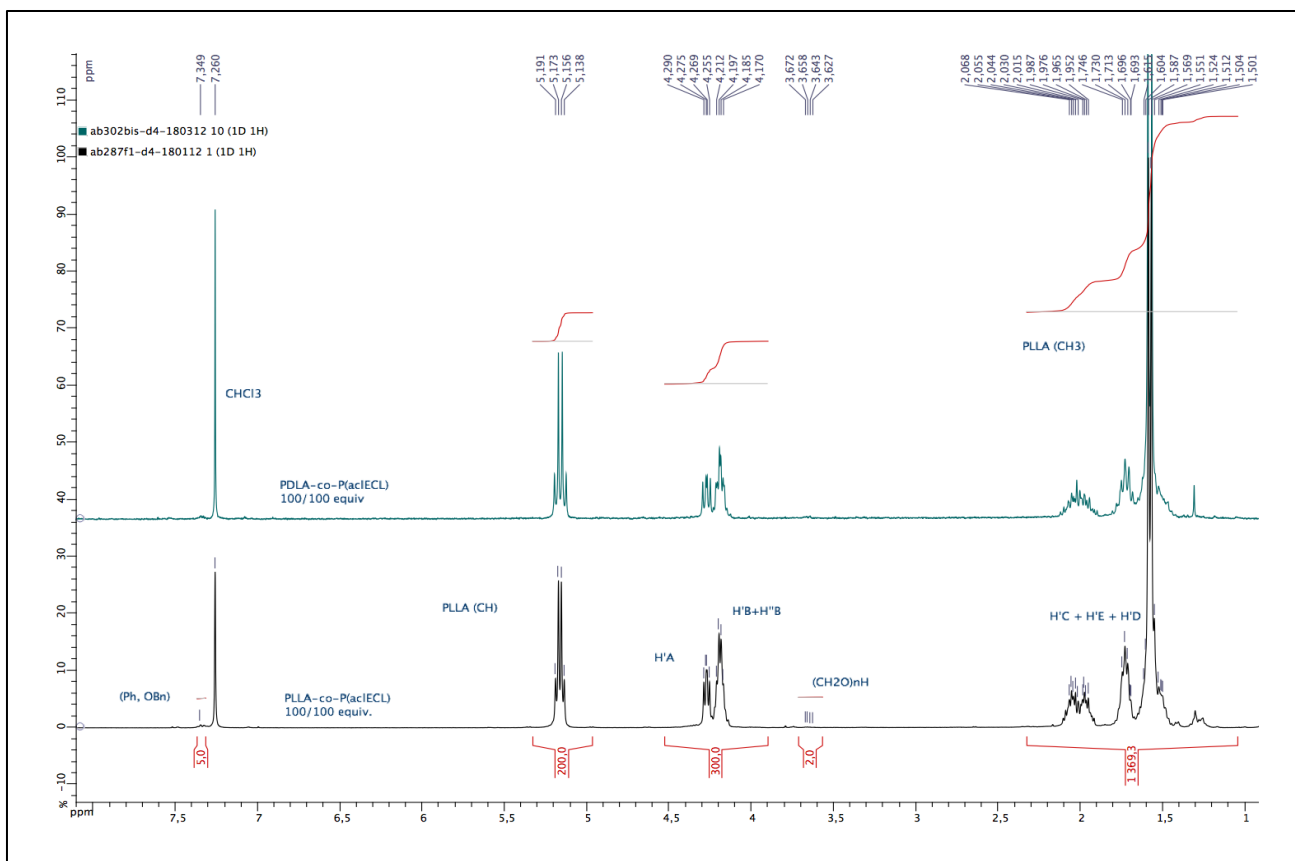


Figure 11: Superimposition of the ^1H NMR spectra (CDCl_3 , 400 MHz) of isolated diblocks prepared by polymerization of: 1). 100 equiv. of *L*- and *D*-lactide using *catalyst 4* system. (conditions: toluene, 80 °C, 9 h, quantitative conv.). 2). 100 equiv. of Cl-CL, RT, 14 h).

As predicted the two diblocks chain lengths match the theoretical values (**entries 1** and **2**, **Table 3**) even if the *PDLA-b-P(Cl-CL)* diblock displays a lower polydispersity (PDI: 1.45) (**Figure 13**) than the *PLLA-b-P(Cl-CL)* diblock (PDI: 1.50) (**Figure 12**).

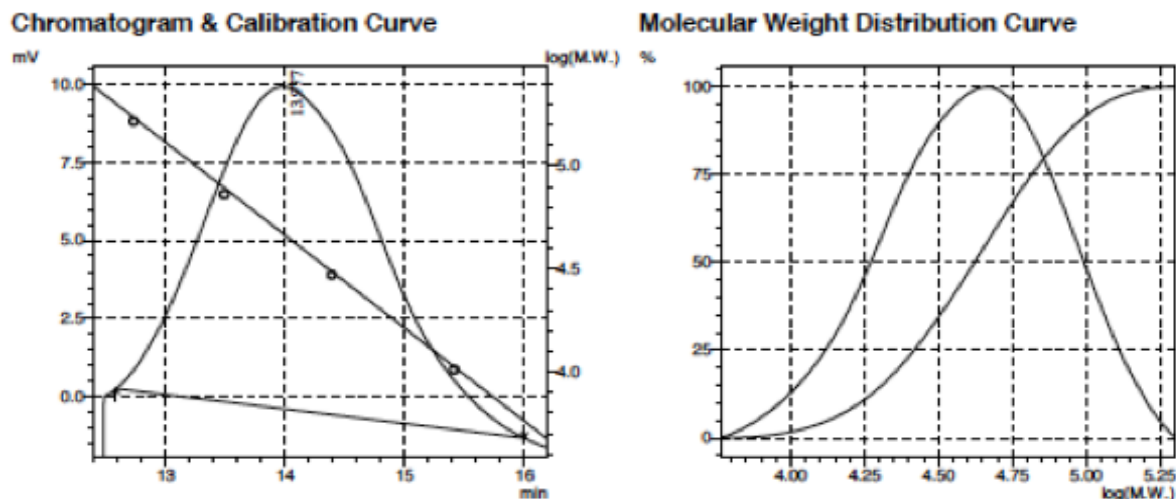


Figure 12: SEC traces of isolated PLLA-*b*-P(Cl-CL) diblock. Conditions: 1) 100 equiv. of *L*-lactide, toluene, 80 °C, 9 h, total conv. 2) 100 equiv. of Cl-CL, toluene, RT, 14 h, quantitative conv.

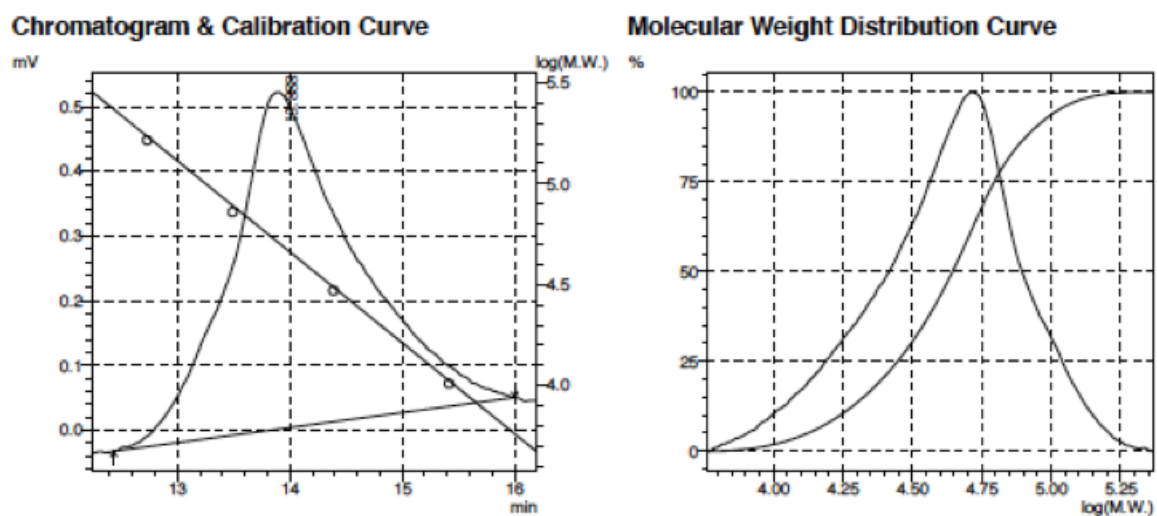


Figure 13: SEC traces of isolated PDLA-*b*-P(Cl-CL) diblock. Conditions: 1). 100 equiv. of *D*-lactide, toluene, 80 °C, 9 h, total conv. 2). 100 equiv. of Cl-CL, toluene, RT, 14 h, quantitative conv.

The ^1H NMR data of other prepared diblock copolymers agree with controlled and expected chain length for both PLA and P(Cl-CL) segments (**Figures 14-16**). Likewise, the GPC traces (**Figure 15**) of the PLLA-*b*-P(Cl-CL) diblocks derived from sequential ROP proceeding by

sequential monomer addition all feature monomodal traces with M_n GPC values in agreement with the theoretical values and narrow polydispersities (**Figures 15, 17 and 19, Table 3**).

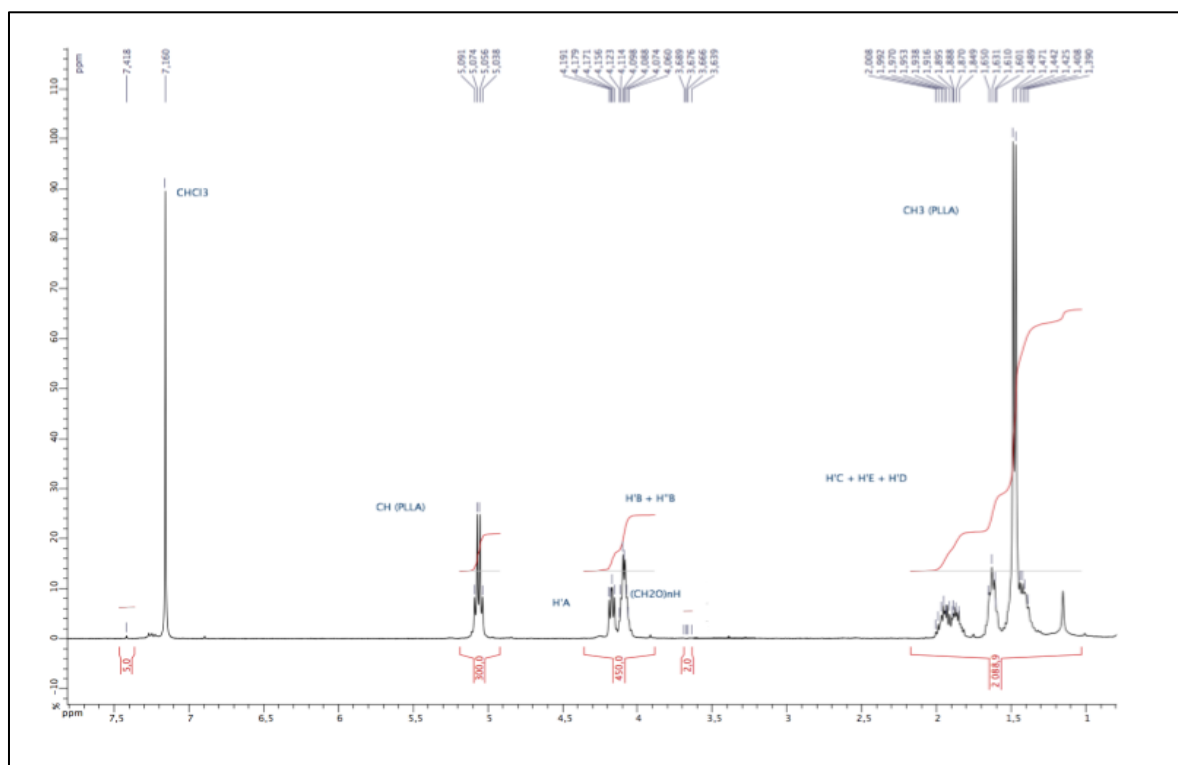


Figure 14: ^1H NMR spectrum (CDCl_3 , 400 MHz) of isolated diblock prepared by polymerization of: 1). 150 equiv. of *L*-lactide using *catalyst 4* system. (Conditions: toluene, 80 °C, 9 h, quantitative conv.). 2). 150 equiv. of Cl-CL, RT, 16 h). Abbreviation: AB306.

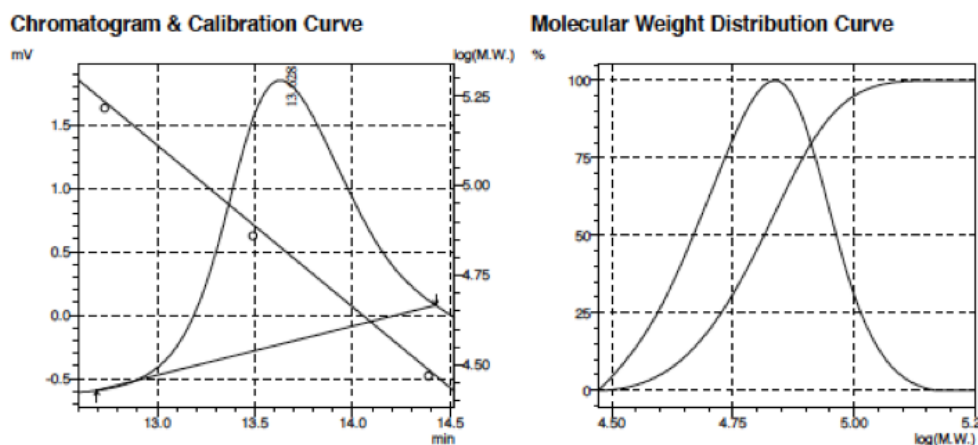


Figure 15: SEC traces of isolated PLLA-*co*-P(Cl-CL) diblock. Conditions: 1) 150 equiv. of *L*-lactide, toluene, 80 °C, 9 h, total conv. 2) 150 equiv. of Cl-CL, toluene, RT, 16 h, quantitative conv.

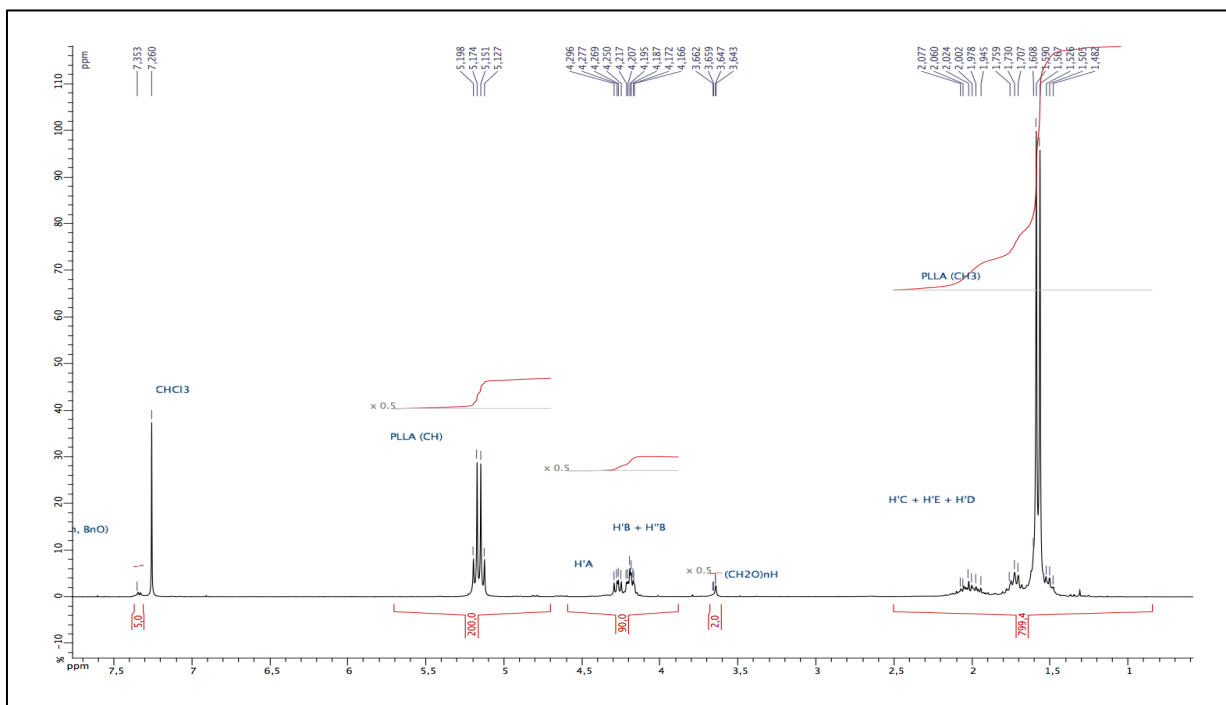


Figure 16: ^1H NMR spectrum (CDCl_3 , 400 MHz) of isolated diblock prepared by polymerization of: 1). 100 equiv. of *L*-lactide using *catalyst 4* system. (Conditions: toluene, 80 °C, 9 h, quantitative conv. 2). 30 equiv. of Cl-CL, RT, 17 h).

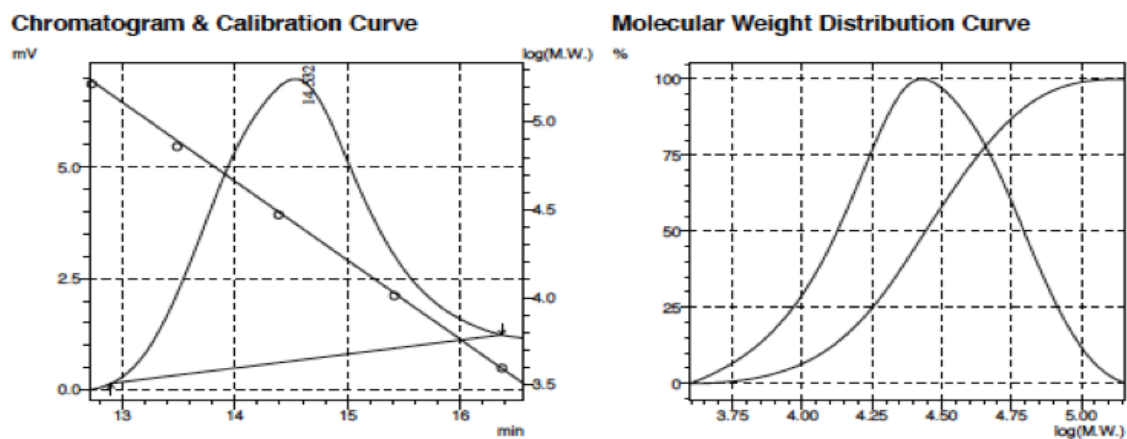


Figure 17: SEC traces of isolated PLLA-*co*-P(Cl-CL) diblock. Conditions: 1). 100 equiv. of *L*-lactide, toluene, 80 °C, 9 h, total conv. 2). 30 equiv. of Cl-CL, toluene, RT, 17 h, quantitative conv.

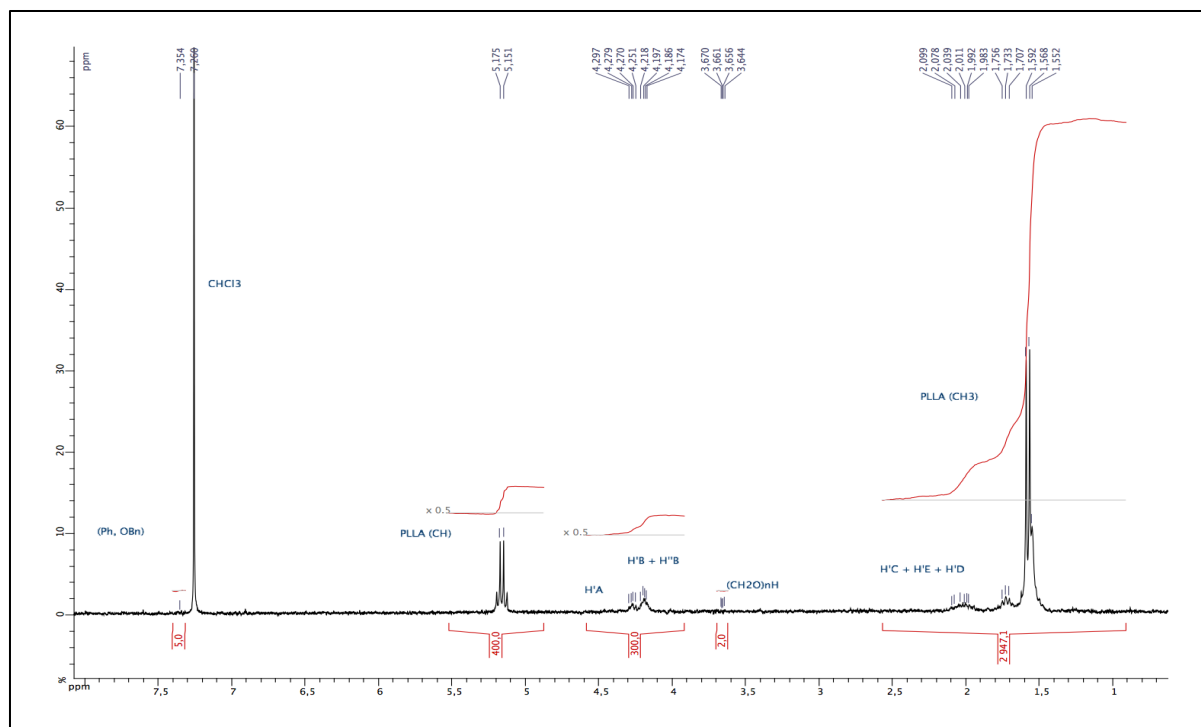


Figure 18: ^1H NMR spectrum (CDCl_3 , 400 MHz) of isolated diblock prepared by polymerization of: 1). 200 equiv. of *L*-lactide using *catalyst 4* system. (Conditions: toluene, 80 °C, 9 h, quantitative conv.) 2). 100 equiv. of Cl-CL, RT, 19 h). Abbreviation: AB318.

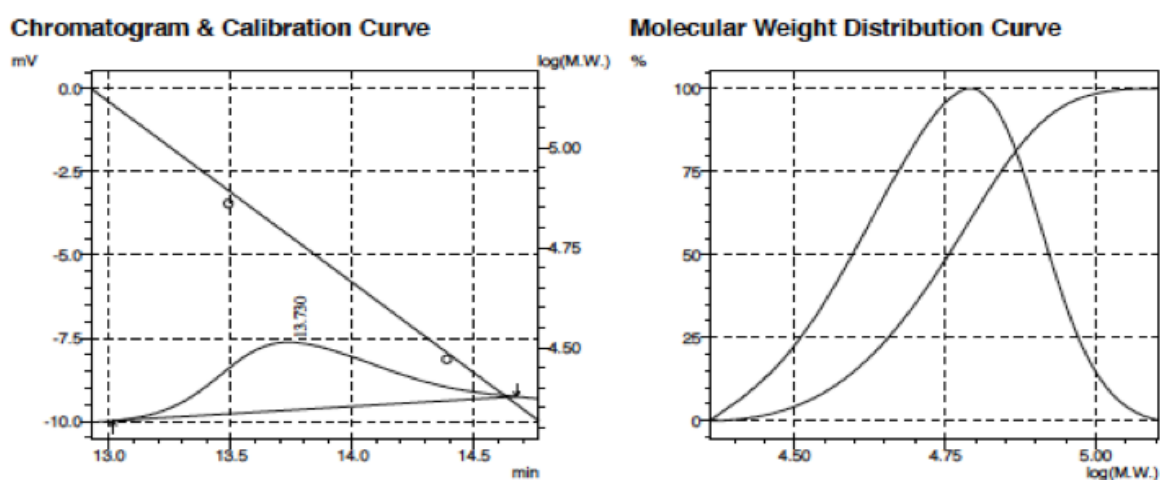


Figure 19: SEC traces of isolated PLLA-*b*-P(Cl-CL). Conditions: 1). 200 equiv. of *L*-lactide, toluene, 80 °C, 9 h, quantitative conv. 2). 100 equiv. of Cl-CL, RT, 19 h, quantitative conv.

III. 2. Stereocomplex formation

In 1987, Ikada *et al.* first reported a PLA stereocomplex of PLLA and PDLA,⁹ the simplest class of polyesters. Blending both PLLA and PDLA polymers lead to the formation of a stereocomplex with a new crystalline structure. The stereocomplex is known to increase thermal, mechanical and material resistance properties of the resulting polymer^{10,11,12} in virtue of the $\text{CH}_3\cdots\text{O}=\text{C}$ hydrogen-bonding interactions between the polymeric enantiomeric chains.¹³



Figure 20: Chain models of PLLA and PDLA
(Scheme source: Ikada *et al.* *Macromolecules*, 1987)¹⁴

Thus, to improve the thermal properties of PLA-*b*-P(Cl-CL) copolymers, a PLLA/PDLA-*b*-P(Cl-CL) stereocomplex was first prepared from PLLA-*b*-P(Cl-CL) 100/100 ratio and PDLA-*b*-P(Cl-CL) 100/100 ratio.

Entry	Diblocks and stereocomplex	PLA/P(Cl-CL) ^a	M _n ^{theo} ^b (g/mol)	M _n ^{GPC} ^c (g/mol)	M _n ^{corr} ^d (g/mol)	PDI
1	PLLA- <i>b</i> -P(Cl-CL) (AB287f1)	100/100	29272	33116	31129	1.50
2	PDLA- <i>b</i> -P(Cl-CL) (AB302bis)	100/100	29272	33741	31717	1.45
3	PLLA- <i>b</i> -P(Cl-CL) + PDLA- <i>b</i> -P(Cl-CL) (AB305bis)	100/100 + 100/100	29272	40047	37644	1.37

^a Equiv versus initiator. ^b Calculated using $[\text{lactide}]_0 \times M_{\text{lactide}} \times \text{conv.} + [\text{Cl-CL}]_0 \times M_{\text{Cl-CL}} \times \text{conv.}$ ^c Measured by GPC in THF (30 °C) using PS standards. ^d ($M_{\text{n corr}} = M_{\text{n GPC}} \times 0.88$) with 0.88: correlation factor obtained **section VIII, Chapter III**).

Table 4: Results of PLLA-*b*-P(Cl-CL), PDLA-*b*-P(Cl-CL) and stereocomplex GPC data

An equal amount of each diblock was dissolved in the same amount of chloroform and then mixed together at room temperature for three hours. The evaporation of the solvent to open air permitted to isolate the solid stereocomplex as crystalline plates (**Figure 21**).

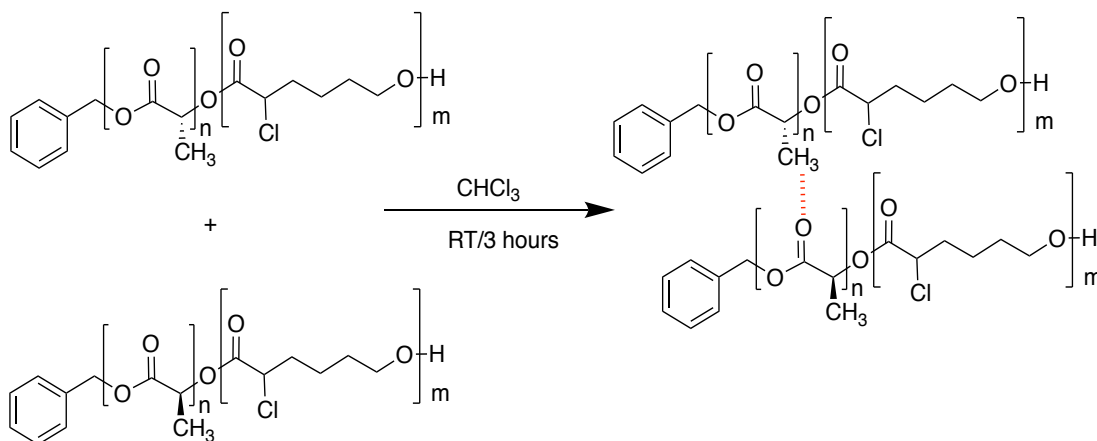


Figure 21: PLA + P(Cl-CL) stereocomplex synthesis

The two enantiomerically pure diblocks have very similar data such as molecular weight and polydispersity (**entries 1 and 2, Table 4**). However, the resulting stereocomplex shows a poor solubility in THF (**entry 3, Table 4**) explaining M_n^{GPC} difference between this latter and the diblocks.

The ^1H NMR spectrum of the stereocomplex (**Figure 22**) and the SEC traces of the isolated stereocomplex (**Figure 23**) are consistent with a well-defined material with controlled chain length.

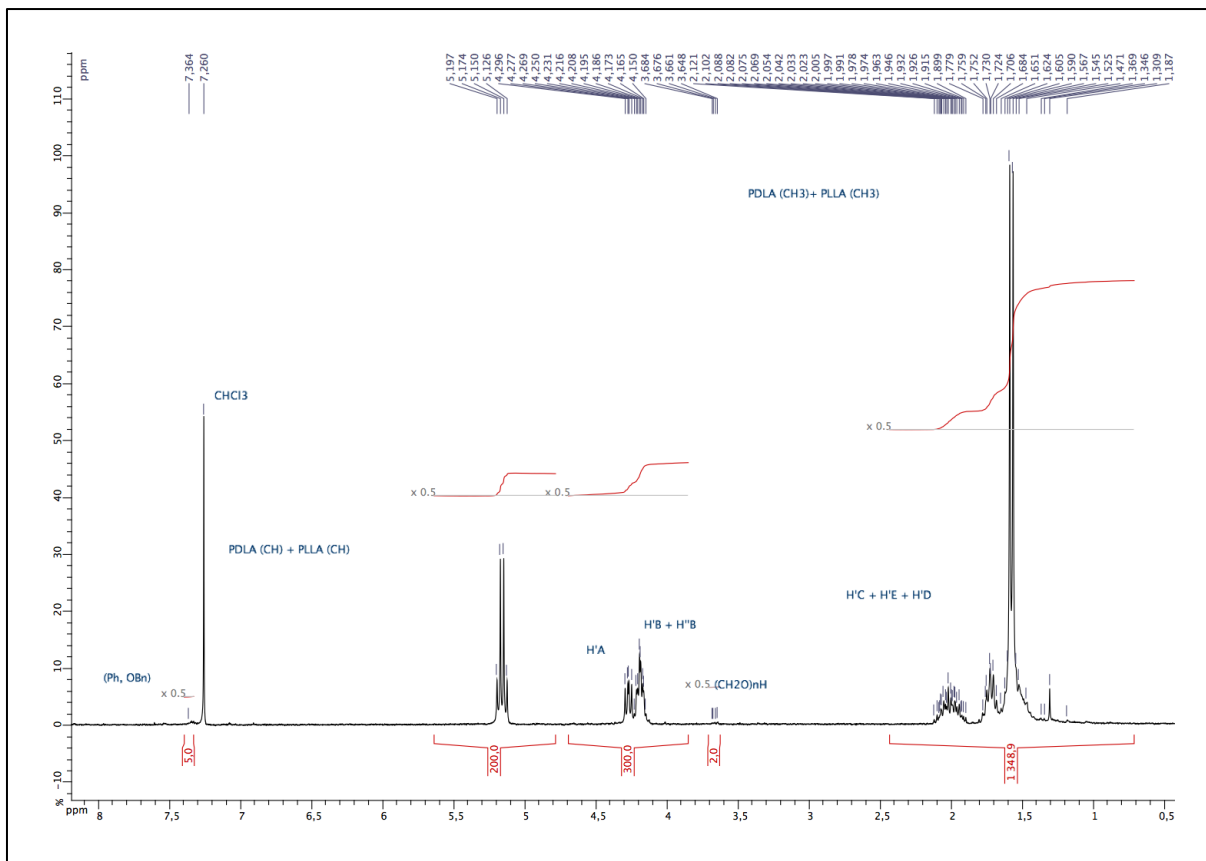


Figure 22: ^1H NMR (CDCl_3 , 400 MHz) of isolated PLA + P(Cl-CL) stereocomplex. (Conditions: $\text{PLLA-}b\text{-P(Cl-CL)}$ 100/100 equiv. + $\text{PDLA-}b\text{-P(Cl-CL)}$ 100/100 equiv., CHCl_3 , RT, 3 h).

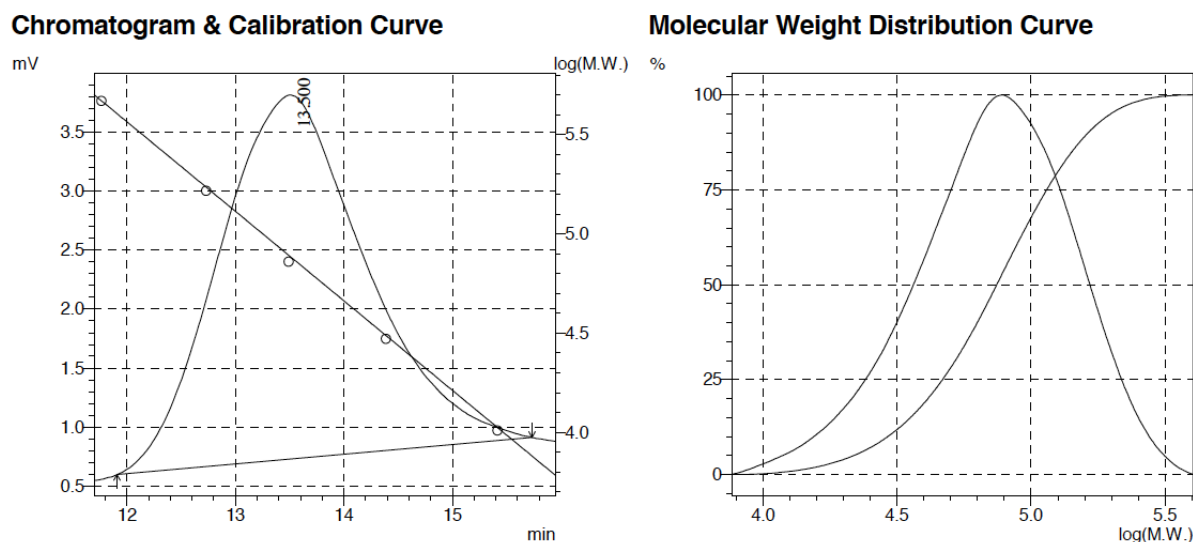


Figure 23: SEC traces of isolated PLA-P(Cl-CL) stereocomplex. (Conditions: PLLA-*b*-P(Cl-CL) 100/100 equiv. + PDLA-*b*-P(Cl-CL) 100/100 equiv., CHCl₃, RT, 3 h).

IV. Thermal gravimetric analysis TGA

IV. 1. Theory about TGA

TGA¹⁵ may be defined as an experimental method for characterizing a system (element, compound or mixture) by measuring the changes in physicochemical properties in a sample that occur at an elevated temperature while the mass sample is varied as a function of increasing temperature according to a controlled temperature program.¹⁶ While heated, materials can undergo various changes accompanied by a loss of mass. For instance, loss processes include the degradation or decomposition, the chemisorption, sublimation, vaporization, oxidative degradation, reduction of metal oxides to metals.

The result of TGA measurements is a thermogravimetric curve that can present the integral form where the mass (in gram or in % of the initial mass) is plotted against time or temperature or it can illustrate the differential form meaning the derivative curve with respect to time or temperature.¹⁷

For the polymers results, TGA allows access to precise information about physicochemical properties of the sample, phase transitions or thermal decompositions. Consequently, in our case, the data collected from the thermal TGA reaction are compiled through a plot of percentage initial mass on the y-axis versus temperature on the x-axis.

IV. 2. P(Cl-CL) homopolymer TGA analysis

P(Cl-CL) homopolymer (100 equivalents of Cl-CL, AB256) has a total mass loss under nitrogen flow. The decomposition occurs in two steps: the first one begins at 220 °C until 340 °C, it is probably the cleavage between the carbone-chlorine bond followed by the second decomposition in a range of 340 °C to 460 °C, temperature at which no sample is left (**Figure 24**). These data are in agreement with those already mentioned in literature by Jérôme *et al.*¹⁸

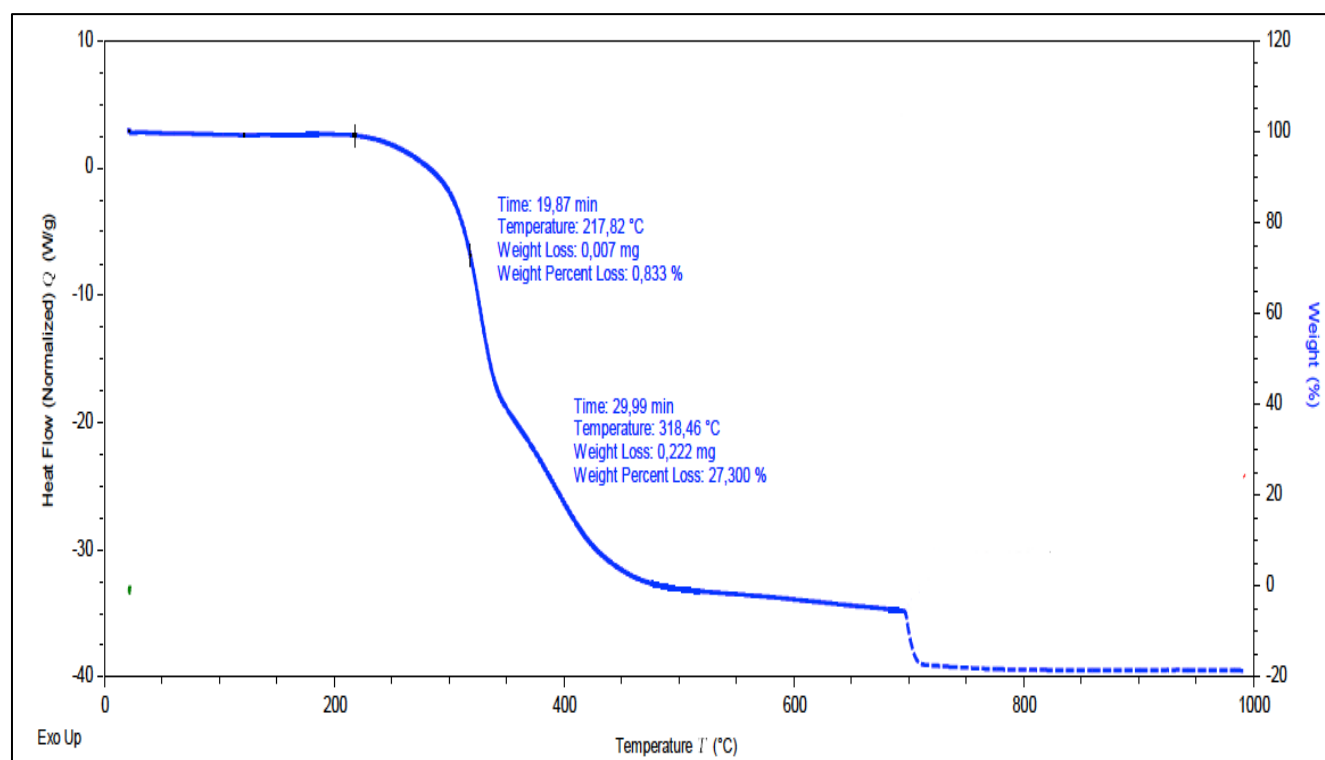


Figure 24: TGA curve for the degradation of P(Cl-CL) heated at 10 °C/min. when is the gas flow switched from nitrogen (100 mL/min.) to air.

By comparison, PCL has a decomposition which occurs at about 430 °C.¹⁹ Thus P(Cl-CL) has a decomposition temperature considerably lower than PCL, probably due the lower stability of the C–Cl upon heating.

IV. 3. Diblocks and stereocomplex TGA studies

All the PLA-*b*-P(Cl-CL) diblocks and the corresponding stereocomplex were also analyzed by TGA (**entries 2 to 6, Table 5**) and the TGA curves are superimposed on the same plot (**Figure 25**).

Entry	References	abbreviation	Initial mass (mg)	Start of decomposition	Residue under N ₂ (%)	Residue under air flow (%)
1	P(Cl-CL) 100 equiv.	AB256	0.8116	After 220 °C	0	/
2	PDLA- <i>b</i> -P(Cl-CL) 100/100 equiv.	AB302bis 1	5.1549	After 280 °C	6.5977	0.4040
3	PLLA- <i>b</i> -P(Cl-CL) 100/30 equiv.	AB303bis 2	5.8197	After 240 °C	4.2864	0.4679
4	PDLA- <i>b</i> -P(Cl-CL) + PLLA- <i>b</i> -P(Cl-CL) 100/100 equiv. + 100/100 equiv.	AB305bis 3	4.3028	After 260 °C	12.99337	6.6136
5	PLLA- <i>b</i> -P(Cl-CL) 150/150 equiv.	AB306 4	4.7446	After 290 °C	5.2364	0.4884
6	PLLA- <i>b</i> -P(Cl-CL) 200/100 equiv.	AB318 5	4.3094	After 220 °C	3.6091	0.0304

Table 5: TGA results for the different samples

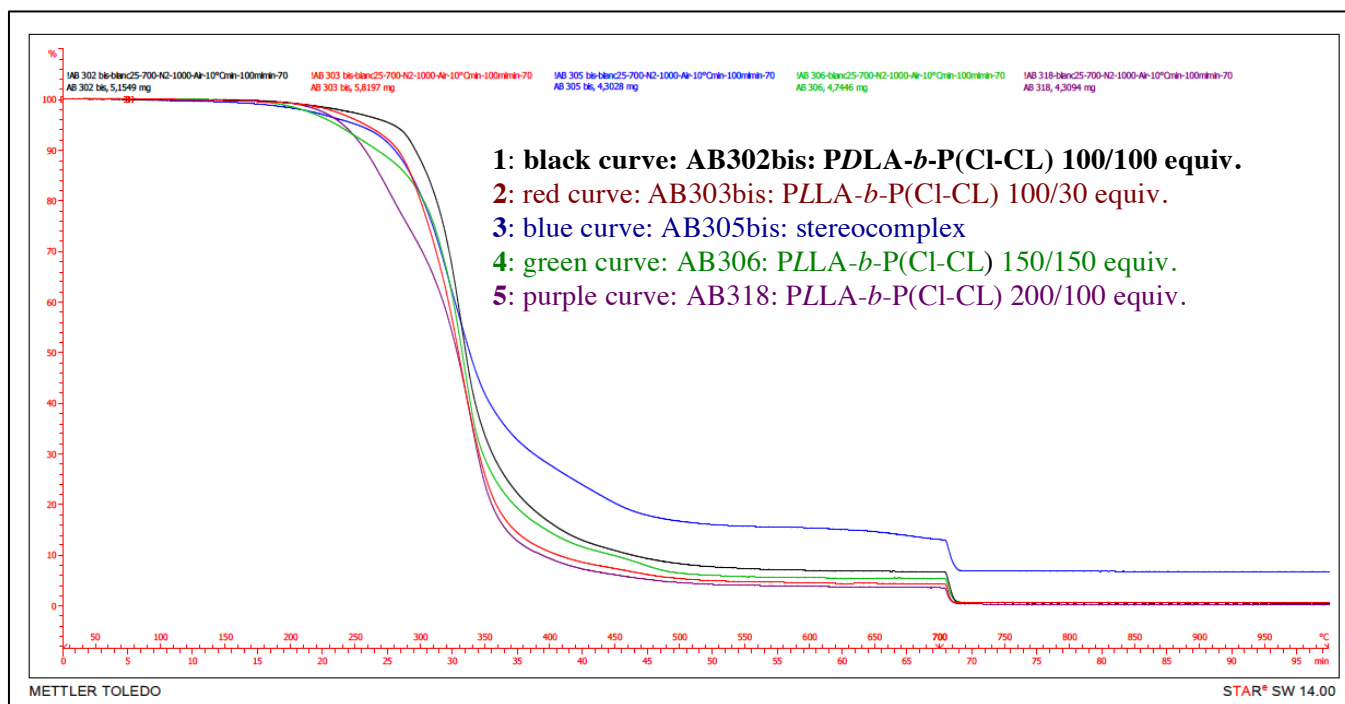


Figure 25: Superimposition of TGA curves for the degradation of diblocks and stereocomplex heated at 10 °C/min. under a nitrogen flow (100 mL/min.) then under air flow. All diblocks and stereocomplex are assigned with a value from 1 to 5.

The transition between the two gases (N_2 and air) is located at 700 °C and all the samples have a high mass loss in contact with air flow. Indeed, adding air gives a more oxidative atmosphere, which allows the pyrolysis of carbon. As seen below P(Cl-CL) has a starting decomposition at 220 °C and PLA about 250 °C.²⁰ Concerning the stereocomplex (3), the residue percentage remains large at 1000 °C (entry 4, Table 5), and is indeed, as planned, the most stable sample. (1) (entry 2, Table 5) shows a first small mass loss on the initial curve before product decomposition (Supporting data: Figure 7). These two effects are interconnected and can't be treated separately. (2) (entry 3, Table 5) shows a similar phenomenon to that discussed for the previous diblock but presents a more important mass loss which is visible just before the decomposition in a range of 190 to 260 °C (Supporting data: Figure 8). (4) (entry 5, Table 5) shows at least three successive mass losses between 180 and 550 °C (Supporting data: Figure 9). The first two are not enough separated to be treated independently. However, the last one is visible but the exact limits are difficult to define. Last, (5) (entry 6, Table 5) has a clear decomposition that occurs in two steps between 200 and 500 °C (Supporting data: Figure 10).

It is relatively simple to compare the stability between **(1)** (**entry 2, Table 5**) and **(4)** (**entry 5, Table 5**). Both are constituted of 50% amount in PLA and have similar starting decomposition temperature about 280-290 °C.

(2) (77% PLLA/23% P(Cl-CL)) (**entry 3, Table 5**) is more resistant than **(5)** (67% PLLA/33% P(Cl-CL)) (**entry 6, Table 5**): these data thus show the diblocks are more stable with a higher content in PLA. As expected, the stereocomplex is the most stable polymer sample thanks to the higher resistance brought by the hydrogen bonds between the polymer enantiomeric chains.

V. DSC studies

V. 1. Theory about DSC

DSC²¹ is a method used to investigate the response of polymers to heating. This technique can be used to study the three characteristic temperatures dependent on the material's properties. The glass transition temperature (T_g)²² is the gradual and reversible transition in the amorphous regions of a polymer designating the transition from a glassy state into a rubbery state.²³ This temperature is always lower than the melting point (T_m) and, if it exists, than the crystallization temperature (T_c) as well. At some point, the macromolecules may gain enough freedom of motion to arrange themselves into a crystalline form. This is known as the crystallization temperature (T_c). This transition from amorphous solid to crystalline solid is an exothermic process. At the melting point (T_m), the polymer chains are able to move around freely and don't have ordered arrangements. Several peaks can be observed if the sample has different sizes and morphologies in the crystalline areas. This process is endothermic.²⁴ The DSC procedure allows accessing to the variation of the enthalpies of crystallization (ΔH_c) and melting (ΔH_m) and to the measurement of the crystallinity of a polymer.²⁵

V. 2. Homopolymers, diblocks and stereocomplex DSC studies

PLLA and P(Cl-CL) homopolymers, the prepared PLLA-*b*-P(Cl-CL) or PDLA-*b*-P(Cl-CL) diblocks, and the PLLA-*b*-P(Cl-CL) + PDLA-*b*-P(Cl-CL) stereocomplex prepared were analyzed by DSC. The corresponding (T_g), (T_m), (T_c), and enthalpies are given in **Table 6**.

Entry	Reference	Ratio/%	T _{g1} (°C)	T _{g2} (°C)	T _m (°C)	ΔH _m (J/g)	T _c (°C)	ΔH _c (J/g)	Crystalline rate ^a %
1	P(Cl-CL) AB256	100 equiv. 100%	-33	-	-	-	-	-	-
2	PLLA AB333	100 equiv. 100%	-	56	165	63	111	-52	60
3	PDLA- <i>b</i> -P(Cl-CL) AB302Bis	100/100 equiv. 50%/50%	-32	55	158	29	106	-22	13
4	PLLA- <i>b</i> -P(Cl-CL) AB303Bis	100/30 equiv. 77%/23%	-29	n.d	155 to 168	41	108	-33	29
5	PDLA- <i>b</i> -P(Cl-CL)+ PLLA- <i>b</i> -P(Cl-CL) AB305Bis	100/100 equiv. + 100/100 equiv. 50%/50%	-30	n.d	191 to 229	53	149	-18	25
6	PLLA- <i>b</i> -P(Cl-CL) AB306	150/150 equiv. 50%/50%	-28	n.d	157	28	93	-18	13
7	PLLA- <i>b</i> -P(Cl-CL) AB318	200/100 equiv. 67%/23%	n.d	n.d	157	32	91	-15	20

n.d: “not determined” because (T_g) is difficult to determine with precision. ΔH_m: melting enthalpy and ΔH_c: recrystallization enthalpy. Crystalline rate calculation: ΔH_{m1} x PLA % x 0.93.²⁶

Table 6: Results of DSC measurements

P(Cl-CL) homopolymer (100 equiv.) (**entry 1, Table 6**) exhibited only a glass transition at -33 °C (**Supporting data: Figure 12**) and thus is an amorphous material. This value can be compared to the PCL, a closely related polymer structure. The different characteristic temperatures for the semi-crystalline PCL are (T_g)= -66 °C, (T_m)= 55 °C and (T_c)= 23 °C.²⁷ Thus, the presence of the chlorine pendant group along with the atacticity of the P(Cl-CL) brings considerably modifications in the material’s properties. PLLA homopolymer (**entry 2, Table 6**) has a (T_g) of 56 °C, and a (T_m) of 165 °C (measured at first ascent) (**Supporting data: Figure 19**). These results are consistent with the literature data: (T_g) PLA = 55-60 °C and (T_m) PLA is 170 °C.²⁸

Regarding the different diblocks (AB302bis, AB303bis, AB306 and AB318), (**entries 3, 4, 6, and 7, Table 6**), a (T_m) is clearly visible for each one. DSC data provide indications about the P(L/D)LA-*b*-P(Cl-CL) diblocks formation. The presence of two different (T_g) temperatures are a first indication that diblocks were formed, one for the P(Cl-CL) part and another for the P(L/D)LA block, with of course different values compared to

homopolymer values. The presence of a (T_c) for all of them constitute the second indication for a diblock character (**Supporting data: Figures 13, 14, 17, and 18**). Indeed, as mentioned above, P(Cl-CL) homopolymer is an amorphous material with thus no (T_c) while PLLA is a highly crystalline homopolymer. Consequently, the (T_c) value comes from the crystalline part of the diblocks. The stereocomplex (AB305bis), (**entry 5, Table 6**) (**Supporting data: Figure 15**) composed by PLLA-*b*-P(Cl-CL) and PDLA-*b*-P(Cl-CL) (AB302bis) shows as expected higher (T_m) and (T_c) values (**Supporting data: Figure 17**).

According to DSC results, the level of crystallinity of (AB306) and (AB318) (**entries 6 and 7, Table 6**) were calculated and follow the ratio PLA/P(Cl-CL): the higher the content in PLA in the diblock, the more crystalline the material is (respectively 13% and 20%). This fact is also confirmed by PLLA-*b*-P(Cl-CL) diblock (AB303bis) containing the highest amount of PLA (77%), which leads to the highest crystallinity (**entry 4, Table 6**).

The formation of PLA-*b*-P(Cl-CL) diblocks thus provides some level of crystallinity to P(Cl-CL)-based materials. Indeed, the PLA block has added crystalline property to the amorphous P(Cl-CL), and further shows that combining the properties of known homopolymers allows the design of a material having a properties synergy.

VI. Conclusion

In summary, the properties of P(Cl-CL) were modified thanks to a copolymerization strategy or the use of a macroinitiator (such as MeO-PEG) leading to the production of diblock copolymers. On the one hand P(Cl-CL) have been modified by adding a m-PEG-OH polymer fragment to act as a hydrophilic counterpart and has allowed the obtention of amphiphilic PEG-*co*-P(Cl-CL) copolymers. These first results were confirmed by NMR and IFT analysis. On the other hand, the use of PLA to perform PLA-*b*-P(Cl-CL) diblocks has provided a crystallinity degree to the completely amorphous P(Cl-CL) and a new PLA-*b*-P(Cl-CL) stereocomplex was successfully produced. Various physicochemical measurements (IFT, TGA, DSC) of these different diblocks and stereocomplex confirmed the enhanced hydrophilicity of PEG-*b*-P(Cl-CL) and the crystallinity of PLA-*b*-P(Cl-CL) materials.

VIII. References

- [1]. S. Magazu, *Physica B Condens Matter*. **1996**, 226, 92-106.
- [2]. J. Drelich, C. Fang, C. L. White, Measurement of interfacial tension in fluid–fluid systems, *Encyclopedia of Surface and Colloid Science*, second ed., vol. 4, CRC Press, Boca Raton, **2006**.
- [3]. D. D. Joseph, M. S. Arney, G. Gillberg, H. Hu, D. Hultman, C. Verdier, T. M. Vinagre, *J. Rheol* **1992**, 36, 621-662.
- [4]. J. J. Elmendorp, G. De Vos, *Polym Eng Sci* **1986**, 26, 415-417.
- [5]. H. H. Hu, D. D. Joseph, *J. Colloid Interface Sci.* **1994**, 162, 331-339.
- [6]. B. Vonnegut, *Rev. Sci. Instr.* **1942**, 13, 6-9.
- [7]. J. D. Berry, M. J. Neeson, R. R. Dagastine, D. Y. C. Chan, R. F. Tabor, *J. Colloid Interface Sci.* **2015**, 454, 226-237.
- [8]. S. Kobayashi, H. Uyama, *J. Polym. Sci. A* **2001**, 40, 192-209.
- [9]. Y. Ikada, K. Jamshidi, H. Tsuji, S. H. Hyon, *Macromolecules* **1987**, 20, 904-906.
- [10]. X. Hu, J. Shao, D. Zhou, G. Li, J. Ding, X. Chen, *J. Appl. Polym. Sci.* **2017**, 134, 44626/1-44626/8.
- [11]. H. Tsuji, *Macromol. Biosci.* **2005**, 5, 569–597.
- [12]. K. Fukushima, Y. Kimura, *Polym. Int.* **2006**, 55, 626–642.
- [13]. J. Zhang, H. Sato, H. Tsuji, I. Noda, Y. Ozaki, *Macromolecules* **2005**, 38, 1822-1828.
- [14]. Y. Ikada, K. Jamshidi, H. Tsuji, S. H. Hyon, *Macromolecules* **1987**, 20, 904-906.
- [15]. E. Ihms, D. Brinkman, *J. Forensic Sci.* **2004**, 49, 505-510.
- [16]. S. Gordon, “Encyclopedia of Science and Technology », McGraw-Hill Co. Inc., New York, Toronto and London, **1960**, p. 556.
- [17]. A. Coats, J. P. Redfern *Analyst* **1963**, 88, 906-924.
- [18]. S. Lenoir, R. Riva, X. Lou, C. Detrembleur, R. Jérôme, P. Lecomte, *Macromolecules* **2004**, 37, 4055-4061.
- [19]. E. M. Abdelrazek, A. M. Hezma, A. El-khodary, A. M. Elzayat, *Egypt. j. basic appl. sci.* **2016**, 3, 10-15.
- [20]. M. H Yang, Y. -H. Lin, *J Test Eval* **2009**, 37, 364-370.
- [21]. W. M. Groenewoud, in *Characterisation of Polymers by Thermal Analysis* (Ed.: W. M. Groenewoud), Elsevier Science B.V., Amsterdam, **2001**, pp. 10-60.
- [22]. C. T. Moynihan, A. J. Easteal, J. Wilder, J. Tucker, *J. Phys. Chem.* **1974**, 78, 2673-2677.

[23]. K. R. Beck, R. Korsmeyer, R. J. Kunz, *J. Chem. Educ.* **1984**, *61*, 668-670.

[24]. Polymerscience.physik.hu-berlin.de/docs/manuals/DSC.pdf

[25]. Y. Kong, J. N. Hay, *Polymer* **2002**, *43*, 3873-3878.

[26]. R. Pantani, A. Sorrentino, *Polym. Degrad. Stab.* **2013**, *98*, 1089-1096.

[27]. A. S. Hadj-Hamou, F. Metref, F. Yahiaoui, *Polym. Bull.* **2017**, *74*, 3833-3853.

[28]. D. Garlotta, *J. Polym. Environ.* **2002**, *9*, 63-84.

Conclusion and Perspectives

The first section of my Ph.D. studies consisted of the synthesis of carbene coordination compounds of the type NHC-MMe₃ acting as efficient ring-opening polymerization initiators of *rac*-lactide, which allowed access to either linear or cyclic PLA depending on the nature of the initiator and the reaction conditions (**Figure 1**). It was shown that for these NHC-MMe₃ systems, the addition of benzyl alcohol acting as a chain transfer agent was beneficial both to ROP activity and control of the polymerization.

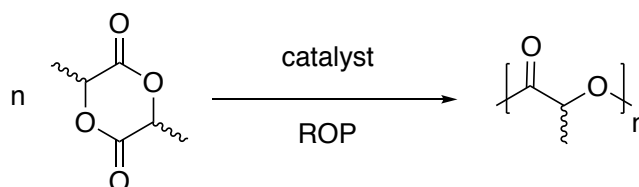


Figure 1: ROP of *rac*-lactide

An (NHC)MMe₃ compound was then ionized via a methide abstraction route with B(C₆F₅)₃ in the presence of diethyl ether as an external Lewis base to afford the corresponding cation of the type [(NHC)MMe₂(L)]⁺ (L labile) as [CH₃B(C₆F₅)₃]⁻ salt. Such cation, which is the first example of a cationic NHC-stabilized alkyl aluminium compound, is stable in solution (CH₂Cl₂) and [(IMes)AlMe₂(Et₂O)]⁺ cationic compound, polymerizes *rac*-lactide at room temperature in the presence of BnOH to produce chain-length controlled with narrow polydispersity indice, constituting a rare case of an Al-based catalyst active at RT in the ROP of lactide.

The second section of this thesis involved the synthesis of PEG-*co*-PLLA amphiphilic copolymers under various conditions using the metal-amido species (*N,O,N*)M-NMe₂ (M= Al, Ga) as ROP catalysts in the presence of MeO-PEG acting as a macroinitiator. Two catalysts incorporating earth-abundant and environmentally friendly metal centers, one with zinc and the other with magnesium, were also used for this copolymerization. The zinc catalyst was shown to be active at 70 °C to produce well-defined copolymer. The best ROP activity was achieved with the Mg(II) catalyst Mg(C₆F₅)₂(THF)₂. The latter is active at low temperature to yield within minutes a chain-length-controlled and monodisperse PEG-*co*-PLLA.

The core chapter of this thesis is the synthesis of the α -chloro- ϵ -caprolactone monomer (Cl-CL). Its ROP was then successfully realized under mild conditions to afford linear poly(Cl-CL) homopolymer using an aluminium salen catalyst (**Figure 2**). Chlorine's presence opens the way on polymer functionalization through nucleophilic substitution to access hydrophilic and biodegradable polymers.

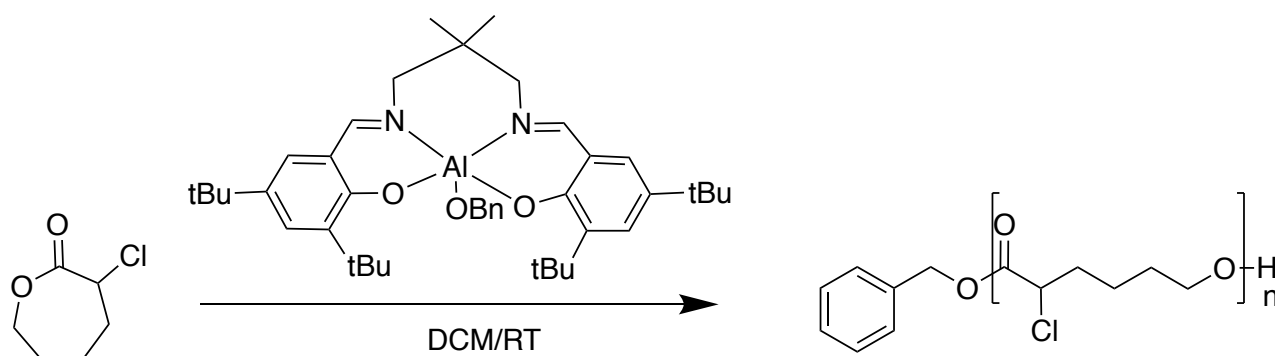


Figure 2: ROP of chloro-caprolactone by a salen catalyst under mild conditions

In order to modify the properties of this homopolymer, on the one hand, a two steps synthesis of PEG-*co*-P(Cl-CL) was performed and three copolymers were obtained in the fourth section. IFT measurements on PEG-*co*-P(Cl-CL) materials have shown that the PEG hydrophilic part provides an amphiphilic nature to the resulting copolymers. On the other hand, a crystalline character has been introduced thanks to the formation of PLA-*b*-P(Cl-CL) diblocks including a new stereocomplex material. Various physicochemical measurements (such as TGA or DSC) were performed on these diblocks and stereocomplex to evaluate the impact of the PLA segment on P(Cl-CL). An important part of the study dealt with the substitution of the chlorine groups in P(Cl-CL) by a hydrophilic group. For that, a two steps synthesis was performed. The introduction of BnO functions to afford P(OBn-CL) material, though subsequent deprotection (to produce P(OH-CL)) led to a mixture of polymers. However, the hydrophilic nature of the final polymers has been validated by their solubility in water, confirming the proposed approach.

As a perspective, it could be interesting to start from a caprolactone with a benzyloxy pendant group. The ROP of this monomer with a salen catalyst could allow direct access to well-defined poly(benzyloxycaprolactone). A subsequent hydrogenation would afford the final hydrophilic P(OH-CL) material (**Figure 3**).

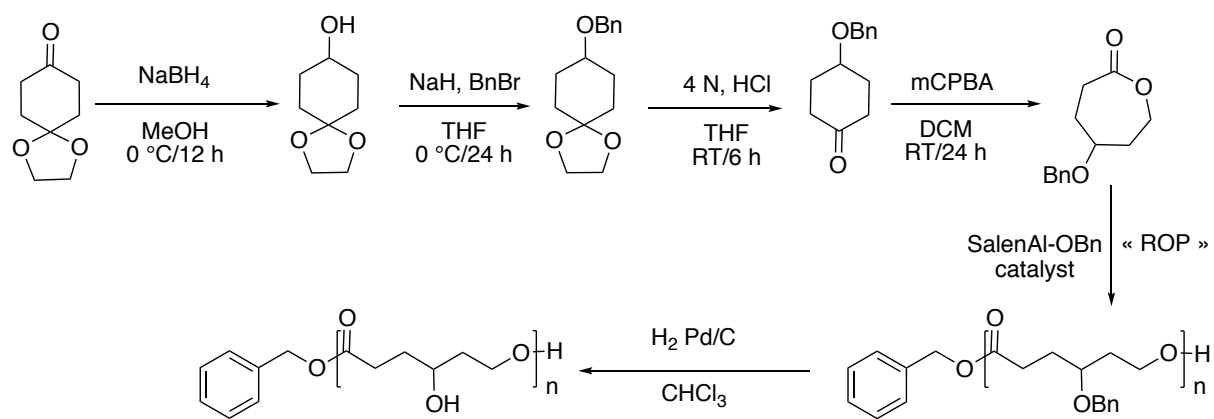


Figure 3: General synthesis for P(OH-CL)

Experimental section

General procedure

Materials

Air sensitive experiments were carried out under N₂ using standard Schlenk techniques or in a nitrogen-filled MBraun Unilab glovebox. Dichloromethane, pentane, toluene and diethylether were first dried through a solvent purification system (MBraun SPS) and stored for at least a couple of days over activated molecular sieves (4 Å) in a glovebox prior to use. Tetrahydrofuran was distilled over Na/benzophenone, methanol, ethanol and DMF were distilled over KOH and stored over activated molecular sieves (4 Å) for a couple of days in a glovebox prior to use. *Rac*, *L* and *D*-lactide were purchased from Aldrich: they were sublimed prior to use. PEG(1900) was purchased from Aldrich too and prior to use was analyzed by GPC and ¹H NMR in order to confirm the M_w. All other chemicals were purchased from Aldrich, T.C.I Europe Corporation and Strem Chemicals and were used as received unless otherwise indicated.

Nuclear Magnetic Resonance

Deuterated solvents were purchased from Eurisotope (CEA, Saclay, France), degassed under a N₂ flow and stored over activated molecular sieves (4 Å) in a glovebox prior to use. NMR spectra were recorded on BrukerAC 300 MHz, 400 MHz, 500 MHz or 600 MHz NMR spectrometers, in Teflon-valved J-Young NMR tubes at ambient temperature unless otherwise indicated. H, F and C chemical shifts are reported vs. SiMe₄ and were determined by reference to the residual H, F and C solvent peaks.¹ Chemical shifts (δ) are given in ppm.

Size-exclusion chromatography (SEC) analysis

The number-average, weight-average molar masses (M_n and M_w, respectively) and molar mass distribution (M_w/M_n) of the polyesters (PLA, P(Cl-CL)) samples were determined by size exclusion chromatography (SEC) at 30 °C with Shimadzu LC20AD ultra-fast liquid chromatography equipped with a Shimadzu RID10A refractometer detector. Tetrahydrofuran (THF) was used as the eluent and the flow rate was set up at 1.0 mL/min. A

Varian PLGel pre-column and a Varian PLGel 5 μm were used. Calibrations were performed using polystyrene standards (400-100000 g/mol) and raw values of M_n (*sec*) were thus obtained.

MALDI-TOF analysis

Mass spectra were acquired on a time-of-flight mass spectrometer (MALDI-TOF-TOF-Autoflex II TOF-TOF, Bruker Daltonics, Bremen, Germany) equipped with a nitrogen laser ($\lambda = 337 \text{ nm}$) at the «Service de Spectrométrie de Masse de l'Institut de Chimie de Strasbourg» (Strasbourg, France) and run in a positive mode. An external multi-point calibration was carried out before each measurement using the singly charged peaks of a standard peptide mixture (0.4 μm in water acidified with FlewAnalysis 3.0 software). α -cyano-4-hydroxy-cinnamic acid (CHCA) was obtained from Sigma (St Louis, MO, USA) and 1,8,9-anthracenetriol (dithranol) from Alfa Aesar (Karlsruhe, Germany). Matrix solutions were freshly prepared: CHCA was dissolved to saturation in H_2O , CH_3CN , HCOOH (50/50.1%) solution and dithranol to saturation in THF. Typically; a 1/1 mixture of the sample solution in CH_2Cl_2 was mixed with the matrix solution and 0.5 μL of the resulting mixture was deposited on the stainless plate.

Elemental analysis

Elemental analysis for all compounds were performed at the “Service de Microanalyse” of the Université de Strasbourg (Strasbourg, France).

X-ray crystallography

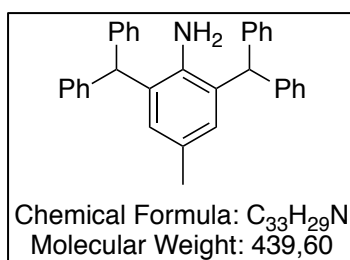
Single crystals of complexes were mounted on glass fibers and data collected on a Nonius Kappa-CCD or Bruker Apex II DUO Kappa-CCD area detector diffractometer (MoK_α $\lambda = 0.71073 \text{ \AA}$). The complete conditions of data collection (Denzo software)² and structure refinements are provided in the different chapter's experimental sections.

All structures were solved using direct methods (SHELXS97) and refined against F^2 and using the SHELXL97 software.³ All non-hydrogen atoms were refined anisotropically.

Chapter I

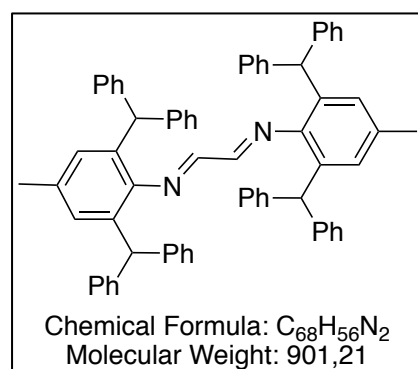
Syntheses

2,6-bis(diphenylmethyl)-4-methylaniline



Diphenylmethanol (10 g, 54.20 mmol) and *p*-toluidine (2.9 g, 27.12 mmol) were heated at 60 °C until the two compounds were liquid, then were refluxed at 160 °C. A solution of $ZnCl_2$ (1.80 g, 13.12 mmol) in aqueous HCl solution 37% (2.27 mL, 27.12 mmol) was added dropwise in the mixture). Then the reaction mixture was heated at 160 °C for one hour. The mixture was then dried under vacuum until the formation of a solid was observed, which was then dissolved in DCM (50 mL). The solution was washed with water (3 times) then brine (3 times). DCM was evaporated by rotatory evaporator affording a brownish solid. The solid was recrystallized in toluene to give after drying a white solid (7.96 g, 67%). 1H NMR (CDCl₃, 400 MHz): δ 2.06 (s, 3H, CH₃), 3.33 (br, 2H, NH₂), 5.49 (s, 2H, CH(Ph)₂), 6.42 (s, 2H, CH_{Ar}), 7.12-7.36 (m, 20H, CH_{Ph}) ppm.

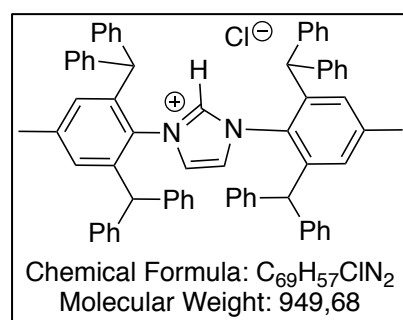
N,N'-bis(2,6-bis(diphenylmethyl)-4-methylphenyl)diazabutadiene



2,6-bis(diphenylmethyl)-4-methylaniline (6 g, 12.20 mmol) was dissolved in 122 mL of DCM (0.10 M) and glyoxal 40% (0.755 mL, 6.10 mmol), 3 g of anhydrous $MgSO_4$ and some drops

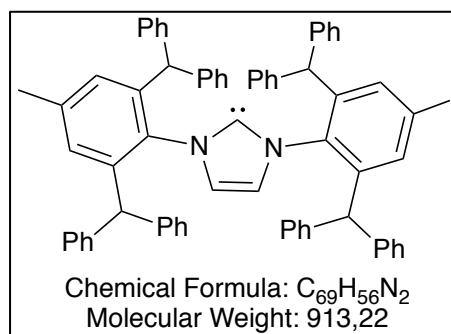
of formic acid were added in the mixture. The mixture was stirred at RT for six days. NMR permits to follow the progress of the reaction. The solution was filtered, dried on MgSO_4 then washed with DCM. A recrystallization in toluene was performed to give after drying a yellow powder (4 g, 52%). **NMR ^1H (CDCl_3 , 400 MHz):** δ 2.04 (s, 6H, CH_3), 5.15 (s, 4H, $\text{CH}(\text{Ph})_2$), 6.58 (s, 4H, CH_{Ar}), 6.88-7.18 (m, 42H, $\text{CH}_{\text{Ph} + \text{HC}=\text{N}}$) ppm.

IPr*. HCl imidazolium salt



N,N'-bis(2,6-bis(diphenylmethyl)-4-methylphenyl)diazabutadiene (4 g, 4.30 mmol) was dissolved in THF (185 mL) then the solution was refluxed at 70 °C. ZnCl_2 (0.71 g, 5.12 mmol) was added in the solution and after ten minutes, paraformaldehyde (0.15 g, 5.12 mmol) then hydrochloride acid in glyoxal 4 M (2.16 mL) were introduced as well. The solution was stirred for two hours at RT, and then THF was evaporated by rotatory evaporator affording a brown solid. The solid was dissolved in ethyl acetate then was filtered and dried under vacuum. Pentane was then added and the solid was filtered to give, once dry, a white powder (1.30 g, 41%). **NMR ^1H (CDCl_3 , 400 MHz):** δ 2.18 (s, 6H, CH_3), 5.28 (s, 4H, $\text{CH}(\text{Ph})_2$), 5.47 (s, 2H, $\text{CH}^{4,5}_{\text{Im}}$), 6.80-7.24 (m, 44H, $\text{CH}_{\text{Ph} + \text{Ar}}$), 13.04 (s, 1H, CH^2_{Im}) ppm.

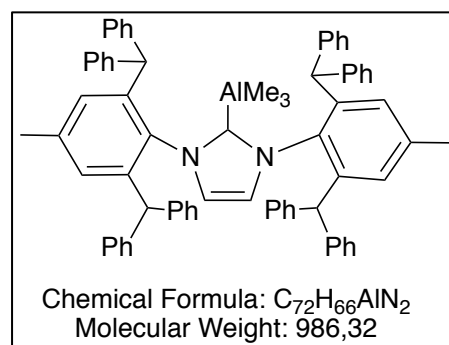
IPr* carbene



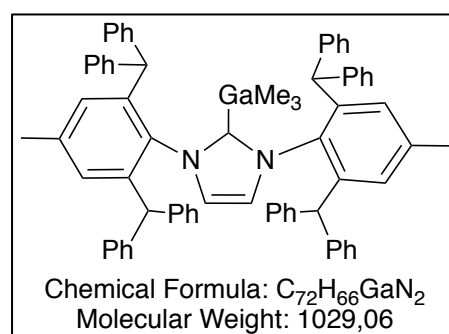
In a glovebox, IPr*.HCl (1.30 g, 1.40 mmol) and KH (0.085 g, 2.01 mmol) were dissolved in THF and the mixture was stirred during one day at RT. Then the mixture was filtered and the solid was dried under vacuum (1 g, 83%). **NMR ^1H (C_6D_6 , 400 MHz):** δ 1.86 (s, 6H, CH_3), 5.78 (s, 2H, $\text{CH}^{4,5}_{\text{Im}}$), 6.03 (s, 4H, $\text{CH}(\text{Ph})_2$), 6.90-7.38 (m, 44H, $\text{CH}_{\text{Ph} + \text{Ar}}$) ppm.

(IPr*)MMe₃ adduct formation

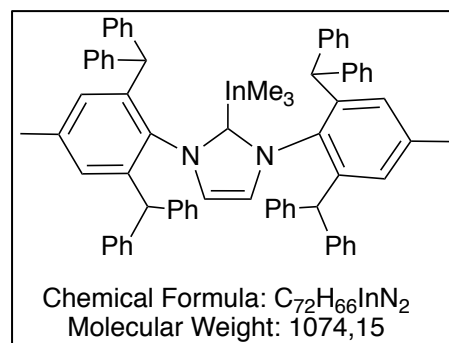
In a glovebox, a toluene solution of free carbene IPr* (400 mg, 0.438 mmol) was added dropwise via a pipette to a toluene solution (10 mL) of MMe₃ (M= Al, Ga or In, 0.438 mmol) under vigorous stirring. The latter mixture was stirred for 1 hour at room temperature then dried *in vacuo* to afford a colourless solid residue that was washed twice with pentane. It was further dried under vacuum to quantitatively afford the corresponding (IPr*)AlMe₃ (**1**), (IPr*)GaMe₃ (**2**) and (IPr*)InMe₃ (**3**) adducts as NMR-pure colourless solids.



(1). 98% yield. X-ray quality crystals were grown from a pentane/toluene solution cooled at -35 °C. **^1H NMR (300 MHz, C_6D_6):** δ -0.34 (s, 9H, $\text{Al}(\text{CH}_3)_3$), 1.76 (s, 6H, *p*- CH_3), 4.99 (s, 2H, $\text{CH}^{4,5}_{\text{Im}}$), 5.69 (s, 4H, $\text{CH}(\text{Ph})_2$), 6.71-6.89 (m, 20H, CH_{Ph}), 6.99 (t, 3H, $^3J=7.5$ Hz, 4H, CH_{Ph}), 7.13 (s, $^3J=7.5$ Hz, 4H, CH_{Ar}), 7.24 (t, $^3J=7.5$ Hz, 8H, CH_{Ph}), 7.58 (d, $^3J=7.5$ Hz, 8H, CH_{Ph}); **$^{13}\text{C}\{^1\text{H}\}$ (500 MHz, C_6D_6):** δ -5.8 ($\text{Al}(\text{CH}_3)_3$), 20.3 (*p*- CH_3), 51.2 ($\text{CH}(\text{Ph})_2$), 122.7 (CH_{Im}), 126.3, 126.9, 128.9, 129.3, 130.1, 133.9, 139.2, 141.5, 142.0, 143.8, 179.0 (C *carbene*) ppm.



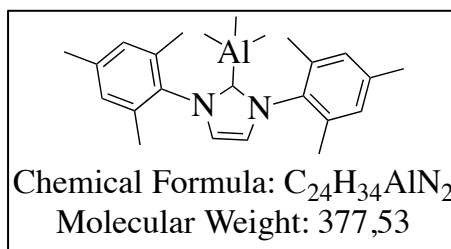
(2). 92% yield. $^1\text{H NMR}$ (300 MHz, C_6D_6): δ -0.08 (s, 9H, $\text{Ga}(\text{CH}_3)_3$), 1.78 (s, 6H, $p\text{-CH}_3$), 5.02 (s, 2H, $\text{CH}^{4,5}_{\text{Im}}$), 5.69 (s, 4H, $\text{CH}(\text{Ph})_2$), 6.74-6.86 (m, 20H, CH_{Ph}), 7.04 (t, $^3J=7.5$ Hz, 4H, CH_{Ph}), 7.14 (s, 4H, CH_{Ar}), 7.20 (t, $^3J=7.5$ Hz, 8H, CH_{Ph}), 7.59 (d, $^3J=7.5$ Hz, 8H, CH_{Ph}); $^{13}\text{C}\{^1\text{H}\}$ (500 MHz, C_6D_6): δ 3.2 ($\text{Ga}(\text{CH}_3)_3$), 21.3 ($p\text{-CH}_3$), 52.2 ($\text{CH}(\text{Ph})_2$), 123.6 (CH_{Im}), 126.6, 127.2, 128.8, 129.8, 130.3, 131.1, 135.1, 140.0, 142.5, 143.2, 144.8, 183.4 (C carbene) ppm.



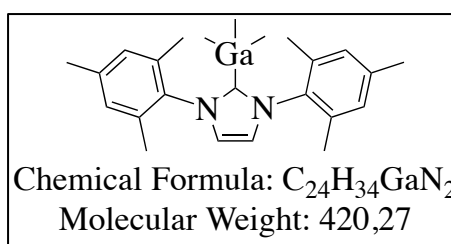
(3). 90% yield. X-ray quality crystals were grown from a pentane/toluene solution cooled at -35 °C. $^1\text{H NMR}$ (300 MHz, C_6D_6): δ -0.11 (s, 9H, $\text{In}(\text{CH}_3)_3$), 1.77 (s, 6H, $p\text{-CH}_3$), 5.11 (s, 2H, $\text{CH}^{4,5}_{\text{Im}}$), 5.66 (s, 4H, $\text{CH}(\text{Ph})_2$), 6.75-6.88 (m, 20H, CH_{Ph}), 7.04 (t, $^3J = 7.5$ Hz, 4H, CH_{Ph}), 7.13 (s, 4H, CH_{Ar}), 7.19 (t, $^3J = 7.5$ Hz, 8H, CH_{Ph}), 7.52 (d, $^3J = 7.5$ Hz, 8H, CH_{Ph}); $^{13}\text{C}\{^1\text{H}\}$ (500 MHz, C_6D_6): δ -7.7 ($\text{In}(\text{CH}_3)_3$), 21.3 ($p\text{-CH}_3$), 52.1 (CH_{Im}), 124.1 ($\text{CH}(\text{Ph})_2$), 126.7, 127.2, 128.4, 128.7, 129.8, 130.5, 131.0, 135.4, 140.1, 142.5, 143.2, 144.5, 185.8 (C carbene) ppm.

IMesMMe₃ adducts formation

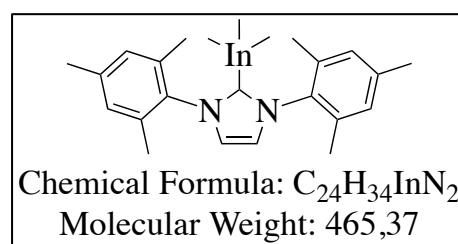
In a glovebox, a toluene solution of free carbene IMes (500 mg, 1.63 mmol) was added dropwise via a pipette to a toluene solution (-35 °C, 10 mL) of MMe₃ (M= Al, Ga or In, 1.63 mmol) under vigorous stirring. The latter mixture was stirred for 1 hour at room temperature then dried *in vacuo* to afford a colourless solid residue that was washed twice with pentane. It was further dried *in vacuo* to quantitatively afford the corresponding IMesAlMe₃ (1), IMesGaMe₃ (2) and IMesInMe₃ (3) adducts as NMR-pure colourless solids.



(1). 95% yield. 1H NMR (CD_2Cl_2 , 400 MHz): δ -1.59 (s, 9H, $AlMe_3$), 2.07 (s, 12H, $o-CH_3$), 2.36 (s, 6H, $p-CH_3$), 7.02 (s, 4H, $m-CH$), 7.07 (s, 2H, CH_{im}) ppm.

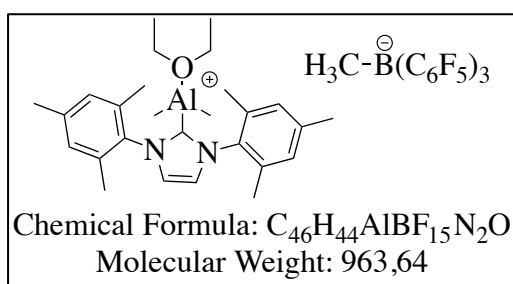


(2). 97% yield. 1H NMR (CD_2Cl_2 , 400 MHz): δ -1.31 (s, 9H, $GaMe_3$), 2.07 (s, 12H, $o-CH_3$), 2.36 (s, 6H, $p-CH_3$), 7.01 (s, 4H, $m-CH$), 7.05 (s, 2H, CH_{im}) ppm.



(3). 98% yield. 1H NMR (CD_2Cl_2 , 400 MHz): δ -1.29 (s, 9H, $InMe_3$), 2.06 (s, 12H, $o-CH_3$), 2.36 (s, 6H, $p-CH_3$), 7.02 (s, 4H, $m-CH$), 7.1 (s, 2H, CH_{im}) ppm.

$[IMesAl(Me)_2OEt_2]^+[MeB(C_6F_5)_3]^-$

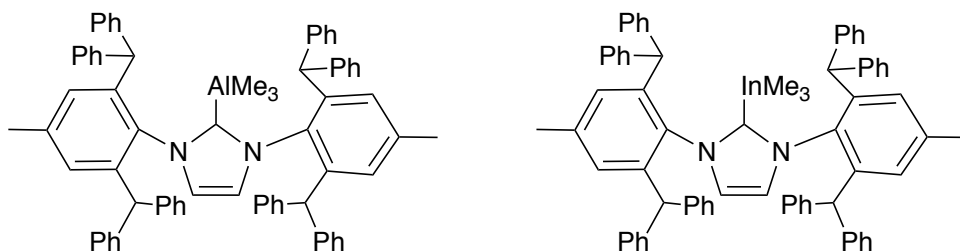


In a glovebox, a precooled ether solution (-35 °C, 5 mL) of free carbene (**1**) (100 mg, 0.27 mmol, 1 equiv.) was added dropwise via a pipette to a precooled ether solution (-35 °C, 10 mL) of tris(pentafluorophenyl)borane (136.4 mg, 0.27 mmol, 1 equiv.) under stirring. The solution was stirred to room temperature overnight and the solvent was removed under vacuum to give a yellowish residue. The latter was washed with pentane then was dried to yield the pure complex as a white powder (231.27 mg, 88%). **¹H NMR (CD₂Cl₂, 400 MHz):** δ -1.13 (s, 6H, AlMe₂), 0.46 (br, 3H, CH₃⁻B(C₆F₅)₃), 1.15 (t, 6H, CH₂ Et₂O), 2.08 (s, 12H, *o*-CH₃), 2.40 (s, 6H, *p*-CH₃), 3.59 (q, 4H, CH₂ Et₂O), 7.11 (s, 4H, *m*-CH), 7.31 (s, 2H, CH_{im}) ppm.

Crystal data

Compound reference:	(IPr*)AlMe ₃	(IPr*)InMe ₃
<i>Chemical formula</i>	C ₇₂ H ₆₆ AlN ₂	C ₇₂ H ₆₅ InN ₂
<i>Formula mass</i>	985.24	1073.08
<i>Crystal system</i>	Monoclinic	Triclinic
<i>a/Å</i>	11.8502(3)	11.7755(10)
<i>b/Å</i>	19.8774(6)	19.8637(17)
<i>c/Å</i>	25.6054(8)	24.519(2)
<i>α/°</i>	90	96.283(2)
<i>β/°</i>	111.240(2)	93.717(2)
<i>γ/°</i>	90	90.052(2)
<i>Unit cell volume/Å³</i>	5621.7(3)	5688.5(9)
<i>Temperature/K</i>	173(2)	173(2)
<i>Space group</i>	P2 1/C	P -1
<i>No. of formula units per cell, Z</i>	4	2
<i>Radiation type</i>	MoK _a	MoK _a
<i>Absorption coefficient, μ/mm⁻¹</i>	0.646	0.460
<i>No. of reflections measured</i>	45922	77431
<i>No. of independent reflections</i>	9881	27504
<i>R_{int}</i>	0.0636	0.1545
<i>Final R₁ values (I > 2σ(I))</i>	0.0489	0.0886
<i>Final wR (F²) values (I > 2σ(I))</i>	0.1191	0.1187
<i>Final R₁ values (all data)</i>	0.0753	0.2006
<i>Final wR (F²) (all data)</i>	0.1330	0.1438
<i>Goodness of fit on F²</i>	1.024	0.987

Table 1: Crystal data and structural refinement for the Al and In, IPr* adducts



Polymer Synthesis

Typical procedure for lactide polymerization

In a glovebox, catalyst (1 equiv.) was charged in a vial equipped with a Teflon™-tight screw cap and a dichloromethane or toluene solution (1 M) of the appropriate amount of monomer was added via a syringe all at once. The resulting solution was vigorously stirred (at room temperature or heated) for the appropriate time. The vial was then removed from the glovebox and the reaction mixture was quenched with MeOH provoking the precipitation of the polymer which was washed several times with MeOH or pentane, dried *in vacuo* until constant weight and subsequently analyzed by ^1H NMR, SEC and by MALDI-TOF spectrometry.

Typical procedure for immortal lactide polymerization

The same procedure as previously described was used for polymerization with the addition of a monomer solution (1 M) containing some known amount of the desired alcohol (BnOH) onto the corresponding initiator.

Polymer characterization

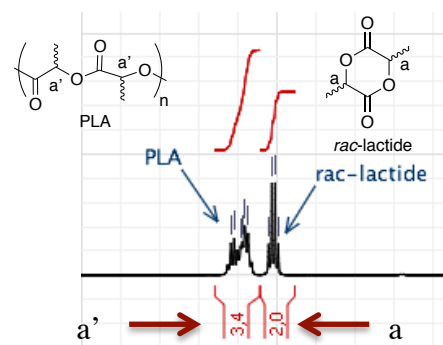
NMR spectroscopy

The monomer to polymer conversion is calculated by ^1H NMR spectroscopy based on the relative integration of the corresponding signals:

Polymer δ^4 (ppm) Monomer δ (ppm)

PLA: 5.20-5.30 *Rac*-lactide: 5.02

^1H NMR spectrum



Size-exclusion chromatography (SEC) analysis

The number-average, weight-average molar masses (M_n and M_w , respectively), and molar mass distribution ($PDI = M_w/M_n$) of PLA samples were determined by size exclusion chromatography (SEC) at 30 °C with Shimadzu LC20AD ultra-fast liquid chromatography equipped with a Shimadzu RID10A refractometer detector. Tetrahydrofuran (THF) was used as the eluent and the flow rate was set up at 1.0 mL/min. A Varian PLGel pre-column 5 μm were used. Calibrations were performed using polystyrene standards (400-100000 g/mol) and the raw values of $M_{n(sec)}$ were thus obtained.

The obtained $M_{n(sec)}$ values were corrected using the correction factor $X = 0.58$ for PLA polymer via the formula: $M_{n(corrected)} = X \cdot M_{n(sec)}^{5.6}$

Supporting data

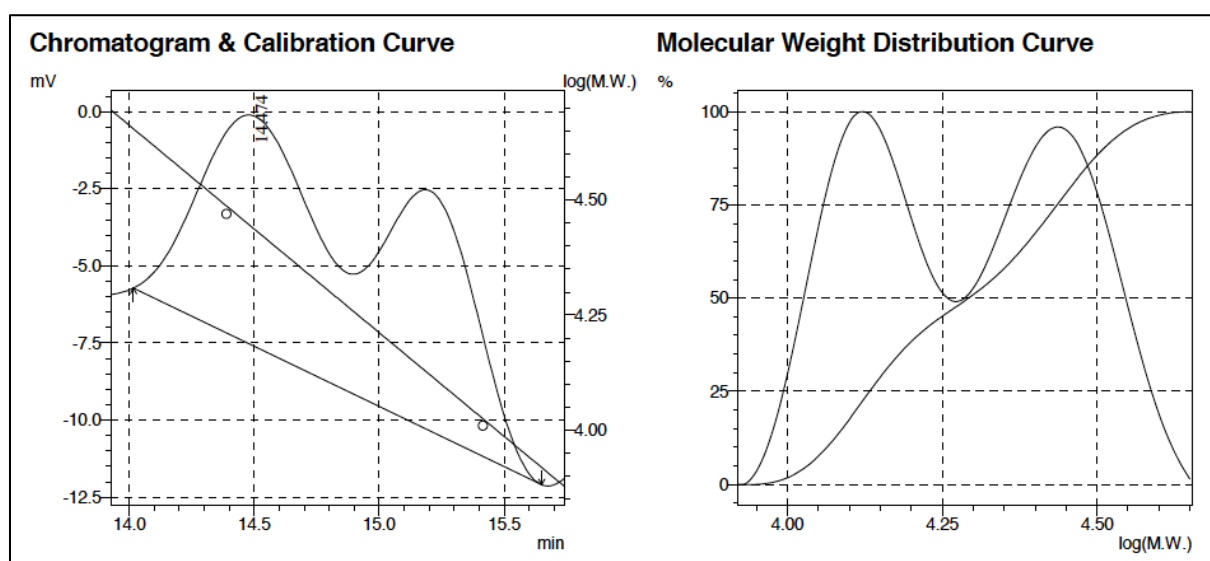
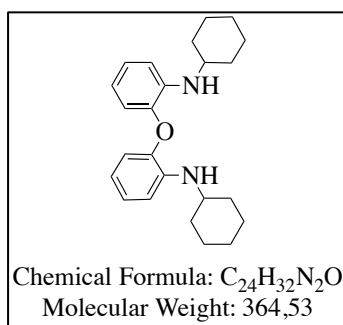


Figure 1: SEC traces of isolated PLA prepared via ROP of *rac*-lactide initiated by the *catalyst 2* system. (Conditions: $[rac\text{-lactide}]_0 = 1 \text{ M}$, 300 equiv. *rac*-lactide, DCM, RT, 12 h, 100% conv.).

Chapter II

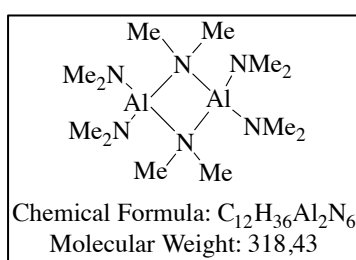
Syntheses

$[(C_6H_{11})NH-C_6H_4]_2O$ (1)



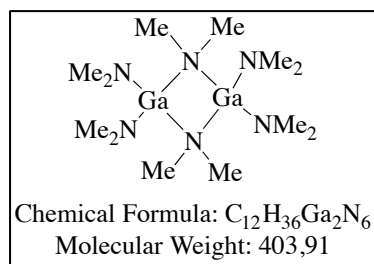
In a 100 mL round-bottom flask, 2,2'-oxydianiline (1.00 g, 5.00 mmol), cyclohexanone (0.95 mL, 10 mmol, 2 equiv.), zinc (3.30 g, 50 mmol, 10 equiv.) and acetic acid (20 mL) were introduced. The mixture was heated at 70 °C under nitrogen for 40 hours. The grey-white suspension containing residual zinc was then cooled to room temperature, and methanol (30 mL) was added. The white precipitate was filtered off and washed with methanol (2 X 30 mL) then the filtrate was concentrated to about 10 mL. Crushed ice (30 g) and dichloromethane (72 mL) were subsequently added, followed by the addition of ammonium hydroxide until pH > 10. The mixture was extracted with dichloromethane (30 mL) and the aqueous layer was further extracted with dichloromethane too (2 X 30 mL), followed by the subsequent drying of the combined organic layers over $MgSO_4$ and evaporating to dryness. A brown oil was obtained, which was purified by column chromatography (SiO_2 , pentane/ethyl acetate (99/1)) to yield compound as a colourless solid (1.30 g, 73% yield), $R_f = 0.64$, UV-revelation. 1H NMR (C_6D_6 , 400 MHz): δ 0.86-1.89 (m, 20H, C_6H_{11}), 3.15 (septet, $^3J=6.5$ Hz, 2H, CH), 4.29 (s, 2H, NH), 6.59 (dt, $^3J=7.8$ Hz, $^4J=1.3$ Hz, 2H, CH_{Ar}), 6.71 (dd, $^3J=7.8$ Hz, $^4J=1.3$ Hz, 2H, CH_{Ar}), 6.92 (dd, $^3J=7.5$ Hz, $^4J=1.5$ Hz, 2H, CH_{Ar}), 7.00 (dd, $^3J=7.5$ Hz, $^4J=1.5$ Hz, 2H, CH_{Ar}) ppm.

$Al_2(NMe_2)_6$ (2a)



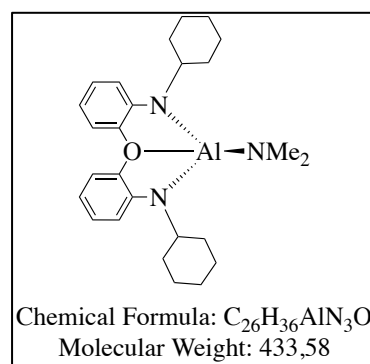
In a glovebox, AlCl_3 (2.00 g, 14.98 mmol, 1 equiv.) and LiNMe_2 (2.50 g, 49.00 mmol, 3.3 equiv.) were introduced in a flask and pentane (250 mL) was added. The mixture was allowed to stir to room temperature for three days. The precipitate was subsequently filtered over celite and the filtrate was evaporated to yield a white powder (2.12 g, 89%). $^1\text{H NMR}$ (C_6D_6 , 300 MHz): δ 2.33 (s, 12H, CH_3), 2.73 (s, 24H, CH_3) ppm.

$\text{Ga}_2(\text{NMe}_2)_6$ (**2b**)



In a glovebox, GaCl_3 (2.00 g, 11.40 mmol, 1 equiv.) and LiNMe_2 (1.91 g, 37.00 mmol, 3.3 equiv.) were introduced in a flask and pentane (250 mL) was added. The mixture was allowed to stir to room temperature for three days. The precipitate was subsequently filtered over celite and the filtrate was evaporated by rotatory evaporator to yield a white powder (1.80 g, 79%). $^1\text{H NMR}$ (C_6D_6 , 300 MHz): δ 2.47 (s, 12H, CH_3), 2.86 (s, 24H, CH_3) ppm.

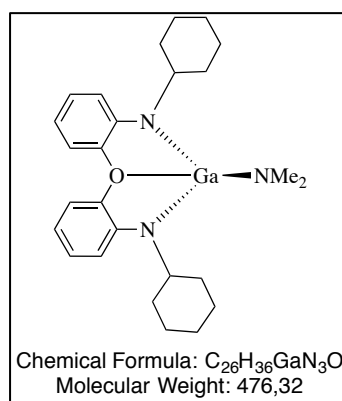
$\kappa^3\text{-N,O,N-}[(\text{C}_6\text{H}_{11})\text{N-C}_6\text{H}_4]_2\text{OAlNMe}_2$ ⁷



In a nitrogen-filled glovebox, the diamino-ether ligand **1** (0.550 g, 1.51 mmol, 1 equiv.), was charged in a vial Schlenk flask and a toluene solution (3 mL) of $\text{Al}_2(\text{NMe}_2)_6$ **2a** (240 mg, 0.75 mmol, 1 equiv.) was added to afford a colourless solution. The reaction mixture was then heated for 72 hours at 110 °C in an oil bath to yield a yellowish solution that was subsequently cooled to room temperature and evaporated to dryness *in vacuo*, affording an

off-white residue. The latter was dissolved in pentane and cooled to $-35\text{ }^{\circ}\text{C}$ over 5 days. The complex precipitated as a white solid that was further dried under vacuum (400 mg, 60%). $^1\text{H NMR}$ (C_6D_6 , 400 MHz): δ 1.12-2.29 (m, 20H, C_6H_{11}), 2.56 (s, 6H, NMe_2), 3.26 (q, $^3J=7.5\text{ Hz}$, 2H, CH), 6.49 (dt, $^3J=7.6\text{ Hz}$, $^4J=1.5\text{ Hz}$, 2H, CH_{Ar}), 6.70 (dd, $^3J=8.5\text{ Hz}$, $^4J=1.3\text{ Hz}$, 2H, CH_{Ar}), 7.03 (dt, $^3J=7.7\text{ Hz}$, $^4J=1.4\text{ Hz}$, 2H, CH_{Ar}), 7.40 (dd, $^3J=8.4\text{ Hz}$, $^4J=1.7\text{ Hz}$, 2H, CH_{Ar}) ppm.

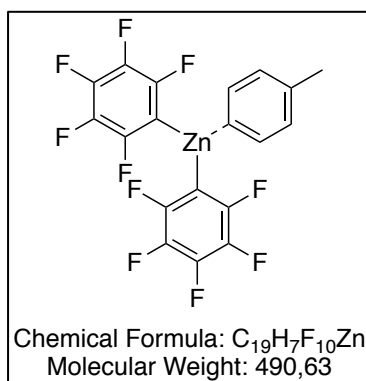
$\kappa^3\text{-}N,O,N\text{-}[(\text{C}_6\text{H}_{11})\text{N-C}_6\text{H}_4]_2\text{OGaNMe}_2$



The Ga amido complex was synthesized by following a procedure identical with that used for $\kappa^3\text{-}N,O,N\text{-}[(\text{C}_6\text{H}_{11})\text{N-C}_6\text{H}_4]_2\text{OAlNMe}_2$. In a nitrogen-filled glovebox, the diamino-ether ligand **1** (0.5 g, 1.37 mmol, 1 equiv.) was charged in a Schlenk flask and a toluene solution (3 mL) of $\text{Ga}_2(\text{NMe}_2)_6$ **2b** (0.275 g, 0.685 mmol, 0.5 equiv.) was added to yield a colourless solution. The reaction mixture was then heated during three days at $130\text{ }^{\circ}\text{C}$ in an oil bath to yield a yellowish solution that was subsequently cooled to room temperature and evaporated to dryness in vacuum, affording a yellowish oil residue. The latter was dissolved in pentane and cooled to $-35\text{ }^{\circ}\text{C}$ over five days. The Ga complex precipitated as a white solid that was further dried under vacuum (0.34 g, 50% yield). X-ray quality crystals were grown from a pentane/toluene solution cooled at $-35\text{ }^{\circ}\text{C}$. $\text{C}_{26}\text{H}_{36}\text{GaN}_3\text{O}$ (476.32): Anal. Calcd. C, 65.56; H, 7.62. Found. C, 65.60; H, 8.36. $^1\text{H NMR}$ (C_6D_6 , 400 MHz): δ 1.42-2.36 (m, 20H, C_6H_{11}), 2.80 (s, 6H, NMe_2), 3.39 (q, $^3J=7.5\text{ Hz}$, 2H, CH), 6.41 (dt, $^3J=7.6\text{ Hz}$, $^4J=1.5\text{ Hz}$, 2H, CH_{Ar}), 6.72 (dd, $^3J=8.4\text{ Hz}$, $^4J=1.3\text{ Hz}$, 2H, CH_{Ar}), 7.04 (dt, $^3J=7.7\text{ Hz}$, $^4J=1.4\text{ Hz}$, 2H, CH_{Ar}), 7.28 (dd, $^3J=8.4\text{ Hz}$, $^4J=1.7\text{ Hz}$, 2H, CH_{Ar}) ppm; $^{13}\text{C}\{^1\text{H}\}$ NMR (C_6D_6 , 500 MHz): δ 26.2 (C_6H_{11}), 26.5 (C_6H_{11}), 26.9 (C_6H_{11}), 35.0 (C_6H_{11}), 35.1 (C_6H_{11}), 42.3 (Ga- NMe_2), 45.3 (CH- C_6H_{11}),

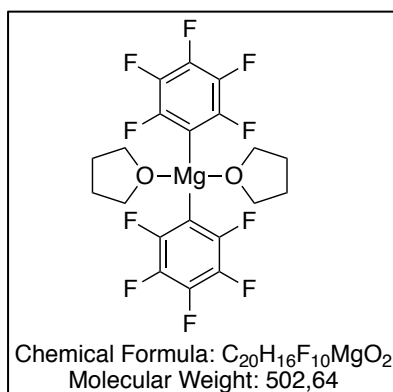
112.8 (CH_{Ar}), 113.7 (CH_{Ar}), 119.7 (CH_{Ar}), 126.0 (CH_{Ar}), 129.6 (CH_{Ar}), 144.9 (C_{ipso}), 146.9 (C_{ipso}) ppm.

Tol•Zn(C₆F₅)₂



A solution of B(C₆F₅)₃ (1 g, 1.95 mmol) in toluene (17 mL) was treated with a solution of ZnMe₂ (0.215 mL, 2.93 mmol) in 6 mL of toluene. The mixture was stirred for 30 minutes at room temperature then the solvent was evaporated under vacuum leading a white solid which was recrystallized overnight in pentane at -35 °C. The supernatant was removed, and the white powder was dried *in vacuo* to produce the zinc complex as a pure white solid (0.950 g, 99%). ¹H NMR (C₆D₆, 300 MHz): δ 2.11 (s, 3H, Me), 6.90-7.13 (m, 5H, Ph) ppm; ¹⁹F NMR (C₆D₆, 500 MHz): δ -118.9 (m, 4F, *o*-F), -153.5 (t, 2F, ³J_{FF} = 19.7 Hz, *p*-F), -161.5 (m, 4F, *m*-F) ppm.

Mg(C₆F₅)₂(THF)₂

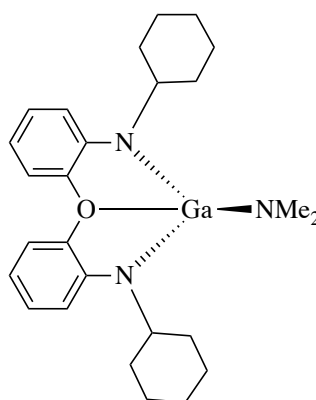


To a precooled solution of 1-bromopentafluorophenylbenzene (1.42 g, 5.77 mmol) dissolved in 5.5 mL of THF was added a solution of dibutylmagnesium (399.69 mg, 2.88 mmol) in 2.9 mL of heptane. The solution was then stirred at room temperature for one hour and the

solvent was removed under vacuum to give a white oil. The white oil was then precipitated in cold pentane then the precipitate was dried under vacuum to produce a white solid (1.54 g, 100%). **¹H NMR (C₆D₆, 300 MHz):** δ 1.42 (m, 8H, CH₂ THF), 3.37 (m, 8H, CH₂ THF) ppm; **¹⁹F NMR (C₆D₆, 500 MHz):** δ -115.3 (m, 4F, *o*-F), -157.8 (t, 2F, ³J_{FF} = 19.6 Hz, *p*-F), -162.1 (m, 4F, *m*-F) ppm.

Crystal data**Compound reference**

<i>Chemical formula</i>	$\text{C}_{26}\text{H}_{36}\text{GaN}_3\text{O}$
<i>Formula mass</i>	476.30
<i>Crystal system</i>	triclinic
<i>a/Å</i>	9.8872(4)
<i>b/Å</i>	10.5152(4)
<i>c/Å</i>	13.3273(5)
<i>$\alpha/^\circ$</i>	82.0320(10)
<i>$\beta/^\circ$</i>	78.8580(10)
<i>$\gamma/^\circ$</i>	62.9080(10)
<i>Unit cell volume/Å³</i>	1208.27(8)
<i>Temperature/K</i>	173(2)
<i>Space group</i>	P-1
<i>No. of formula units per cell, Z</i>	2
<i>Radiation type</i>	MoK _a
<i>Absorption coefficient, μ/mm^{-1}</i>	1.161
<i>No. of reflections measured</i>	19723
<i>No. of independent reflections</i>	7046
<i>R_{int}</i>	0.0170
<i>Final R₁ values (I > 2σ(I))</i>	0.0259
<i>Final wR (F²) values (I > 2σ(I))</i>	0.0629
<i>Final R₁ values (all data)</i>	0.0307
<i>Final wR (F²) (all data)</i>	0.0652
<i>Goodness of fit on F²</i>	1.043

Table 2: Crystal data and structural refinement for the Ga amido complex

Polymer synthesis

Typical procedure for lactide polymerization

In a glovebox, catalyst (1 equiv.) was charged in a vial equipped with a Teflon™-tight screw cap and a dichloromethane or toluene solution (1 M) of the appropriate amount of monomer was added via a syringe all at once. The resulting solution was vigorously stirred (at room temperature or heated) for the appropriate time. The vial was then removed from the glovebox and the reaction mixture was quenched with MeOH provoking the precipitation of the polymer which was washed several times with MeOH or pentane, dried *in vacuo* until constant weight and subsequently analysed by ¹H NMR, SEC and by MALDI-TOF spectrometry.

Typical procedure for immortal lactide polymerization

The same procedure as previously described was used for polymerization with the addition of a monomer solution (1 M) containing some known amount of the desired alcohol (m-PEG-OH) onto the corresponding initiator.

Polymer characterization

NMR spectroscopy

As previously described, the monomer to polymer conversion is calculated by ¹H NMR spectroscopy based on the relative integration of the corresponding signal. (**Experimental Section, “Chapter I”-Polymer characterization-NMR spectroscopy**).

Size-exclusion chromatography (SEC)

The obtained $M_{n(sec)}$ values were corrected using the correction factor **X**, as described in the **Experimental section chapter I** for *rac*-lactide. The determination of the real M_n for PEG-*co*-PLLA with the mono-capped methoxy ether PEG(1900) was calculated from the formula: $((M_{n_GPC} \times X) - 1900) + 1900$. The corrected factor for PLA is 0.58 so $((M_{n_GPC} \times 0.58) - 1900) + 1900$.

Supporting data

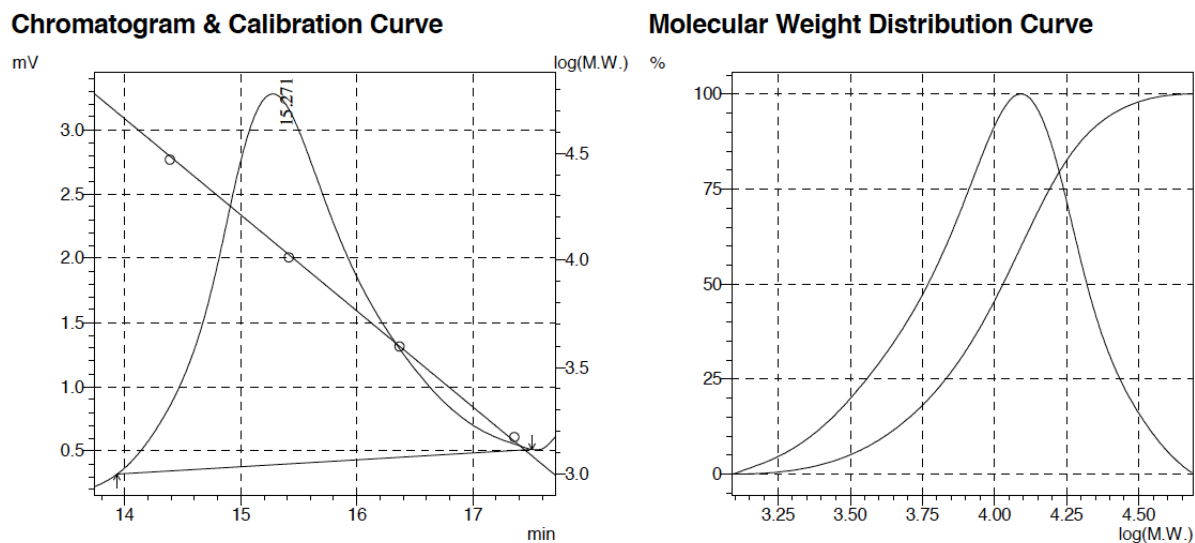


Figure 1: SEC traces of isolated PEG-*co*-PLLA prepared by polymerization of *L*-lactide initiated by *catalyst 2*/PEG system. (Conditions: $[Lactide]_0 = 1$ M, 100 equiv. *L*-lactide, 5 equiv. PEG, toluene, 90 °C, 1h17, total conv.).

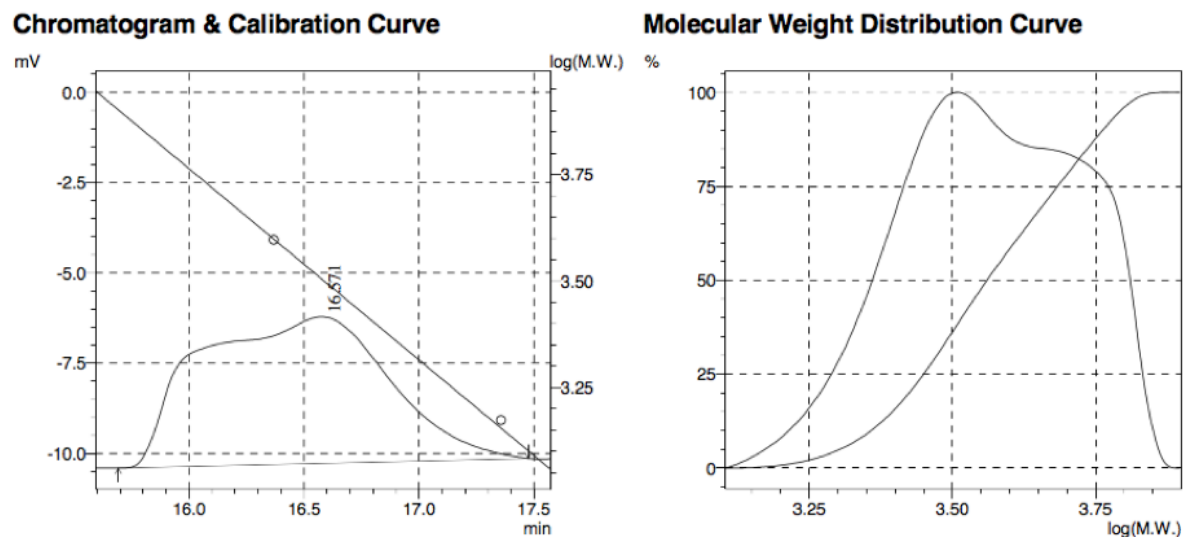


Figure 2: SEC traces of isolated PEG-*co*-PLLA prepared by polymerization of *L*-lactide initiated by *catalyst 4*/PEG system. (Conditions: $[L-lactide]_0 = 1$ M, 100 equiv. *L*-lactide, 5 equiv. PEG(1900), DCM, RT, quantitative conv.).

Chapter III

Typical procedure for Cl-CL polymerization

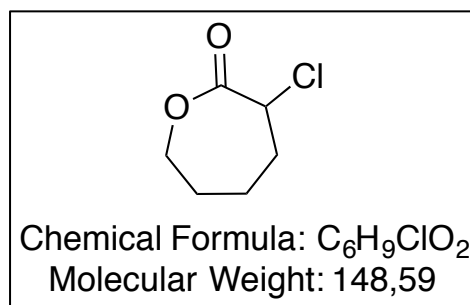
In a glovebox, catalyst (1 equiv.) was charged in a vial equipped with a Teflon™-tight screw cap and a dichloromethane or toluene solution (1 M) of the appropriate amount of monomer was added via a syringe all at once. The resulting solution was vigorously stirred (at room temperature or heated) for the appropriate time. The vial was then removed from the glovebox and the reaction mixture was quenched with pentane provoking the precipitation of the polymer which was washed several times with pentane, dried under vacuum until constant weight and subsequently analysed by ^1H NMR, SEC and by MALDI-TOF spectrometry.

Typical procedure for immortal Cl-CL polymerization

The same procedure as previously described was used for polymerization with the addition of a monomer solution (1 M) containing a known amount of the desired alcohol (BnOH) onto the corresponding initiator.

Syntheses

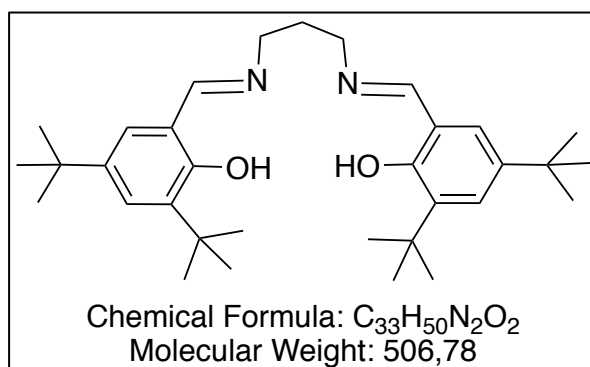
α -chloro- ϵ -caprolactone⁸



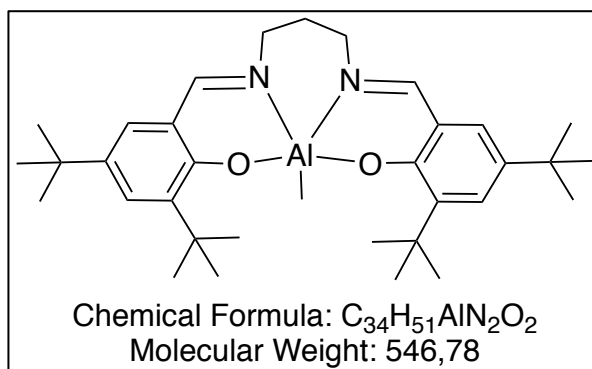
20 g (81 mmol) of *m*CPBA (70%) was added to a solution of 10 g (75 mmol) of 2-chlorocyclohexanone in 100 mL of dichloromethane at room temperature. The reaction was stirred at room temperature for 96 hours, then the flask was cooled overnight at $-20\text{ }^\circ\text{C}$ in order to precipitate *m*-chlorobenzoic acid. The precipitate was removed by filtration and the solution was washed with a saturated aqueous solution of NaHSO_3 (three times), an aqueous

solution of NaHCO_3 (three times), and finally with water. After drying over MgSO_4 , the organic phase was filtered, and the solvent was removed under reduced pressure to give a yellow oil. The oil was purified by silica column chromatography using pentane/ethyl acetate (82/18) as eluent separating α -chloro- ϵ -caprolactone and ϵ -chloro- ϵ -caprolactone and then increasing polarity pentane/ethyl acetate (70:30) for collection of α -chloro- ϵ -caprolactone. The solvent was removed by rotatory evaporator, and the colourless oil was dried under vacuum for two days (5 g, 67%), $R_f = 0.36$, UV-revelation. $\text{C}_6\text{H}_9\text{ClO}_2$ (**148.03**): Anal. Calcd. C, 48.50, H 6.11; Anal Found. C, 48.47, H 6.12. $^1\text{H NMR}$ (CDCl_3 , 300 MHz): δ 1.76-2.22 (m, 6H, CH_2), 4.19-4.27 (m, 1H, COOCH_2), 4.56-4.67 (m, 1H, COOCH_2), 4.78-4.81 (dd, 1H, CHCl) ppm.

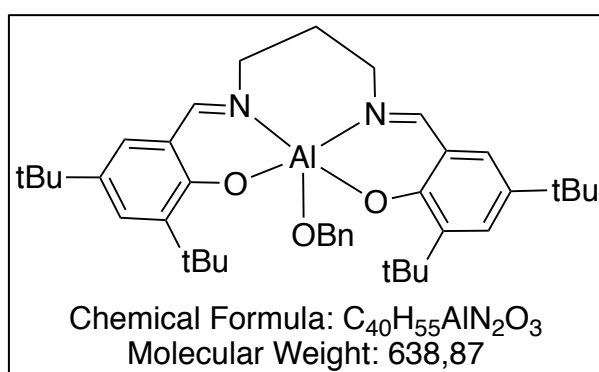
1,3-Diamino- N,N' -bis(3,5-di-*tert*-butylsalicylidene)propane



0.257 g (3.2 mmol, 1 equiv.) of 1,3-diaminopropane was dissolved in 5 mL of absolute ethanol, and a solution of 1.5 g (6.4 mmol, 2 equiv.) of 3,5-di-*tert*-butylsalicylidene in 10 mL of absolute ethanol was added. The solution was then heated to reflux for 12 hours under stirring to afford a yellow suspension. After filtration, rotatory evaporator removed the solvent. (1.29 g, 80%). $^1\text{H NMR}$ (CDCl_3 , 400 MHz): δ 1.31 (s, 18H, $\text{C}(\text{CH}_3)_3$), 1.46 (s, 18H, $\text{C}(\text{CH}_3)_3$), 2.13 (q, $^3J = 6.7$ Hz, 2H, $\text{CH}_2\text{CH}_2\text{CH}_2$), 3.71 (t, $^3J = 6.7$ Hz, 4H, $\text{CH}_2\text{CH}_2\text{CH}_2$), 7.08 (d, $^2J = 2.4$ Hz, 2H, CH_{Ar}), 7.39 (d, $^2J = 2.4$ Hz, 2H, CH_{Ar}), 8.39 (s, 2H, NCH_{Ar}), 13.80 (s, 2H, OH) ppm.

[*N,N'*-bis(3,5-di-*tert*-butylsalicylidene)-1,3-diaminopropanato]aluminium(III) methyl

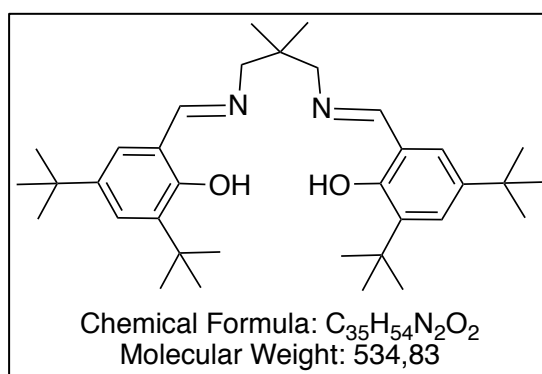
N,N'-bis(3,5-di-*tert*-butylsalicylidene)-1,3-diaminopropane (0.200 g, 0.394 mmol) was dissolved in 5 mL of toluene. To this stirred solution, $AlMe_3$ (28.37 mg, 0.394 mmol) in 2 mL of toluene was added dropwise. The reaction was allowed to stir at 110 °C for 12 hours. The solvent was evaporated under vacuum to give a yellow powder; this powder was washed three times with pentane and was dried *in vacuo*. (0.209 g, 96%). 1H NMR (C_6D_6 , 400 MHz): δ - 0.34 (s, 3H, $AlCH_3$), 1.38 ((m, 2H, $N(CH_2CH_2CH_2)N$ and (s, 18H, $C(CH_3)_3$)), 1.79 (s, 18H, $C(CH_3)_3$), 2.76 (m, 2H, $N(CHHCH_2CHH)N$), 3.08 (m, 2H, $(CHHCH_2CHH)$), 6.90 (d, $^2J=2.4$ Hz, 2H, CH_{Ar}), 7.38 (s, 2H, NCH_{Ar}), 7.76 (d, $^2J=2.4$ Hz, 2H, CH_{Ar}) ppm.

[*N,N'*-bis(3,5-di-*tert*-butylsalicylidene)-1,3-diaminopropanato]aluminium(III) benzyloxide⁹

In a glovebox, [*N,N'*-bis(3,5-di-*tert*-butylsalicylidene)-1,3-diaminopropanato]aluminium(III) methyl (0.20 g, 0.366 mmol) was dissolved in anhydrous toluene, and $BnOH$ (1 equiv., 0.040 g) was subsequently added. The reaction mixture was heated at 110 °C overnight. After

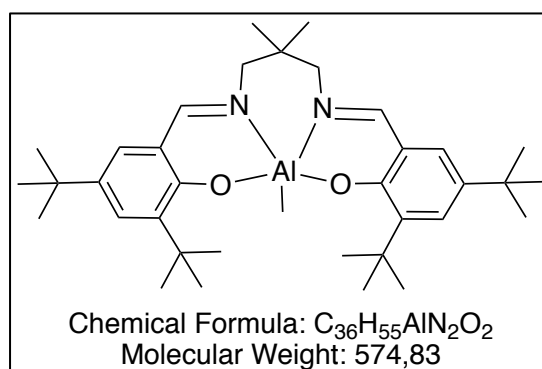
evaporation of the solvent, the residue was washed with pentane to give the product as a white powder (0.222 g, 100%). $^1\text{H NMR}$ (C_6D_6 , 400 MHz): δ 1.37 (m, 2H, $\text{N}(\text{CH}_2\text{CH}_2\text{CH}_2)\text{N}$ and (s, 18H, $\text{C}(\text{CH}_3)_3$), 1.73 (s, 18H, $\text{C}(\text{CH}_3)_3$), 2.78 (m, 2H, $\text{N}(\text{CHHCH}_2\text{CHH})\text{N}$), 3.45 (m, 2H, $(\text{CHHCH}_2\text{CHH})$), 5.21 (br, 2H, CH_2Ph), 6.88 (d, $^2J=2.4$ Hz, 2H, CH_{Ar}), 7.07-7.20 (m, 5H, CH_{Ar}), 7.38 (s, 2H, NCH_{Ar}), 7.72 (d, $^2J=2.4$ Hz, 2H, CH_{Ar}) ppm.

1,3-Diamino-*N,N'*-bis(3,5-di-*tert*-butylsalicylidene)-2,2'-dimethylpropane



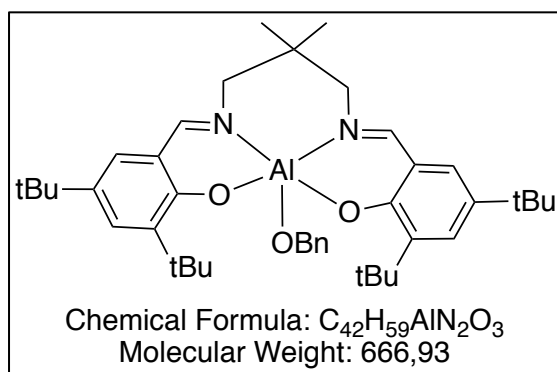
0.251 g (2,13 mmol, 1 equiv.) of 1,3-diamino-2,2'-dimethylpropane was dissolved in 5 mL of absolute ethanol, and a solution of 1 g (4.26 mmol, 2 equiv.) of 3,5-di-*tert*-butylsalicylidene in 10 mL of absolute ethanol was added. The solution was then heated to reflux for 12 hours under stirring to produce a yellow suspension. After filtration, the product was removed by rotatory evaporator (1 g, 90%). $^1\text{H NMR}$ (CDCl_3 , 400 MHz): δ 1.10 (s, 6H, $\text{CH}_2\text{C}(\text{CH}_3)_2\text{CH}_2$), 1.31 (s, 18H, $\text{C}(\text{CH}_3)_3$), 1.47 (s, 18H, $\text{C}(\text{CH}_3)_3$), 3.48 (s, 4H, $\text{CH}_2\text{CMe}_2\text{CH}_2$), 7.10 (d, $^2J=2.4$ Hz, 2H, CH_{Ar}), 7.39 (d, $^3J=2.4$ Hz, 2H, CH_{Ar}), 8.36 (s, 2H, NCH_{Ar}), 13.83 (s, 2H, OH) ppm.

[*N,N'*-bis(3,5-di-*tert*-butylsalicylidene)-1,3-diamino-2,2'-dimethylpropanato]aluminium(III) methyl



N,N'-bis(3,5-di-*tert*-butylsalicylidene)-1,3-diaminopropane (0.300 g, 0.560 mmol) was dissolved in 1 mL of toluene. To this stirred solution, AlMe_3 (40.37 mg, 0.560 mmol) in 1 mL of toluene was added dropwise. The reaction was allowed to stir at 110 °C for 12 hours. The solvent was evaporated under vacuum to give a yellow powder; this powder was washed three times with pentane and was dried under vacuum. (0.300 g, 93%). $^1\text{H NMR}$ (C_6D_6 , 400 MHz): δ - 0.42 (s, 3H, AlCH_3), 0.40 (s, 3H, $\text{CH}_2\text{C}(\text{CH}_3)_2\text{CH}_2$), 0.57 (s, 3H, $\text{CH}_2\text{C}(\text{CH}_3)_2\text{CH}_2$), 1.38 (s, 18H, $\text{C}(\text{CH}_3)_3$), 1.84 (s, 18H, $\text{C}(\text{CH}_3)_3$), 2.65 (d, $^3J=12.3$ Hz, 2H, $\text{N}(\text{CHH}\text{CMe}_2\text{CHH})\text{N}$), 2.89 (d, $^3J=12.3$ Hz, 2H, $\text{N}(\text{CHH}\text{CMe}_2\text{CHH})\text{N}$), 7.0 (d, $^2J=2.4$ Hz, 2H, CH_{Ar}), 7.50 (s, 2H, NCH_{Ar}), 7.77 (d, $^2J=2.4$ Hz, 2H, CH_{Ar}) ppm.

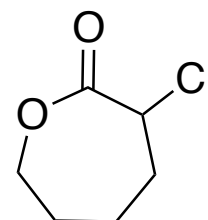
[*N,N'*-bis(3,5-di-*tert*-butylsalicylidene)-1,3-diamino-2,2'-dimethylpropanato] aluminium(III) benzyloxide¹⁰



In a glovebox, [*N,N'*-bis(3,5-di-*tert*-butylsalicylidene)-1,3-diamino-2,2'-dimethylpropanato] aluminium(III) methyl (0.20 g, 0.348 mmol) was dissolved in anhydrous toluene, and BnOH (1 equiv., 0.037 g) was subsequently added. The reaction mixture was heated at 110 °C overnight. After evaporation of the solvent, the residue was washed with pentane to give the product as a white powder (0.232 g, 100%). $^1\text{H NMR}$ (C_6D_6 , 400 MHz): δ 0.41 (s, 3H, $\text{CH}_2\text{C}(\text{CH}_3)_2\text{CH}_2$), 0.58 (s, 3H, $\text{CH}_2\text{C}(\text{CH}_3)_2\text{CH}_2$), 1.38 (s, 18H, $\text{C}(\text{CH}_3)_3$), 1.81 (s, 18H, $\text{C}(\text{CH}_3)_3$), 2.65 (d, $^3J=12.3$ Hz, 2H, $\text{N}(\text{CHH}\text{CMe}_2\text{CHH})\text{N}$), 3.24 (d, $^3J=12.3$ Hz, 2H, $\text{N}(\text{CHH}\text{CMe}_2\text{CHH})\text{N}$), 4.97 (br, 2H, CH_2Ph), 6.99 (d, $^2J=2.4$ Hz, 2H, CH_{Ar}), 7.13-7.27 (m, 5H, CH_{Ar}), 7.52 (s, 2H, NCH_{Ar}), 7.77 (d, $^2J=2.4$ Hz, 2H, CH_{Ar}) ppm.

Crystal data**Compound reference:** **α -chloro- ϵ -caprolactone**

<i>Chemical formula</i>	C ₆ H ₉ ClO ₂
<i>Formula mass</i>	148.59
<i>Crystal system</i>	orthorhombic
<i>a/Å</i>	7.1919(2)
<i>b/Å</i>	8.9752(3)
<i>c/Å</i>	21.8531(7)
<i>α/°</i>	90
<i>β/°</i>	90
<i>γ/°</i>	90
<i>Unit cell volume/Å³</i>	1410.59
<i>Temperature/K</i>	173(2)
<i>Space group</i>	Pbca
<i>No. of formula units per cell, Z</i>	16
<i>Radiation type</i>	MoK _{α}
<i>Absorption coefficient, μ/mm⁻¹</i>	None
<i>No. of reflections measured</i>	11782
<i>No. of independent reflections</i>	1603
<i>R_{int}</i>	0.0796
<i>Final R₁ values (I > 2σ(I))</i>	0.0398
<i>Final wR (F²) values (I > 2σ(I))</i>	0.0981
<i>Final R₁ values (all data)</i>	0.0476
<i>Final wR (F²) (all data)</i>	0.01080
<i>Goodness of fit on F²</i>	1.110

**Table 3: Crystal data and structural refinement for the α -chloro- ϵ -caprolactone**

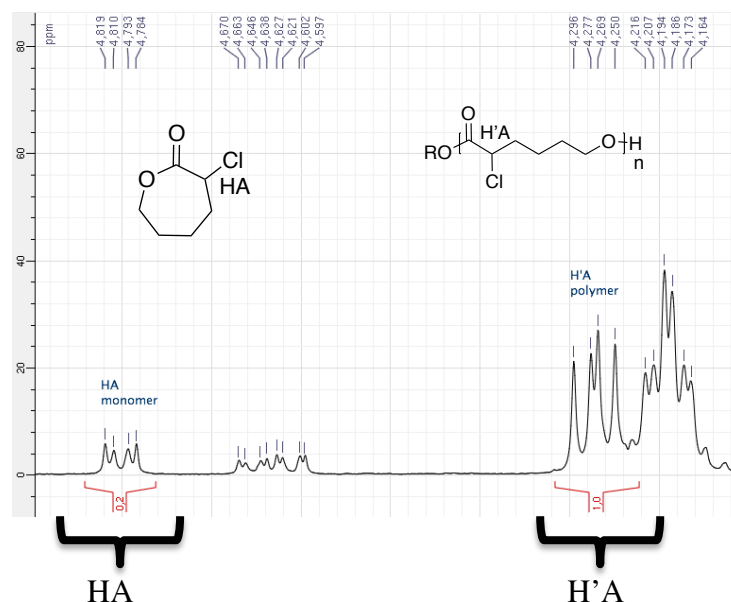
P(Cl-CL) characterization

NMR spectroscopy

The monomer to polymer conversion is calculated by ^1H NMR spectroscopy based on the relative integration of the corresponding signal:

Polymer δ (ppm) Monomer δ (ppm)

4.78-4.82 4.25-4.27



Size-exclusion chromatography (SEC) analysis

The number-average, weight-average molar masses (M_n and M_w , respectively) and molar mass distribution ($\text{PDI} = M_w/M_n$) of the polyester P(Cl-CL) samples were determined by size exclusion chromatography (SEC) at 30 °C with Shimadzu LC20AD ultra-fast liquid chromatography equipped with a Shimadzu RID10A refractometer detector. Tetrahydrofuran (THF) was used as the eluent and the flow rate was set up at 1.0 mL/min. A Varian PLGel pre-column 5 μm were used. Calibrations were performed using polystyrene standards (400-100000 g/mol) and the raw values of $M_n(\text{sec})$ were thus obtained.

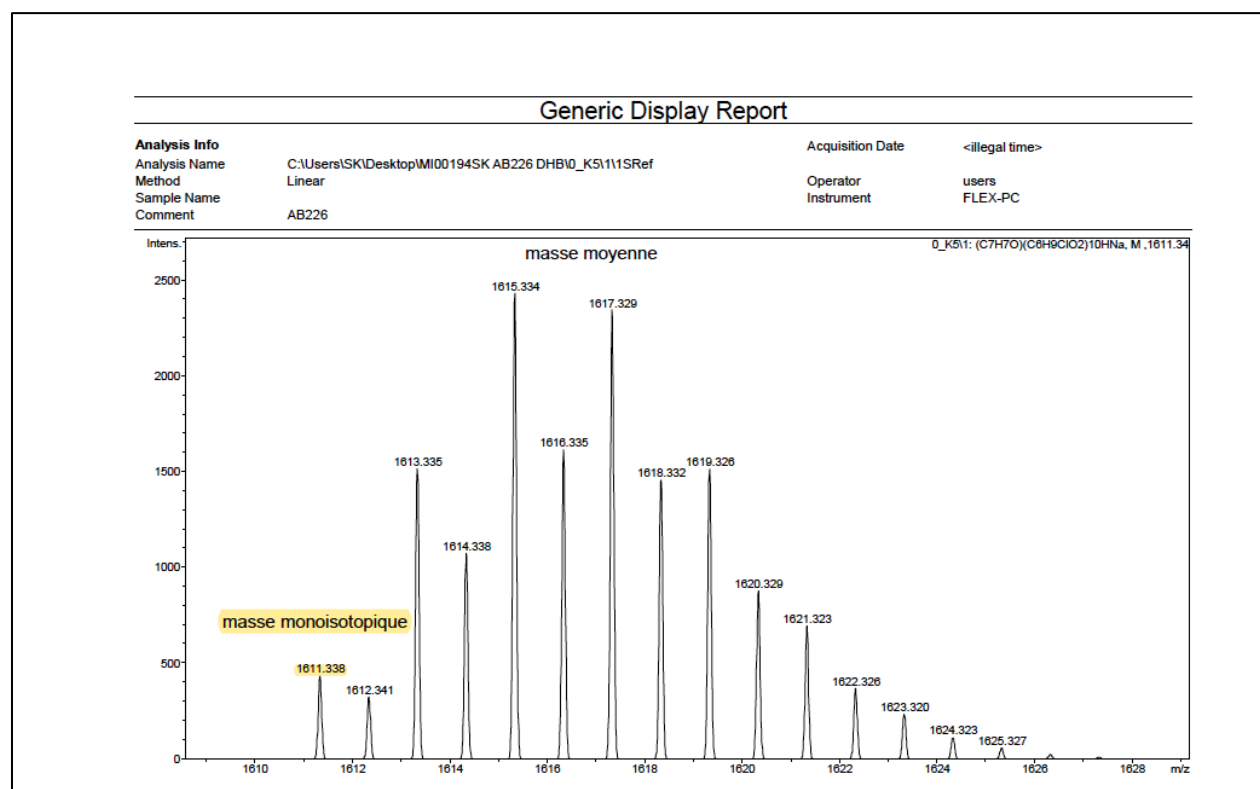
General procedure for Williamson reaction

NaH was placed in excess in cold anhydrous THF and benzyl alcohol was added dropwise whilst stirring the solution. The mixture was stirred during 1 hour at 0 °C. P(Cl-CL) in anhydrous THF was added (1mL/min.) to the mixture under nitrogen then the mixture was stirred at RT for 14 hours. The solvent was evaporated by rotatory evaporator, and then dissolved in EtOAc, washed three times with brine and three times with water. The organic

layer was then dried over MgSO_4 then the solvent removed by rotatory evaporation. The oily residue was then washed with pentane and dried under vacuum.

Supporting data

a.



b.

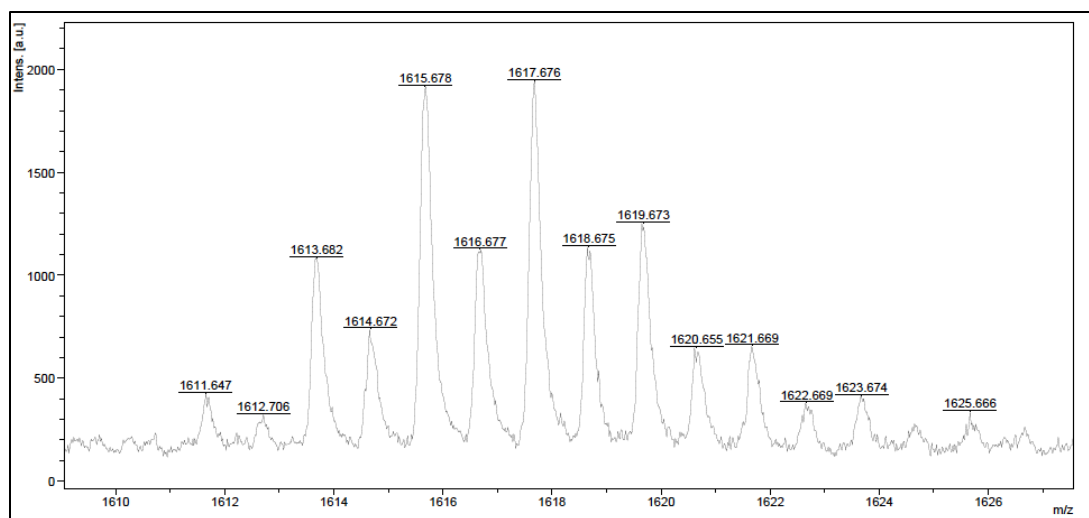
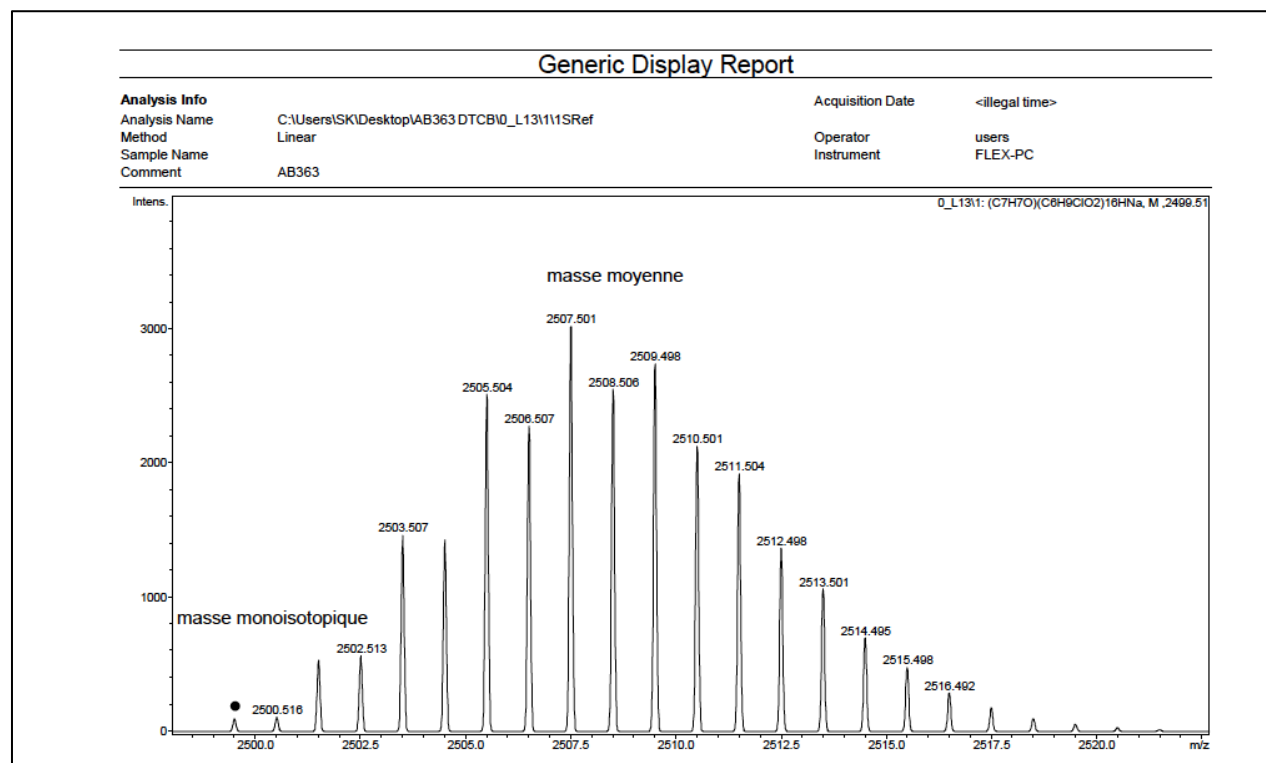


Figure 1: a. Generic display report of the average mass for the peak m/z : 1615 illustrating the monoisotopic mass m/z : 1611.647; $(\text{BnOH} + [\text{Cl-CL}]_{10} + \text{Na}^+) = 108.06 + 10 \times 148.03 + 22.99 = 1611.35$ b. Zoom-in of the peak for m/z : 1615.678 (Figure 48, Chapter III), P(Cl-CL) prepared by ROP of Cl-CL initiated by the *catalyst 4* system. (Conditions $[\text{Cl-CL}]_0 = 1$ M, 100 equiv. of Cl-CL, DCM, RT, polymer isolated at 100% conv. in P(Cl-CL)).

a.



b.

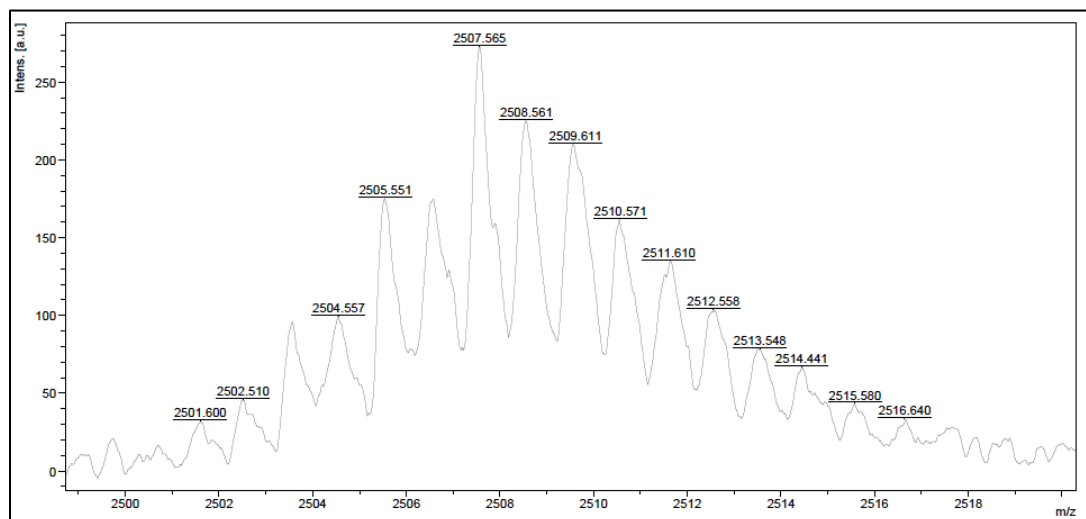
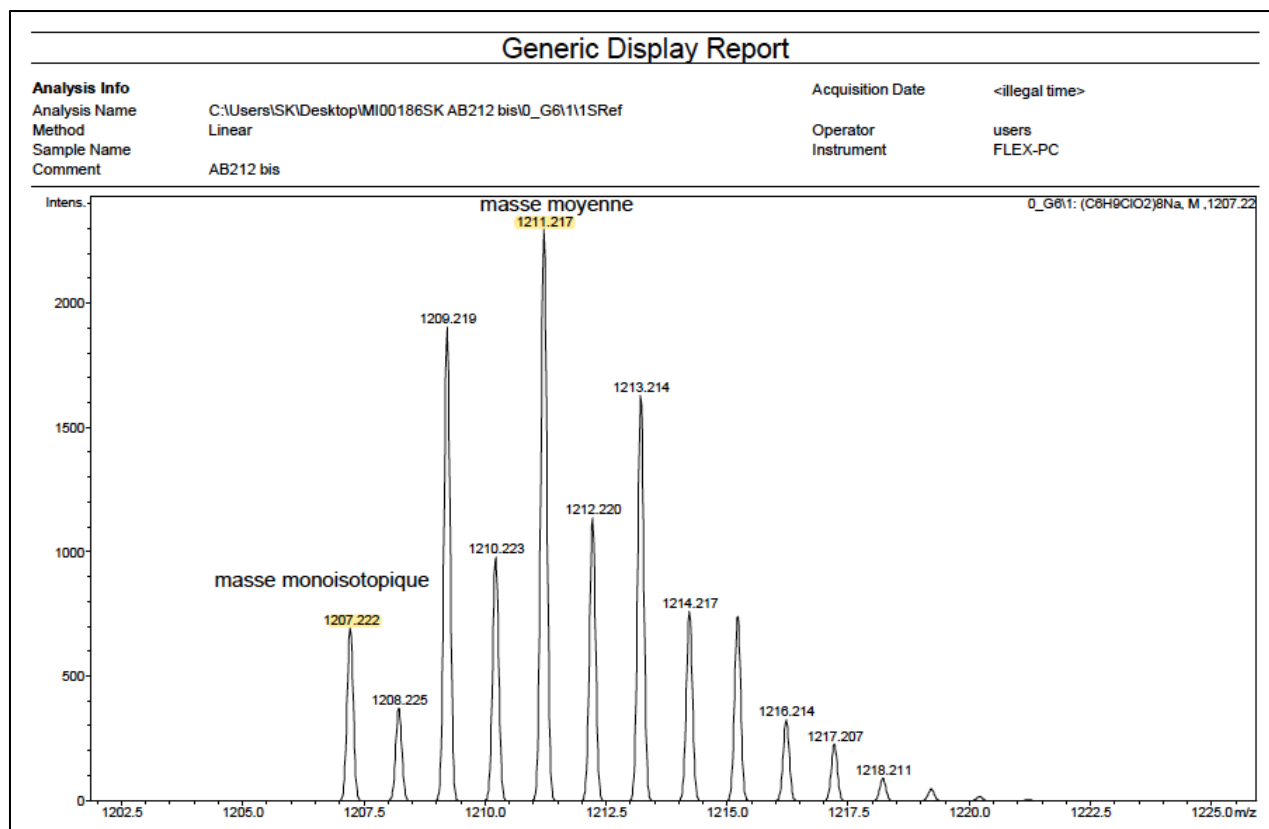


Figure 2: a. Generic display report of the average mass for the peak m/z : 2507.565 illustrating the monoisotopic mass m/z : 2499.53; $(\text{BnOH} + [\text{Cl-CL}]_{16} + \text{Na}^+) = 108.06 + 16 \times 148.03 + 22.99 = 2499.53$ b. Zoom-in of the peak for m/z : 2597.565 (Figure 54, Chapter III) MALDI-TOF spectrum of the P(Cl-CL) prepared by ROP of Cl-CL initiated by the *catalyst 4* system. (Conditions $[\text{Cl-CL}]_0 = 1$ M, 250 equiv. of Cl-CL, DCM, RT, polymer isolated at 100% conv. in P(Cl-CL)).

a.



b.

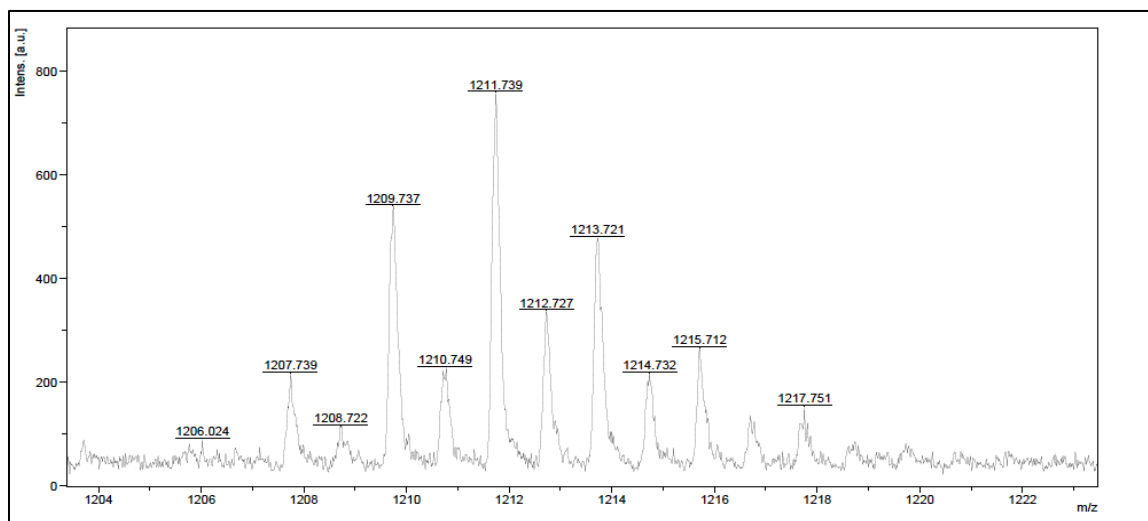


Figure 3: a. Generic display report of the average mass for the peak m/z : 1211.217 illustrating the monoisotopic mass m/z for the cyclic polymer: 1207.222; $([Cl-CL]_8 + Na^+) = 8 \times 148.03 + 22.99 = 1207.23$ b. Zoom-in of the peak for m/z : 1211.739, “Figure 57 Chapter III”: MALDI-TOF spectrum of the P(Cl-CL) prepared by ROP of Cl-CL initiated by the *catalyst 4* system. (Conditions: $[Cl-CL]_0 = 1$ M, 500 equiv. of Cl-CL, DCM, RT, polymer isolated at 100% conv. in P(α cl ϵ CL)). c. For the linear polymer see (Figure 1. a) m/z : 1615.334

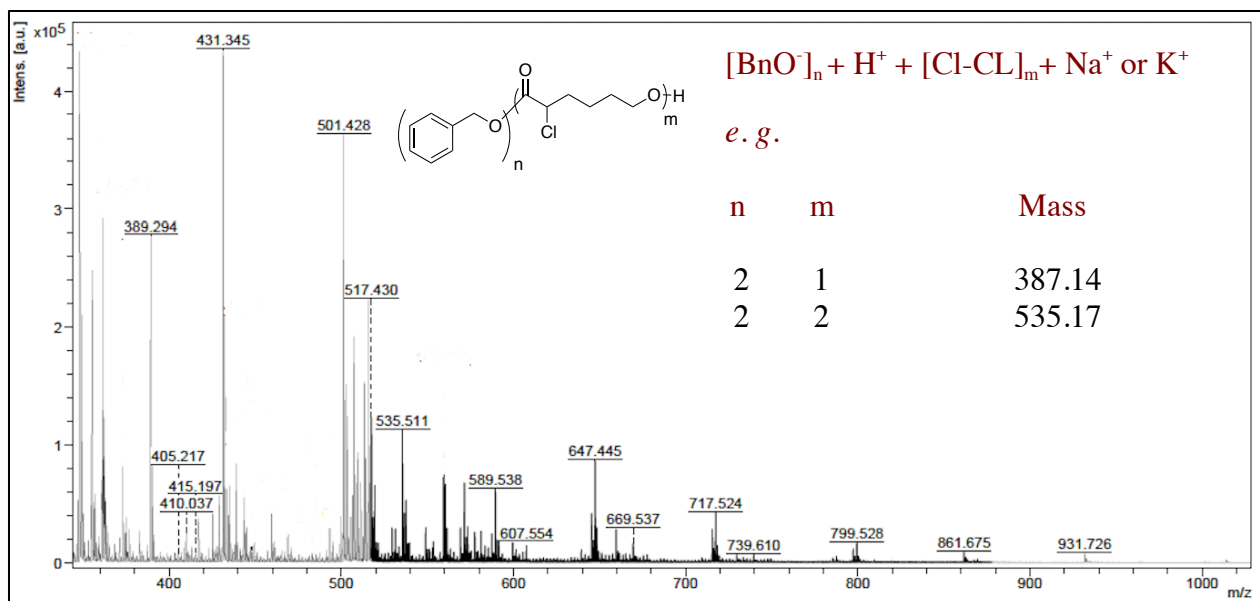


Figure 4: Zoom-in of the MALDI-TOF spectrum of the P(Cl-CL) prepared by immortal ROP of Cl-CL initiated using the complex 4. (Conditions: [Cl-CL]₀ = 1 M, 1000 equiv. of Cl-CL, 5 equiv. of BnOH, DCM, RT, 110 min., total conv.). For the good assignments look at Figures 4a, 4b, and 4c.

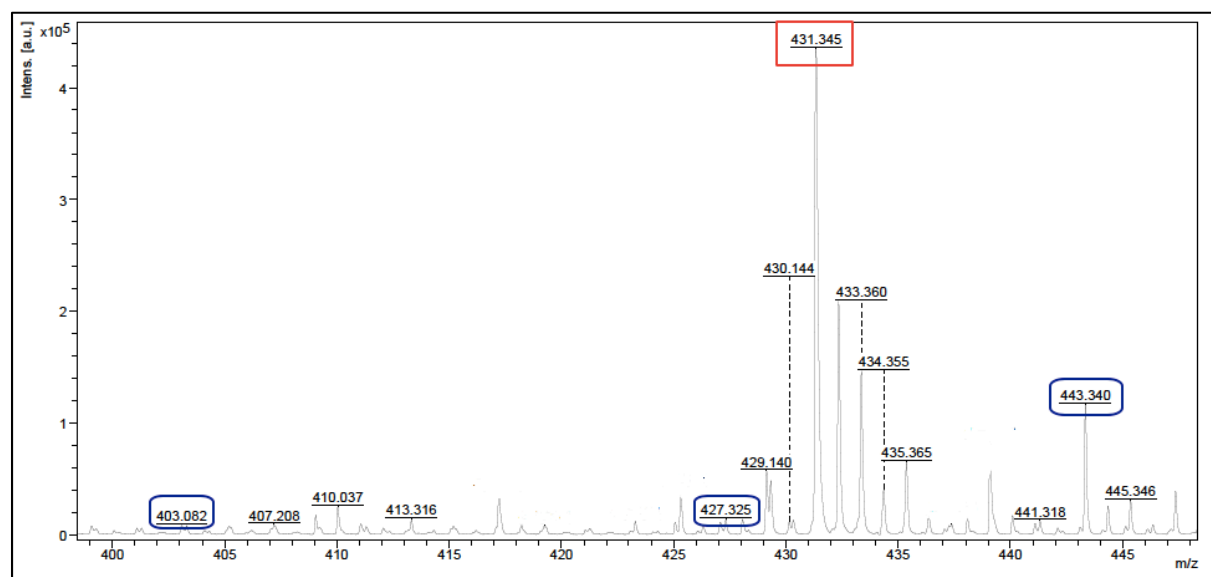


Figure 4a: Zoom of the region's massive from m/z: 403.082 to 445.346. Good assignments for the m/z peaks at 403.082: $(\text{BnOH})_2 + \text{P}(\text{Cl-CL}) + \text{K}^+ = 108.06 \times 2 + 148.03 + 39.09 = 403.24$ then 427.325: $\text{BnOH} + \text{P}(\text{Cl-CL})_2 + \text{Na}^+ = 108.06 + 148.03 \times 2 + 22.99 = 427.11$, and 443.340: $\text{BnOH} + \text{P}(\text{Cl-CL})_2 + \text{K}^+ = 108.06 + 148.03 \times 2 + 39.09 = 443.21$.

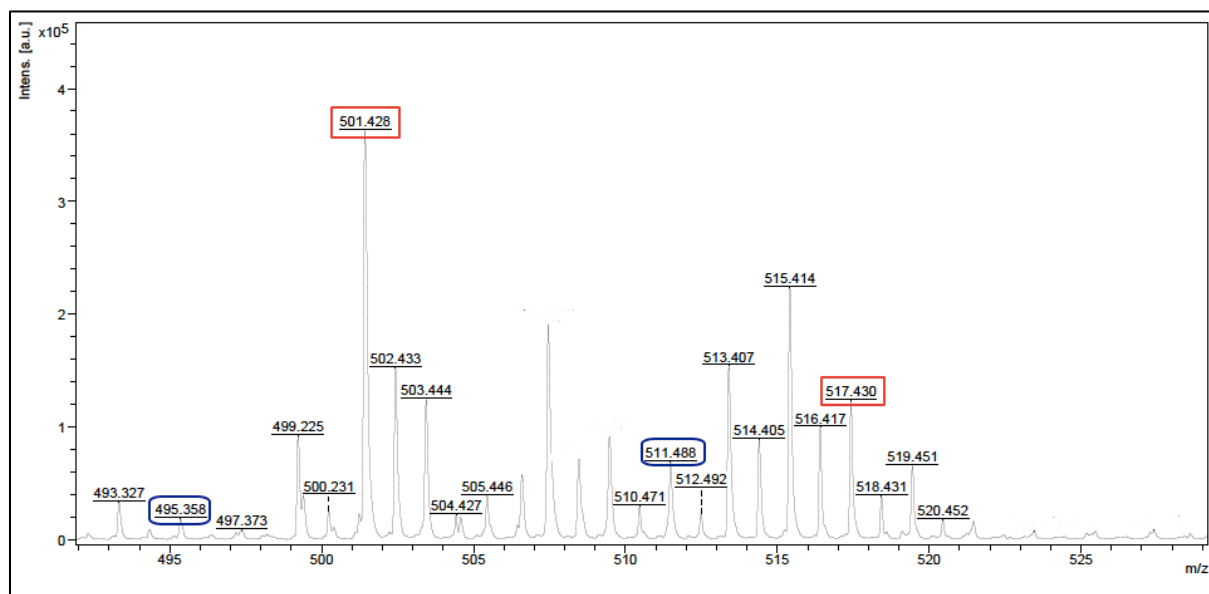


Figure 4b: Zoom of the region's massive from m/z: 493.327 to 520.452. Good assignments for the m/z peaks at 495.358: $(\text{BnOH})_3 + \text{P}(\text{Cl-CL}) + \text{Na}^+ = 108.06 \times 3 + 148.03 + 22.99 = 495.20$, and 511.488: $(\text{BnOH})_3 + \text{P}(\text{Cl-CL}) + \text{K}^+ = 108.06 \times 3 + 148.03 + 39.09 = 511.30$.

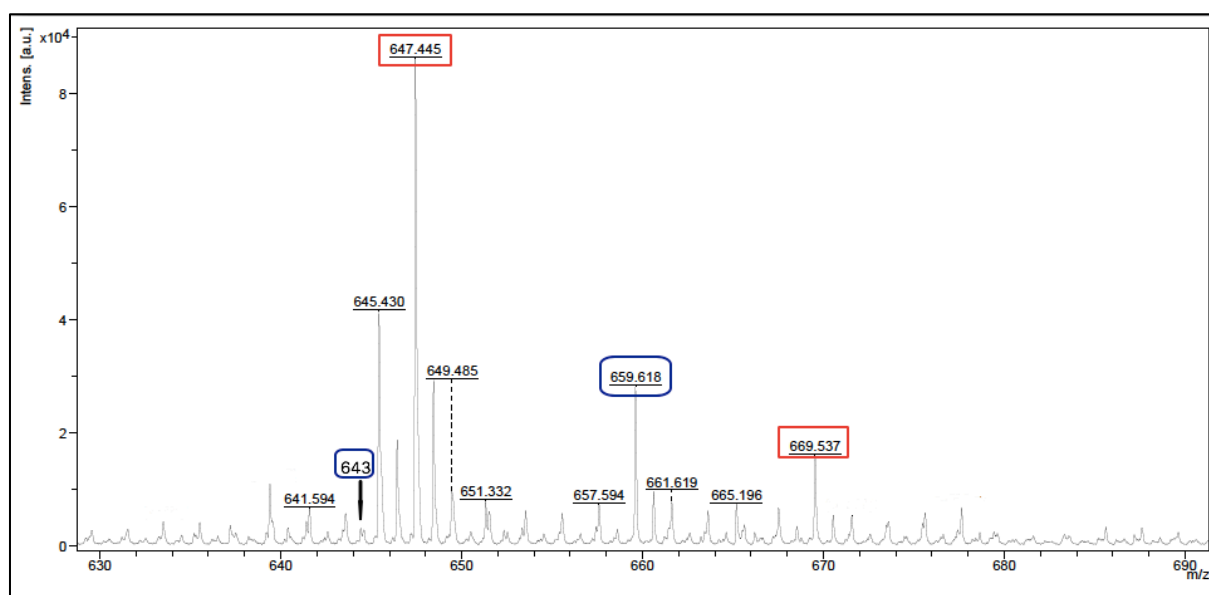


Figure 4c: Zoom of the region's massive from m/z: 641.594 to 669.537. Good assignments for the m/z peaks at 643: $(\text{BnOH})_3 + \text{P}(\text{Cl-CL})_2 + \text{Na}^+ = 108.06 \times 3 + 148.03 \times 2 + 22.99 = 643.23$, and 659.618: $(\text{BnOH})_3 + \text{P}(\text{Cl-CL})_2 + \text{K}^+ = 108.06 \times 3 + 148.03 \times 2 + 39.09 = 659.33$.

(Red squares: average mass, blue squares: monoisotopic mass)

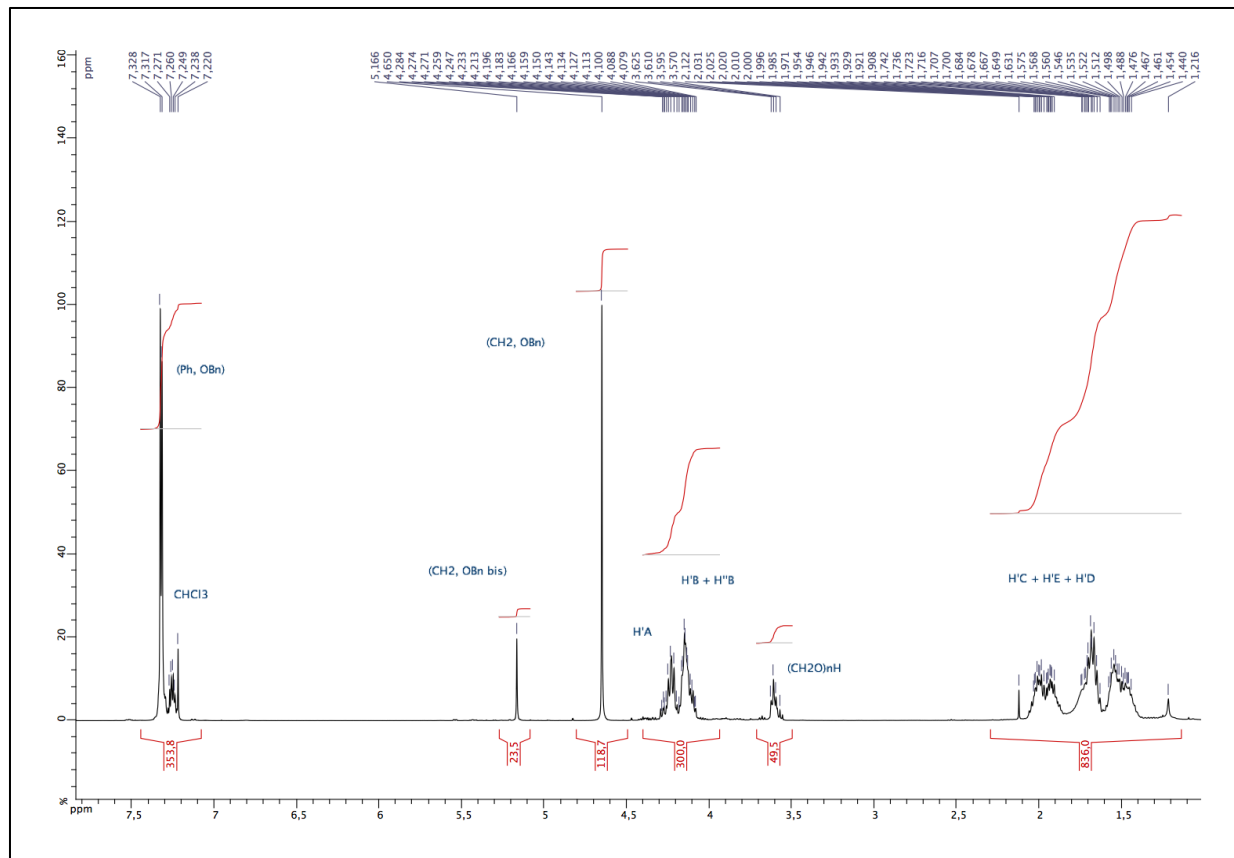


Figure 5: ^1H NMR (CDCl_3 , 400 MHz): 1). 0.7 equiv. BnOH, 0.9 equiv. NaH (conditions: anhydrous THF, 1 h, 0 °C) then addition of P(Cl-CL) $n=100$ in anhydrous THF, overnight, RT, 73% yield).

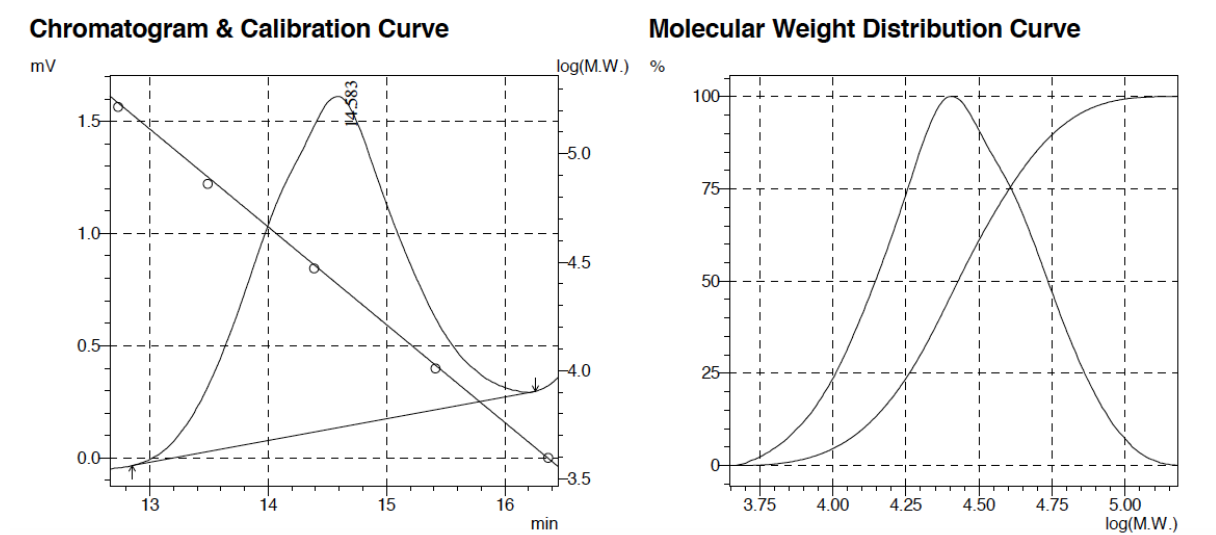


Figure 6: SEC traces of isolated polymer prepared via Williamson reaction on P(Cl-CL) (Conditions: P(Cl-CL) with $n=100$, 0.7 equiv. BnOH vs. P(Cl-CL), RT, anhydrous THF, isolated polymer, bimodal).

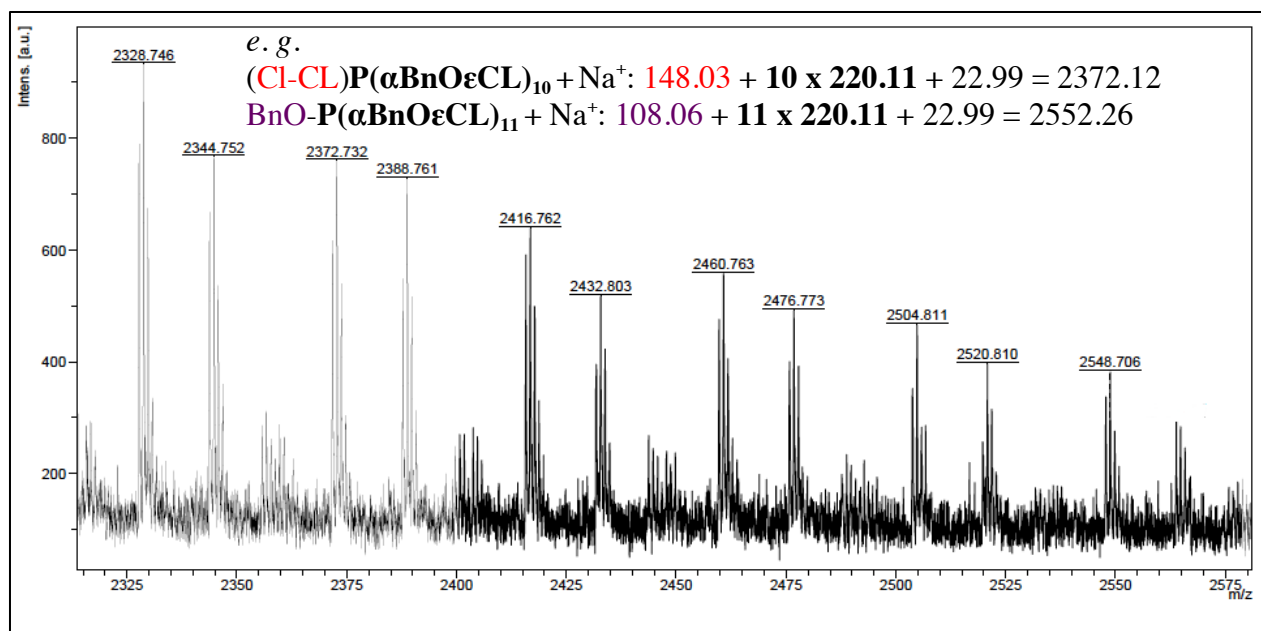


Figure 7: Zoom-in of the MALDI-TOF of the Williamson reaction using NaH/BnOH system. (Conditions: P(Cl-CL) with $n=100$, 0.7 equiv. BnOH vs. P(Cl-CL), anhydrous THF, RT, overnight).

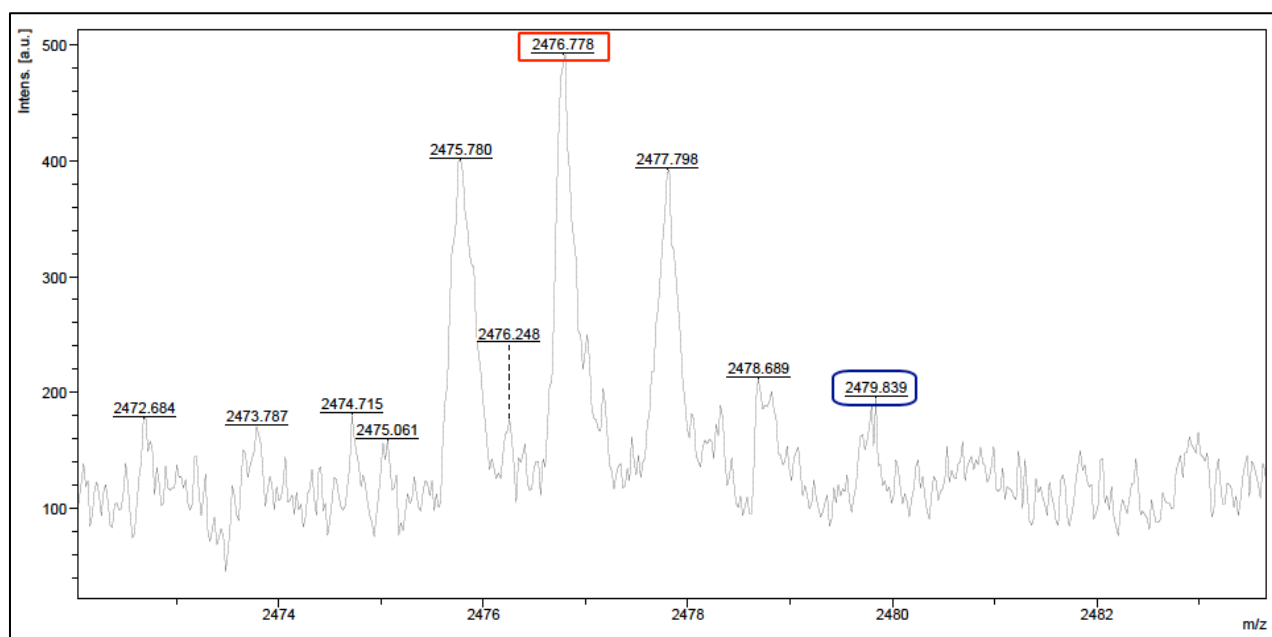


Figure 7a: Zoom of the region's massive from m/z : 2472 to 2480. Good assignment for the m/z peak at 2479.839; $\text{BnOH} + \text{Cl-CL} + [\text{P}(\alpha\text{OBn}\epsilon\text{CL})]_{10} + \text{Na}^+ = 108.06 + 148.03 + 10 \times 220.11 + 22.99 = 2480.18$; $\text{BnO-P}(\text{Cl-CL})\text{P}(\alpha\text{BnO}\epsilon\text{CL})_{10} + \text{Na}^+$.

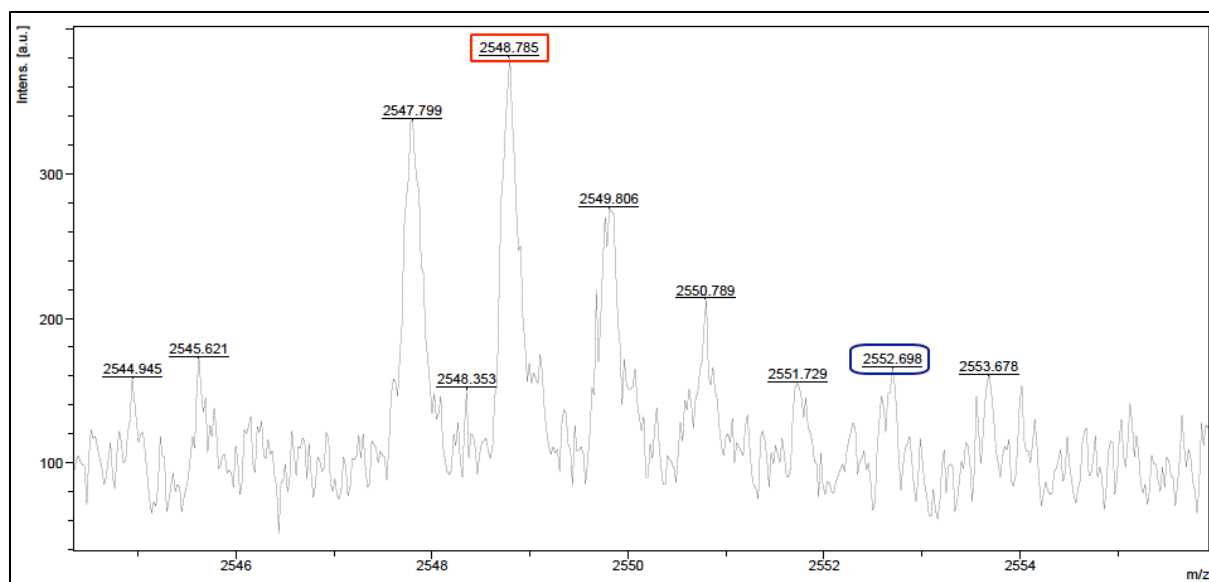


Figure 7b: Zoom of the region's massive from m/z: 2544 to 2553. Good assignation for the m/z peak at 2552; $\text{BnOH} + [\text{P}(\alpha\text{OBn}\epsilon\text{CL})]_{11} + \text{Na}^+$: $108.06 + [220.11]_{11} + 22.99 = 2552.26$; $\text{BnO-P}(\alpha\text{BnO}\epsilon\text{CL})_{11} + \text{Na}^+$.

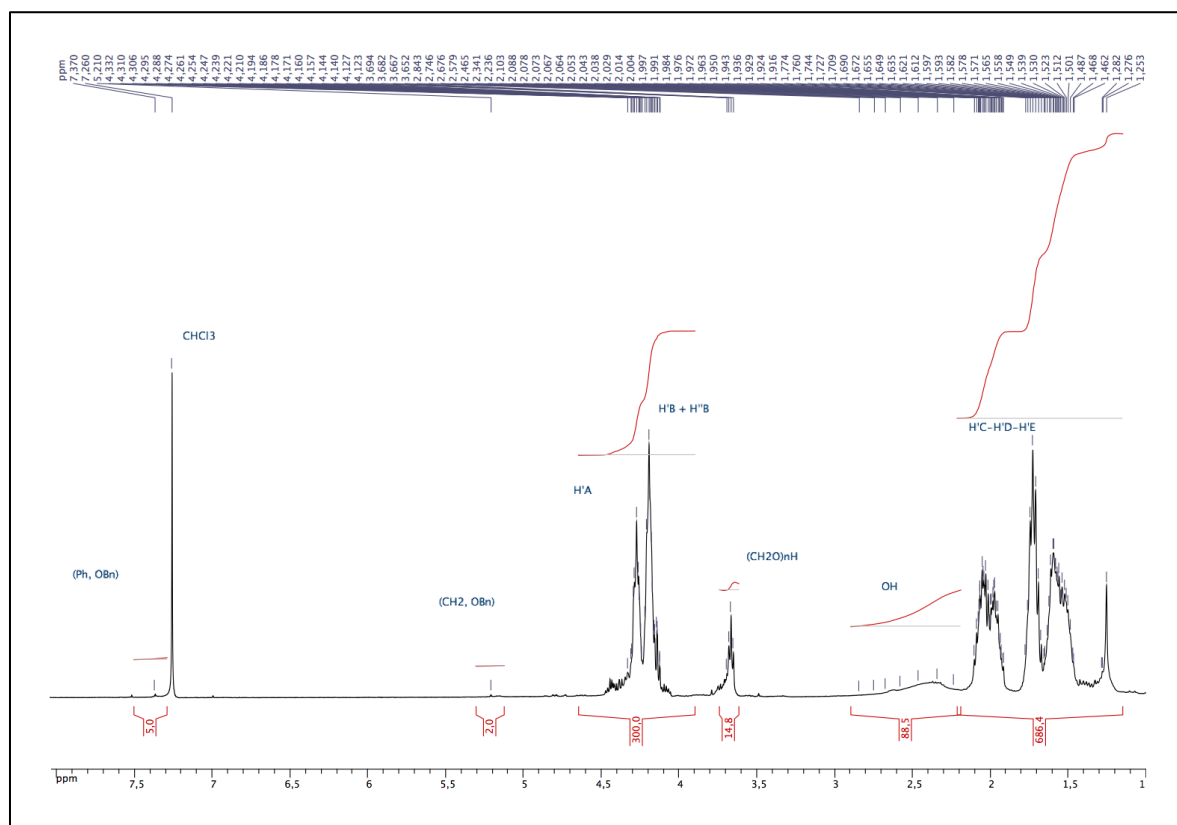


Figure 8: ^1H NMR (CDCl_3 , 400 MHz), hydrogenation of the polymer mixture obtained after Williamson reaction on $\text{P}(\text{Cl-CL})$ with $n=100$. (Conditions: CDCl_3 , RT, H_2 (1 atm.), 15 min. total conversion in OH, quantitative yield).

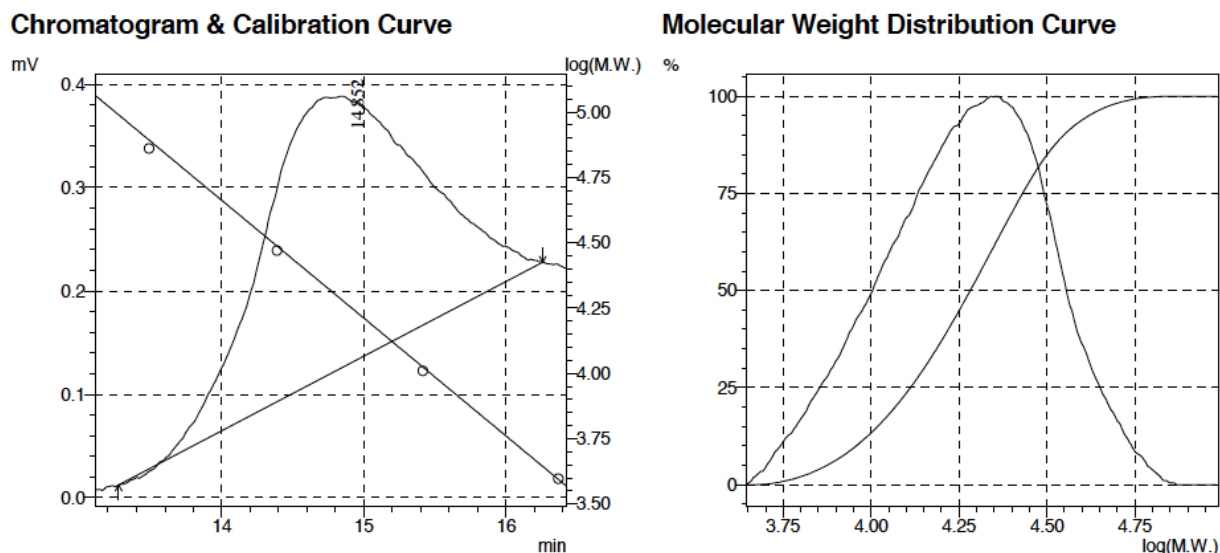


Figure 9: SEC traces of isolated polymer after hydrogenation reaction. (Conditions: CDCl_3 , RT, 15 min., isolated polymer).

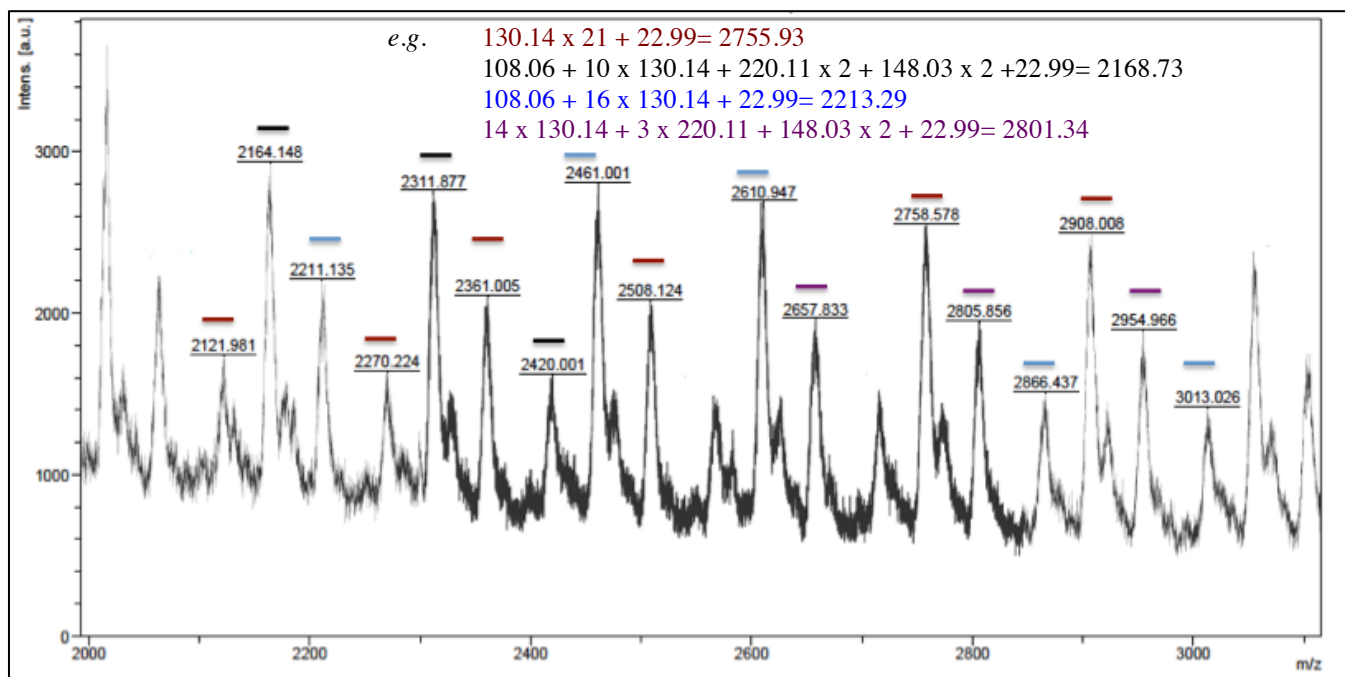


Figure 10: Zoom-in of the MALDI-TOF of the isolated polymer after hydrogenation of the polymer obtained after Williamson reaction on P(Cl-CL) with $n=100$. (Conditions: CDCl_3 , RT, H_2 (1 atm.), 15 min., isolated polymer).

Legend: **red lines:** cyclic P($\alpha\text{OH}\epsilon\text{CL}$), **black lines:** mainly linear P($\alpha\text{OH}\epsilon\text{CL}$) chain initiated including some P($\alpha\text{OBn}\epsilon\text{CL}$) units and (Cl-CL) fragments, **blue lines:** linear P($\alpha\text{OH}\epsilon\text{CL}$) bonded on the ester end at the OBn initiator, **purple lines:** mainly cyclic P($\alpha\text{OH}\epsilon\text{CL}$) with some P($\alpha\text{OH}\epsilon\text{CL}$) units and Cl-CL fragments.

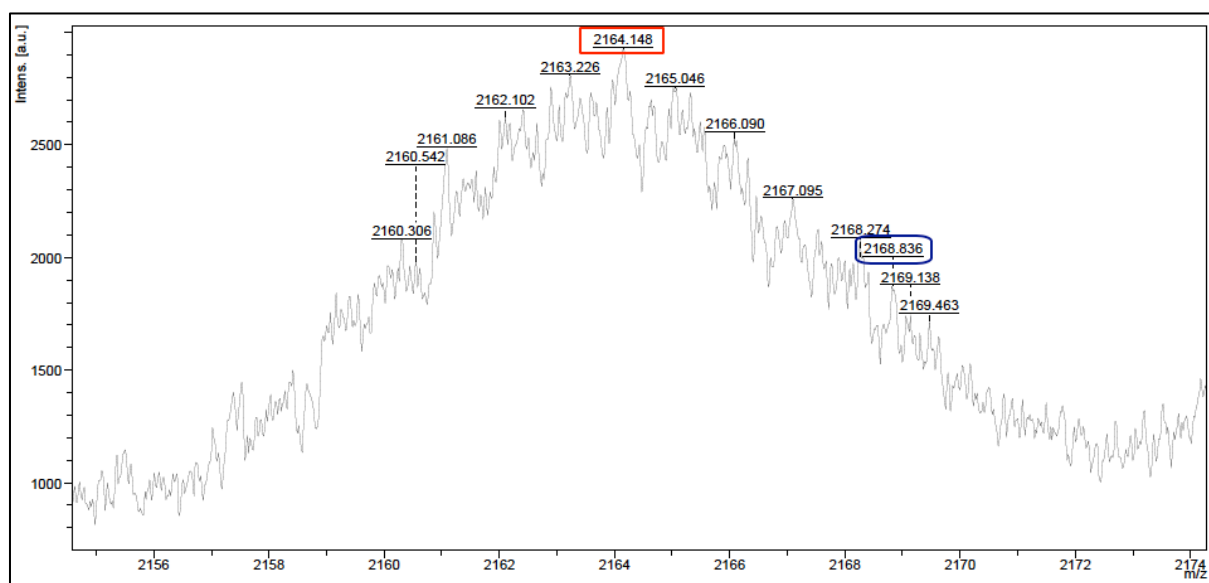


Figure 10a: Zoom of the region's massive from m/z : 2160 to 2170. Good assignment for the m/z peak at 2168.836; $\text{BnOH} + [\text{P}(\alpha\text{OH}\epsilon\text{CL})]_{10} + [\text{P}(\alpha\text{OBn}\epsilon\text{CL})]_2 + [\text{P}(\text{Cl-CL})]_2 + \text{Na}^+ : 108.06 + 10 \times 130.14 + 2 \times 220.11 + 2 \times 148.03 + 22.99 = 2168.73$; $\text{BnO-P}(\alpha\text{BnO}\epsilon\text{CL})_{11} + \text{Na}^+$

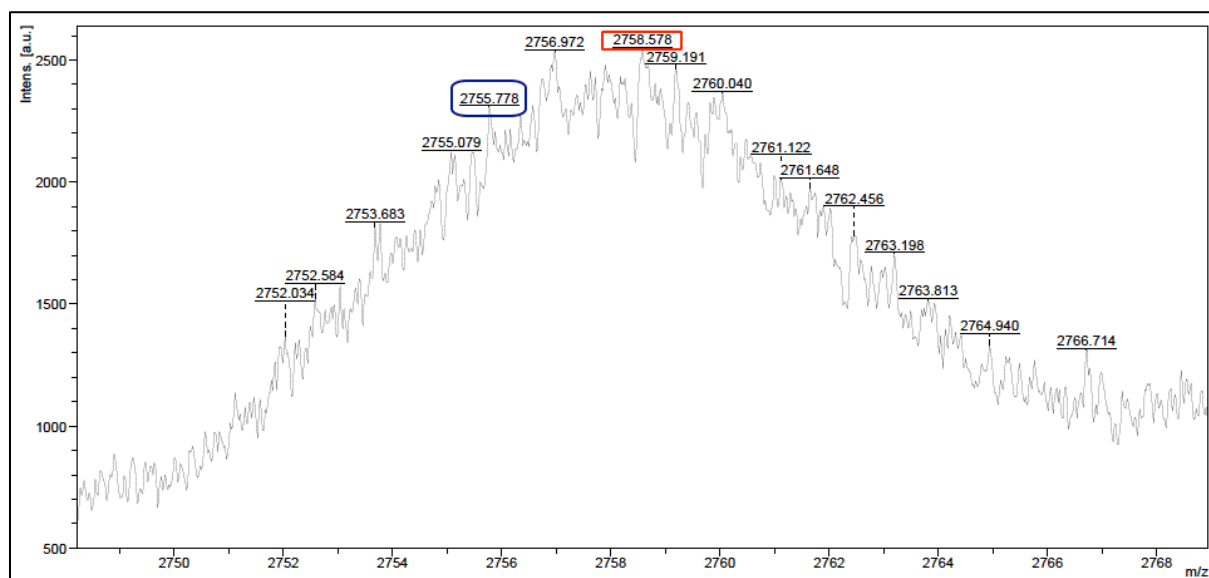


Figure 10b: Zoom of the region's massive from m/z : 2752 to 2766. Good assignment for the m/z peak at 2755.778; $[\text{P}(\alpha\text{OH}\epsilon\text{CL})]_{21} + \text{Na}^+ : 21 \times 130.14 + 22.99 = 2755.93$.

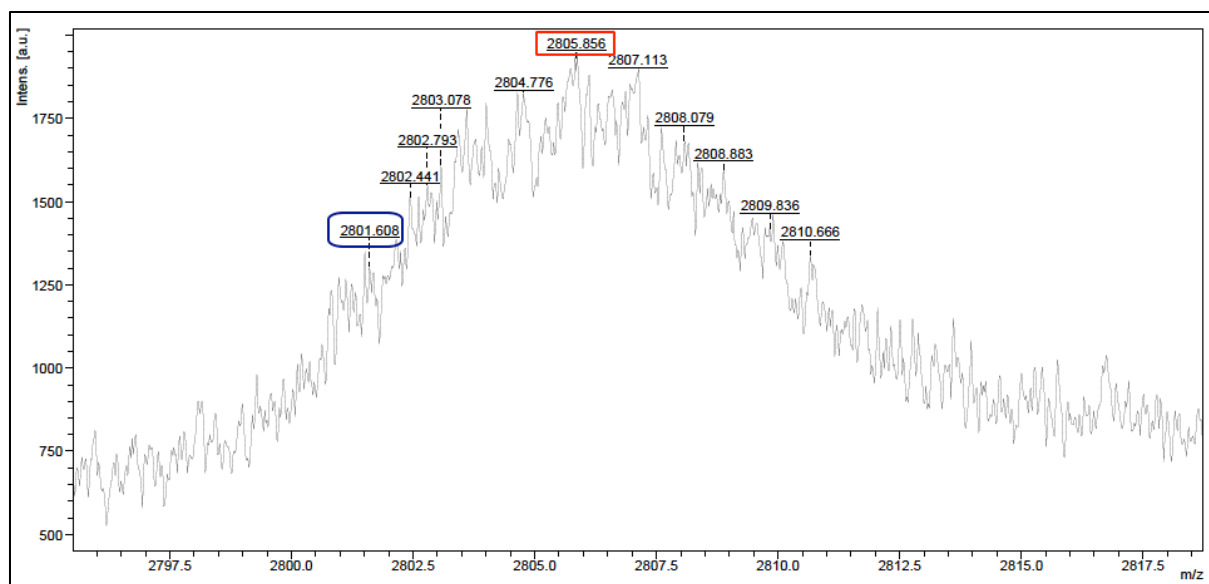


Figure 10c: Zoom of the region's massive from m/z: 2801 to 2810. Good assignment for the m/z peak at 2801; $[P(\alpha OH\epsilon CL)]_{14} + [P(\alpha OBn\epsilon CL)]_3 + [P(Cl-CL)]_2 + Na^+ = 14 \times 130.14 + 3 \times 220.11 + 2 \times 148.03 + 22.99 = 2801.34$.

Chapter IV

Polymer characterization

For NMR spectroscopy and size-exclusion chromatography (SEC) analysis: **P(CI-CL) characterization-Chapter III**

IFT measurements

Copolymers' IFT measurements were performed at SNF_{sas} (St Etienne, Andrezieux, France) with a spinning drop tensiometer SVT20N Dataphysics. The measurements were obtained at RT with a spinning rate of 5000 rpm, a concentration of 1500 ppm in copolymer using [dodecane/water] solvents.

Thermogravimetric Analysis (TGA)

TGA measurements for AB302bis, AB303bis, AB305bis, AB306, and AB318 samples were effected at the “Institut Charles Sadron”, (Strasbourg, France) and were taken using a TGA2 (Mettler-Toledo). Samples mass about 5 mg powder were heated from room temperature to 1000 °C from 0.02 to 150 °C/min. The TGA data were plotted as temperature versus weight percent, from which onset and final decomposition temperatures were obtained. The analytical method used for all these samples is 25 °C to 700 °C at 10 °C/min. under a nitrogen flow of 1000 mL/min. and 700 °C to 1000 °C at 10 °C/min. under an air flow of 100 mL/min. Concerning AB256 sample, TGA measurement was performed at the “Chemlab Platform”, (Strasbourg, France) using an ATG SDT 650 TA instrument using the same method as for the previous samples.

Differential Scanning Calorimetry (DSC)

DSC measurements were carried out using a DSC Q200 thermal analyser instrument. Powdered sample (about 5 mg) were loaded and sealed in a stainless steel high volume pan. Samples were heated from -80 °C to 550 °C using nitrogen gas vector. The glass transition temperature, the melting temperature and crystallization temperature were measured after heating the samples up to 180 °C and cooling to -80 °C. Thermograms were recorded during

first cycle at 10 °C/min. Results and measurements were effected with the TA universal Analysis software.

General procedure for diblock's formation

L- or *D*-lactide was dissolved in toluene and *catalyst 4* (1 equiv.) was added to the mixture which was stirred for 9 hours at 80 °C. To this PLA mixture was added the appropriate Cl-CL amount then the mixture was stirred at room temperature until the total conversion in P(Cl-CL). The toluene was evaporated and the obtained solid was washed three times with pentane then was dried under vacuum.

Stereocomplex formation

10 mg of *PLLA-b-P(Cl-CL)* and 10 mg of *PDLA-b-P(Cl-CL)* were slowly dissolved together in CHCl₃. The mixture was then stirred at room temperature for 3 hours then the solvent was evaporated at open air to give the *PLLA-b-P(Cl-CL) + PDLA-b-P(Cl-CL)* stereocomplex as a white powder.

Supporting data

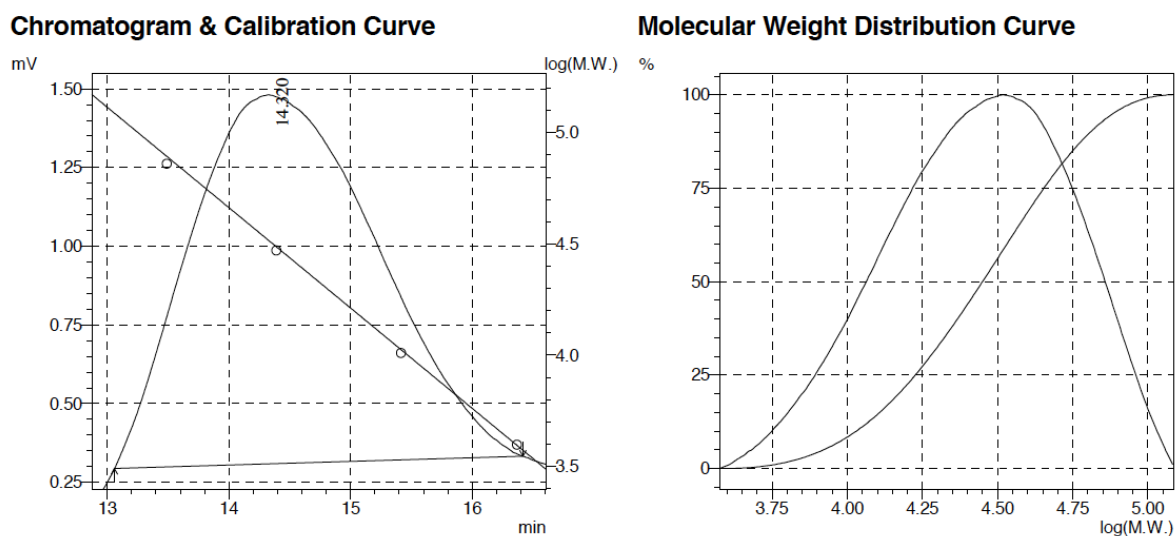


Figure 1: SEC traces of isolated PEG-co-P(Cl-CL) prepared via ROP of Cl-CL initiated by the *catalyst 4*/PEG(1900) system. (Conditions: $[\text{Cl-CL}]_0 = 1 \text{ M}$, 100 equiv. of Cl-CL, 5 equiv. of PEG (1900), RT, DCM, 6 h, 100% conv.).

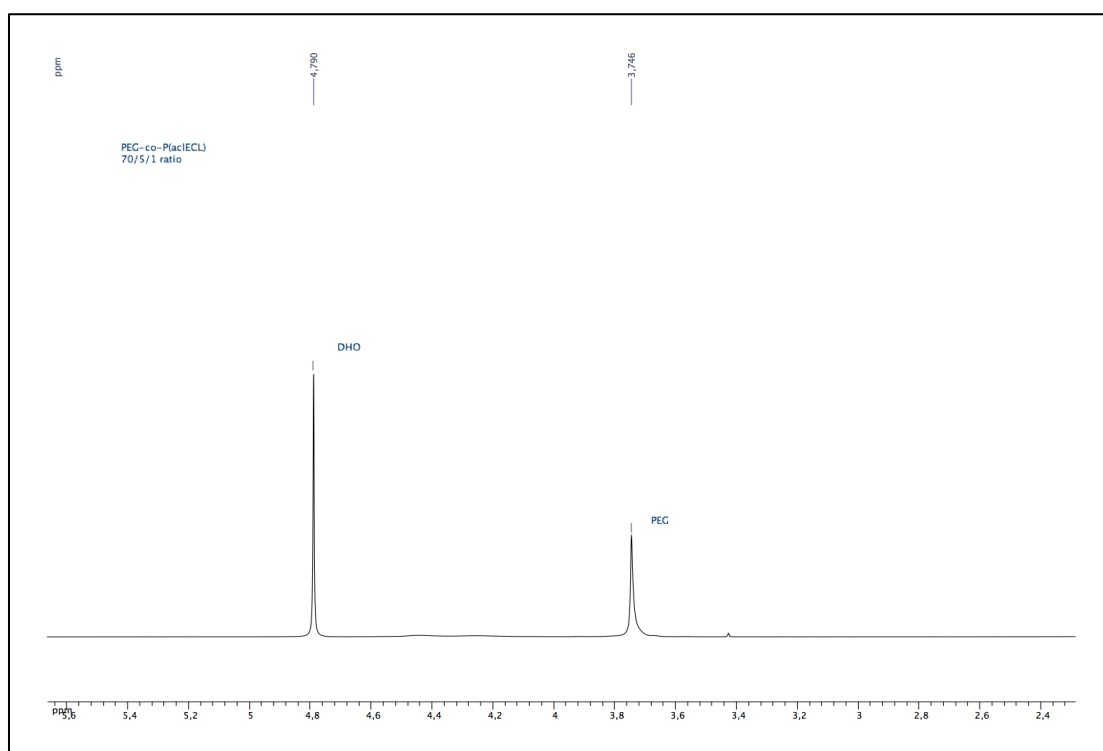


Figure 2: ^1H NMR (D_2O , 400 MHz) of isolated PEG-co-P(Cl-CL) prepared by ROP of Cl-CL initiated by *catalyst 4*/PEG system. (Conditions: $[\text{Cl-CL}]_0 = 1 \text{ M}$, 70 equiv. of Cl-CL, 5 equiv. of PEG vs. *catalyst*, RT, DCM, 3.5 h, quantitative conv.).

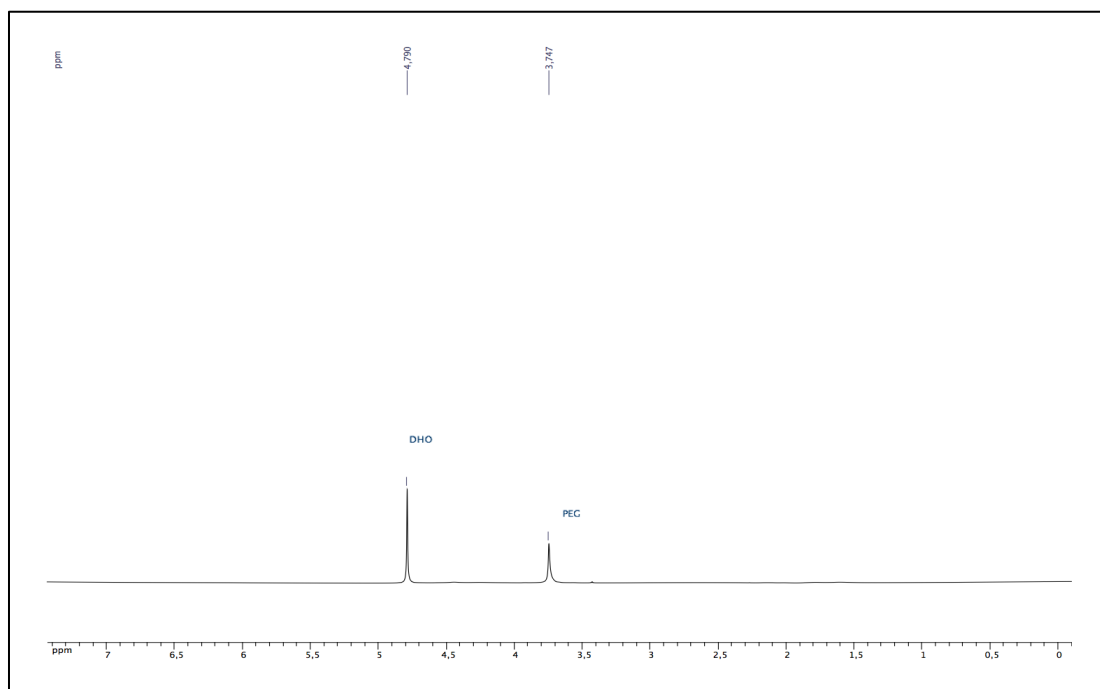


Figure 3: ¹H NMR (D₂O, 400 MHz) of isolated PEG-*co*-P(Cl-CL) prepared by ROP of Cl-CL initiated by *catalyst 4*/PEG system. (Conditions: [Cl-CL]₀= 1 M, 100 equiv. of Cl-CL, 5 equiv. of PEG *vs.* catalyst, RT, DCM, 6 h, quantitative conv.).

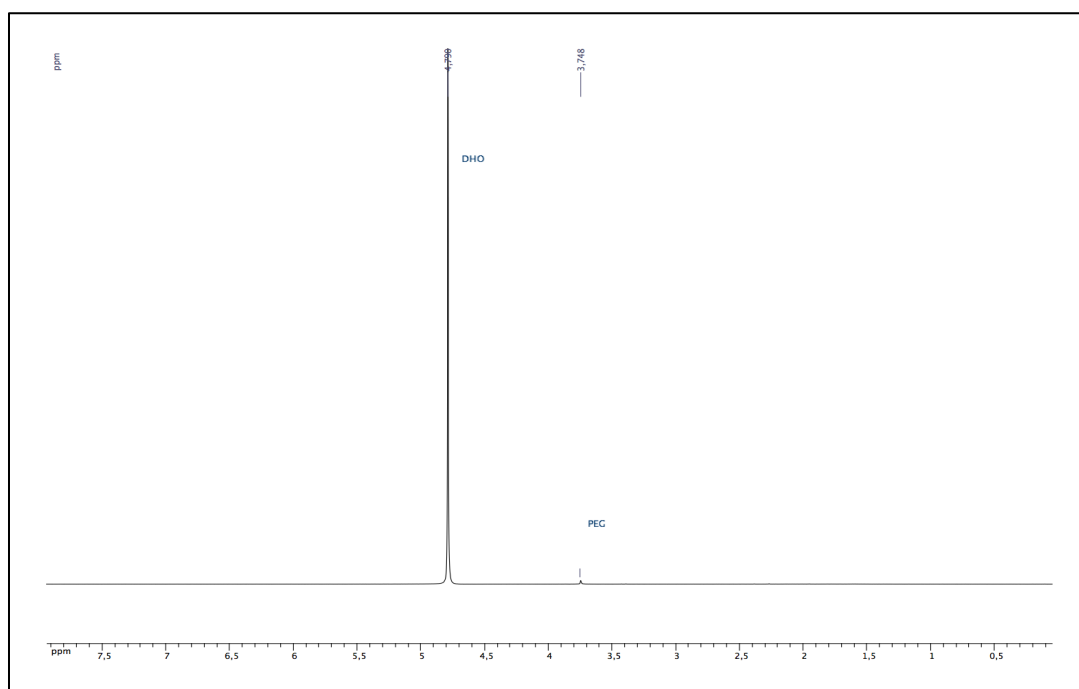


Figure 4: ¹H NMR (D₂O, 400 MHz) of isolated PEG-*co*-P(Cl-CL) prepared by ROP of Cl-CL initiated by *catalyst 4*/PEG system. (Conditions: [Cl-CL]₀= 1 M, 500 equiv. of Cl-CL, 5 equiv. of PEG *vs.* catalyst, RT, DCM, 9 h, quantitative conv.).

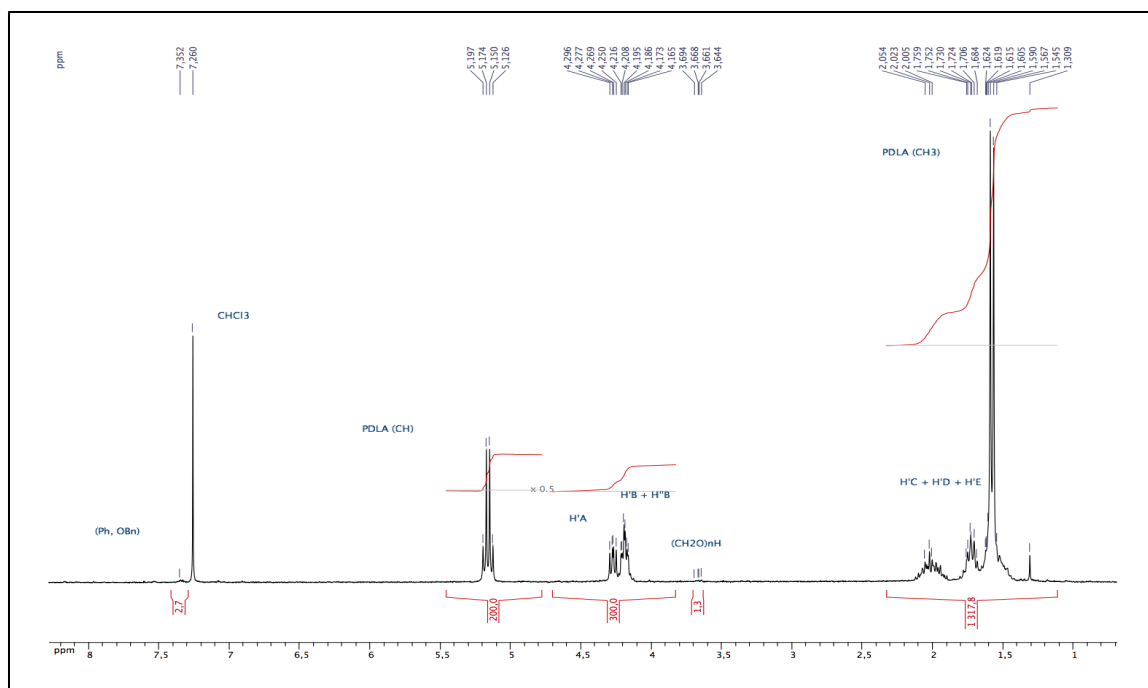


Figure 5: ^1H NMR spectrum (CDCl_3 , 400 MHz) of isolated diblock prepared by polymerization of: 1). 100 equiv. of *D*-lactide using *catalyst 4* system (conditions: $[\text{Lactide}]_0 = 1 \text{ M}$, toluene, 80°C , 9 h, quantitative conv.). 2). $[\text{Cl-CL}]_0 = 1 \text{ M}$, 100 equiv. of Cl-CL, RT, 14 h). Abbreviation: AB302bis.

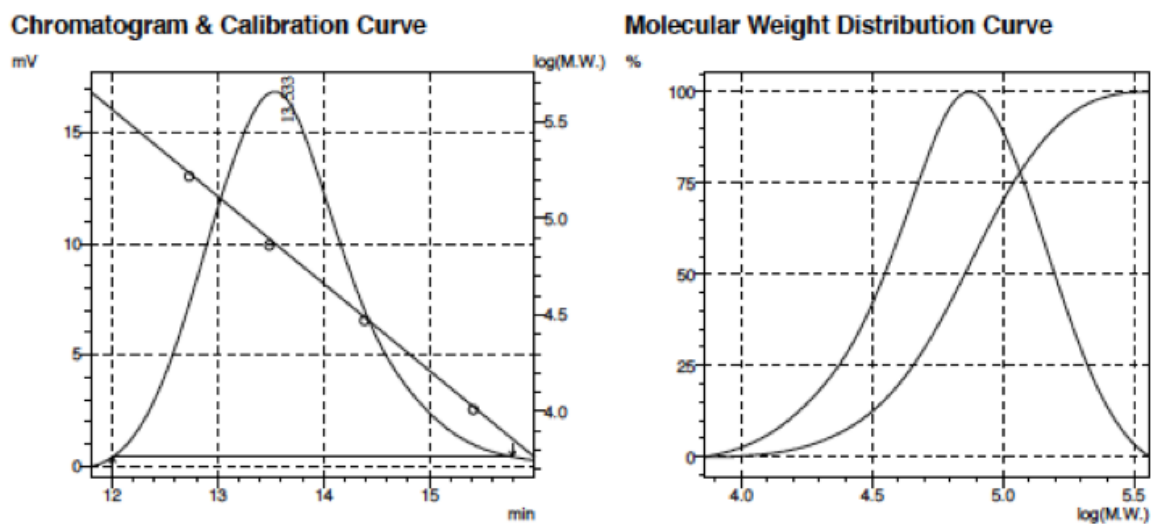


Figure 6: SEC traces of isolated PLLA-*co*-P(Cl-CL) diblock. (100 equiv. of *L*-lactide, 30 equiv. of Cl-CL). Abbreviation: AB303bis

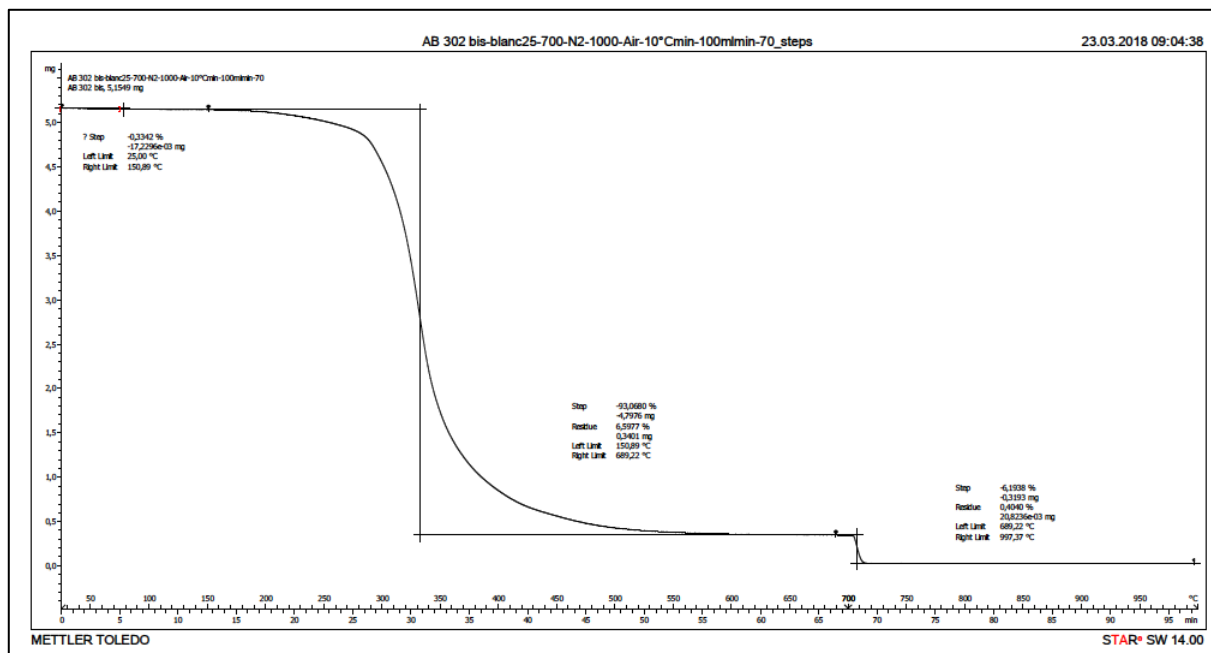


Figure 7: TGA performed on isolated PDLA-*b*-P(Cl-CL) diblock (100 equiv. of *D*-lactide, 100 equiv. of P(Cl-CL)). AB302bis

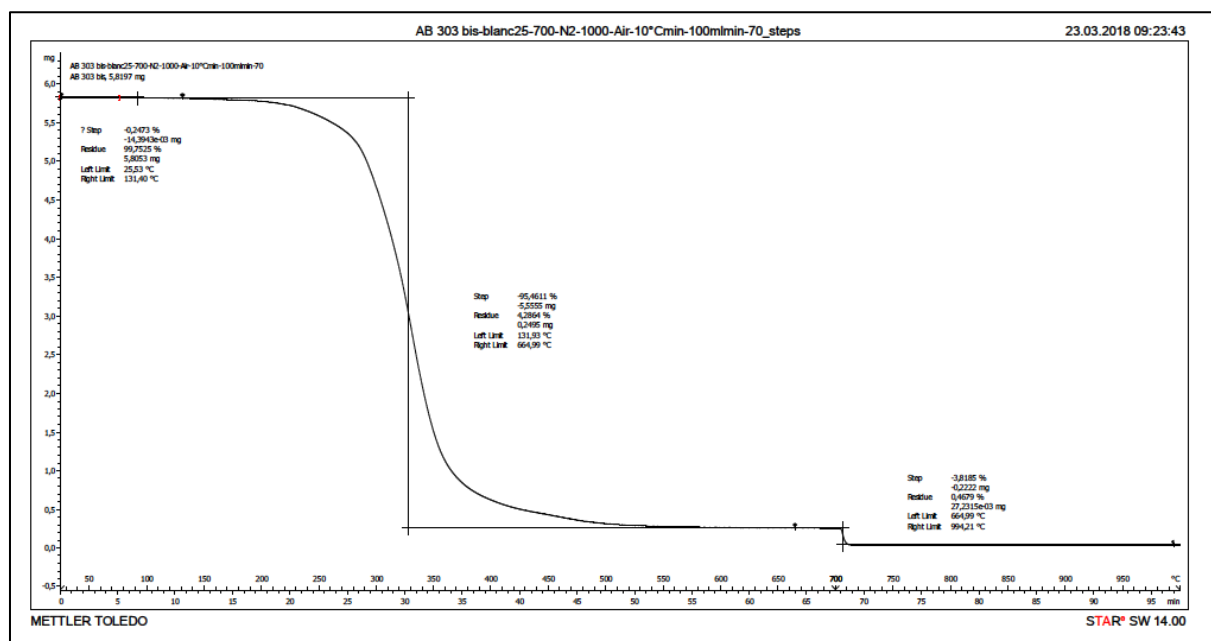


Figure 8: TGA performed on isolated PLLA-*b*-P(Cl-CL) diblock (100 equiv. of *L*-lactide, 30 equiv. of P(Cl-CL)). AB303bis

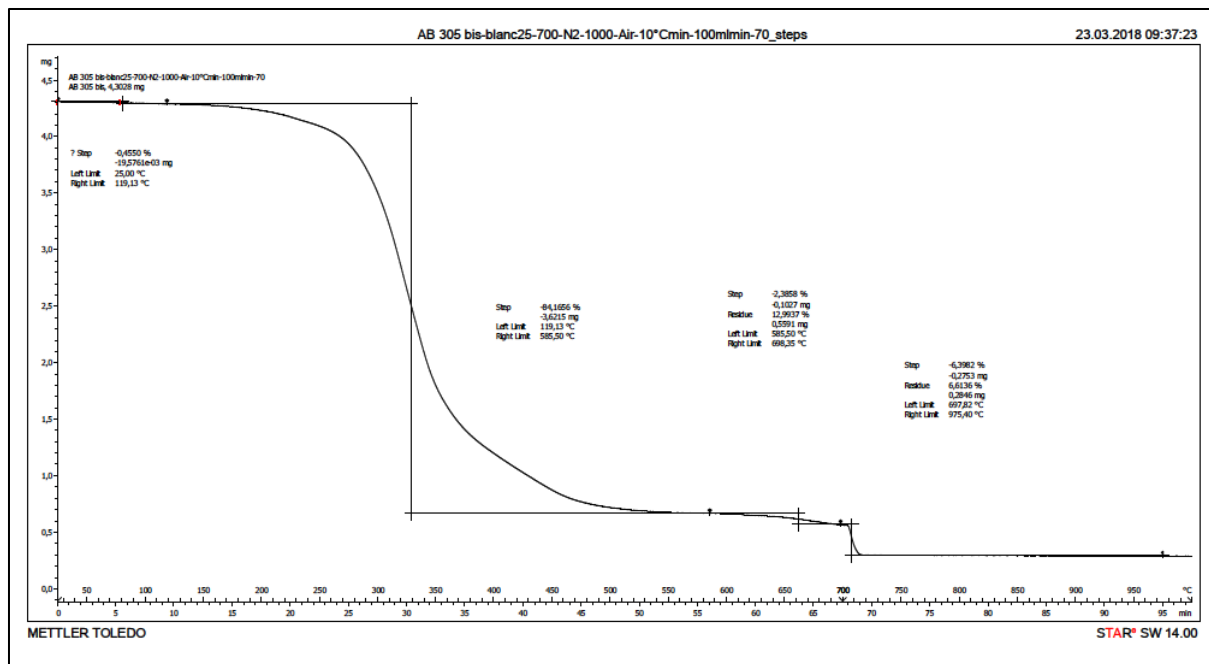


Figure 9: TGA performed on isolated PLLA-*b*-P(Cl-CL) + PDLA-*b*-P(Cl-CL) stereocomplex. (PLLA-*b*-P(Cl-CL) + PDLA-*b*-P(Cl-CL): Mixture of PLLA-*b*-P(Cl-CL) diblock: 100 equiv. of PLLA + 100 equiv. of P(Cl-CL) and PDLA-*b*-P(Cl-CL) diblock: 100 equiv. of *D*-lactide + 100 equiv. of P(Cl-CL). AB305bis

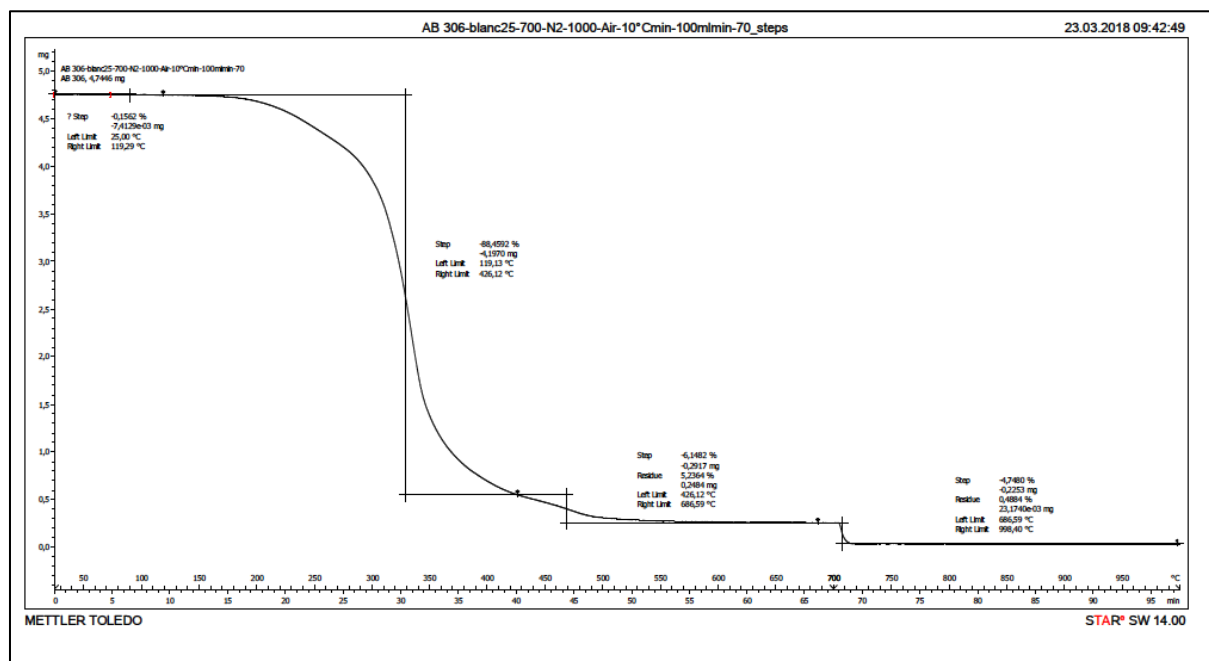


Figure 10: TGA performed on PLLA-*b*-P(Cl-CL) diblock (150 equiv. of *L*-lactide, 150 equiv. of P(Cl-CL)). AB306

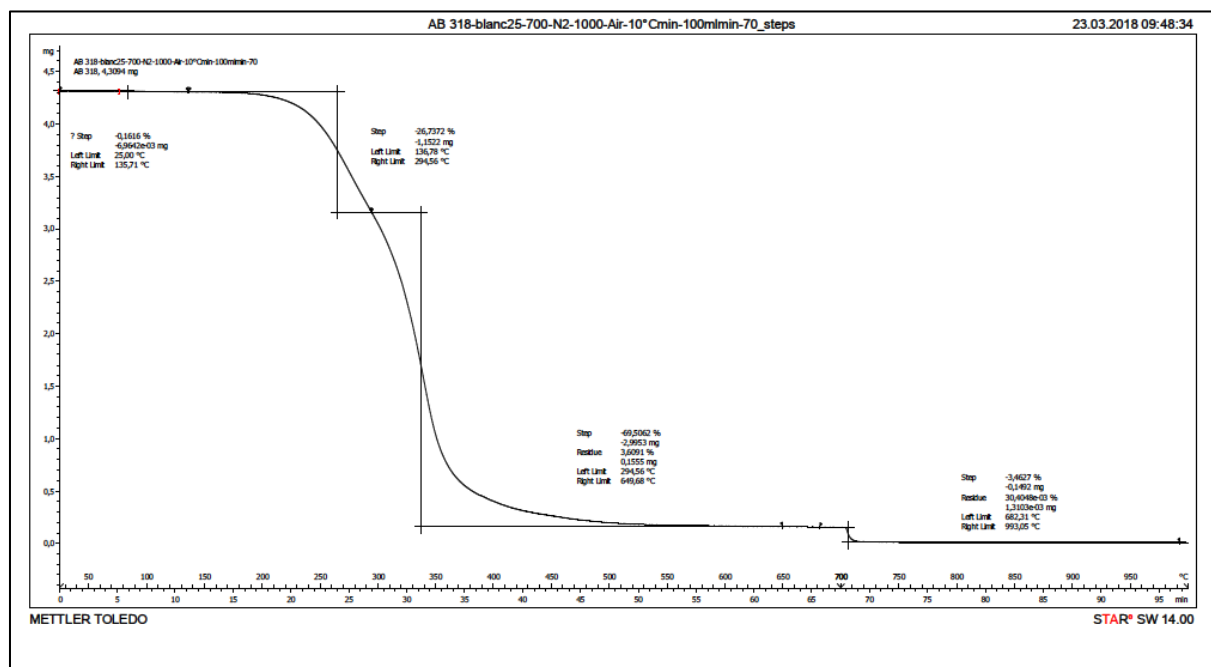


Figure 11: TGA performed on PLLA-*b*-P(Cl-CL) diblock (200 equiv. of *L*-lactide, 100 equiv. of P(Cl-CL)). AB318

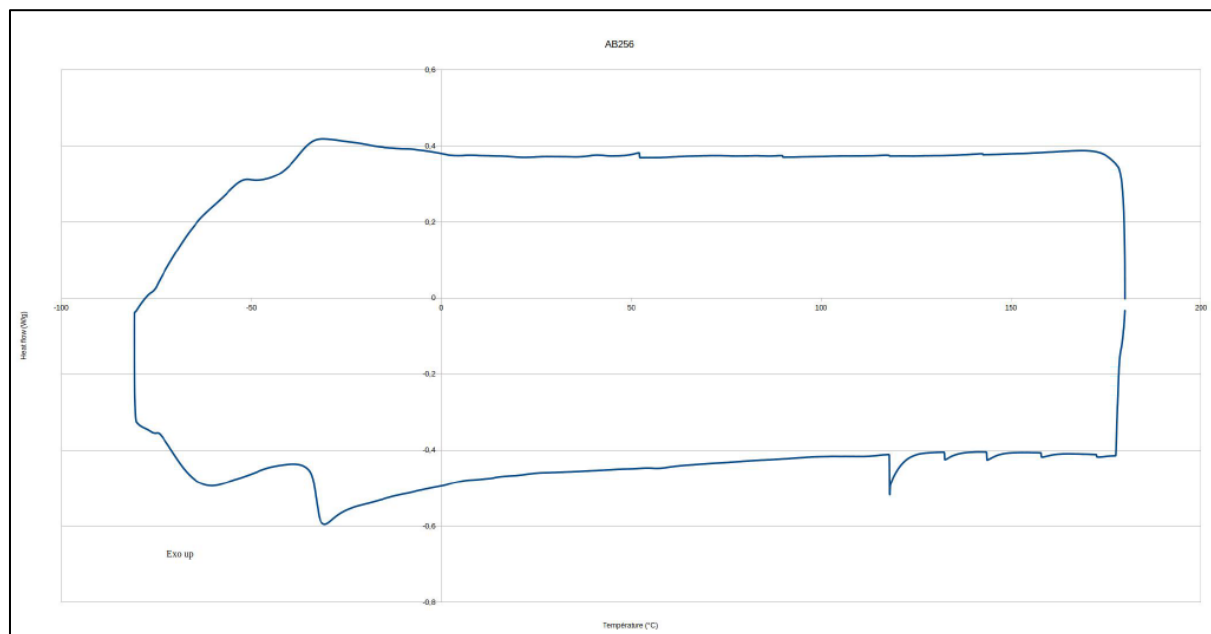


Figure 12: DSC curve of AB256 homopolymer sample (100 equiv. of P(Cl-CL)). Cycle: 180 °C; -80 °C; 180 °C; 25 °C. Rate: 10 °C/min.

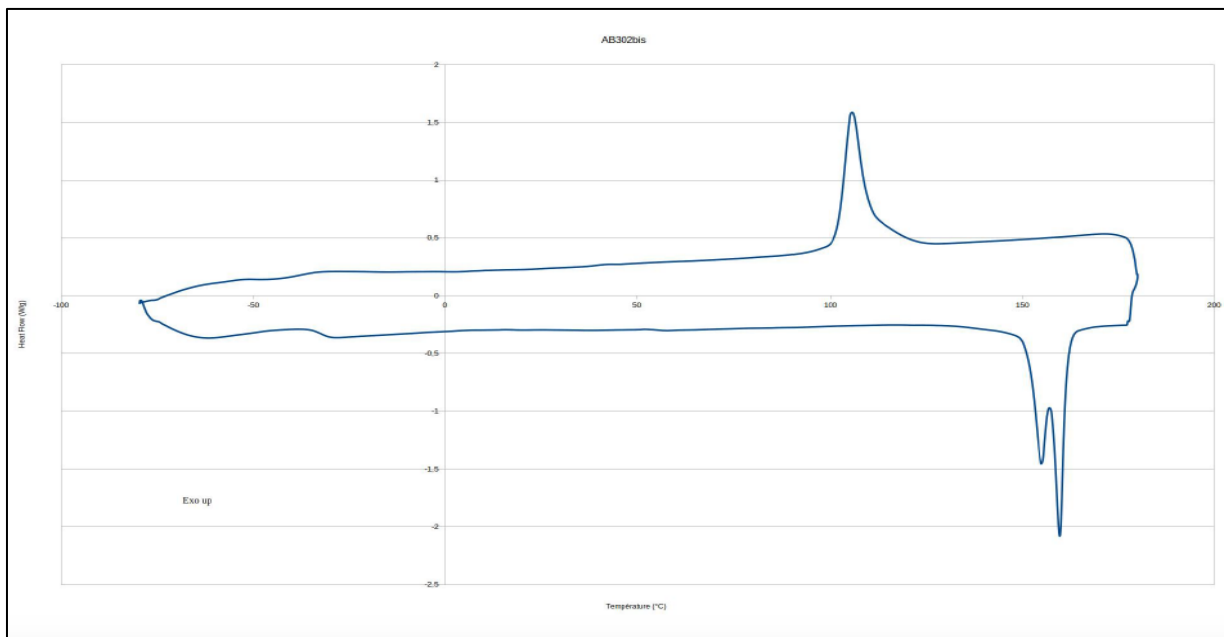


Figure 13: DSC curves of AB302bis diblock sample (100 equiv. PDLA + 100 equiv. P(Cl-CL)). Cycle: 180 °C; -80 °C; 180 °C; 25 °C. Rate: 10 °C/min.

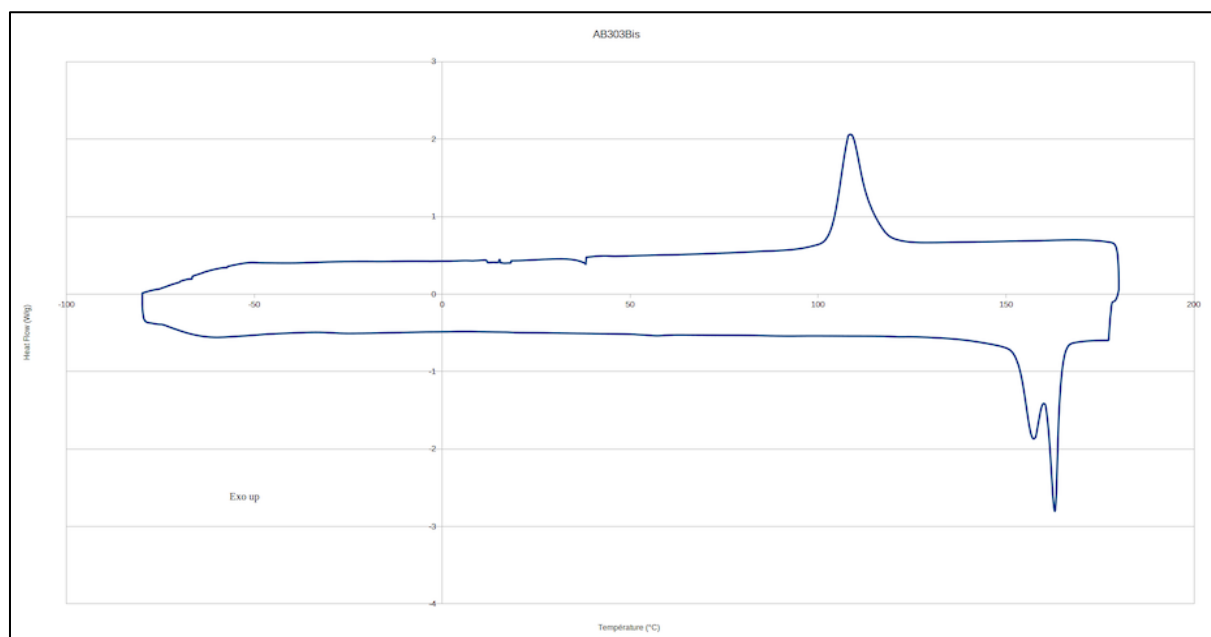


Figure 14: DSC curve of AB303bis diblock sample (100 equiv. of L-lactide + 30 equiv. of P(Cl-CL)). Cycle: 180 °C; -80 °C; 180 °C; 25 °C. Rate: 10 °C/min.

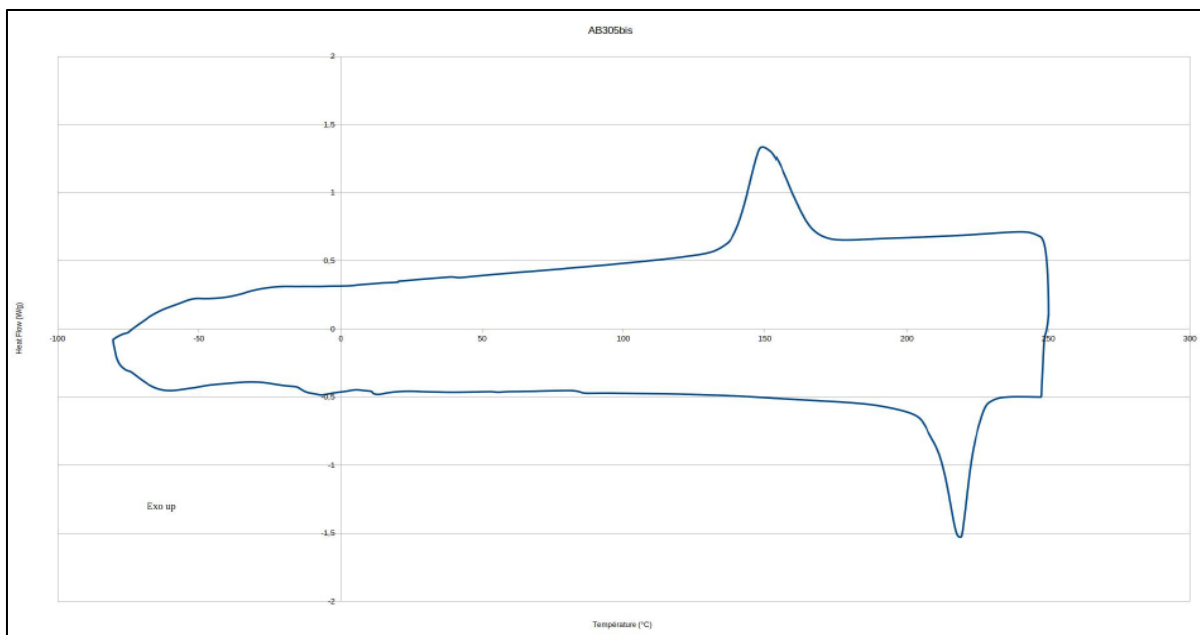


Figure 15: DSC curves of AB305bis stereocomplex sample (PLLA-*b*-P(Cl-CL): 100 equiv. of *L*-lactide + 100 equiv. of P(Cl-CL) + PDLA-*b*-P(Cl-CL): 100 equiv. of *D*-lactide + 100 equiv. of P(Cl-CL)). Cycle: 180 °C; -80 °C; 180 °C; 25 °C. Rate: 10 °C/min.

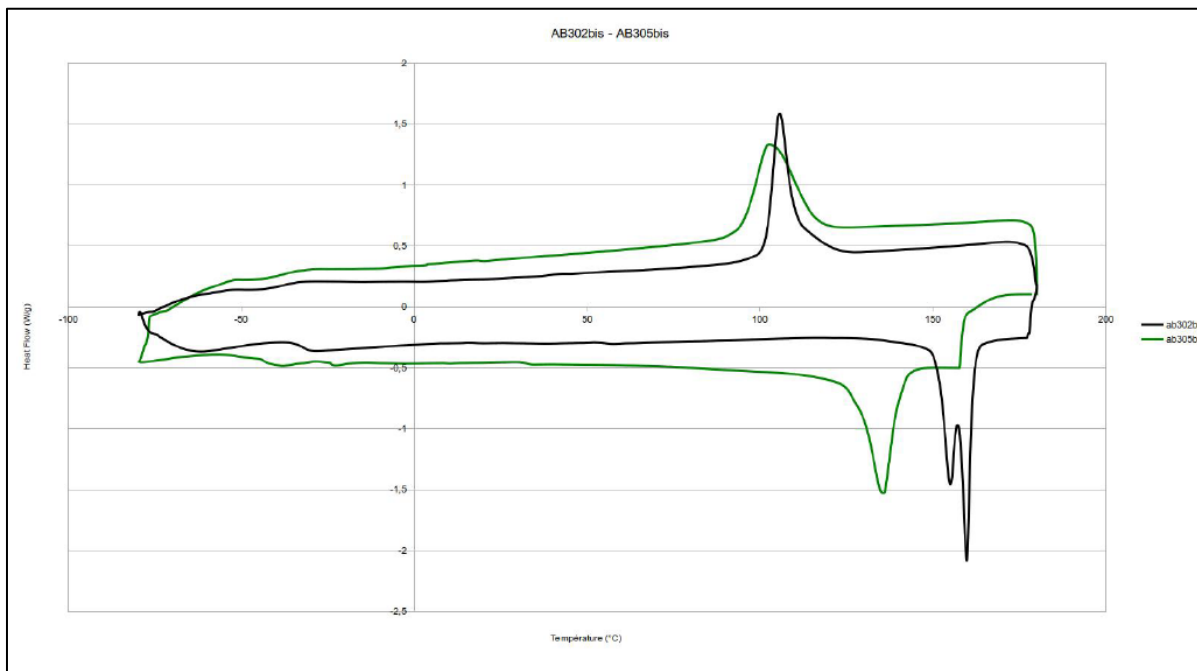


Figure 16: Superimposition of AB305bis stereocomplex DSC (green curve) to AB302bis diblock DSC (black curve). Cycle: 180 °C; -80 °C; 180 °C; 25 °C. Rate: 10 °C/min.

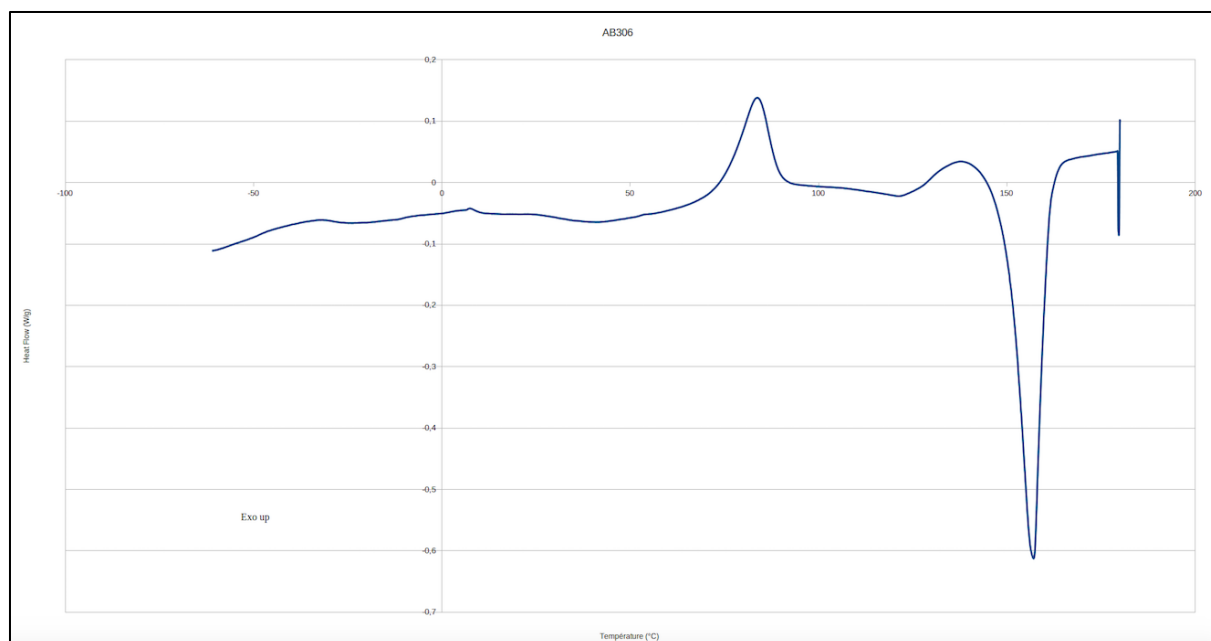


Figure 17: DSC curves of AB306 diblock sample (150 equiv. of *L*-lactide, 150 equiv. of P(Cl-CL)). Cycle: 180 °C; -80 °C; 180 °C; 25 °C. Rate: 10 °C/min.

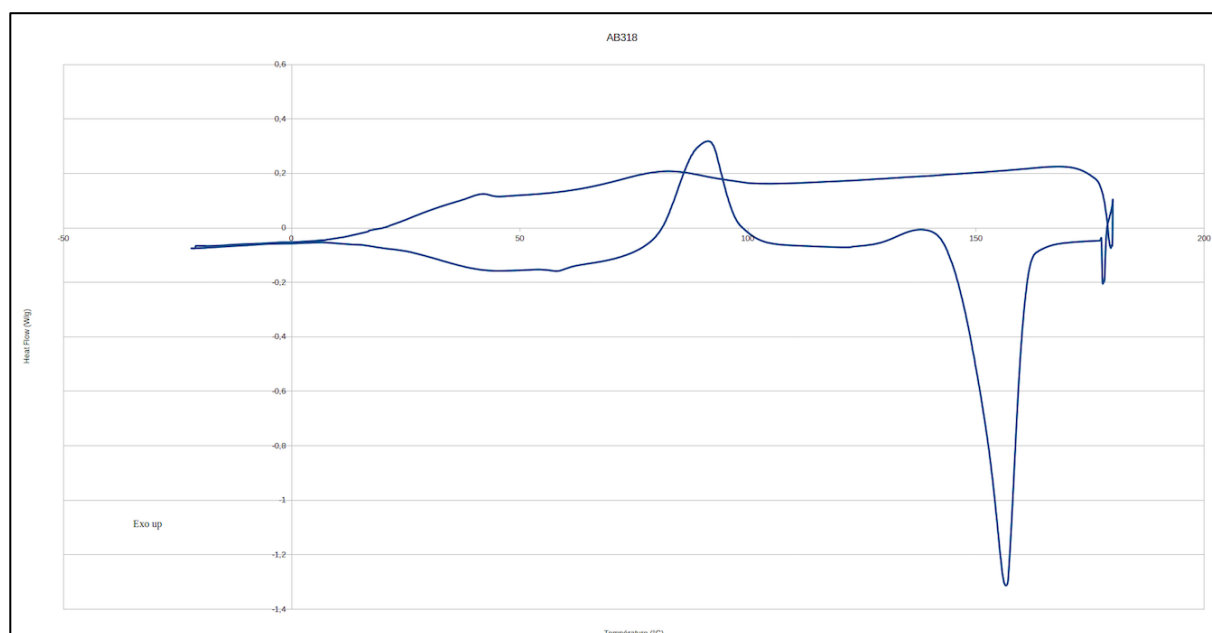


Figure 18: DSC curves of AB318 diblock sample (200 equiv. of *L*-lactide, 100 equiv. of P(Cl-CL)). Cycle: 180 °C; -80 °C; 180 °C; 25 °C. Rate: 10 °C/min.

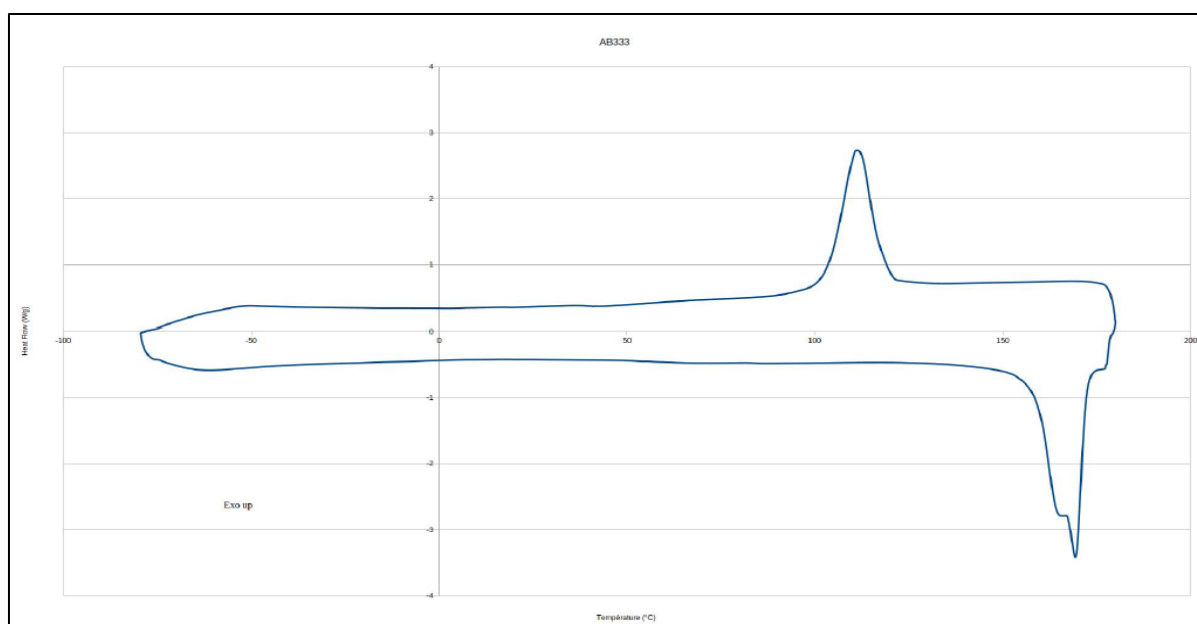


Figure 19: DSC curves of AB333 PLLA sample (100 equiv. PLLA. Cycle: 180 °C; -80 °C; 180 °C; 25 °C. Rate: 10 °C/min.).

References

- [1]. G. R. Fulmer, A. J. M. Miller, N. H. Sherden, H. E. Gottlieb, A. Nudelman, B. M. Stolz, J. E. Bercaw, K. I. Goldberg, *Organometallics*, **2010**, *29*, 2176.
- [2]. *Kappa CCD Operation Manual*, B. V. Nomius, Ed.; Delft: The Netherlands, **1997**.
- [3]. G. –M. Sheldrick, SHELXL97, *Program for the refinement of Crystal Structures*; University of Göttingen: Göttingen, Germany, **1997**.
- [4]. CDCl₃, 25 °C
- [5]. A. Kowalski, A. Duda, S. Penczek, *Macromolecules* **1998**, *21*, 2114
- [6]. M. Save, M. Schappacher, A. Soum, *Macromol. Chem. Phys.* **2002**, *203*, 889.
- [7]. F. Hild, L. BreLOT, S. Dagorne, *Organometallics* **2011**, *30*, 5457-5462.
- [8]. S. Lenoir, R. Riva, X. Lou, C. Detrembleur, R. Jérôme, P. Lecomte, *Macromolecules* **2004**, *37*, 4055-4061.
- [9]. D. J. A. Cameron, M. P. Shaver, *Journal of Polymer Science Part A: Polymer Chemistry* **2012**, *50*, 1477-1484.
- [10]. N. Nomura, R. Ishii, Y. Yamamoto, T. Kondo, *Chem. Eur. J* **2007**, *13*, 4433-4451

Résumé des résultats importants

Une série de catalyseurs de type NHC a été synthétisée à partir du carbène libre 1,3-dimésitylimidazol-2-ylidène qui a lui-même été coordonné avec des métaux du groupe 13, stabilisés par des groupements alkyles (M= Al, Ga, et In respectivement). Ces adduits ont ensuite été testés avec succès dans la ROP du *rac*-lactide en présence d'un alcool jouant le rôle d'agent de transfert de chaîne. Chacune de ces polymérisations a également été réalisée en l'absence d'agent de transfert de chaîne afin d'identifier le rôle de ce dernier.

En présence d'un agent de transfert de chaîne, dans notre cas l'alcool benzylique, les polymérisations se sont avérées relativement rapides, avec des conversions totales du *rac*-lactide en poly(*rac*-lactide) à température ambiante en 30 minutes pour le catalyseur à base d'indium. La durée s'est avérée considérablement plus longue pour le catalyseur de gallium. En parallèle, l'adduit d'aluminium a subi une réaction d'abstraction d'un méthyle par l'acide de Lewis $B(C_6F_5)_3$ en présence d'un solvant coordinant (Et_2O), menant à une espèce cationique stable $[IMesAlMe_2(OEt_2)]^+$ en solution (ex: CH_2Cl_2) et du sel $[CH_3B(C_6F_5)_3]^-$. Cette espèce cationique a également été testée dans la ROP du *rac*-lactide. Ce dernier catalyseur s'est révélé être inactif à température ambiante. La polymérisation a dû être effectuée à 90 °C, et une conversion totale a été obtenue au bout de 40 minutes. Grâce au tracé des courbes $\ln(M_0/M) = f(\text{temps})$ et $M_{n, \text{exp}} = f(\text{conversion})$, les ROP sont cohérentes avec une cinétique de pseudo-ordre un. Une corrélation linéaire entre la masse moléculaire du PLA formé et la conversion du monomère durant la réaction est observée, confirmant la formation contrôlée du PLA. La spectrométrie de masse en mode MALDI-TOF du polymère obtenu est en accord avec un polymère linéaire portant un groupement benzyloxy en bout de chaîne. Ce qui suggère ainsi un mécanisme de polymérisation opérant via le mécanisme classique de coordination-insertion.

En l'absence d'initiateur, les polymérisations se sont déroulées avec des temps de conversion beaucoup plus lents (ex: 83 h). Le tracé des courbes $\ln(M_0/M) = f(\text{temps})$ et $M_{n, \text{exp}} = f(\text{conversion})$, révèle des cinétiques également de pseudo-ordre un pour chaque polymérisation, et un contrôle de la formation du polymère en fonction de la conversion en monomère. Ces polymérisations sont bien contrôlées et les spectres MALDI-TOF en absence d'alcool ont permis de définir la forme du polymère final (cyclique, linéaire).

La synthèse de copolymères PEG-*co*-PLLA a été effectuée avec différents catalyseurs (connus ou nouvellement synthétisés) et les conditions optimales ont été définies pour chacune de ces polymérisations. Ces copolymères sont de nature amphiphile grâce à la partie

PEG qui leur confère un caractère hydrophile. Le PLA, qui est un polymère biodégradable, apporte une contribution hydrophobe (**Figure 1**).

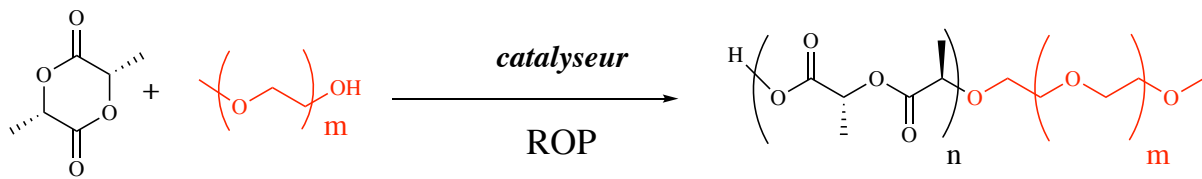


Figure 1: ROP du *L*-lactide par un système catalyseur/*m*-PEG-OH pour l'obtention de copolymère PEG-*co*-PLLA

La synthèse a d'abord été réalisée avec des catalyseurs de types *N,O,N* dont l'un à base d'amido aluminium déjà connu, et son analogue, avec comme métal le gallium qui constitue un nouveau catalyseur. Ces deux catalyseurs sont différents uniquement par la nature du centre métallique. Le premier possède un centre métallique aluminium alors que le second complexe est coordonné à du gallium.

Les polymérisations du PEG-*co*-PLA avec ces deux catalyseurs ont été effectuées à 90 °C. Grâce au spectre de masse en mode MALDI-TOF, nous avons confirmé l'obtention des copolymères de façon contrôlée. Nous avons pu remarquer que le catalyseur avec comme centre métallique le gallium avait une activité plus rapide dans cette polymérisation que celui avec l'aluminium. Un troisième catalyseur a été synthétisé. Il comprend comme métal le zinc, métal possédant des propriétés intéressantes. Naturellement présent dans l'air, l'eau ou les sols, ce métal est également peu onéreux et biocompatible. La polymérisation a été effectuée à 70 °C et nous avons obtenu le copolymère souhaité, confirmé par l'analyse de masse. Enfin, un dernier catalyseur, à base de magnésium a permis cette polymérisation et s'est avéré être le plus intéressant pour cette copolymérisation. La conversion totale a été obtenue en seulement quatre minutes avec une température basse pour un meilleur contrôle de l'activité. Les conditions industrielles ont également été réalisées pour la formation de ce copolymère. Il s'agit des conditions dites «conditions bulk» réalisées sans solvant. Nous avons appliqué ce procédé pour chacun des catalyseurs préalablement utilisés. Ainsi, pour les quatre différentes polymérisations, les résultats obtenus confirment que ces polymérisations sont capables de se réaliser dans de telles conditions. Pour chaque copolymère, un spectre de masse en mode MALDI-TOF confirme la formation du copolymère PEG-*co*-PLLA.

La plus grande partie de ma thèse s'inscrit dans la polymérisation linéaire et contrôlée à température ambiante de la Cl-CL, au préalable synthétisée, via la réaction d'oxydation de Bayer-Villiger de la chloro-cyclohexanone par le *m*CPBA (**Figure 2**).

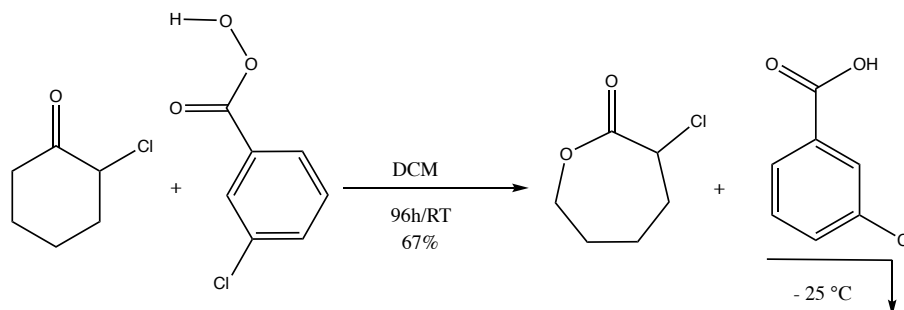


Figure 2: Oxydation de la 2-chlorocyclohexanone en Cl-CL

La ROP de 100 équivalents en monomère, catalysée par un salen d'aluminium a mené à une conversion totale en polymère en seulement 7 minutes avec un indice de polydispersité fin (1.17). Ce succès nous a permis de synthétiser la P(Cl-CL) avec différents ratios en monomère. C'est ainsi que la longueur de chaîne polymérique a d'abord été augmentée à 250 équivalents. La polymérisation a atteint une conversion totale en polymère après une durée de 130 minutes et nous avons observé un indice de polydispersité fin (PDI: 1.25). Les études cinétiques dans les deux polymérisations précédentes catalysées par le salen d'aluminium sont en accord avec une ROP procédant de façon contrôlée. Nous avons obtenu une corrélation linéaire entre la valeur de la masse moléculaire du P(Cl-CL) formé et la conversion du monomère durant la polymérisation. Cela illustre un accroissement de la chaîne polymérique de façon linéaire avec la conversion. Le tracé du graphique du logarithme népérien $\ln(M_0/M)$ en fonction du temps a confirmé une cinétique d'ordre un pour la formation en P(Cl-CL) qui est également en accord avec un processus de ROP contrôlé via un mécanisme de coordination-insertion. La polymérisation a aussi été réalisée avec un ratio de 500 équivalents en Cl-CL. Cependant, la réaction est considérablement plus longue (7 heures) dans les mêmes conditions, que celles utilisées précédemment et nous obtenons un indice de polydispersité large (PDI: 1.56). La GPC indique un tracé bimodal et un faible poids moléculaire par comparaison avec ceux obtenus pour un ratio de 100 équivalents en monomère puis de 250 équivalents. La RMN ^1H ainsi que le spectre de masse en mode MALDI-TOF, permettent de conclure d'une part à la formation d'un polymère cyclique de P(Cl-CL), mais aussi d'un polymère linéaire de P(Cl-CL) portant un groupement benzyloxy en bout de chaîne.

Afin de modifier les propriétés de ce polymère, des copolymères amphiphiles ont été synthétisés. Ces derniers sont conçus avec une chaîne hydrophile de polyéthylène glycol et d'une partie hydrophobe de P(Cl-CL). Des tests de solubilité dans l'eau deutéré ainsi que des mesures de tension interfaciale, ont permis d'attribuer un caractère amphiphile ou hydrophobe, selon la longueur de chaîne de PEG par rapport à celle en P(Cl-CL) à ces copolymères. Des diblocs P(D)LA-*b*-P(Cl-CL) selon différentes proportions en chacun des monomères comme l'indique le tableau ci-dessous (**tableau 1**), ont été formés dans le but d'apporter cette fois-ci un caractère cristallin grâce au lactide sur le P(Cl-CL) qui est un polymère amorphe.

	<i>L</i> -lactide / <i>D</i> -lactide (équivalents)	Cl-CL (équivalents)	PLA/P(Cl-CL) (%)
PLA homopolymère	100	/	100/0
PLLA- <i>b</i> -P(Cl-CL)	100	20	83/17
PLLA- <i>b</i> -P(Cl-CL)	100	30	76/23
PLLA- <i>b</i> -P(Cl-CL)	200	100	66/34
PLLA- <i>b</i> -P(Cl-CL)	150	150	50/50
PLLA- <i>b</i> -P(Cl-CL)	100	100	50/50
PDLA- <i>b</i> -P(Cl-CL)	100	100	50/50
P(Cl-CL) homopolymère	0	100	0/100

Tableau 1: Résumé des différents diblocs P(D)LA-*b*-P(Cl-CL) formés

Parallèlement à la formation de ces diblocs, nous avons effectué un nouveau stéréocomplexe: PLLA-*b*-P(Cl-CL) + PDLA-*b*-P(Cl-CL). Différentes mesures physico-chimiques ont ensuite été établies sur ces différents diblocs et sur le stéréocomplexe. Des mesures d'analyses thermogravimétriques ont permis de mesurer la variation de masse des différents copolymères (**Tableau 1**), de l'homopolymère, et du stéréocomplexe, en fonction du temps, et de comparer les températures de décomposition de chacun des échantillons, ainsi que leur quantité résiduelle. L'homopolymère P(Cl-CL) s'avère être très sensible, ce qui est probablement dû à la présence de liaisons carbone-chlore. Comme nous l'avions prévu, le stéréocomplexe quant à lui, est le plus résistant des matériaux. Des mesures de calorimétrie à balayage différentiel nous ont permis de déterminer les températures caractéristiques (fusion, cristallisation,..) des homopolymères, diblocs et du stéréocomplexe. Des réactions de Williamson ont été réalisées

sur la P(Cl-CL) grâce à l'alcool benzylique, suivies d'hydrogénation dans le but d'obtenir l'alcool correspondant, menant ainsi à un polymère hydrophile.

Après plusieurs essais avec 1 équivalent en alcool benzylique par rapport à la P(Cl-CL), le nombre encore très important de fonctions benzyloxy non déprotégées apparents en MALDI-TOF, a laissé supposer que ce groupement volumineux empêchait par encombrement stérique, l'approche d'un certain nombre de centres à substituer. Ainsi nous avons choisi de diminuer la stoechiométrie et de mettre l'alcool benzylique en défaut (0.7 équivalents). La réaction de Williamson tout comme celle procédée avec 1 équivalent d'alcool benzylique mène au clivage du polymère obtenu. En effet, en RMN du proton, deux signaux différents CH_2 -Ph sont visibles, et le bout de chaîne de fin du polymère est plus intense que ce que nous attendions. Cela implique une coupure du polymère en oligomères plus petits, sans doute obtenus par une réaction de transestérification du polymère avec BnOH. La réaction d'hydrogénation appliquée sur ce mélange est quantitative en RMN. Après avoir pressurisé les polymères avec du dihydrogène (1 atm.) dans du chloroforme deutéré catalysé par du Pd/C et après 15 minutes à température ambiante, le suivi RMN montre la disparition complète des signaux du benzyloxy, et la quantité en toluène fournie n'augmente plus. La spectrométrie de masse nous permet d'identifier un mélange de P(α OH ϵ CL) cyclique et linéaire ainsi que la présence de polymère cyclique linéaire avec des fragments P(α OBn ϵ CL) du polymère non déprotégé et d'unités (Cl-CL). Pour savoir si le polymère final avait tout de même acquis un caractère hydrophile, il a été étudié en RMN dans de l'eau deutéré. La présence de signaux bien définis tant en RMN du proton que du carbone, nous permet de valider ainsi l'approche recherchée.

Catalyse de la polymérisation pour l'obtention de polyesters à caractères hydrophile biodégradable

Résumé

Des adduits carbéniques à base de métaux du groupe 13 (aluminium, gallium et indium) ainsi qu'un nouveau cation d'aluminium stabilisé par des groupements alkyles, ont permis la ROP du lactide dans des conditions réactionnelles douces et simples. Dans un second temps, des copolymères amphiphiles ont été synthétisés par la ROP du lactide en présence de poly(éthylène glycol) menant aux PEG-co-PLLA désirés. Les complexes organométalliques ont encore mis en avant leurs avantages grâce à l'utilisation de salen d'aluminium qui permet d'ouvrir la voie sur la ROP de l' α -chloro- ϵ -caprolactone menant à la poly(α -chloro- ϵ -caprolactone). La synthèse de nouveaux copolymères, diblocs et stéréocomplexe a permis de moduler les propriétés de l'homopolymère obtenu, telles qu'ont pu le confirmer les diverses mesures physico-chimiques effectuées sur ces derniers. Enfin, la post-fonctionnalisation partielle, grâce à la réaction de Williamson, suivie par la réaction d'hydrogénation a permis l'obtention de polymères hydrophiles.

Mots-clés: Chimie organométallique, polymérisation par ouverture de cycle, polymères biodégradables, polymères amphiphiles.

Abstract

Carbene adducts with Group 13 metal (aluminium, gallium and indium) and a new aluminium cation stabilized by alkyl groups, have allowed the ROP of lactide under mild and simple conditions. In a second step, amphiphilic copolymers were synthesized with poly(ethylene glycol) leading to the desired PEG-co-PLLA. Organometallic complexes have still put forward their advantages by the use of aluminium's salen allowing to open the way on the ROP of the α -chloro- ϵ -caprolactone leading to the poly(α -chloro- ϵ -caprolactone). The formation of new copolymers, diblocks and stereocomplex has afforded to modulate the obtained homopolymer's properties, confirmed by the use of the various physicochemical measurements effected on the latter. Finally, the partial post-functionalization according to the Williamson reaction followed by the hydrogenation reaction has led to the obtaining of hydrophilic polymers.

Keys-words: Organometallic chemistry, Ring Opening Polymerization, biodegradable polymers, amphiphilic polymers.